

Shear Capacity of Concrete Members under Monotonic and Cyclic Loading

Sara Javidmehr

Institut für Baustoffe, Massivbau und Brandschutz (iBMB)
Materialprüfanstalt für das Bauwesen (MPA) Braunschweig

Heft 238

Braunschweig
ISBN 978-3-89288-223-7
ISSN 1439-3875

2019

Von der Fakultät Architektur, Bauingenieurwesen und Umweltwissenschaften
der Technischen Universität Carolo-Wilhelmina zu Braunschweig
zur Erlangung des Grades einer Doktoringenieurin (Dr.-Ing.)
genehmigte Dissertation

Eingereicht am: 11. Januar 2019

Disputation am: 29. August 2019

Berichterstatter:

Prof. Dr.-Ing. Martin Empelmann

Prof. Dr. sc. techn. Klaus Thiele

Diese Dissertation ist über die Internetseite der Universitätsbibliothek
Braunschweig online zugänglich.

Bibliografische Information der Deutschen Nationalbibliothek

Die Deutsche Nationalbibliothek verzeichnet diese Publikation in der Deutschen
Nationalbibliografie; detaillierte bibliografische Daten sind im Internet über
<http://dnb.dnb.de> abrufbar.

Bibliographic information published by the Deutsche Nationalbibliothek

The Deutsche Nationalbibliothek lists this publication in the Deutsche
Nationalbibliografie; detailed bibliographic data are available on the Internet at
<http://dnb.dnb.de>

Information bibliographique de la Deutsche Nationalbibliothek

La Deutsche Nationalbibliothek a répertorié cette publication dans la Deutsche
Nationalbibliografie; les données bibliographiques détaillées peuvent être consultées
sur Internet à l'adresse <http://dnb.dnb.de>

Abstract

Shear Capacity of Concrete Members under Monotonic and Cyclic Loading

To date, a reliable assessment of shear safety of concrete members is a challenging task for evaluation of existing concrete structures such as bridges. Available investigations and models for determination of shear capacity are often based on diagonally cracked members and assure the shear safety mainly based on provided shear reinforcement. Application of such models results often in a calculated lack of shear resistance due to deficient shear reinforcement, although existing concrete members are often free from diagonal cracks. To avoid over-conservative evaluations in such cases, the shear capacity provided by concrete tensile strength would be evaluated in this thesis. A safe consideration of this load-bearing mechanism for members subjected to cyclic service loads e.g. traffic loads requires, however, an adequate consideration of cyclic damage on concrete tensile behaviour.

At first, concrete tensile behaviour under uniaxial tension is investigated using conducted tensile tests on cyclically damaged members and a compiled database of cyclic tensile tests. The findings are used to propose a tensile curve for cyclically damaged concrete.

In the second part, cracking of concrete members under shear loading is evaluated using provided mechanical models and shear tests in the technical literature. A database of monotonic and cyclic shear tests on reinforced and prestressed concrete members without shear reinforcement with provided data on diagonal cracking is compiled. Based on monotonic tests of the database, a mechanical model is proposed for a better approximation of diagonal cracking load. This model is adapted later on to derive mechanical models, which account for prestressing as well as cyclic damage.

In a higher approximation level, some benchmark shear tests are evaluated using nonlinear finite element (FE) analysis to propose a refined model configuration for reliable assessment of diagonal cracking of shear critical members. The refined model configuration is validated in a further step using the monotonic tests in the shear database. In addition, recommendations are made for numerical prediction of the diagonal cracking load of cyclically damaged concrete members.

Finally, the results of the theoretical, experimental and numerical investigations are summarized in proposals for determination of the shear capacity of members under monotonic and cyclic shear loads at the state of diagonal cracking using mechanical and numerical models.

Kurzfassung

Querkrafttragfähigkeit von Betonbauteilen unter monoton steigender und zyklischer Beanspruchung

Eine zuverlässige Bewertung der Tragsicherheit von Betonbauteilen ist bislang eine herausfordernde Aufgabe bei der Bewertung bestehender Bauwerke wie Brücken. Vorhandene Untersuchungen und Modelle zur Bestimmung der Querkrafttragfähigkeit basieren oft auf Bauteile, die bereits Schrägrisse aufweisen und bei denen die Querkrafttragfähigkeit über die vorhandene Querkraftbewehrung sichergestellt wird. Die Anwendung solcher Modelle führt oft zu einer rechnerischen defizitären Querkrafttragfähigkeit, obwohl die bestehenden Bauteile oft frei von Schrägrissen sind. Um in solchen Fällen eine zu konservative Bewertung zu vermeiden, wird in dieser Arbeit der Betonzugtraganteil unter Querkraftbeanspruchung bewertet. Eine sichere Berücksichtigung dieses Traganteils für Bauteile wie Brücken, die zyklischen Betriebslasten ausgesetzt sind, erfordert jedoch eine angemessene Berücksichtigung der zyklischen Schädigung.

In dieser Dissertation wird hierzu in einem ersten Schritt das einaxiale Betonzugtragverhalten mithilfe eigener Zugversuche an zyklisch vorgeschädigten Proben und einer erstellten Datenbank zu zyklischen Zugversuchen untersucht. Aus den Ergebnissen wird eine Arbeitslinie für zyklisch vorgeschädigten Beton vorgeschlagen. In einem zweiten Schritt wird die Schrägrissbildung von Betonbauteilen anhand vorhandener mechanischer Modelle sowie vorhandener Querkraftversuche in der Fachliteratur mit dokumentierten Schrägrisslasten bewertet. Hierzu wird eine Datenbank zu monotonsteigend und zyklisch durchgeführten Querkraftversuchen an Stahlbeton- und Spannbetonbalken ohne Querkraftbewehrung aufgebaut. Mithilfe der Datenbank wird ein vorhandener mechanischer Ansatz ausgewählt, optimiert und zur Herleitung weiterer Modelle für die rechnerische Bewertung der Schrägrisslasten von vorgespannten Bauteilen und zyklisch vorbelasteten Stahlbetonbauteilen modifiziert. In einer höheren Nachweisstufe wird anhand von FE-Analysen von Querkraftversuchen eine verfeinerte Modellkonfiguration ausgewählt, welche mit den monotonen Datenbankversuchen validiert wird. Darüber hinaus werden Empfehlungen für die numerische Modellierung der Schrägrissbildung von zyklisch vorgeschädigten Stahlbetonbauteilen gegeben.

Schließlich werden die Ergebnisse der theoretischen, experimentellen und numerischen Untersuchungen in Vorschläge zur Bewertung der Schrägrissbildung von Bauteilen unter monotoner und zyklischer Querkraftbeanspruchung zusammengefasst.

Acknowledgements

This thesis concludes the research done in three unforgettable years at iBMB, Division of Concrete Constructions of TU Braunschweig. It was encouragement, support and love of many people who accompanied me, to whom I owe many thanks.

First and foremost, I would like to thank my supervisor Univ. Prof. Martin Empelmann for his wise guidance and trust. Without his understanding, critical remarks on my work and the provided academic freedom, I would not have been able to complete this thesis. I would also like to thank my second examiner Univ. Prof. Dr. sc. techn. Klaus Thiele for his critical review and helpful comments on my thesis.

My special thanks go to Dr.-Ing. Vincent Oettel for his support and encouraging as well as constructive comments on my work. I would also like to thank all my friends and colleagues at Division of Concrete Construction: Angelika Schukmann, Daniel Busse, Jörn Remitz, Marcel Wichert, Henrik Matz, Jonas Cramer, Jan-Paul Lanwer and the Colleagues in the testing Hall of iBMB Bernd Schiedung, Matthias Kloss, Philip Hirschfeld and Michael Brüggem. Many thanks also to the members of Graduate School 2075 for sharing their expertise and ideas during our discussions. I would also like to thank Oliver Dienelt for his support by finding the most unfindable literature.

Huge thanks to Christian, who has supported me in the past years with his love and for being always there for me. You make me feel so fortunate and loved! Many thanks also to his family for making me feel at home in Germany.

Last, but not least, I would like to thank my family, my parents who have sparked my interest on research and make me feel so loved and blessed and my brother for his unconditional love and support.

Braunschweig, January 2019

Sara Javidmehr

Table of Contents

	Page
Table of Contents	I
Notations	IV
1 Introduction	1
1.1 Background	1
1.2 Aim and objectives	2
1.3 Outline	3
2 Monotonic and cyclic concrete tensile behaviour	5
2.1 Uniaxial concrete tensile behaviour	5
2.1.1 Tensile cracking and softening behaviour	5
2.1.2 Parameters of the concrete tensile curve	8
2.1.3 Factors affecting concrete tensile strength	11
2.2 Uniaxial cyclic tensile behaviour of concrete	13
2.2.1 Concrete behaviour under cyclic tension	13
2.2.2 Parameters of the cyclic concrete tensile curve	15
2.3 Concluding remarks	18
3 Experimental investigation of tensile cyclic damage	20
3.1 General remarks	20
3.2 Database of cyclic tensile tests	20
3.2.1 Overview of database	20
3.2.2 Comparison of tensile strength values	21
3.2.3 Evaluation of fatigue tensile strength	23
3.3 Experimental Investigations	23
3.3.1 Experimental programme and tests specimens	23
3.3.2 Test specimens and concrete	24
3.3.3 Test setup and testing procedure	24
3.3.4 Evaluation of test data	26
3.4 Concluding remarks	32
4 Diagonal cracking under monotonic and cyclic loading	34
4.1 Behaviour of concrete members under monotonic shear loads	34
4.1.1 Stress state in concrete members and theoretical diagonal cracking	34
4.1.2 Experimental diagonal cracking	36
4.1.3 Influencing parameters on diagonal tension under shear	39
4.1.4 Shear capacity under diagonal tension and further load-bearing mechanisms	42

Table of Contents

4.1.5	Mechanical approaches for evaluation of monotonic diagonal cracking load	43
4.2	Behaviour of concrete members under cyclic shear loads	48
4.2.1	Experimental investigations under combined flexure and shear	48
4.2.2	Mechanical approaches for evaluation of cyclic diagonal cracking load	50
4.3	Concluding remarks	51
5	Database of shear tests	53
5.1	General remarks and selection criteria	53
5.2	Overview on database	54
5.3	Location and shape of critical diagonal crack	57
5.4	Evaluation of diagonal cracking load	60
5.5	Concluding remarks	61
6	Diagonal cracking load under monotonic and cyclic shear	63
6.1	General remarks	63
6.2	Monotonic diagonal cracking load of RC members	63
6.2.1	General approach	63
6.2.2	Evaluation of mechanical approaches	65
6.2.3	Modified mechanical model	68
6.3	Derived model for diagonal cracking of prestressed members	70
6.4	Derived model for cyclic diagonal cracking	72
6.5	Concluding remarks	77
7	Nonlinear finite element evaluation of diagonal cracking	79
7.1	Scope and objectives	79
7.2	Modelling orthotropic damage in shear critical members	80
7.3	Element size and crack band width	82
7.4	Loading and analysis procedure	83
7.5	Description of numerical models	84
7.5.1	Geometry and model discretization	84
7.5.2	Material parameters	85
7.5.3	Analysis procedure	86
7.6	Scope of reference investigations	87
7.6.1	Models with rotating cracks (R)	88
7.6.2	Models with fixed cracks (F)	91
7.6.3	Comparison of results and provisional conclusion	94
7.7	Proposed iterative-incremental approach	96
7.8	Proposed rotating to fixed crack model (RF)	99
7.9	Concluding remarks	100

8 Numerical simulation of experiments in shear database	102
8.1 Outline	102
8.2 General approach	102
8.3 Diagonal cracking of RC members under monotonic shear loads	103
8.3.1 Diagonal cracking and failure loads	103
8.3.2 Load-displacement curves and crack propagation	105
8.3.3 Brittleness of critical diagonal cracking and prior notice	110
8.4 Evaluation of the rotating to fixed crack model (RF crack model)	114
8.4.1 Diagonal cracking and failure loads	114
8.4.2 Parametric study	119
8.5 FE simulation of RC members under cyclic loading	123
8.6 Concluding remarks	126
9 Proposals for evaluation of shear capacity under monotonic and cyclic loading	128
9.1 General	128
9.2 Analytical approach	128
9.3 Numerical approach	131
9.4 Conceptual approach	133
10 Conclusions and outlook	135
10.1 Conclusion	135
10.2 Outlook	137
11 References	138
Appendix A: Database of cyclic tensile tests	A-1
Appendix B: Documentation of cyclic tensile tests	B-1
B-1 Concrete mixture	B-1
B-2 Concrete properties	B-1
B-3 Overview of results	B-2
B-4 Failure sections and surfaces	B-3
Appendix C: Shear database	C-1
C-1 Calculation of concrete properties	C-1
C-2 Shear tests on RC members with diagonal cracking load (mRC-V)	C-3
C-3 Shear tests on RC members with crack detail (mRC-D)	C-11
C-4 Shear tests on PC members with diagonal cracking load (mPC)	C-17
C-5 Shear tests on RC members under cyclic loading (cRC)	C-19
Appendix D: Finite Element Models	D-1
D-1 Input	D-1
D-2 Results of benchmark models	D-6
D-3 Results of mRC beams	D-9

Notations

Upper case Latin letters

A	Cross-section area / constant	A_p	Cross-section area of prestressing steel
A_s	Cross-section area of longitudinal tensile reinforcement	$A_{s,2}$	Cross-section area of longitudinal compressive reinforcement
C	Constant	D	Constant
D_ε	Strain-based damage parameter	D_σ	Stress-based damage parameter
D_ϕ	creep-based damage parameter	E_c	Elasticity modulus of concrete
$E_{c,N}$	Elasticity modulus of concrete after N applied cycles	E_s	Elasticity modulus of steel reinforcement
F	Applied force / force	F_0	Basis load level
F_{cc}	Normal force in concrete compression zone	F_m	Mean load level
F_{max}	Maximum applied force	F_s	Tensile force in longitudinal reinforcement
G_E	Elastic energy	$G_{E,N}$	Elastic energy after N cycles
G_F	Fracture energy	$G_{F,c}$	Compressive fracture energy
$G_{F,N}$	Fracture energy after N cycles	I	Second moment of area (moment of inertia)
K_f	Fracture toughness	M	Bending moment
M_R	Calculated bending resistance	M_{sup}	Bending moment under upper load
M_u	Ultimate bending moment at failure	N	Number of applied load cycles
N_{cr}	Number of applied load cycles until diagonal cracking	N_{crit}	Number of applied load cycles until critical cracking
N_f	Number of applied load cycles until fatigue failure	S	Stress level
$S(z)$	First static moment of area	S_{inf}	Lower stress level
S_{sup}	Upper stress level	V	Applied shear load
V_A	Shear resistance provided by aggregate interlock	V_{cc}	Shear resistance of concrete compression zone
V_{cr}	Diagonal cracking load	$V_{cr,cal}$	Calculated diagonal cracking load
$V_{cr,cycl,cal}$	Calculated cyclic diagonal cracking load	$V_{cr,exp}$	Applied shear load at diagonal cracking
V_D	Shear resistance provided by dowel action of longitudinal reinforcement	V_{inf}	Lower level of applied shear force
V_R	Shear resistance provided by residual tensile strength in fracture process zone	V_{sup}	Upper level of applied shear force
W	work	W	Moment of resistance
W_f	Fracture work	W_{in}	Internal elastic work
W_{out}	Total applied work		

Lower case Latin letters

a	Shear span	b	Beam width
d	Effective depth of cross-section	d_g	Maximum aggregate size
dx	Length of infinitesimal element	d_0	Reference effective depth
f_c	Concrete compressive strength	f_{ct}	Concrete tensile strength
$f_{ct,cal}$	Calculated concrete tensile strength	$f_{ct,ef}$	Effective concrete tensile strength
$f_{ct,fat}$	Fatigue concrete tensile strength	$f_{ct,fl}$	Flexural concrete tensile strength
$f_{ct,fl}$	Flexural concrete tensile strength	$f_{ct,fat,cal}$	Calculated fatigue concrete tensile strength
$f_{ct,fat,exp}$	Experimental fatigue concrete tensile strength	$f_{ct,ef}$	Effective concrete tensile strength
$f_{ct,mod}$	Modified concrete tensile strength	$f_{ct,ref}$	Reference concrete tensile strength
$f_{ct,res}$	Residual concrete tensile strength	$f_{ct,sp}$	Splitting concrete tensile strength
f_{st}	Ultimate stress of steel reinforcement	f_{sy}	Yield stress of steel reinforcement
h	Beam height / height of tensile specimen	h_c	Depth of concrete compression zone
h_{cb}	Crack band width	h_{ct}	Depth of concrete tensile zone
h_E	Element size	h_{ef}	Effective depth of a member after primary cracking
$h_{ef,1}$	Effective depth of member at first load cycle	$h_{ef,N_{cr}}$	Effective depth of member after N_{cr} load cycles
h_p	Additional effective depth due to prestressing	h_{sb}	Width of the shear band
h_λ	Beam depth with a crack inclination of 45 degrees	i	increment
l	length	l_{ch}	Characteristic length
l_{cr}	Crack length	l_{eff}	Effective length
l_{FPZ}	Length of fracture process zone	m	Mean value / median
s	Standard deviation	s_r	Crack distance
t	Depth	u	Step size
u_{in}	Initial step size	v	Variation coefficient
w_{cr}	Crack width	$w_{cr,1}$	Threshold crack width at tensile unstable cracking
$w_{cr,2}$	Ultimate crack width	x_{cr}	Crack distance from support axis
$x_{cr,apr,RC}$	Approximated crack distance from support axis of RC members	$x_{cr,apr,PC}$	Approximated crack distance from support axis of PC members
$x_{cr,exp}$	Experimental crack distance from support axis of PC members	$x_{cr,FE}$	Numerical crack distance from support axis of PC members
z	Lever arm of internal forces		

Notations

Upper case Greek letters

ΔK	Stress intensity	$\Delta\gamma$	Shear strain increment
------------	------------------	----------------	------------------------

Lower case Greek letters

α	Ratio / inclination of principal stress	α_{cp}	Reduction factor due to lateral compression
$\alpha_{N_{cr}}$	Factor after N_{cr} cycles	α_R	Threshold angle
α_0	Shape factor of aggregate	α_{Rcr}	Crack angle
β	Shear retention factor	γ	Shear strain
γ_{mod}	Model safety factor	δ	deflection
$\delta_{cr,1}$	Displacement at tensile macrocracking	$\delta_{cr,2}$	Ultimate tensile displacement
δ_{ct}	Tensile displacement	δ_{el}	Elastic displacement
δ_{in}	Initial step size	δ_{tot}	Total displacement
ε	Strain	ε_{cr}	Crack strain
$\varepsilon_{cr,1}$	Threshold crack strain at tensile instable cracking	$\varepsilon_{cr,2}$	Ultimate crack strain
ε_{el}	Elastic strain	ε_{nn}	Normal crack strain
$\varepsilon_{nn,lim}$	Threshold normal strain	ε_s	Strain in longitudinal reinforcement
ε_{sh}	Hardening strain	ε_{su}	Ultimate strain of steel reinforcement
$\varepsilon_{sup,1}$	Upper strain at first load step	$\varepsilon_{sup,N}$	Upper strain at Nth load step
ε_{tt}	Tangential crack strain	η	Brittleness factor
η_{cr}	Brittleness factor based on diagonal cracking and ultimate shear load	η_g	Brittleness factor based on energy release during diagonal cracking
η_δ	Brittleness factor based on maximum deflection at state of diagonal cracking	θ	Inclination of principal compressive stress trajectory
κ	Calculated curvature	κ_{sh}	Curvature caused by shrinkage
μ	Damage factor of tensile stiffness	ν	POISSON's ratio
ξ	Relative depth of concrete compression zone	$\xi_{N_{cr}}$	Relative depth of concrete compression zone at diagonal cracking
ξ_1	Relative depth of concrete compression zone at first load step	ρ_l	Longitudinal reinforcement ratio
σ	stress	σ_c	Compressive stress at extreme fibre of member
σ_{cp}	Normal stress caused by prestressing	σ_{cr}	Normal stress in crack
σ_{ct}	Tensile stress	σ_{inf}	Lower applied stress
σ_{pl}	Stress in prestressing steel	σ_{sup}	Upper applied stress
σ_x	Normal stress to cross-section	σ_1	Principal tensile stress
σ_2	Principal compressive stress	$\sigma_{\phi,res}$	Internal damage stress

τ	Shear stress	τ_{cr}	Shear stress in crack
$\tau_x(z)$	Shear stress normal to x-plane and variable in z-direction	τ_u	Ultimate shear resistance
τ_u	Ultimate shear resistance	ϕ_{cycl}	Cyclic creep coefficient
$\phi_{cycl,exp}$	Experimental cyclic creep coefficient		

Other notations

\emptyset	diameter	\emptyset_{sl}	Diameter of longitudinal reinforcement
∂	Partial differential	d	differential Partial differential

Abbreviations

c	cyclic	CL	Centreline
F	Fixed	LEFM	Linear elastic fracture mechanics
LVDT	Linear variable differential transformers	m	monotonic
NA	Neutral axis	PC	Prestressed concrete
R	rotating	RC	Reinforced concrete
RF	Rotating to fixed	TB	Technical bending theory

1 Introduction

1.1 Background

According to assessment and inspection guidelines for existing concrete structures, specific interventions such as detailed measurements or service load limitations are required as soon as diagonal cracks are documented. Frequently, results of bridge inspections in Germany show no documented diagonal cracks on concrete bridges with calculated lack of shear resistance [Mar-2015], [Fis-2014]. Therefore, service shear load level causing a major diagonal crack (diagonal cracking load) signifies a crucial state for such structures.

Diagonal cracks can emerge under in-plane loads, as soon as the diagonal tension caused by shear loading overstep the concrete tensile capacity. Such cracks are often classified according to their shape as web shear cracks or flexure shear cracks. In profiled (often prestressed) members, web shear cracks are formed in sections with limited flexural crack depths or uncracked sections. Quite the contrary, the flexure shear cracks emerge as an extension of existing flexural cracks, which implies that the diagonal crack formation is influenced by interacting flexure and shear (compare Figure 1-1).

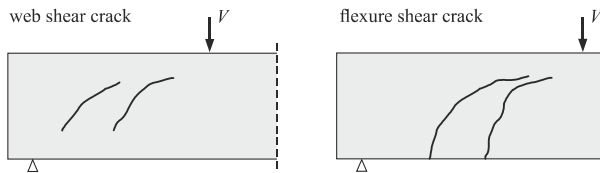


Figure 1-1: web shear crack (left) and flexural shear crack (right)

After diagonal cracking, the provided shear reinforcement is activated and causes a higher ultimate shear load. For members with lower provided shear reinforcement ratios in comparison to the required value, the currently often used strut and tie models ([Mar-1985], [Sch-1987]) are not appropriate. This is based on the fact that in contrast to assumptions of strut and tie models, the diagonal cracks in a member with a low amount of shear reinforcement are not finely distributed in shear span [Kle-2016] and therefore, no parallel strut and ties can be formed [Fro-2000], [Her-2016]. The shear behaviour of such members is defined predominantly by the behaviour of a major diagonal crack, similar to members without shear reinforcement. For this reason, the focus of several current studies is on shear resistance of beams without shear reinforcement (e.g. [Hub-2016], [Her-2017], [Fus-2017], [Tew-2014], [Tra-2015], [Tue-2015], [Sch-2014], [Zin-2000], [Gör-2004], [Fis-2017], [Mar-2014], [Yan-2014]).

In real structures, both webs shear cracks and flexure shear cracks can be formed. However, the applied shear load causing a major flexure shear crack is lower compared to the load causing a major web shear crack due to mentioned effects caused by interacting flexure and shear. For this reason and with respect to current theoretical and experimental investigations in the technical literature, the focus of the present doctoral thesis will be on the determination of diagonal cracking load of members with a potential flexure shear crack.

Most evaluations on members without shear reinforcement focus however on ultimate shear resistance, which includes different load-bearing mechanisms provided by longitudinal reinforcement as well as concrete at ultimate failure state. The derived models using such observations are generally defined based on diagonally cracked members and do not account for the behaviour of member at the state of major diagonal cracking. The main motivation of the present thesis is to evaluate the diagonal tension caused by shear loads using mechanically sound models. Using such mechanical models, the diagonal cracking load can be determined by limiting the acting diagonal tension to the provided tensile resistance of concrete (available concrete tensile strength).

For existing structures such as bridges, the provided tensile resistance by the uncracked concrete under shear loads should be determined under consideration of cyclic service loads such as traffic loads. Whilst existing research on cyclic shear behaviour of members without shear reinforcement focuses primarily on shear resistance and prediction of a fatigue life, the main objective of the present study will be the assessment of damage caused by cyclic preloading at the assessment time. For this aim, knowledge about effects of cyclic tensile preloading on macroscopic parameters of concrete is required. Furthermore, methods and models are required, which facilitate the implementation of possible effects of cyclic preloading in assessment models.

1.2 Aim and objectives

The aim of the present doctoral thesis is to quantify the shear capacity of members with potential flexure shear cracks under monotonic and cyclic loads. For this purpose, reinforced and prestressed concrete members without shear reinforcement and with a rectangular cross-section are investigated theoretically and numerically. Based on the evaluations, recommendations would be provided for a calculative determination of diagonal cracking load under monotonic shear loads. To further comprehend the effects of cyclic loading on residual concrete resistance to tension, uniaxial tensile tests are conducted within an experimental programme on cyclically preloaded specimens. With the obtained knowledge about cyclic damage phenomena on concrete tensile behaviour using conducted tests accompanied by evaluations of a compiled tensile database, the provided numerical and theoretical models would be adapted for evaluation of diagonal cracking

load of cyclically damaged members. To this end, the thesis distinguishes the following three objectives:

- Finding a mechanical consistent model to determine diagonal tension caused by monotonic shear loads at the state of major diagonal cracking for reinforced and prestressed concrete members
- Developing a theoretical approach to account for cyclic damage on shear capacity under cyclic diagonal tension
- Validation and enhancement of numerical models for the evaluation of diagonal cracking (load and cracking section) as well as ultimate shear loads

Based on theoretical, experimental and numerical evaluations, a mechanically sound model for the prediction of diagonal cracking load of concrete members will be provided and recommendations for numerical approximation of diagonal cracking are made.

1.3 Outline

Chapters 2 contains the basic principles of tensile behaviour of concrete under monotonic as well as cyclic loading.

In the third chapter, concrete tensile behaviour under cyclic loads is evaluated theoretically and experimentally. The available cyclic tensile tests in the literature conducted as fatigue tensile tests and residual tensile tests (monotonic tests on cyclically damaged specimens) are composed in a tensile database. Since number of residual tensile tests in the technical literature is limited and for a better understanding of the mechanisms of damage in such tests, further residual tensile tests are conducted within this thesis. Based on the comparison of own experimental results with the tensile database. The results of investigations are discussed further in this chapter and are the basis of a proposed new concrete tensile curve.

Chapter 4 contains basic knowledge on diagonal cracking of members with a potential flexure shear crack under monotonic and cyclic shear loading. The key influencing parameters on the diagonal cracking (load and pattern) at the state of major diagonal cracking are indicated and existing mechanical approaches for prediction of diagonal cracking load are introduced.

Chapter 5 presents the developed shear database including tests under monotonic and cyclic shear loads. The effects of key influencing parameters on the diagonal tension at the state of major diagonal cracking and the shape as well as location of critical diagonal crack are discussed in this chapter. Based on experimental results, the role of the shape and location of the major diagonal crack is indicated, which is not a priori and needs to be approximated with decent methods.

Introduction

The shear database is used in Chapter 6 for the evaluation of the mechanical models presented in Chapter 4. On this basis, modified new models are developed and extended using findings in Chapter 2 and 3 for the evaluation of diagonal cracking load of prestressed members as well as cyclically damaged members. The proposed models are validated using the shear database.

In order to provide recommendations for numerical prediction of diagonal cracking load and location of the critical section, the potentials of nonlinear finite element (FE-) simulations are evaluated using some benchmark tests in Chapter 7. The main influencing parameters and existing approaches for modelling of diagonal cracking are assessed. On the basis of calculations, a refined iterative-incremental approach and a new crack model are proposed for assessment of shear critical members.

In chapter 8, documented shear tests in the database on reinforced concrete members are investigated numerically with the proposed model configurations in the previous chapter. Based on this, the objectivity and meaningfulness of the numerically predicted diagonal cracking load and critical section are analysed. The results are further used to develop concepts for investigation of failure brittleness and prior notice of concrete members under monotonic shear loads. In a further step, the new crack model is evaluated using selected shear tests and adjustment for the model parameters are suggested based on a parametric study. Additionally, the new concrete tensile curve is implemented in the numerical model for evaluation of diagonal cracking load of cyclically damaged members. Numerical evaluations of selected cyclic shear tests are used to evaluate the prediction accuracy of the proposed method.

Chapter 9 summarizes the developed models and methods in the thesis as proposals for determination of the shear capacity of members under monotonic and cyclic shear loads at the state of diagonal cracking using mechanical, numerical and conceptual approaches. The main conclusions and an outlook for potential future research possibilities are given in chapter 10.

2 Monotonic and cyclic concrete tensile behaviour

2.1 Uniaxial concrete tensile behaviour

2.1.1 Tensile cracking and softening behaviour

Cracking of concrete is mainly described using uniaxial concrete tensile behaviour, which can be optimally determined within uniaxial tensile tests. During a monotonic uniaxial tensile test, the applied tension on test specimens can be increased as constant load increments in a so-called load-controlled scheme or be adapted to measured displacement of a control length in a displacement-controlled manner. Independent from the loading scheme, same cracking behaviour in microscale can be assumed, which includes the formation of new microcracks in addition to existing ones caused by hydration of cement and shrinkage. During the ascending tensile loading, almost a linear correlation can be observed between the tensile stress σ_{ct} and the tensile deformation of the specimen δ_{ct} . In a load-controlled scheme, a rapid localisation of microcracks at a section with least concrete tensile strength ends the tensile test at a peak tensile load F_{max} . The uniaxial concrete tensile strength f_{ct} can be calculated using the peak load and the area of fracture cross-section A as F_{max} / A . In a displacement-controlled scheme, a reduction of stiffness due to excessive microcracking can also be documented in the ascending branch of the load-displacement curve (Figure 2-1, point A). A stress level for initiation of softening due to excessive microcracking is provided e.g. in [Rei-2013] as $70 \% \cdot f_{ct}$ or equal to $90 \% \cdot f_{ct}$ according to [fib-2008].

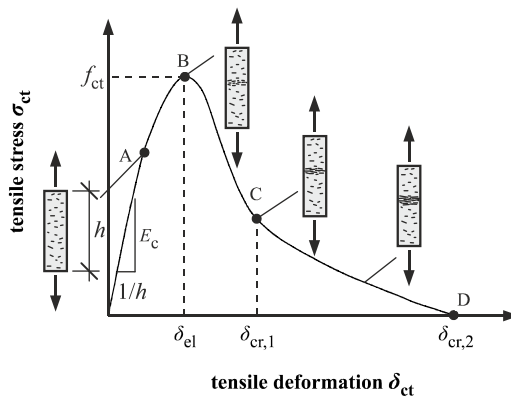


Figure 2-1: Tensile stress-displacement curve and different cracking states under monotonic uniaxial tension (according to [Mal-2006] and [Kes-2002])

A displacement-controlled loading enables additionally an evaluation of concrete tensile softening, since a reduction of applied stress after the peak stress f_{ct} is possible. With the

beginning of macroscopic damage at the peak stress f_{ct} , the applied stress descends until point C (compare Figure 2-1) in a gentle and stable manner due to microcrack localisation in a fracture process zone. The applied stress at this point is determined as $0.15 \cdot f_{ct}$ according to [fib-90] and [Wit-1983] or corresponds to $0.2 \cdot f_{ct}$ according to [fib-2010]. This stage of stable crack propagation is followed by a rather rapid instable crack propagation until failure, with a significant reduction of applied stress. The effective tensile strength can be defined as the applied stress in each phase and correlates with the displacement of the control length δ_{ct} .

Due to the brittle nature of the tensile failure, stable crack propagation in the descending branch can only be achieved if the control length is kept smaller than a characteristic length l_{ch} proposed as a material parameter by HILLERBORG et al. [Hil-1976]. Assuming that the total applied work on the specimen can be divided into an elastic W_{in} and a fracture work W_f , the released elastic work at the state of cracking should be smaller than or equal to the fracture work to ensure a stable crack propagation.

$$W_{out} = W_{in} + W_f \quad \text{Eq. 2-1}$$

For the assumed control length equal to the specimen length l , the total work W_{out} can be extended as follows:

$$F \cdot \delta_{tot} = A \cdot G_E + A \cdot G_F \quad \text{Eq. 2-2}$$

Elastic energy G_E and fracture energy G_F are defined as the work per cross-section area A according to following equations (compare Figure 2-2):

$$G_E = \frac{l \cdot f_{ct}^2}{2 \cdot E_c} \quad \text{Eq. 2-3}$$

$$G_F = \int_{\delta_{cr,1}}^{\delta_{cr,2}} f_{ct,ef}(\delta_{cr}) \cdot d\delta_{cr} \quad \text{Eq. 2-4}$$

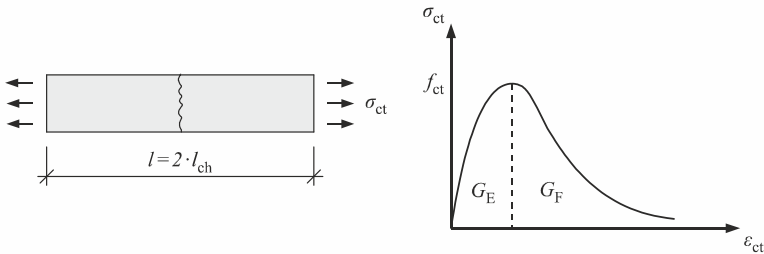


Figure 2-2: Elastic energy, fracture energy and the defined characteristic length l_{ch} according to [Hil-1976]

Due to an equilibrium between elastic and fracture energy, the characteristic length l_{ch} can be subsequently determined as:

$$l_{ch} = \frac{E_c \cdot G_F}{f_{ct}^2} \quad \text{Eq. 2-5}$$

According to HILLERBORG, l_{ch} defines the length of a cohesive crack, which makes a back-calculation of measured displacement to a theoretical crack width w_{cr} possible (compare Figure 2-3, left). Based on this assumption, a theoretical crack width w_{cr} can be correlated to effective tensile strength in the descending branch of concrete tensile curve. These assumptions are the fundamentals of the proposed cohesive crack model by HILLERBORG et al. [Hil-1976] denoted as fictitious crack model which is one the most commonly used existing cohesive crack models for concrete. The total displacement δ_{tot} is divided in this model into an elastic deformation δ_{el} and a crack width w_{cr} .

$$\delta_{tot} = \delta_{el} + w_{cr} \quad \text{Eq. 2-6}$$

To enable a transition between elastic deformation phase and cracked concrete phase, the load-displacement curve can be defined as a tensile stress-strain curve using a reformulation of fictitious crack model in the crack band model of BAŽANT / OH [Baž- b1983]. The smeared crack consideration in this model assumes a cracked region in a fracture process zone as a crack band with the width h_{cb} (compare Figure 2-3, right).

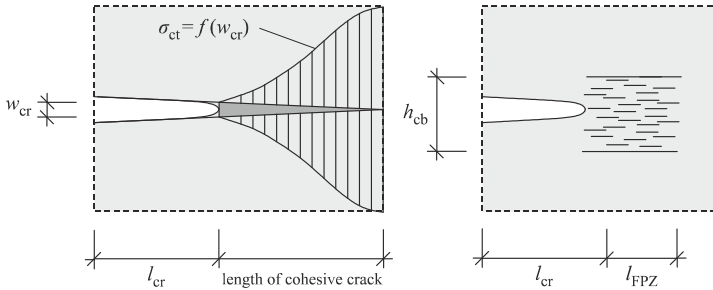


Figure 2-3: Stress distribution in fracture process zone in the fictitious crack model of [Hil-1976] (left) and crack band model of [Baž- b1983] (right) shown according to [Tru-1999]

With the defined crack band width h_{cb} , the crack width w_{cr} can be converted to a crack strain ε_{cr} and Eq. 2-1 can be rewritten as:

$$\varepsilon = \varepsilon_{el} + \varepsilon_{cr} = \frac{f_{ct}}{E_c} + \frac{w_{cr}}{h_{cb}} \quad \text{Eq. 2-7}$$

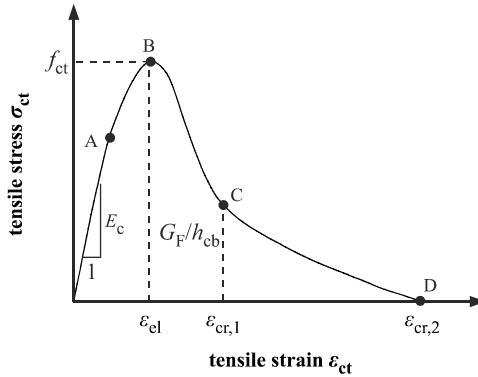


Figure 2-4: Tensile curve of concrete based on crack band width model

The crack band width approach is the basis of numerical simulation of concrete cracking using smeared crack models.

2.1.2 Parameters of the concrete tensile curve

To define the tensile curve of concrete using fictitious crack model, tensile strength f_{ct} , elasticity modulus E_c , fracture energy G_F , ultimate crack width $w_{cr,2}$ and the shape of the softening curve should be defined.

The tensile strength of concrete can be determined using direct tensile test (as discussed in section 2.1.1.) or indirectly based on splitting tests on cylindrical specimens or bending tests or prismatic beams (compare Figure 2-5). Whilst indirect tests are conducted based on standards and guidelines, there is almost no standardized approach for a direct tensile test. As a result, the direct tensile tests are conducted on specimens with different

- cross-sections (circular, cylindrical, with or without a notch, variable over specimen length for dog-bone specimens)
- control lengths and
- boundary conditions (glued on loading plates, bolted or pinned to loading plates, with rotating or non-rotating loading plates etc.).

In uniaxial tensile tests, installation of tensile specimens in the testing frame, stiffness of the testing frame and the used control system is known to influence the test stability and the achieved softening curves [van-2007]. Since this testing procedure is accompanied with more effort, many researchers revert to indirect tensile tests. However, the ultimate loads of indirect tests should be back-calculated with regard to stress distribution over fracture cross-section into a uniaxial tensile strength. The stress distribution over the fracture cross-section is rather disturbed in notched specimens [Ar-1982], for which reason they are

categorized as an indirect tensile test. In both direct and indirect test methods, the experimental concrete tensile strength is afflicted with a large scatter. Therefore, for calculative approaches, empirical correlations are proposed for the calculation of concrete tensile strength based on the value of concrete compressive strength f_c .

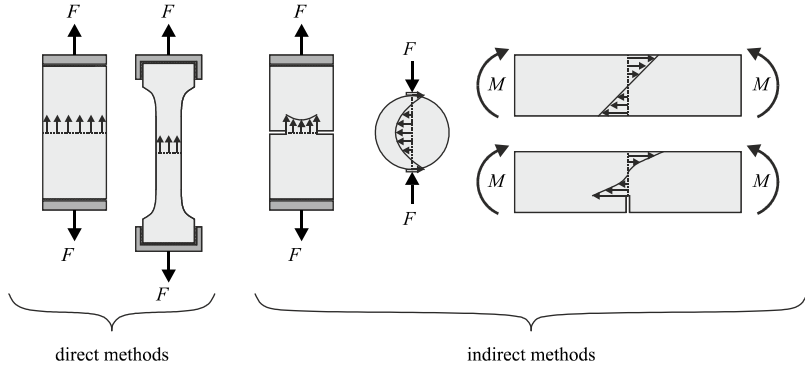


Figure 2-5: Test methods for determination of uniaxial tensile strength f_{ct}

For normal strength concrete, a common correlation between f_{ct} and f_c is the one suggested by HEILMANN [Hei-1969] with the following general form:

$$f_{ct,cal} = a \cdot f_c^{2/3} \quad \text{Eq. 2-8}$$

For the mean value of concrete tensile strength is the factor a equal to 0.3 according to [DIN-1992-1-1]. The equation in [DIN-1992-1-1] is based on the characteristic concrete compressive strength f_{ck} , which is calculated as $(f_c - 8)$ in general and is set as $(f_c - 4)$ for value of the concrete compressive strength of laboratory tests. The tensile strength of high strength concrete ($> C50/60$) is typically calculated using the suggested correlation of [Rem-1994].

$$f_{ct,cal} = b \cdot \ln \left(1 + \frac{f_c}{10} \right) \quad \text{Eq. 2-9}$$

The value of b is set to 2.12 in DIN 1992-1-1 [DIN-1992-1-1]. This equation is modified by REINHARDT to the following power function with the correlation:

$$f_{ct} = 1.115 \cdot f_{ck}^{1/3} \quad \text{for } > C50/60 \quad \text{Eq. 2-10}$$

For a calculative estimation of the critical crack width $w_{cr,1}$ and also the ultimate crack width $w_{cr,2}$ of plain concrete under tension, tensile fracture energy G_F of concrete and the shape of tensile softening curve should be provided. The value of G_F depends on various properties of concrete mix such as concrete strength f_c , water / cement ratio (w/c), shape factor of aggregates α_0 ($\alpha_0 = 1$ for round aggregates and $\alpha_0 = 1.44$ for angular aggregates), as well as maximum aggregate size d_g . These properties are considered in the proposed empirical correlation according to [Baž-2002].

$$G_F = \frac{2.5}{1000} \cdot \left(\alpha_0 \cdot \left(\frac{f_c}{0.051} \right)^{0.46} \cdot \left(1 + \frac{d_g}{11.27} \right)^{0.22} \cdot \left(\frac{W}{c} \right)^{-0.3} \right) \quad \text{Eq. 2-11}$$

From the mentioned factors are maximum aggregate size and concrete compressive strength considered in CEP-*fib* 90 [fib-90] for a simpler estimation of fracture energy G_F according to the following equation:

$$G_F = G_{F,0} \cdot \left(\frac{f_c}{10} \right)^{0.7} \quad \text{Eq. 2-12}$$

Herein is the basis value of fracture energy $G_{F,0}$ [N/mm] defined according to:

$$G_{F,0} = \frac{1}{1000} \cdot (0.0469 \cdot d_g^2 - 0.5 \cdot d_g + 26) \quad \text{Eq. 2-13}$$

A higher value of G_F [N/mm] is suggested in Model Code 2010 [fib-2010] solely based on concrete compressive strength f_c :

$$G_F = 0.073 \cdot f_c^{0.18} \quad \text{Eq. 2-14}$$

The shape of softening curve is often determined by data-fitting using experimental tensile softening curves. Exponential approximations are provided by HORDIJK [HOR-1992], DUDA [DUD-1991], GOPALARATHNAM [Gop-1987] etc.. A commonly used exponential softening curve is the proposed correlation of HORDIJK with the following equation:

$$\frac{f_{ct,ef}(w_{cr})}{f_{ct}} = \left(1 + \left(3 \cdot \frac{w_{cr}}{w_{cr,2}} \right)^3 \right) \cdot e^{\left(-6.93 \cdot \frac{w_{cr}}{w_{cr,2}} \right)} - 0.0274 \cdot \frac{w_{cr}}{w_{cr,2}} \quad \text{Eq. 2-15}$$

The ultimate crack width $w_{cr,2}$ of this curve is equal to:

$$w_{cr,2} = 5.136 \cdot \frac{G_F}{f_{ct}} \quad \text{Eq. 2-16}$$

Further multilinear simplifications of the tensile softening curve of concrete are also available such as the ones proposed in Model Code 2010 [fib-2010] (compare Figure 2-6).

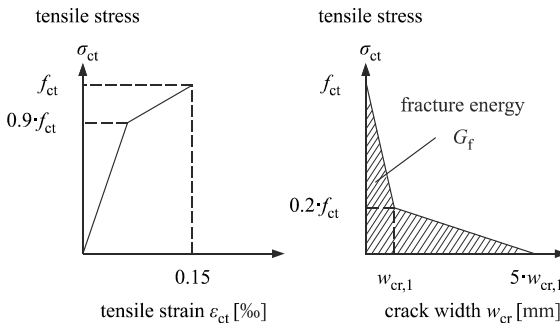


Figure 2-6: Tensile curve of concrete according to Model Code 2010 [fib-2010]

According to Model Code 2010, the tensile curve is defined using a bilinear tensile stress-strain curve in the ascending branch and a bilinear tensile strength-crack width curve in softening branch. Based on the assumed values in Figure 2-6, the crack width at the initiation of an instable crack growth $w_{cr,1}$ can be calculated as

$$w_{cr,1} = \frac{G_F}{f_{ct}} \quad \text{Eq. 2-17}$$

2.1.3 Factors affecting concrete tensile strength

In a uniaxial stress state, macroscopic tensile cracking can be defined using the concrete tensile strength f_{ct} . With the presence of lateral compression, experimental evidence shows that tensile cracking occurs under lower tensile stress than f_{ct} (KUPFER / GERSTLE [Kup-a1973], HUSSEIN [Hus-2006] und HAMPEL / CURBACH [Ham-2006]). A commonly used failure envelope under biaxial stress state is the one proposed by KUPFER / GERSTLE [Kup-a1973], [Kup-b1973].

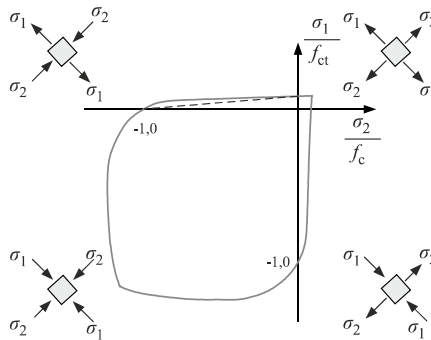


Figure 2-7: Failure envelope proposed in [Kup-a1973] for different stress states and the linear approximation of tensile strength with lateral compression

For concrete members with a normal compression (e.g. due to prestressing) or for tensile cracking in a biaxial stress state (as under shear forces), the tensile cracking should be defined using a modified concrete tensile strength $f_{ct,mod}$. In a linear approximation of the depicted failure envelope in Figure 2-7, the modified tensile strength can be determined by means of tensile and compressive strength of concrete and the lateral principal compressive stress σ_2 .

$$f_{ct,mod} = \frac{1 - \frac{|\sigma_2|}{f_c}}{1 - \frac{f_c}{f_{ct}}} \cdot f_{ct} \quad \text{Eq. 2-18}$$

A further influencing parameter on concrete tensile strength is the effect of differential shrinkage, which reduces the concrete tensile strength at extreme fibre of the specimen

as figured out by HEILMANN [Hei-1969]. This effect is not negligible in uniaxial tensile tests (compare Figure 2-8). Due to the superposition of external tensile stresses and internal eigenstresses caused by (drying) shrinkage, the local reduction of concrete tensile strength causes tensile failure of the specimens. According to REINHARDT [Rei-2013], the splitting tensile tests are not affected by shrinkage as the point of crack initiation (maximal tensile strength) is far from the extreme fibre of the specimen, where the local eigenstresses according to shrinkage act.

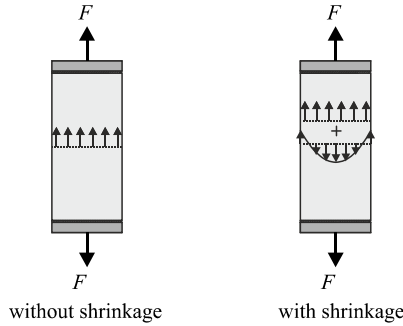


Figure 2-8: Influence of eigenstresses caused by shrinkage in uniaxial tensile specimens

For reinforced concrete members, the restraint caused by longitudinal reinforcement during shrinkage affects the cracking load of the members. The restraint amount depends on the longitudinal reinforcement ratio. To consider this restraint in structural scale, GILBERT / RANZI [Gil-2010], [Gil-2011] suggest considering an initial curvature κ_{sh} as a function of longitudinal reinforcement ratio ρ_l (compare Eq. 2-19), which considers the effects of shrinkage before cracking.

$$\kappa_{sh} = (100 \cdot \rho_l - 2500 \cdot \rho_l^2) \cdot \left(\frac{d}{0.5 \cdot h} - 1 \right) \cdot \left(1 - \frac{A_{s,2}}{A_s} \right)^{1.3} \cdot \left(\frac{\varepsilon_{sh}}{h} \right) \quad \text{Eq. 2-19}$$

Here is d the effective depth of the section, h is the overall section depth, A_s and $A_{s,2}$ are cross-section areas of the longitudinal reinforcement in tension and compression zone, respectively and ε_{sh} denotes the value of shrinkage strain. In ultimate limit state, the concrete tensile strength does not influence the flexural resistance and therefore, effects of shrinkage are negligible in this limit state. However, the diagonal cracking under shear loading is known to be influenced by drying shrinkage. HYODO [Hyo-2013] and GÖRTZ [Gör-2004] suggest considering the influence of shrinkage on diagonal cracking of reinforced concrete members. GÖRTZ proposes a constant reduction factor equal to 79 % based on a database evaluation. HYODO suggests an equivalent longitudinal tensile reinforcement ratio $\rho_{l,eq}$ according to Eq. 2-20 to account for the influence of experimentally measured strain in longitudinal tensile reinforcement at the age of loading $\varepsilon_{s,0,exp}$ (compare Figure 2-9).

$$\rho_{l,eq} = \frac{\varepsilon_s}{\varepsilon_s - \varepsilon_{s,0,exp}} \cdot \rho_l \quad \text{Eq. 2-20}$$

Based on the equivalent reduced longitudinal reinforcement ratio, the change in applied moment at flexural cracking $M_{fl,sh}$ as well as applied moment at diagonal cracking under consideration of shrinkage $M_{DT,sh}$ is predictable (compare Figure 2-9) according to HYODO.

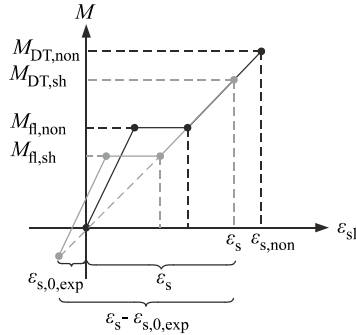


Figure 2-9: Simplified correlation between flexural moment and shrinkage-induced strain in steel reinforcement according to [Myo-2013]

As apparent from Eq. 2-19 and Eq. 2-20, the value of shrinkage strain should be provided for an adequate consideration of shrinkage effects on diagonal cracking, as it depends on curing method, age, cement type etc..

Another influencing factor is the so-called size effect, which was investigated experimentally and theoretically in [Baž-1984], [Leo-1962], [Hub- a2014], [Cao-2001]. It is observed that the tensile strength does not grow proportionally with the growing cross-section, which is justified by increasing the probability of the internal defects and consequently the sum of the local stress concentrations according to WEIBULL.

2.2 Uniaxial cyclic tensile behaviour of concrete

2.2.1 Concrete behaviour under cyclic tension

Similar to tensile tests under monotonic tension, uniaxial cyclic tensile tests can be conducted as load-controlled or displacement-controlled tests. The aim of load-controlled tests is often the prediction of a fatigue life within fatigue tensile tests. It is known based on fatigue tests, that the damage process under cyclic loading increases with a higher load amplitude as well as an increasing number of cycles, and depends on loading frequency and lower and upper stress levels (σ_{inf} and σ_{sup} respectively) [Rei-1981], [Cor-1981]. After N_f number of cycles in a fatigue test, a fatigue failure occurs and the upper stress level σ_{sup}

denotes the fatigue tensile strength $f_{ct, fat}$. If the specimen deformation is measured during load-controlled cyclic tests, a general increase in the measured deformation can be observed, which is mainly caused by microcracking in the cement matrix and damage between different concrete phases. The development of deformation under an increasing number of load cycles comply with a similar regime as depicted in Figure 2-10.

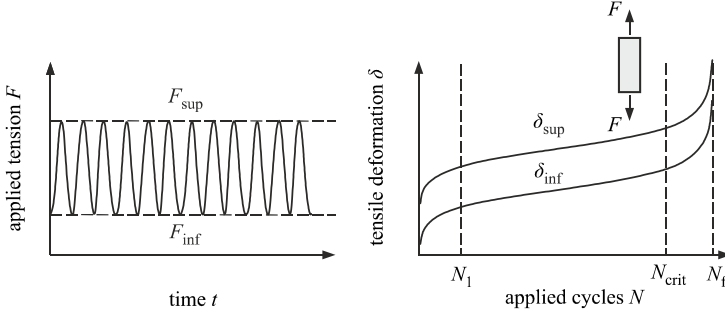


Figure 2-10: Schematic view loading in a load-controlled tensile fatigue test (left) and corresponding cyclic creep curve (right)

This deformation evolution can be divided into three phases. The first branch with a rapid microcracking and tensile deformation of the specimen under first loading, accompanied by a secondary branch with a nearly linear correlation between the number of load cycles and deformation growth. The third phase begins from a critical number of load cycles N_{crit} , from which a rather accelerated crack growth and a deformation gain are observed until the number of cycles to fatigue are reached. This characteristic curve is often termed as cyclic creep curve. For definition of a damage factor within fatigue tests, the ascending slope of deformation in the secondary branch is proposed in [Wei-1987] and [Cor-1984] to quantify the cyclic damage on tensile specimens. Based on the measured values of total tensile strain and elastic strain, a cyclic creep factor was defined in [Cor-1984] as follows:

$$\varphi_{cycl}(N) = \frac{\varepsilon_{tot}(N) - \varepsilon_{el}}{\varepsilon_{el}} = \frac{\varepsilon_{tot}(N) - \varepsilon_{el}}{\varepsilon_{el}} \quad \text{Eq. 2-21}$$

The damage factor is defined by CORNELISSEN [Cor-1984] using the cyclic creep factor for a given number of load cycles and with regard to the upper stress level S_{sup} (σ_{sup} / f_{ct}) accordingly:

$$D_{\varphi}(N) = S_{sup} \cdot \sqrt{1 + \varphi_{cycl}(N)} \quad \text{Eq. 2-22}$$

The applied cyclic tension can be also displacement-controlled during the tests. For this test procedure, after one or several displacement cycles with a constant size, the applied displacement is increased with a constant step $\Delta\delta$. Examples of such tensile tests are documented in [Rei-1986], [Kes-2002] and [Che-2016].

2.2.2 Parameters of the cyclic concrete tensile curve

As for monotonic tensile softening, tensile strength f_{ct} , elasticity modulus E_c , fracture energy G_F , ultimate crack width $w_{cr,2}$ and the shape of softening curve should be available for adaption of fictitious crack model under cyclic loads.

The available adaptations of parameters are often of empirical nature. For instance, the tensile strength is reduced in accordance with the tensile fatigue strength $f_{ct,fat}$ of concrete. For this aim, a commonly used correlation is the proposed equation by CORNELISSEN [Cor-1984], which is derived using a regression analysis of cyclic tests and considers lower stress level and number of cycles.

$$f_{ct,fat} = \frac{f_{ct,ref}}{14.52} \cdot \left(14.81 + 2.79 \cdot \frac{\sigma_{inf}}{f_{ct,ref}} - \log N_f \right) \quad \text{Eq. 2-23}$$

Considering the lower stress level in Eq. 2-23 a more differentiated specification of tensile fatigue strength of concrete is available in comparison to the suggested correlation of [fib-2010] (compare Eq. 2-24):

$$f_{ct,fat} = f_{ct,ref} \cdot \left(\frac{\log N_f}{12} - 1 \right) \quad \text{Eq. 2-24}$$

For the value of fracture energy, the accumulated work during the cyclic loading process and its division into reversible and irreversible parts are mostly based on phenomenological models and experimental observations. Therefore, the existing assumptions are as different as the existing experimental observations. CORNELISSEN, HORDIJK and REINHARDT observed during first displacement-controlled monotonic and cyclic tests, that the envelope curve of tensile stress-displacement hysteresis of cyclic loads resembles $\sigma_{ct} - \delta_{ct}$ curve of monotonic tests. They concluded that for each concrete, a unique curve describes the crack formation and softening [Cor-1986], which is independent from the loading sequence. Later on, HORDIJK [Hor-1992] investigated the displacement behaviour within monotonic and cyclic tensile loads to find similarities between achieved values of displacement. He concluded that the ultimate tensile strains reached in a load-controlled fatigue test are higher than monotonic ultimate tensile strain values and could observe almost no correlation between the cyclic and monotonic tensile displacements (compare Figure 2-11). Quite the contrary, BALÁZS proposed that the displacement at the initiation of a critical crack propagation (N_{crit}) during a cyclic test corresponds to the elastic displacement of monotonic tensile tests δ_{el} [Bal-1991]. THUN et al. [Thu-2011] proved the plausibility of this assumption based on a comparison between the displacement attained during monotonic uniaxial tensile tests and cyclic fatigue tests on cast and drilled preloaded concrete samples.

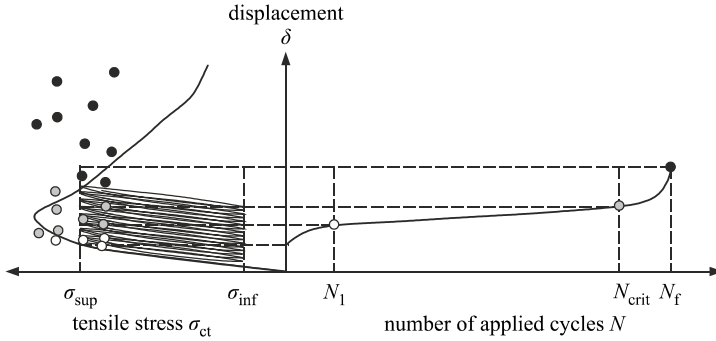


Figure 2-11: Comparison between measured displacements in fatigue tests and the monotonic tensile curve in accordance with [Hor-1992]

Like HORDIJK, KESSLER-KRAMMER [Kes-2002] observed during his displacement-controlled cyclic tensile tests that the monotonic and cyclic displacements are not directly comparable. He could show further, that with an increasing number of cycles to failure, the energy consumption for a fatigue failure decreases. This indicates the area beneath the hysteresis envelope, i.e. the cyclic fracture energy. Based on displacement controlled cyclic tests with different numbers of load cycles to failure, KESSLER-KRAMER proposed a reduction of fracture energy for cyclically loaded specimens according to the following equation:

$$G_F(N) = G_F - 0.0214 \cdot \log N \tag{Eq. 2-25}$$

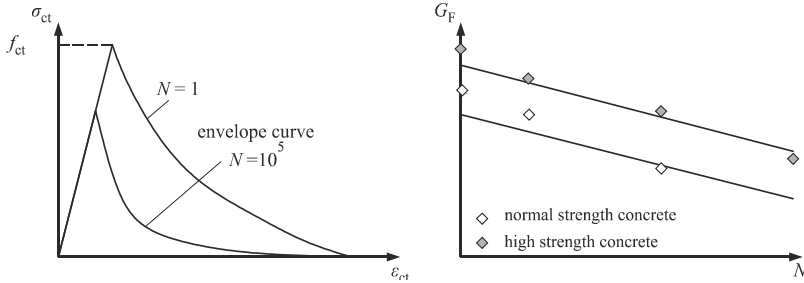


Figure 2-12: Change of envelope curve of cyclic tensile tests with the number of applied cycles (left) and reduction of fracture energy (right) illustrated schematically based on [Kes-2002]

Even during load-controlled cyclic tensile tests, CHEN [Che-2017] defined an accumulated damage value based on the area within each loading and unloading curve. This accumulated damage energy indicates the amount of energy, which is dissipated in the damage process and increases with the number of applied cycles.

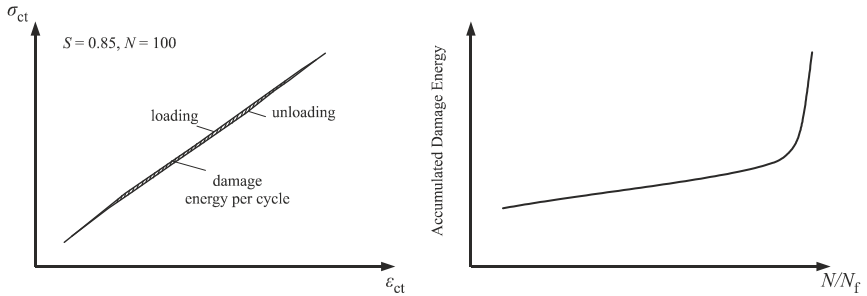


Figure 2-13: Calculation of dissipated energy in each load step (left) and the increase of accumulated energy with the number of applied load cycles (right) by [Che-2017]

Based on the discussed experimental observations, theoretical models are developed for the consideration of cyclic damage in the cohesive crack models. The most of existing models, however, focus on an exact description of loading and unloading in hysteresis loops such as the model proposed by HORDIJK [HOR-1992] or the suggested one by YAN-KELEVSKY / REINHARDT [YAN-1989].

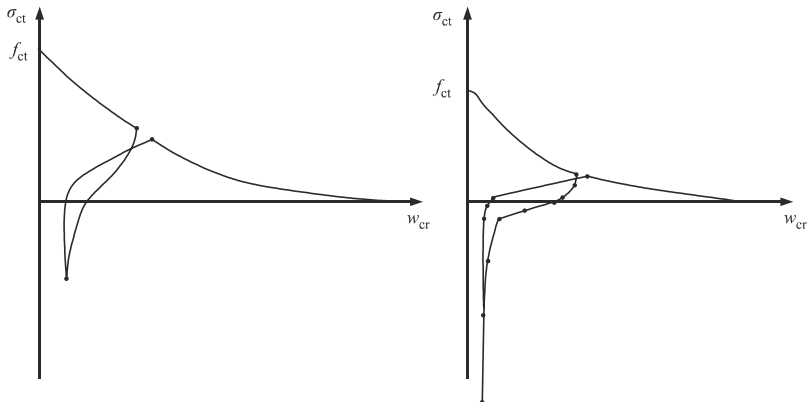


Figure 2-14: Models for tensile softening according to [HOR-1992] (left) and [YAN-1989] (right)

For an engineering application, rather straightforward methods are needed, which consider the effects of damage on concrete behaviour after a certain number of cyclic loads. Such engineering models considering actual accumulated damage on parameters of a cohesive crack model are proposed for example by PFANNER [Pfa-2003] and SKAR et al. [Ska-2017].

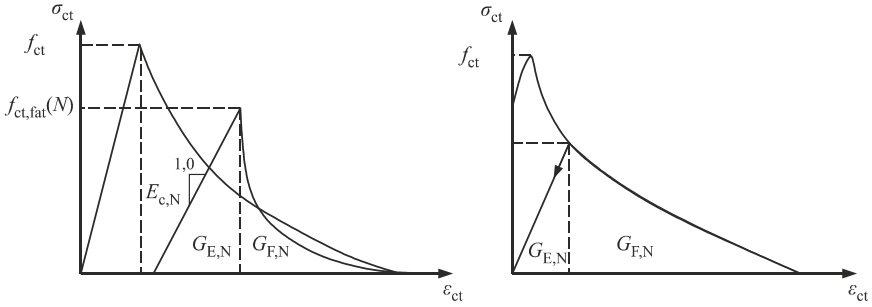


Figure 2-15: Tensile curve of cyclically damaged concrete according to PFANNER [Pfa-2003] (left) and according to SKAR et al. [Ska-2017] (right)

The basis of both approaches is an energy-based definition of damage, where the applied energy is divided into a dissipated part in damage, a reversible energy $G_{E,N}$ and a modified fracture energy $G_{F,N}$. In the proposed model of PFANNER [Pfa-2003], the macroscopic damage caused by cyclic loading is considered as a change of material parameters such as stiffness and tensile strength as well as a predefined deformation caused by cyclic creep. The tensile curve of SKAR et al. [Ska-2017] considers predefined initial stress caused by cyclic damage and a constant stiffness to the unloading curve after the first loading. The different energy components can be defined only using cyclic tensile tests, e.g. the reduced fracture energy after cyclic damage can be determined using the correlation suggested by KESSLER-KRAMER (compare Eq. 2-25). Further experiments are required to make a statement about the stiffness of cyclically damaged specimens.

2.3 Concluding remarks

The basics of tensile cracking and softening behaviour under monotonic and cyclic tension were briefly introduced in this chapter. The required parameters for modelling of tensile cracking using fictitious crack model were summarized and provided models for a damage consideration are discussed. An overview of the literature shows that the effects of cyclic damage on macroscopic material parameters of concrete include cyclic creep, reduction of tensile strength to a fatigue tensile strength $f_{ct,fat}$ and a reduction of fracture energy G_F . However, the existing knowledge on cyclic damage focuses mainly on detailed evolution of cyclic hysteresis, including loading and unloading paths. For high-cycle fatigue in structural scale, modelling of the whole loading sequence is rather a time consuming and inefficient procedure. To provide information about the current state of the existing cyclically preloaded structures, convenient engineering models are needed which should be able to determine the tensile behaviour based on the existing damage at the assessment time. Two examples of such models were introduced which accentuates the controversial viewpoints for the definition of concrete tensile curve in damaged state.

Despite differences in models, some similar observations exist, such as a continuous increasing deformation under cyclic loading known as cyclic creep. To obtain a better insight in the phenomena engaged in cyclic damage and its effects on parameters of the concrete tensile curve, an evaluation of existing cyclic tests and further experimental investigations can be helpful.

3 Experimental investigation of tensile cyclic damage

3.1 General remarks

For a safe approximation of effects of cyclic loading on concrete tensile capacity, profound knowledge about the cyclic damage processes in concrete and their influence on macroscopic tensile parameters of concrete are required. Cyclic damage development in concrete can be described ideally using direct uniaxial tensile tests. In general, some well-documented laboratory tests are available, which are conducted for the evaluation of fatigue tensile strength $f_{ct,fat}$ (FT tests) or to determine residual tensile strength $f_{ct,res}$ of cyclically preloaded specimens (RT tests). The first group of tests are more common and are conducted until a fatigue failure is reached. The value of upper stress level σ_{sup} defines in such tests the tensile resistance of concrete at the state of fatigue failure. In contrast, in tensile tests on cyclically preloaded specimens, the specimens are often partially or completely unloaded after a preloading phase and subsequently loaded monotonically until failure. The peak stress σ_{max} of the second monotonic load phase describes in such tests the tensile resistance of cyclically damaged concrete subsequently termed as residual tensile strength $f_{ct,res}$. The idea of this chapter is to compare these two types of concrete tensile strengths and point out the similarities and differences between the obtained test results.

In a first step, available tensile fatigue tests (FT) and residual tensile tests (RT) are collected in a tensile database. The ultimate tensile strength values of both test types are compared and analysed. Residual tensile tests are not as common as tensile fatigue tests. For this reason and also to better comprehend the results of database evaluation, residual tensile tests are conducted at iBMB, Division of concrete construction of TU Braunschweig within this thesis. The experimental programme involves load-controlled tensile tests on undamaged as well as on cyclically preloaded tensile specimens. The findings of the database evaluations are compared with the test results. The test data and provided theoretical background in chapter 2 are used to quantify the effects caused by cyclic damage.

3.2 Database of cyclic tensile tests

3.2.1 Overview of database

Cyclic tensile tests are compiled in a tensile database, which includes tensile fatigue tests under constant loading amplitudes (FT) and monotonic tests conducted on cyclically preloaded specimens (RT). In fatigue tensile tests, the specimens fail after N_f load cycles in the cyclic loading phase and the fatigue tensile strength $f_{ct,fat}$ corresponds to the value of upper stress σ_{sup} . The latter test type is conducted often on run-out specimens of fatigue

tests (specimens, which did not fail within fatigue tests) or after a lower number of applied load cycles $N < N_f$. The residual tensile strength $f_{ct,res}$ signifies the peak stress of the monotonic loading phase.

The developed database includes 170 FT tests and 74 RT tests, which are summarized in Table 3-1. The available datasets are documented in detail in Appendix A.

The upper and lower stress levels (S_{sup} and S_{inf}) are calculated as the ratio of upper and lower stresses (σ_{sup} and σ_{inf}) and the reference tensile strength according to:

$$S = \frac{\sigma}{f_{ct,ref}} \quad \text{Eq. 3-1}$$

Table 3-1: Overview of the tests in the tensile database

Author	Test type	Ref.	geometry	No.	S_{sup}	S_{inf}	N	frequency	$f_{ct,ref}$
			[-/mm]	[-]	[-]	[-]	[-]	[Hz]	[N/mm ²]
CORNELISSEN	FT	[Cor-1984], [Cor-1981]	cylinder (dogbone) 120 x 175	218	0.6-0.9	0.1	10^4 - 10^5	6	2.5-3.0
KESSLER-KRAMER	FT	[Kes-2002]	prism (dogbone) 60 x 100 x 220	10	0.75-0.85	-	10^3 - $2.7 \cdot 10^4$	10	3.5-5.4
CHEN	FT	[Che-2017]	cylinder 73 x 205	51	0.8-0.95	-	10^1 - $3 \cdot 10^5$	4	3.6
CORNELISSEN	RT	[Cor-1984]	cylinder (dogbone) 120 x 175	28	0.4-0.7	0-0.4	10^5 - $2 \cdot 10^6$	6	~2.9
BLASCHKE	RT	[Blu-1993]	prism 200 x 200 x 1000	27	0.6-0.75	0.1	10^4 - 10^5	0.01-1.0	1.3-2.0
MENG / SONG	RT	[Men-2007]	prism (dogbone) 100 x 100 x 110	19	0.75-0.85	-	10^3 - $1.5 \cdot 10^4$	-	~2.7

3.2.2 Comparison of tensile strength values

The values of peak stress reached in each test type ($f_{ct,fat}$ in FT tests and $f_{ct,res}$ in RT tests) have been compared with the reference value of concrete tensile strength $f_{ct,ref}$ as provided in respective reference. For a comparison between cyclic damage within a fatigue tensile test (FT) and a monotonic test on cyclically damaged members (RT), relative tensile strength is determined using the ratio between resulted tensile strength and reference tensile strength for RT tests determined as $f_{ct,res} / f_{ct,ref}$ and for FT tests as the ratio $f_{ct,fat} / f_{ct,ref}$. Within the database evaluations, the focus is on influence of applied number of cycles (N_f or N). Based on the existing tests, no correlation could be observed between $f_{ct,fat}$ or $f_{ct,res}$ and the value of loading frequency f .

The correlation between relative tensile strength values and the number of applied load cycles is evaluated using Figure 3-1.

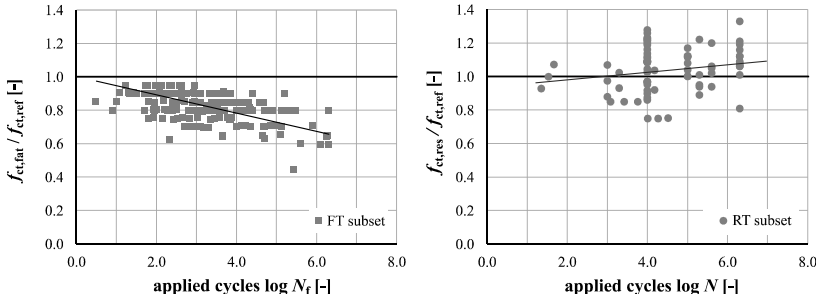


Figure 3-1: Relative fatigue tensile strength (left) and relative residual tensile strength (right)

As depicted in Figure 3-1 (left), higher upper stress level leads to a shorter fatigue life. Therefore, the fatigue tensile strength $f_{ct,fat}$ decreases with the number of applied cycles as suspected. In contrary, the resulted residual tensile strength values $f_{ct,res}$ (Figure 3-1, right) remain unaffected by the applied cyclic preloading and show a slight gain even after 10^6 applied load cycles. CORNELISSEN [Cor-1984] mentions stress redistribution at low stress levels as a possible reason for the strength gain after cyclic preloading. According to BLASCHKE [BLA-1994], the randomness of concrete tensile strength is responsible for this observation. This statement was verified by the tests conducted by BLASCHKE, in which the first crack was closed using an epoxy-based adhesive and the specimens were loaded afterwards. It is reported that the subsequent cracks appear under a higher load level in all cases. Based on same considerations, random tensile strength distribution implemented in the crack model according to EMPELMANN [Emp-1995] considers the first crack to appear at a section with a concrete tensile strength equal to characteristic concrete tensile strength f_{ctk} (5%-quantile), followed by further cracks at sections with higher random concrete tensile strength values. According to MENG / SONG [Men-2007], despite the gain in concrete tensile strength in RT test, the probability of failure grows with the increasing number of applied load cycles. For evaluation of randomness of concrete tensile strength and selection of a representative probability distribution function, more RT tests are required. The same applies for the evaluation of failure probability.

In comparison to FT test, RT tests are conducted less often and generally without required information on strain development during the tests. To figure out the similarities and differences between response of specimens in RT and FT tests, further experiments with continuous measurements are required. For the evaluation of strength of cyclically damaged structures, it should be clarified whether a cyclic damage occurs within RT tests and how this damage is to be taken into account in structural scale.

3.2.3 Evaluation of fatigue tensile strength

To evaluate the existing correlations for a calculative approximation of concrete tensile fatigue strength $f_{ct,fat}$, the prediction accuracy of two introduced approaches for the evaluation of tensile resistance obtained from fatigue tests i.e. fatigue tensile strength has been evaluated using the FT tests in tensile database. The evaluated equations include the correlation proposed by CORNELISSEN [Cor-1984] (Eq. 2-23) and the correlation according to Model Code 2010 [fib-2010] (Eq. 2-24). The model safety factor for the predicted value of fatigue tensile strength is determined according to the following correlation:

$$\gamma_{mod} = \frac{f_{ct,fat,exp}}{f_{ct,fat,cal}} \quad \text{Eq. 3-2}$$

Based on an assumed normal distribution for tensile strength values, the prediction accuracy of both approaches is evaluated based on mean value (m), standard deviation (s) and variation coefficient (v) of the model safety factors.

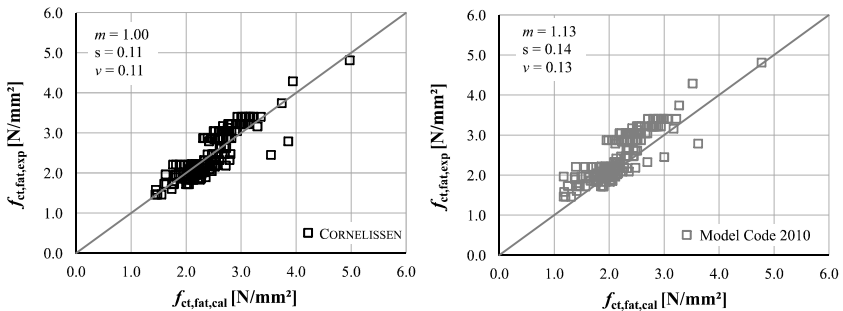


Figure 3-2: Prediction of fatigue tensile strength according to [Cor-1984] (left) and according to [fib-2010] (right)

According to the evaluations, it is evident that both equations are based on the same dataset and the equation of Model code 2010 is probably a simplified version of the equation according to CORNELISSEN. It can be concluded that for evaluation of mean values of fatigue tensile strength, the suggested correlation of CORNELISSEN is more suitable.

3.3 Experimental Investigations

3.3.1 Experimental programme and tests specimens

Monotonic load-controlled uniaxial tensile tests were conducted on 7 reference specimens and 14 cyclically preloaded specimens within the experimental programme. The tensile strength of reference specimens was compared with those of cyclically preloaded

specimens to quantify the damage caused by cyclic preloading on concrete tensile behaviour. The effects of the number of applied load cycles are evaluated for different applied upper and lower load levels. During the cyclic loading, further damage indicators such as local strain and deformation of the specimens are continuously measured and evaluated.

3.3.2 Test specimens and concrete

The concrete was mixed in two similar batches with a target strength class of C30/37 and a maximum aggregate size of $d_g = 16$ mm. The specimens were cast in horizontal coated prismatic formworks on a shaking table (compare Figure 3-3). After one day of curing in wrapped and sealed formworks, the specimens were cured for 28 days in water and stored afterwards under constant conditions (temperature = 20.5°C and relative humidity = 68 %) in a climate chamber until the testing day. To apply tension on specimens, two steel plates with central drilled threaded bores were glued on two specimen sides. The surfaces of both specimen sides were mechanically treated and roughened in order to reach a better adhesion between the specimen and the glued steel plates. The dimensions and weight of each specimen were measured before testing and considered in calculated stresses.

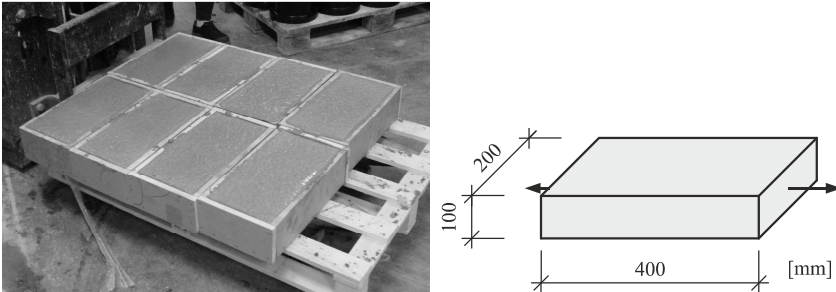


Figure 3-3: Placed and compacted concrete in horizontal formwork (left) and dimensions of specimens (right)

3.3.3 Test setup and testing procedure

Tensile tests were conducted in the precision testing room of iBMB, TU Braunschweig with a constant temperature of 23.5 °C and relative humidity of 50 %. The arrangement of tests and the applied sensors were as illustrated in Figure 3-5. The specimens were installed in the testing machine using a hinged support construction, which enables compensation of possible eccentricities. The tests were carried out in a rigid two-column servo-hydraulic testing machine with a mounted hinged fixture between two actuators.

The monotonic tensile tests were conducted as reference tests on undamaged specimens with similar geometry and test setup at different ages. For damage evaluation, the specimens were cyclically preloaded and loaded afterwards monotonically until failure. Within the cyclic preloading phase, the specimens were loaded first to a basis load level of $F_0 = 5$ kN and afterwards until the target mean load level (F_m). Originating from the mean load level, a sinusoidal cyclic load with a constant amplitude and a loading frequency of 0.5 Hz was applied on each specimen until a specific number of load cycles was reached. The loading frequency was selected using previous preliminary tests to minimize the objectionable effects of back-oscillation of specimens between unloading and loading phases. After the cyclic preloading phase, the specimens were unloaded toward F_0 and loaded afterwards monotonically until failure. The resulted maximum stress σ_{max} specifies the concrete residual tensile strength $f_{ct,res}$.

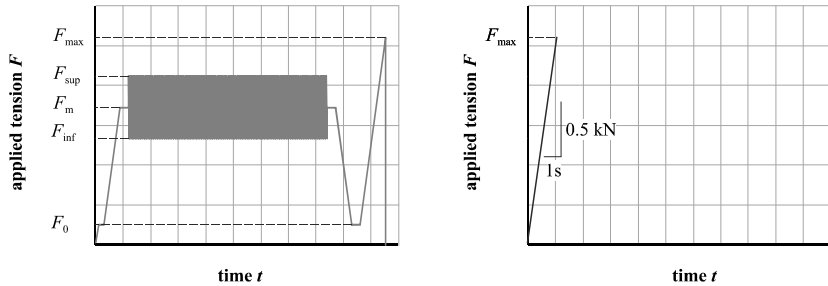


Figure 3-4: Loading scheme during residual tensile tests (left) and monotonic tests (right)

During the tests, local tensile strains are measured at three points on each north and south faces of the specimens. The total displacements of specimens are additionally measured on both specimen sides using linear variable differential transformers (LVDT). The measured values during the cyclic phase are the peak values of strain and displacement in every 60 seconds. During the monotonic phase, a continuous measurement with a rate of 100 Hz is attended.

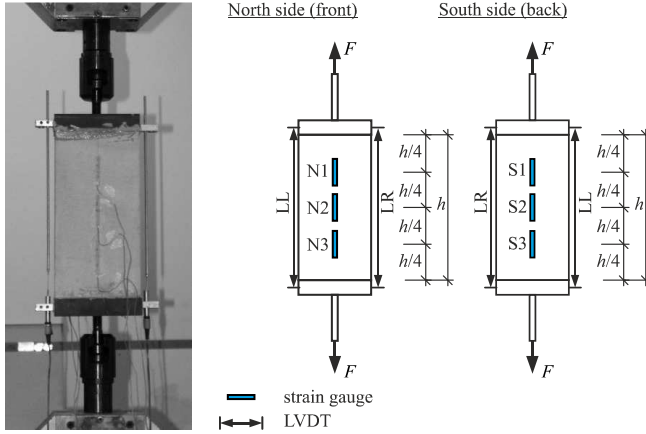


Figure 3-5 Tests setup (left) and position of applied sensors as strain gauges and LVDTs (right)

3.3.4 Evaluation of test data

A total number of 21 tests are conducted, including 7 reference tests and 14 cyclic tests. An overview of conducted tests and their results are given in Table 3-2. Further results are documented in Appendix B.

To evaluate the influence of cyclic damage, the ultimate peak stress reached in the monotonic load phase specifies the experimental residual tensile strength $f_{ct,res}$. The values of $f_{ct,res}$ listed in Table 3-2 are calculated for each specimen using the measured self-weight, ultimate failure load and cross-section dimensions of the specimen. The influence of cyclic loading on strain development of the specimens is also assessed based on the upper strain level of the first load cycle $\varepsilon_{sup}(1)$ and the last load cycle $\varepsilon_{sup}(N)$ as well as the ultimate failure strain of the specimens $\varepsilon_{ct,max}(N)$. It should be noted that the maximum value of measured strain in each specimen is only documented and evaluated here. The residual concrete tensile strength of a specimen after N applied load cycles corresponds to:

$$f_{ct,res} = \sigma_{max}(N) = \frac{F_{max}(N)}{A} \quad \text{Eq. 3-3}$$

Table 3-2: Overview of the results of tensile tests

Spec.	age	preloaded	S_{sup}	S_{inf}	N	$\epsilon_{sup} (I)$	$\epsilon_{sup} (N)$	ϵ_{max}	σ_{max}
	[days]		[-]	[-]	[-]	[$\mu\text{m/m}$]	[$\mu\text{m/m}$]	[$\mu\text{m/m}$]	[N/mm^2]
ZP1	47		-					76.7	2.2
ZP2	47		-					73.8	2.3
ZP3	47	x	0.7	0.4	1000				2.3
ZP4	48	x	0.7	0.4	2460				2.5
ZP5	49		-					68.4	2.3
ZP6	49		-					104.3	2.0
Z1	120		-					95.6	2.3
Z2	118	x	0.7	0.5	10336			166.9	2.3
Z3	119	x	0.8	0.4	10124			165.1	2.5
Z4	119	x	0.8	0.5	31053			116.1	2.3
Z5	120		-					107.3	2.3
ZO1*	254	x	1.2	0.7	10	-	-	-	2.6
ZO2*	255	x	1.1	0.7	3	-	-	-	2.3
ZO3	254	x	0.8	0.5	16183	92.3	147.9	168.3	2.1
ZO4	327		-					107.7	1.9
ZO5	327	x	0.8	0.5	43200	71.4	142.2	146.5	2.3
ZO6	328	x	0.9	0.6	86400	91.4	136.6	150.9	2.5
ZO7*	334	x	0.9	0.4	3530	87.5	173.0	173.7	2.1
ZO8	335	x	0.9	0.6	129600	106.5	258.9	257.8	2.4
ZO9	348	x	0.7	0.4	129600	67.5	233.8	233.8	2.6
ZO10	350	x	0.7	0.4	86400	58.5	114.3	114.3	2.42

Three specimens undergone a premature failure during the cyclic loading phase after a few load steps (marked with "*" in Table 3-2) and could not therefore be considered for the evaluation of residual tensile strength.

The values of the relative residual concrete tensile strength (ratio between the residual tensile strength and reference tensile strength) are calculated and illustrated in Figure 3-6 (left). In addition, the failure point of cyclically preloaded members with regard to their ultimate strengths and failure strains are illustrated in comparison to the concrete tensile curve of reference tensile tests. The softening branch of the curve is calculated according to the exponential correlation according to HORDIJK [HØR-1992] (calculated based on Eq. 2-15) for the sake of comparison.

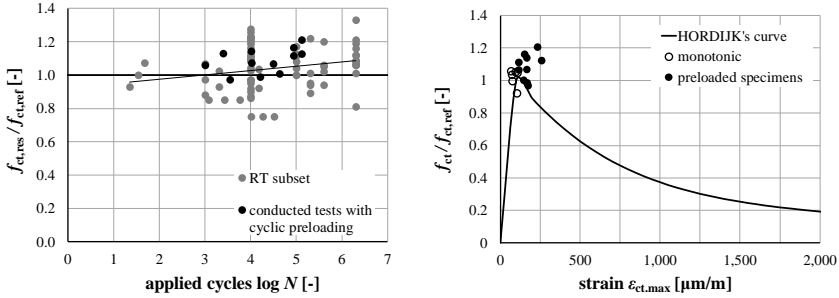


Figure 3-6: Correlation between the residual tensile strength and the reference tensile strength for conducted tests and tests in RT subset of tensile database (left) and ultimate stress and strain of monotonic and cyclic preloaded tests in comparison to monotonic tensile curve according to [HØR-1992] (right)

The correlation between relative $f_{ct,ref}$ values and the number of applied load cycles N in Figure 3-6 (left) shows a slight increase in values of residual tensile strength after a cyclic preloading. The results correspond with the results of tests in RT subset of tensile database.

Based on Figure 3-6 (right), it can be seen that, similar to observations within fatigue tests (compare section 2.2), the ultimate strains of specimens at failure state have a comparably larger scatter and are in all cases higher than failure strains of reference monotonic tensile tests. It is also apparent from the comparison that even for reference tests, the values of local strain is afflicted with a large scatter.

To quantify the cyclic damage, the evolution of the upper strain level during the cyclic loading phase for each test is evaluated. The considered values correspond to the maximum measured local strain. The strain evolution curves of specimens ZO5 to ZO10 with the number of load steps $N_{max} > 30,000$ are depicted in Figure 3-7, left. The value of cyclic creep within the cyclic phase is calculated based on Eq. 3-4 as an experimental creep coefficient:

$$\varphi_{cyl,exp}(N) = \frac{\Delta \varepsilon_{sup}}{\varepsilon_{sup,1}} = \frac{\varepsilon_{sup,N} - \varepsilon_{sup,1}}{\varepsilon_{sup,1}} \quad \text{Eq. 3-4}$$

The experimental creep values are illustrated in correlation to the number of applied load cycles in Figure 3-7, right.

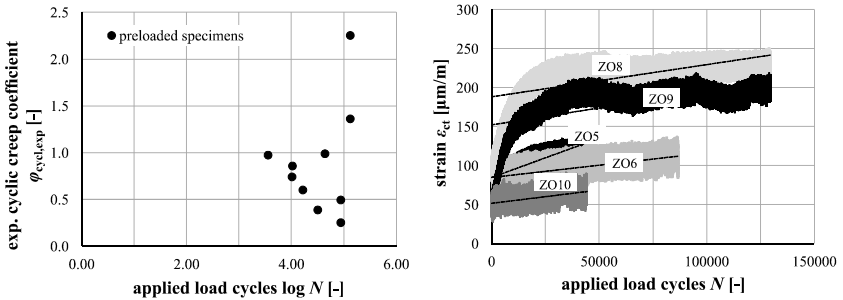


Figure 3-7: Relation between the strain evolution and number of applied load cycles

It is evident from Figure 3-7 that the absolute values of strain increase within the first 10,000 load cycles rapidly, followed by an almost linear strain gain similar to illustrated cyclic creep curve in Figure 2-10. According to strain gain and increasing cyclic creep depicted in Figure 3-7, it can be concluded that even before macroscopic damage, microscopic damage processes in different concrete phases such as microcracking of cement matrix, damage of aggregates and softening of the interfacial transition zone between aggregate and cement paste cause a gradual strain gain. However, no correlation could be observed between the slope of linear phase and upper and lower stress levels or the ultimate tensile strength. Since the strain gauges provide only data on local strain development, this deviation can be explained by the heterogeneous concrete structure. Due to the time-dependent material parameters of concrete and different displacement types (reversible and irreversible deformations), the measured displacement cannot be directly associated with irreversible damage in the specimen.

Damage effects were also visually detectable based on the shaped slates on fracture surface. Additionally, analysis of fracture surfaces under a digital microscope showed a qualitative lower roughness of damaged regions of fracture surfaces for specimens with higher number of applied load cycles. This is illustrated exemplarily in Figure 3-8 for specimens ZO2 ($N = 3.0$) and ZO9 ($N \sim 1.29 \cdot 10^5$).

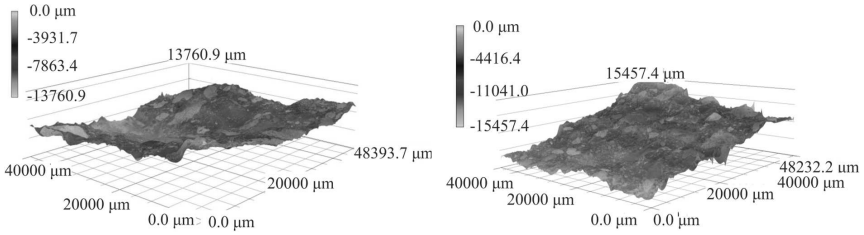


Figure 3-8: Fracture surface of specimens ZO2 ($N = 3.0$) and ZO9 ($N = 129,600$) measured by a digital microscope

To account for different stress levels, the suggested damage factor by CORNELISEN $D_\phi(N)$ was additionally evaluated using Eq. 2-22. The correlation between number of applied load cycles and creep-based damage factor is shown in Figure 3-9.

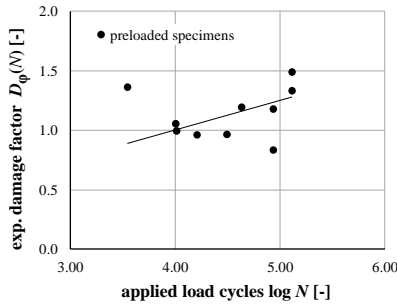


Figure 3-9: Linear correlation between creep-based damage factor $D_\phi(N)$ and the number of applied preloading cycles

A clear tendency is observed during the monotonic loading phase of preloaded specimens (with the number of load steps $N_{max} > 30,000$) between the stiffness of preloaded specimens and the strain gain due to cyclic creep. This correlation is illustrated in Figure 3-10.

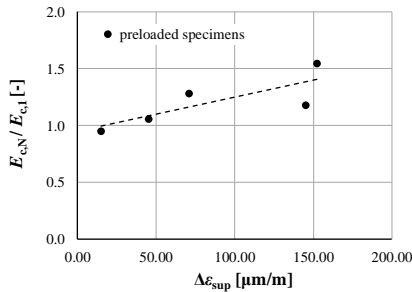


Figure 3-10: Linear correlation between strain gain during cyclic tests and increase in stiffness of specimen in subsequent monotonic loading

Although the hysteresis curves during cyclic loading show a reduction of concrete stiffness during cyclic loading (compare chapter 2), the preloading and cyclic creep in RT tests reduces the strain to peak stress as also shown in previous investigations such as in [Coo-1981]. With the almost unchanged values of failure peak stress, the lower required strain to peak stress is captured as a higher stiffness of preloaded specimens.

This observation can also be justified by the partial unloading of the specimens, which enables apparently a new stress distribution and change of stress path in the specimen, leading to higher macroscopic stiffness and slightly higher tensile strength values. It is worth noting that such stress distribution is only possible for limited lengths of microcracks as illustrated in Figure 3-11. During the cyclic loading phase, local microcracks with limited lengths are formed in sections with relatively lower tensile strength. Since the local microcracks appear in the weaker parts of the specimens, the intact specimen regions tend to have a higher tensile strength. After an unloading or partial unloading, the microcracks close and a redistribution of stresses to parts of specimens with a higher strength is possible according to Figure 3-11, left. In the subsequent monotonic loading phase is therefore often a higher peak stress reached. During fatigue tests, such stress redistribution is only possible in a limited extent based on the lower stress level and the loading frequency. For this reason, the macroscopic behaviour is mainly influenced by the behaviour of the damaged regions of the specimen.

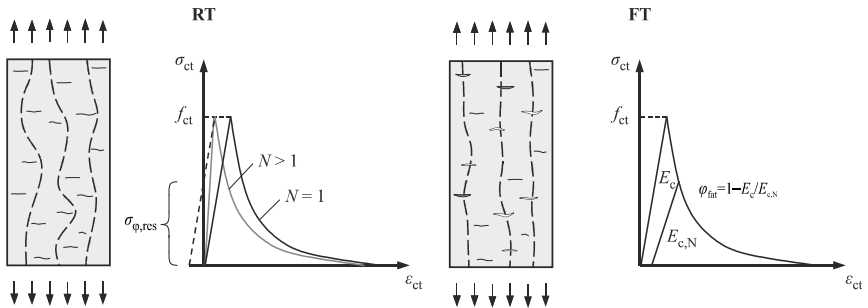


Figure 3-11: Qualitative change of stress path during a RT test and corresponding change of concrete tensile curve (left) in comparison to the loading and unloading stress path during an FT test and the corresponding concrete tensile curve (right)

A common observation during both RT and FT tests is the cyclic creep phenomenon. In RT tests, this leads to a higher stiffness, whereas in FT tests, a reduction of stiffness is often reported. The cyclic creep coefficient in FT tests corresponds to:

$$\varphi_{fat}(N) = 1 - \frac{E_c}{E_{c,N}} \quad \text{Eq. 3-5}$$

Conducted RT tests show a correlation between stiffness gain in the monotonic loading phase and the cyclic creep (compare Figure 3-10). Assuming a constant modulus of elasticity E_c (according to Figure 3-11, left), the cyclic creep for the applied number of cycles N in FT tests can be represented for RT tests as a damage induced equivalent stress $\sigma_{\varphi, \text{res}}$, which can be calculated based on:

$$\sigma_{\varphi, \text{res}}(N) = f_{\text{ct}} \cdot \left(\frac{E_c}{E_{c,N}} - 1 \right) \quad \text{Eq. 3-6}$$

Based on value of internal stress value $\sigma_{\varphi, \text{res}}$, a modified concrete tensile curve is proposed (compare Figure 3-12), which considers the effects of a previous cyclic preloading on tensile behaviour of the specimen in a preceding monotonic loading phase.

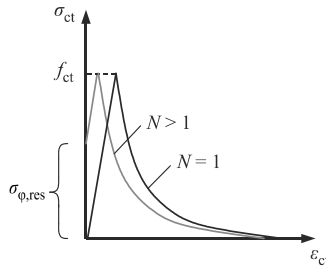


Figure 3-12: Proposed modified tensile curve

The proposed curve can be used for numerical stationary monotonic (displacement-controlled) evaluation of cyclically preloaded structures.

3.4 Concluding remarks

After a literature review, a database of two different types of cyclic tensile tests, i.e. fatigue tests (FT) and residual tensile tests (RT) was developed and evaluated. Whereas in FT tests, a lower fatigue tensile strength with increasing number of load steps was observed as supposed, the values of residual tensile strength showed a slight gain. The different responses of concrete tensile specimens within these two test types were analysed and indicated the necessity of a better insight in cyclic damage phenomena. Furthermore, two introduced models for determination of fatigue tensile strength were evaluated using the FT subset of the tensile database. The proposed equation by CORNELISSEN showed good results for the approximation of fatigue tensile strength.

To investigate the possible damage within RT tests and evaluate its impact on macroscopic tensile behaviour of concrete, response of cyclically preloaded specimens was evaluated within an experimental programme. Based on the conducted RT tests, a general increase in residual tensile strength and ultimate failure strain was evident from the test results, which confirmed the reported results in the technical literature. Furthermore, a

higher concrete stiffness $E_{c,N}$ was observed during the monotonic loading of cyclically preloaded specimens, which was based on the reduced strain to failure caused by cyclic creep. It was shown for the conducted tests within the experimental programme that the stiffness gain correlates with the experimental cyclic creep coefficient. This observation was used to define a new modified tensile curve for cyclically preloaded members. The applicability of proposed adjusted tensile curve in structural scale for the cyclically preloaded concrete should be validated using test data.

4 Diagonal cracking under monotonic and cyclic loading

4.1 Behaviour of concrete members under monotonic shear loads

4.1.1 Stress state in concrete members and theoretical diagonal cracking

Shear behaviour of reinforced concrete (RC) and prestressed concrete (PC) members can be described using stress states at different depths of cross-section of the members. Based on the principal stress trajectories for a homogenous and linear elastic concrete (according to HOOK's law), three main stress states can be observed and evaluated using the MOHR's circle of stresses.

In the extreme tensile fibre (point 1), the infinitesimal elements are only opposed to tensile principal stress σ_1 acting parallel to beam axis. In point 2, for converting the rotated tensile and compressive principal stresses σ_1 and σ_2 to stresses parallel to beam axis, an auxiliary term as shear stress $\tau_x(z)$ should be defined according to the MOHR's circle of stresses. In point 3, a compressive principal stress σ_2 is acting along the beam axis.

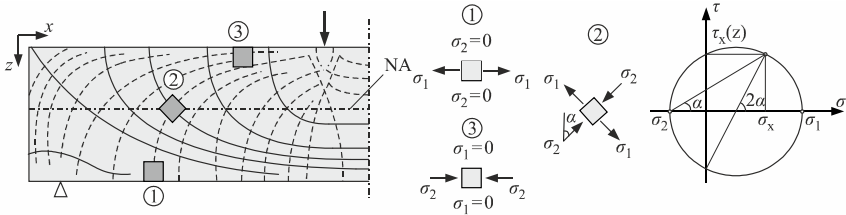


Figure 4-1: Principal stress trajectories, stress state in different depths of the section and MOHR's circle of stresses at neutral axis of the member ([Bus-2019], [Hub-2016])

Based on the MOHR's circle of stresses, shear stress $\tau_x(z)$ can be calculated using the principal tensile stress σ_1 and normal stress along the beam axis $\sigma_x(z)$, which is variable over the beam depth.

$$\tau_x(z) = \sigma_1 \cdot \sqrt{1 - \frac{\sigma_x(z)}{\sigma_1}} \quad \text{Eq. 4-1}$$

For a practical application, a correlation between the applied moment M and shear V is needed to calculate the stresses. A common approach is suggested in the technical bending theory (TB) that is based on EULER-BERNOULLI's beam theory. This theory is valid in beam regions without stress concentrations (B regions) and as long as plane sections remain plane and normal to the axis of the member after bending. Based on these assumptions, the sum of normal and shear stresses for an infinitesimal element of the beam

with a length dx is used to derive a correlation between normal and shear stresses. This is shown for a beam with a rectangular cross-section in Figure 4-2.

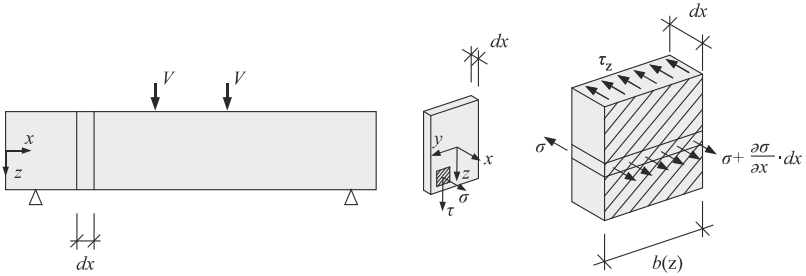


Figure 4-2: Normal and shear stresses for a beam section [Gro-2014]

The equilibrium conditions for the illustrated beam section with a cross-section area of A^* is according to the following equation:

$$-\tau_x(z) \cdot b(z) \cdot dx - \int_{A^*} \sigma \cdot dA + \int_{A^*} \left(\sigma + \frac{\partial \sigma}{\partial x} \right) \cdot dA = 0 \quad \text{Eq. 4-2}$$

This equation can be rewritten as:

$$\tau_x(z) \cdot b(z) = \int_{A^*} \frac{\partial \sigma}{\partial x} \cdot dA \quad \text{Eq. 4-3}$$

The definition of shear load as the variation of moment over the beam length can be used to rewrite the term $\partial M / \partial x$ into:

$$\frac{\partial \sigma}{\partial x} = \frac{\partial M}{\partial x} \cdot z = \frac{V}{I} \cdot z \quad \text{Eq. 4-4}$$

Eq. 4-3 and Eq. 4-4 result in the following correlation:

$$\tau_x(z) \cdot b(z) = \frac{V}{I} \int_{A^*} z \cdot dA \quad \text{Eq. 4-5}$$

Here is the integral term the first static moment of the area $S(z)$, so the shear stress $\tau_x(z)$ can be calculated using the applied shear load as:

$$\tau_x(z) = \frac{V \cdot S(z)}{I \cdot b(z)} \quad \text{Eq. 4-6}$$

For a beam without normal stresses, Eq. 4-1 presumes that the maximum σ_1 is reached at the neutral axis of the beam (where the flexural normal stresses $\sigma_x(z)$ are zero). If the principal tensile stress at this point exceeds the effective concrete tensile strength $f_{ct,ef}$, a diagonal crack emerges and the diagonal cracking load can be determined using the following correlation:

$$V_{cr,cal} = \frac{I}{S(z)} \cdot b(z) \cdot f_{ct,ef} \cdot \sqrt{1 - \frac{\sigma_x(z)}{f_{ct,ef}}} \quad \text{Eq. 4-7}$$

It is apparent from the basic equation according to TB (Eq. 4-7) that the diagonal cracking load can be defined based on following terms:

- $I / S(z)$ depending on cross-section geometry
- Depth dependent beam width $b(z)$
- Failure criterion of concrete under tension defined by the effective concrete tensile strength $f_{ct,ef}$
- Effects of normal stresses $\sigma_x(z)$ (if available) at the cracking depth

For a rectangular reinforced concrete beam with a width b and height h without normal loads Eq. 4-7 can be rewritten as:

$$V_{cr,cal} = \frac{2}{3} \cdot b \cdot h \cdot f_{ct,ef} \quad \text{Eq. 4-8}$$

The assumptions of TB are also advantageous, as the theoretical inclination of the diagonal crack caused by rotated principal tensile stresses can be calculated using shear and normal stresses of the section (compare Eq. 4-9).

$$\tan 2\alpha = \frac{2 \cdot \tau_x(z)}{\sigma_x} \quad \text{Eq. 4-9}$$

According to Eq. 4-9, the theoretical inclination of diagonal crack at the neutral axis of the section corresponds to 45° . The expression according to TB (Eq. 4-8) are valid if the principal stresses at point 1 and 3 in Figure 4-1 do not violate the concrete failure criterion.

4.1.2 Experimental diagonal cracking

For reinforced concrete members with a rectangular cross-section, flexural cracks appear prior to diagonal cracking when the concrete tensile strength is reached at the extreme tensile fibre of the member. Such primary flexural cracks develop in the section until a stabilized flexural cracking state is reached and are perpendicular to beam axis or slightly inclined. The primary cracking causes, however, no global damage for shear critical members [Tue-2015], [Fus-2017]. With increasing applied load, the primary flexural cracks rotate further and form several diagonal cracks in shear span. This rotation of cracks can be explained by the rotation of principal stress trajectories. Under combined flexure and shear, the principal tensile stresses and the general diagonal tension are affected by the existing flexural cracks and deviate from the illustrated trajectories in Figure 4-1.

In the further sequence of shear tests, a diagonal crack stands out based on its shape, location or kinematics (relative displacement of crack faces, crack width development

and speed of crack propagation), which is often termed as a critical diagonal crack or a major diagonal crack (noticeable based on line thickness in Figure 4-3). To define a point for initiation of the critical diagonal crack, different criteria are used based on experimental observations. The shape of critical diagonal crack influences the definition of critical diagonal cracking and the associated mechanisms with it. Different observations regarding the initiation of the critical diagonal cracking complicates the experimental documentation of the applied shear load at the state of critical diagonal cracking, subsequently termed as experimental diagonal cracking load $V_{cr,exp}$. Furthermore, comparing the crack pattern at the state of stabilized flexural cracking (Figure 4-3, left) and possible critical diagonal crack shapes (Figure 4-3, right), three main mechanisms can be associated with the critical diagonal cracking.

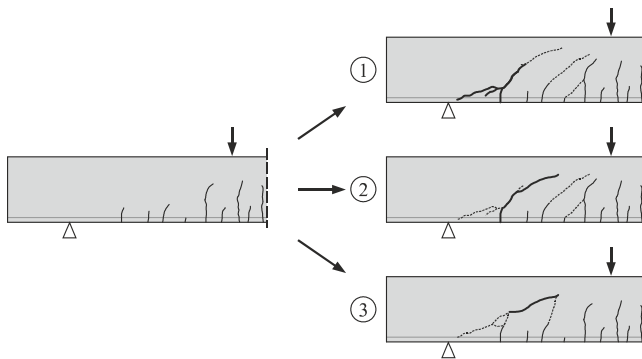


Figure 4-3: Primary cracks and possible critical diagonal crack shapes

Different diagonal cracking mechanisms are indeed one of the main reasons, for which the number of provided tests with documented $V_{cr,exp}$ is limited (compare chapter 5) and explains the larger scatter generally associated with the experimental diagonal cracking loads in comparison to maximum shear loads $V_{u,exp}$ [Baž-1984]. Some experimental observations notice that a critical cracking initiates as an inclined crack emerges close to an existing primary crack at the depth of longitudinal tensile reinforcement (Figure 4-3, crack type 1). The first crack rotation is reported by several shear tests at this beam depth e.g. in MOODY et al. [Moo-1954]. This criterion for critical diagonal cracking can be based on a bond loss at the depth of longitudinal tensile reinforcement, which disturbs the normal stress transfer from longitudinal reinforcement to concrete. A critical vertical displacement at the depth of longitudinal tensile reinforcement was proposed by [Van-2016] to signify such critical diagonal cracking state.

The most commonly used convention considers documenting experimental diagonal cracking loads $V_{cr,exp}$ at the depth of neutral axis (NA) or at mid-depth (ML) of the beam ([Van-1962], [Pod-1998], [Kre-1966], [Mat-1963], [Xie-1994], [Mph-1984], [Mph-1984]). For instance, optical

observations of the crack growth during the shear tests in [Pod-1998] show that diagonal cracks become first visible at a crack depth around the beam centreline. A significant rotation in crack path is reported in several shear tests at the depth of neutral axis. In this case, a rapid crack formation due to diagonal tension and an increase in crack width are the significant phenomena associated with critical diagonal cracking (Figure 4-3, crack type 2). This crack type is used to report the diagonal cracking load by VAN DEN BERG [VAN-1962]. He documented the load at which the first diagonal crack is formed as $V_{cr,exp}$. MATHEY / WATSTEIN [Mat-1963] defined the diagonal cracking load as the load magnitude at which the critical diagonal crack reaches the depth of neutral axis of the beam. KREFFELD [Kre-1966] defined $V_{cr,exp}$ as the load magnitude short before the critical diagonal crack penetrates the concrete compression zone. GÖRTZ [Gör-2004] characterizes a significant rotation of the critical crack at the neutral axis as the beginning of an instable critical crack growth.

Another type of critical diagonal cracking occurs between two adjacent primary cracks (Figure 4-3, crack type 3), which is designated as tooth break in tooth and tie models (such as the model proposed by KANI [Kan-1979], REINECK [Rei-1991] and TUE [Tue-2014]). This type of cracking is often observed for members with high shear span to depth ratios or high longitudinal reinforcement ratios (compare 4.1.3), where several almost vertical primary cracks with low crack distances s_r are formed before diagonal cracking.

After a critical diagonal cracking, the shear failure can occur as destruction of concrete compression zone, further increase in width of critical diagonal crack or debonding of longitudinal reinforcement. The failure mode is strongly dependent on the structural system and loading conditions and influences the ultimate shear load $V_{u,exp}$. In a number of existing tests in the technical literature, the failure load of members with a failure due to diagonal cracking is reported as diagonal cracking load. The number of experiments with an explicit documentation of diagonal cracking load based on one of above-mentioned definitions are limited. The general crack pattern including distance of primary cracks s_r and the inclination of primary cracks affects the experimental shear capacity under diagonal tension and also the shear resistance of the members [Gör-2004], [Cav-2017], [Kle-2016].

Previous evaluations suggest some values for primary crack distance s_r such as $0.4 - 0.8 \cdot d$ at the mid-depth of the beam according to [Kha-2013] or $0.7 \cdot (d - h_c)$ according to REINECK [Rei-1990]. Based on the failure crack shape and crack distances s_r simplified crack patterns are provided in [Rüs-1967], [Hol-2014] and [Rei-1990].

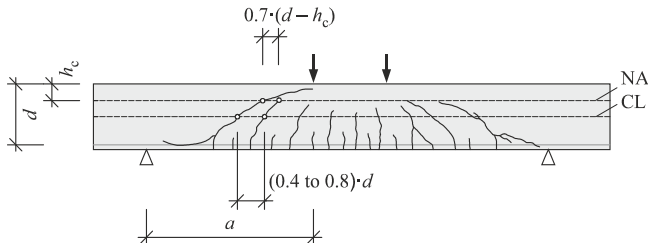


Figure 4-4: Schematic crack pattern and defined crack distances according to [Kho-2013] and [Rei-1990]

There are also some equations for simplified approximation of shape of the critical diagonal cracks. Examples of such formulations determined using a fitted curve to experimental failure crack paths are introduced in [Gör-2004] and [Fus-2017].

In contrast to flexural cracking, the initiation of diagonal cracks as well as formation of the critical diagonal crack are generally not discernible based on the load-deflection curve of the member [Kre-1966]. Hence, extensive measurements are needed for the documentation of diagonal cracks. Common measurement methods include continuous optical documentation of crack propagation, vertical displacement measurements using LVDTs, local strain measurements in shear span, measurement of beam curvature using inclinometers [Sch-2014], photogrammetric measurement or documentation of crack kinematics using image correlation techniques (e.g. [Hub-2016], [Cam-2013], [Cav-2017], [Fus-2017]) as well as fibre-optic sensing [Fis-2017].

For defining a specific threshold for initiation of a critical diagonal crack based on measurements, various observations exist. Using vertical displacement measurements in shear span, BRESLER / SCORDIS [Bre-1963] observed an accelerated increase in vertical displacement of LVDTs by initiation of a critical diagonal crack. SCHACHT associates based on photogrammetric measurements the initiation of a critical diagonal cracking with an instable crack propagation, which can be detected as an accelerated crack propagation [Sch-2014], [Hol-2014]. According to [Fus-2017], a sudden instable diagonal cracking initiates with a change of crack inclination to 45° , as the released tensile force due to cracking gets a significant vertical component and cannot be intercepted by the existing load-bearing mechanisms.

4.1.3 Influencing parameters on diagonal tension under shear

For members with a potential flexure shear crack, the critical diagonal crack emerges in a previously cracked section. Therefore, the stress state at diagonal cracking deviates from the depicted principal stress trajectories in Figure 4-1.

KANI [Kan-1968] and LEONHARDT / WALTHER [Leo-1962] were the first to mention the influence of ratio between flexural moment and shear load M/V as a critical parameter on diagonal cracking and shear failure mode. M/V ratio is often provided relative to effective depth of the section as shear span to depth ratio a/d or shear slenderness λ , which specifies the value of the maximum moment at mid-span M to the constant shear load in shear span V . According to KANI, from a certain shear slenderness ($a/d \sim 2,0$), the failure load deviates from the maximum load corresponding to bending resistance M_R and the concrete member can be specified as a shear critical member. Based on these observations, beams with a shear slenderness between 2 and 8 are located in the so-called KANI's valley and reach a significantly lower ultimate load in comparison to the load corresponding to M_R (compare Figure 4-5).

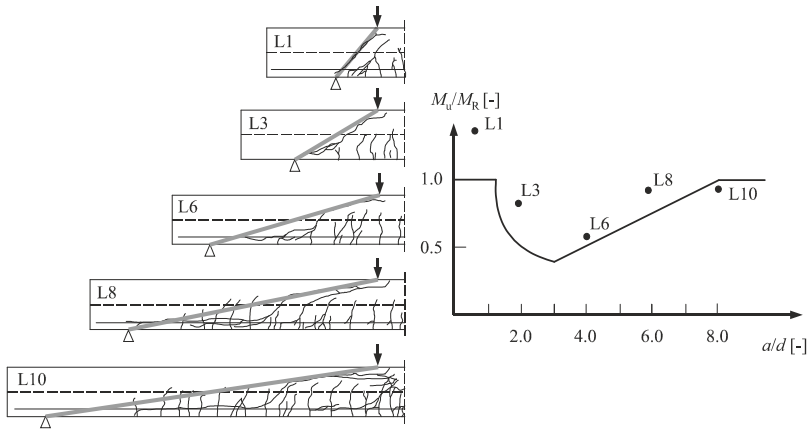


Figure 4-5: Comparison of crack pattern and direct compression strut for shear tests of LEONHARDT / WALTHER with different values of shear slenderness (left) as well as the ratio between ultimate failure moment M_u and bending resistance M_R in relation with KANI's valley (according to [Cav-2017])

In this range of shear slenderness, the cracking depends significantly on the shear span to depth ratio, as it influences the load-bearing mechanism under shear [Cav-2017]. An evaluation of crack patterns in beams 1 to 10 examined by LEONHARDT / WALTHER shows that a direct compression strut can be formed even after a critical diagonal cracking for shear span to depth ratios $2.5 < a/d < 4.0$, which results in a significant difference between the diagonal cracking and the ultimate failure loads for members. A major reduction of ultimate loads take place for a shear slenderness between 2.5 and 4.0.

A detailed view of this stress state can be observed using nonlinear simulation of beams as represented in Figure 4-6.

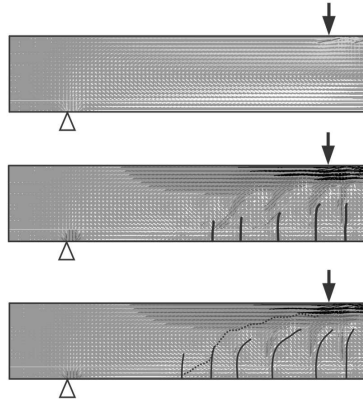


Figure 4-6: Stress trajectories in uncracked state (up), after stabilized flexural cracking (middle) and close to critical diagonal cracking state (down)

A comparison between principal stress trajectories in uncracked state (Figure 4-6, up), after stabilized flexural cracking (Figure 4-6, middle) and shortly before critical diagonal cracking (Figure 4-6, down) shows that the existing flexural cracks cause a tensile stress concentration at crack front and also form compressive struts between adjacent cracks. Single compressive struts between cracks, potential direct compressive strut between loading point and support, as well as inclination, distance and depth of primary cracks define the altered stress trajectories short before critical diagonal cracking and the resulted diagonal crack paths. For instance, if the direct strut is steeper than the inclination of altered stress trajectories at the intersection point with existing primary cracks, the critical diagonal crack forms as a single diagonal crack. If the inclination of direct strut and stress trajectories coalesces at intersection points, the critical diagonal crack is formed as assumed in tooth and tie models between two flexural cracks.

The stress state at diagonal cracking and pattern of primary cracks are affected in structural scale by loading parameters and member configurations such as

- shear span to depth ratio (a/d),
- longitudinal reinforcement ratio (ρ_l),
- concrete strength (f_{ct} or f_c) and
- width (b) and effective depth (d) of the longitudinal tensile reinforcement.

The above-mentioned influencing parameters are the basis of most data fittings and regression analyses for development of empirical shear models for determination for diagonal cracking load and are also used in available mechanical models.

4.1.4 Shear capacity under diagonal tension and further load-bearing mechanisms

Before a diagonal crack is formed, concrete tensile resistance to diagonal tension mainly fulfils the equilibrium condition in the critical section. After critical diagonal cracking, the released forces perpendicular to crack path should be redistributed between other load-bearing mechanisms. The diagonally cracked section as depicted in Figure 4-7 is considered to derive the equilibrium condition for existing mechanical models in the technical literature for evaluation of ultimate shear resistance. In this state, the uncracked (effective) depth of the beam is limited to the compression zone of the member. The assumed shear stress distribution is often defined according to MÖRSCH [Mör-1907] with a parabolic part in compression zone and a constant value in the cracked depth of the section. The shear resistance provided by the compression zone V_{cc} is considered using the assumption of TB [Zin-2000] or under consideration of an activated arching action as proposed in [Mar-2014]. The constant component of shear resistance in cracked region is attributed with following load-bearing mechanisms:

- Aggregate interlock V_A
- Dowel action of longitudinal reinforcement V_D
- Residual tensile strength in the fracture process zone V_R

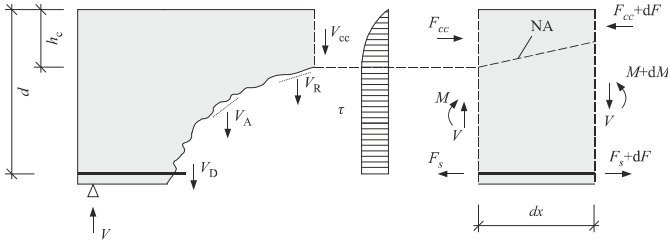


Figure 4-7: load-bearing mechanisms after a critical diagonal cracking (left) and assumed shear stress distribution according to [Mör-1907] (right)

The contribution of aggregate interlock and dowel action is considered differently in existing mechanical models and is the basis of several contradicting ideas. This is mainly based on simultaneous involvement of different constructing and destructing mechanisms. For instance, the contribution of aggregate interlock depends on roughness of crack face, crack width and relative displacement of crack faces. With a higher depth of concrete compression zone h_c , the relative lateral displacement of crack faces is reduced which decreases the contribution of aggregate interlock. At the same time, the diagonal crack widths of such members (high $\alpha\rho$) are relatively small and hence the aggregate interlock is activated by a smaller relative lateral displacement of crack faces [Wal-1980], [Cam-2013], [Cav-2017], [Wal-1981]. A lateral vertical displacement activates simultaneously the dowel action of longitudinal reinforcement, which also depends on several factors such

as available aggregate interlock. Some approaches imply that aggregate interlock and dowel action can be ignored as the intact concrete compression zone avoid a lateral relative displacement along the diagonal cracks [Zar-2003], [Cho-2007]. Other observations such as in [Cao-2001] show that the calculated dowel action by most approaches cannot develop in real shear tests on normal concrete members because splitting tensile cracks emerge parallel to longitudinal reinforcement prior to an adequate lateral vertical displacement and cause debonding between concrete and longitudinal reinforcement.

For development of mechanical models, evaluation of state of diagonal cracking instead of shear failure state is beneficial, as the considered load-bearing mechanisms are limited. However, due to combined influence of shear and flexure loading on development of flexure shear cracks, the approach based on TB (compare chapter 4.1.1) is not valid anymore and further adjustments are needed for a calculative determination of concrete tensile capacity.

Evaluation of state of diagonal cracking instead of shear failure state is beneficial for development of mechanical approaches, as the considered load-bearing mechanisms are limited. However, due to combined influence of shear and flexure loading on development of flexure shear cracks, the approach based on TB (compare section 4.1.1) is not valid anymore and further adjustments are needed for a calculative determination of shear capacity caused by concrete resistance to diagonal tension. However, it is worth noting that the determined values of diagonal cracking in such cases define a lower bound of concrete tensile capacity as in tests, aggregate interlock might be activated in early stages of cracking and plays an important role on crack pattern in the shear span.

4.1.5 Mechanical approaches for evaluation of monotonic diagonal cracking load

In this chapter, existing mechanical models in the technical literature for the evaluation of diagonal cracking load $V_{cr,cal}$ are introduced. The considered models assume a sudden formation of critical diagonal crack caused by diagonal tension and are derived based on assumptions of TB. However, due to the existing flexural cracks, the basic equation of TB (Eq. 4-7) results in an overestimation of diagonal cracking load [Jav-2017], [Jav-2018a], [Roo-2018] (compare 6.2.2).

A common method for modification of the approach according to TB is to adapt the effective depth of member h_{ef} based on an assumed stress distribution over the section depth. The mentioned different experimental observations regarding the shape of critical diagonal crack (compare Figure 4-3) result in various suppositions for the adaptation of h_{ef} and the stress distribution at the state of critical diagonal cracking.

Model according to HONG /HA

HONG / HA [Hon-2012] follow the definition of diagonal cracking load according to MOODY, which implies that the diagonal crack initiates at the depth of longitudinal tensile reinforcement. In this approach, the equilibrium condition (Figure 4-8) is developed for a concrete shell element adjacent to longitudinal reinforcement. The tensile stress in longitudinal reinforcement σ_x is assumed to be equal to the bond stress between the observed shell element and reinforcement τ_x .

$$\tau_x \cdot b \cdot dx + \sigma_x \cdot b \cdot dx = dF \tag{Eq. 4-10}$$

Due to the correlation between σ_x and τ_x according to MOHR's circle of stresses, shear stress τ_x can be determined using Eq. 4-11. Here, the partial force dF can be converted using partial bending moment dM and effective lever arm z as dM / z so that Eq. 4-10 can be rewritten as:

$$\tau_x = \frac{2}{1 + 2\sqrt{5}} \cdot f_{ct} \tag{Eq. 4-11}$$

Calculated diagonal cracking load $V_{cr,cal}$ according to the model of HONG / HA equals:

$$V_{cr,cal} = \tau_x \cdot b \cdot z = b \cdot z \cdot \frac{2}{1 + 2\sqrt{5}} \cdot f_{ct} \tag{Eq. 4-12}$$

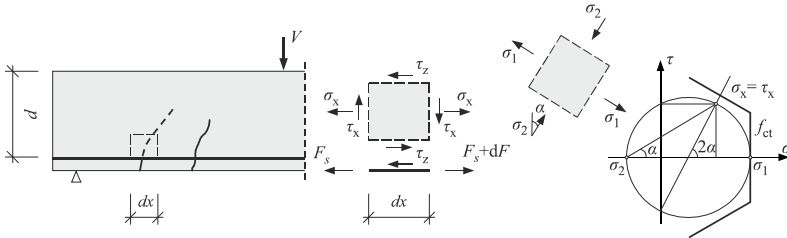


Figure 4-8: Distribution of normal and shear stresses in the initiation point of diagonal crack and failure criterion according to HONG / HA [Hon-2012]

For an assumed value of z equal to $0.9 \cdot d$, the proposed equation for calculation of diagonal cracking load can be rewritten as follows:

$$V_{cr,cal} = 0.33 \cdot b \cdot d \cdot f_{ct,sp} \tag{Eq. 4-13}$$

The concrete tensile strength considered for the evaluation of $V_{cr,cal}$ is the splitting tensile strength $f_{ct,sp}$ (compare .

Model according to GALLEGO et al.

GALLEGO et al. [Gal-2014] proposed a model which adapts the effective depth of the member h_{ef} based on the depth of existing flexural crack at the state of diagonal cracking. In this case, Eq. 2-33 can be rewritten as:

$$V_{cr,cal} = \frac{2}{3} \cdot b \cdot h_{ef} \cdot f_{ct,fl} \quad \text{Eq. 4-14}$$

To determine h_{ef} , a linear normal stress distribution over the depth of member and a parabolic distribution of shear stresses according to TB is considered. The effective depth can be determined based on normal stress distribution using the compressive strength σ_c and tensile strength f_{ct} at both extreme fibres of the member (compare Figure 4-9). The effective depth can be divided into a tension zone h_{ct} and a compression zone h_c .

$$h_{ef} = h_c + h_{ct} = h_c \cdot \left(1 + \frac{f_{ct,fl}}{\sigma_c} \right) \quad \text{Eq. 4-15}$$

The compression zone is calculated using a force equilibrium under pure bending as follows:

$$h_c = \xi \cdot d = \left(-\alpha \cdot \rho_l + \sqrt{(\alpha \cdot \rho_l)^2 + 2 \cdot \alpha \cdot \rho_l} \right) \cdot d \quad \text{Eq. 4-16}$$

Where the coefficient α is equal to:

$$\alpha = E_s/E_c \quad \text{Eq. 4-17}$$

The longitudinal reinforcement ratio ρ_l is defined based on the effective depth of the longitudinal reinforcement using:

$$\rho_l = \frac{A_s}{b \cdot d} \quad \text{Eq. 4-18}$$

The concrete tensile strength in the model according to GALLEGO et al. is considered to be the flexural tensile strength $f_{ct,fl}$ according to [DIN-1992-1-1] with an adaption to account for effects of lateral compression on concrete tensile criterion.

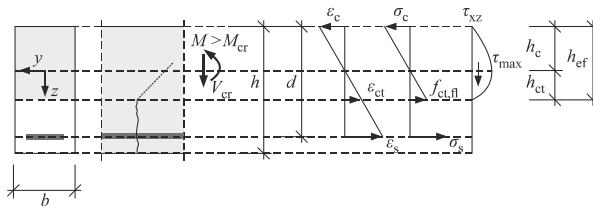


Figure 4-9: Normal and shear stress distribution over cross-section of the member according to GALLEGO et al. [Gal-2014]

Model according to TRAN ET AL.

Similar to the model according to GALLEGO et al., the critical diagonal cracking arises according to TRAN / KOHOUTEK / GRAUBNER [Tra-2015], [Tra-2017] due to a sudden development of a diagonal crack in tension zone of the specimen. For the calculation of the effective depth, however, the residual tensile strength in tensile softening zone is considered. Hence, the tension zone of effective depth can be divided into an uncracked region $h_{ct,1}$ and a cracked region $h_{ct,2}$ within which the crack width does not exceed a critical crack width $w_{cr,1}$. The crack width at the depth of diagonal crack initiation is determined using a linear crack width distribution between effective depth of longitudinal reinforcement (d) and the depth of diagonal crack initiation ($h_c + h_{ct,1}$):

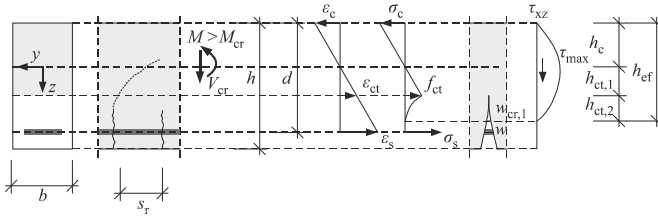


Figure 4-10: Normal and shear stress distribution over cross-section of the member according to TRAN et al. [Tra-2015]

$$h_{ct} = h_{ct,1} + h_{ct,2} = \frac{w_{cr,1}}{w} \cdot (d - h_c) \quad \text{Eq. 4-19}$$

The crack width w is determined in this model using the crack distance s_r according to REINECK [Rei-1990] (compare Figure 4-4) and the strain in longitudinal reinforcement ϵ_s accordingly:

$$w = s_r \cdot \epsilon_s \quad \text{Eq. 4-20}$$

The value of ϵ_s is determined using calculated curvature κ with regard to the applied moment M in the state of diagonal cracking.

$$\epsilon_s = \kappa \cdot (d - h_c) \quad \text{Eq. 4-21}$$

The calculated concrete tensile capacity $V_{cr,cal}$ correspond to

$$V_{cr,cal} = 2/3 \cdot b \cdot (h_c + h_{ct}) \cdot f_{ct} \quad \text{Eq. 4-22}$$

According to the model proposed by TRAN et al. the implemented concrete tensile strength f_{ct} is the uniaxial concrete tensile strength as defined in DIN EN 1992-1-1 [DIN-1992-1-1].

Model according to TUE ET AL.

The model of TUE et al. [Tue-2014] can be regarded as a further model, which considers the initiation of critical diagonal cracking in concrete tensile zone. In this case, the crack tip

is located in a shear band with a band width h_{sb} depending on longitudinal reinforcement ratio ρ_l and concrete compressive strength f_c . One of the weaknesses of this approach is the proposed empirical equation for the calculation of shear bandwidth h_{sb} .

$$h_{sb} = 0.5 \cdot \frac{(100 \cdot \rho_l)^{0.9}}{f_c} \quad \text{Eq. 4-23}$$

Based on the width of shear band, a normal stress caused by bending moment σ_x is considered at the crack process zone in shear band according to:

$$\sigma_x = \begin{cases} f_{ct} \cdot \left(1 - 0.5 \frac{h_{sb}}{h_{ct,1} + h_{ct,2}}\right) & h_{sb} < h_{ct,1} + h_{ct,2} \\ f_{ct} \cdot \left(0.5 \frac{h_{sb}}{h_{ct,1} + h_{ct,2}}\right) & h_{sb} \geq h_{ct,1} + h_{ct,2} \end{cases} \quad \text{Eq. 4-24}$$

Based on this normal stress σ_x , the ultimate shear stress is defined by inserting f_{ct} (uniaxial tensile strength as defined in DIN EN 1992-1-1 [DIN-1992-1-1]) as ultimate principal tensile stress in Eq. 4-1.

$$\tau_u = \sqrt{f_{ct} \cdot (f_{ct} - \sigma_x)} \quad \text{Eq. 4-25}$$

The shear stress at the neutral axis of the beam should be determined in this model using the assumed distribution and equilibrium conditions using the following equation:

$$\tau_{max} = \frac{\tau_u}{1 - (h_{ct,1}/h_c)^2} \quad \text{Eq. 4-26}$$

Depth of uncracked tensile zone can be calculated in this approach with the following correlation with a linear normal strain distribution over effective depth:

$$h_{ct,1} = \frac{f_{ct}/E_c}{\varepsilon_s} \cdot (d - h_c) \quad \text{Eq. 4-27}$$

For the depth of the cracked zone, following equation is suggested, in which the crack width of primary flexural cracks is predicted based on recommended characteristic crack width w_k according to DIN EN 1992-1-1 and critical crack width $w_{cr,1}$.

$$h_{ct,2} = \frac{w_{cr,1}}{w_k} \cdot (d - h_c - h_{ct,1}) \quad \text{Eq. 4-28}$$

The supposed crack distance s_r for calculation of w_k is approximated as $0.7 \cdot d$ in this model. The diagonal cracking load $V_{cr,cal}$ is subsequently calculated using a mean shear stress in accordance with the depicted stress distribution in Figure 4-11.

$$V_{cr,cal} = \frac{2}{3} \cdot \tau_{max} \cdot h_c + \frac{1}{2} \cdot (\tau_{max} + \tau_u) \cdot h_{ct,1} + \tau_u \cdot (d - h_c - h_{ct,1}) \quad \text{Eq. 4-29}$$

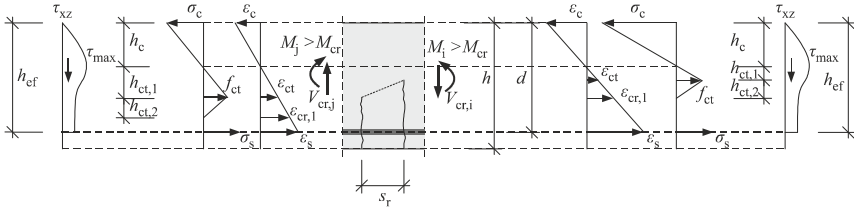


Figure 4-11: Normal and shear stress distribution over the cross-section of the member according to TUE et al. [Tue-2014]

4.2 Behaviour of concrete members under cyclic shear loads

4.2.1 Experimental investigations under combined flexure and shear

Within shear tests under cyclic loading, the same cracking sequence can be observed for members with a potential flexure shear crack. For members with an upper stress level lower than monotonic critical diagonal cracking load, a flexural cracking occurs due to the applied upper load level. With increasing number of cycles, a gradual change in beam stiffness caused by cyclic creep and crack propagation is observed. However, the global damage of shear critical members under cyclic loading begins analogously to experiments under monotonic shear with the formation of critical diagonal crack [Cha-1958b].

In the past decades, the influence of cyclic loads on shear resistance of concrete beams has been studied in several experimental programmes within three- or four-point bending tests. The main objective of such tests was the evaluation of shear fatigue life, for which reason only the number of cycles to fatigue failure N_f are mainly provided.

A comprehensive experimental programme was conducted by CHANG / KESLER [Cha-1958b], which showed that with increasing number of load cycles, width and depth of existing primary cracks increase. The fatigue life depends beside the upper shear load level V_{sup} also on the ratio between lower and upper shear load level V_{inf} / V_{sup} . The tests of CHANG / KESLER were conducted under a constant shear span to depth ratio $a/d = 3.72$ but with variable load levels and longitudinal reinforcement ratios ρ_l . Based on stress level, different failure modes are often documented which include failure of longitudinal reinforcement, crushing of concrete along the critical diagonal crack (Figure 4-11, up) or increase in width of diagonal cracks and a subsequent diagonal tensile failure (Figure 4-11, down).

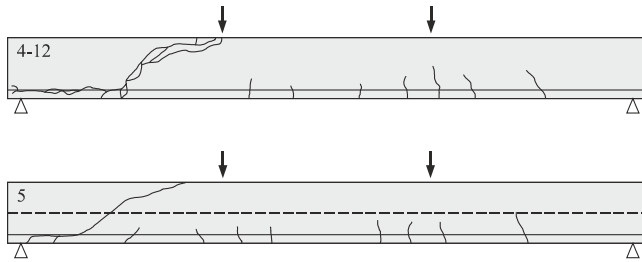


Figure 4-12: Fatigue failure due to concrete compression failure (up) or concrete diagonal tensile failure (down) according to CHANG / KESLER [Cha- b1958]

UEDA / OKAMURA [Ued-1982] conducted 16 tests on rectangular beams without shear reinforcement with a shear span to depth ratio of $a/d = 3.5$ and figured out a change in the location of critical diagonal crack x_{cr} , which affects the rate of crack propagation and the probability of fatigue failure. Based on the experimental investigation of UEDA / OKAMURA, a significant number of further load cycles can be applied after a diagonal cracking.

KOHL [Koh-2014] conducted twenty cyclic shear tests with a 3-point bending configuration, a constant shear span to depth ratio of $a/d = 5.0$ and a constant longitudinal reinforcement ratio $\rho_l = 1.57\%$. During the tests, the failure mode, crack path and inclination of critical diagonal crack as well as contribution of different load-bearing mechanism were evaluated. KOHL concluded that the path and inclination of diagonal crack do not change with the applied cycles and the main load-bearing mechanism can be attributed to concrete compression zone.

A review of above-mentioned experimental observations shows that the effects of cyclic loading on diagonal cracking and failure mode is more conspicuous for members with low shear span to depth ratios. The same conclusion was made HIGAI [Hig-1978], who conducted an experimental programme with different shear span to depth ratios. His observations confirmed the fact that depending on shear slenderness, additional load cycles can be applied after critical diagonal cracking until ultimate failure. The failure mode is in such cases due to a failure of compressive strut. The difference between number of cycles to diagonal cracking N_{cr} and number of cycles to failure N_f changes therefore based on the proceeding failure mode, which can be caused by failure of compressive strut or a tensile failure due to diagonal cracking (compare Figure 4-13).

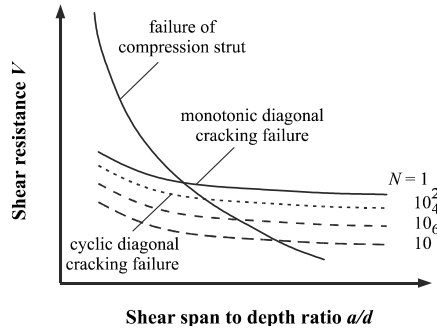


Figure 4-13: Influence of shear span to depth ratio on failure mode under cyclic shear [Hig-1978]

4.2.2 Mechanical approaches for evaluation of cyclic diagonal cracking load

For an explicit evaluation of the diagonal cracking under cyclic loads, the stress state after cyclic damage should be considered for derivation of the diagonal tension caused by shear. The resulted diagonal tensile stress should be afterwards limited to tensile strength of damaged concrete. The stress state is also affected by changes in concrete strength and damage of bond between concrete and longitudinal reinforcement. Such damage phenomena are included in the model according to MAEKAWA et al. [Mae-2006], [Fuj-2013], [Geb-2008], which considers a reduction of stiffness due to accumulation of plastic damage in the concrete compression zone, a change of the bond behaviour under cyclic loading and a decrease of the aggregate interlock present at diagonal crack faces. Similar phenomena are also considered in the model according to PFANNER [Pfa-2003]. This model is suitable for a numerical investigation of the load-bearing and the deformation behaviour of members under consideration of cyclic damage [Koh-2014], is however too complex for an analytical solution. Most of the existing models, including the above-mentioned ones focus on shear failure state and degradation phenomena acting on a diagonally cracked member. Therefore, the influence of cyclic loading on the resistance of concrete to diagonal tension is often disregarded or considered inadequately.

To have mechanically reasoned closed-form analytical models for diagonal cracking, a group of approaches are available, which are based on linear elastic fracture mechanics (LEFM). The basic equation of such models is the PARIS / ERDOGAN law, which emphasizes that based on stress intensity ΔK at crack tip and fracture toughness K_{Ic} , an existing crack propagates with respect to number of applied cycles N . The PARIS / ERDOGAN law is defined originally for ductile materials such as steel and was adapted by BAŽANT [Baž-1991] for application to quasi-brittle materials such as concrete. The change of crack length l_{cr} per load cycle is determined using Eq. 4-30 under consideration of size effect constant parameter (by the constant C in Eq. 4-30).

$$\frac{dl_{cr}}{dN} = C \cdot \left(\frac{\Delta K}{K_f} \right)^m \quad \text{Eq. 4-30}$$

The constant values of C and m should be determined based on experimental evidence and an assumed shape for the crack. On the basis of this equation, a mechanically reasoned equation (Eq. 4-31) was proposed by GALLEGO et al. [Gal-2014], [Rui-2015].

$$\log N_{cr} = A \cdot (1 - S_{sup})^B \left(\frac{\sigma_{1,sup}}{f_{ct,ef}} \right)^C \quad \text{Eq. 4-31}$$

In this equation, the upper stress level $\sigma_{sup,1}$ is determined as follows:

$$\sigma_{1,sup} = \frac{2}{3} \cdot \frac{V_{sup}}{b \cdot h_{ef}} \quad \text{Eq. 4-32}$$

The constants A , B and C was fitted to a database with documented number of cycles to diagonal cracking equal to $A = 3.01$, $B = -0.08$ and $C = -0.99$, which is a weak point of this model.

Although the effects of crack propagation in macroscale are considered in this model, the cyclic creep phenomenon is not acknowledged. The cyclic creep is mainly caused by growth of subcritical microcracks and was studied by BAŽANT / HUBLER [Baž-2014] based on PARIS / ERDOGAN law for cyclic compressive loading. A superposition of attained equations for macrocrack propagation and growth of subcritical cracks is however not possible, as the stress intensity ΔK differs for different crack shapes.

4.3 Concluding remarks

Diagonal tension caused by shear was analysed based on available experimental and theoretical investigations in the literature. It can be stated that critical diagonal cracking is an important cracking stage as it specifies the initiation of global damage in shear critical members. For members with a potential flexure shear crack, effects of interacting flexure and shear caused by primary cracks should be considered on the stress state at critical diagonal cracking. Major influencing parameters such as longitudinal reinforcement ratio (ρ_l), width (b) and effective depth (d) of the beam and shear span to depth ratio (a/d) affect the diagonal tension at the state of diagonal cracking. Hence, a reliable mechanical model should account for such major influencing parameters.

Existing mechanically based approaches for evaluation of monotonic diagonal cracking load $V_{cr,cal}$ were introduced. It should be noted that only comparable approaches are selected, which are derived under consideration of existing primary cracks in a section without diagonal cracks. In such approaches, the calculated diagonal tensile stress is limited to concrete tensile strength.

Diagonal cracking under monotonic and cyclic loading

Experimental and theoretical evaluations of diagonal cracking under cyclic loading are rather limited in the technical literature. The available mechanical approaches are mainly based on LEFM, which demand a data fitting and depend on the assumed shape of crack. Therefore, a concurrent consideration of macrocrack propagation and growth of subcritical microcracks is not possible. Comprehensive analytical mechanically based approaches, which consider both microcrack and macrocrack propagation are missing.

5 Database of shear tests

5.1 General remarks and selection criteria

The discussed physical mechanisms of diagonal cracking in chapter 3 are based mainly on existing shear tests on reinforced and prestressed concrete members. The available experimental evidence has been previously implemented to derive several empirical and semi-empirical approaches for the evaluation of diagonal cracking load and ultimate shear resistance. The test data are also commonly used for validation of existing mechanical approaches. Since there is still no generally accepted mechanical approach for the evaluation of shear resistance, several shear tests are available and would also be conducted in the future.

To cover a wide range of influencing parameters and test setups, numerous databases of beam tests under monotonic and cyclic loading are already built up (e.g. in [Rei-2012], [Col-2008], [Gal-2014], [Koh-2014]). In case of monotonic tests, it was found that a large part of these tests are already included in the ACI-DAfStb database [Rei-2012], which was created by the joint work of DAfStb and ACI Subcommittee 445-D and is continuously updated and controlled [Dun-2018]. The number of shear tests under cyclic loading is limited and covered by most of existing databases. For the evaluation of concrete tensile capacity, however, the value of diagonal cracking load should be provided, which is not documented in most databases. Furthermore, for investigation of effects of cyclic loading on the concrete tensile capacity, shear tests with an upper shear load level V_{sup} beneath the diagonal cracking load and documented number of cycles to diagonal cracking N_{cr} are required. To have uniform datasets with reliable test data, a database was developed under consideration of the following criteria:

- Concrete members (RC and PC) with rectangular cross-section without shear reinforcement
- Shear tests under point loads not applied near support (shear span to depth ratio $a/d \geq 2.0$)
- No plain longitudinal reinforcement bars

The developed database includes

- Shear tests on reinforced concrete (RC) beams under monotonic load (mRC),
- Shear tests on prestressed concrete (PC) beams under monotonic load (mPC) and
- Shear tests on reinforced concrete (RC) beams under cyclic load (cRC).

The prestressed members (PC) in mPC subset were prestressed with straight tendons without additional longitudinal tensile reinforcement for both prestressed and post-tensioned types of prestressing.

An overview of the tests in the database and the constellation of datasets is given in upcoming chapter. The detailed database is documented in Appendix C.

5.2 Overview on database

For the development of shear database, after an extensive literature review, datasets in ACI-DAfStb database were supplemented with some new tests, experimental diagonal cracking loads $V_{cr,exp}$ and definition of critical diagonal cracking (compare chapter 4). Besides, diagonal crack paths (in general failure crack path) were documented using existing pictures or sketches.

For mRC datasets, the diagonal cracking load was provided for 204 tests (mRC-V) from 1190 existing datasets compiled in ACI-DAfStb database. For 308 tests, some available detail on diagonal crack path regarding measured distance of diagonal crack from support or failure crack paths were documented (mRC-D). The first group includes tests in [Bha-1968], [Bre-1963], [Dia-1960], [Kre-1966], [Mat-1963], [Moo-1954], [Mor-1956], [Van-1962], [Xie-1994], [Sch-2014], [Slo-2014], which are mainly used for theoretical investigation of diagonal cracking load. As most of introduced approaches in chapter 4.1.5 are based on members without longitudinal reinforcement in compression zone, only such tests are included in mRC-V subsets. The second subset mRC-D is evaluated in the present chapter to investigate influencing factors on shape of the critical diagonal crack.

The number of datasets in mPC subset of database is rather limited, as only for 47 tests in [Kar-1969] and [Söz-1957] diagonal cracking loads were provided. These references do not provide any information on shape or location of the critical diagonal crack.

For the evaluation of cyclic tensile capacity of concrete under shear, a total number of 204 datasets of existing cyclic shear tests on reinforced concrete members (cRC) are collected in a database. As only shear tests with upper shear load V_{sup} below the calculated diagonal cracking load $V_{cr,cal}$ comply with the aim of the evaluation, the proposed model in the following chapter is used for calculation of monotonic diagonal cracking load $V_{cr,cal}$ and compared with the experimental upper shear load level $V_{sup,exp}$. This condition is only fulfilled for 161 datasets, from which only for 57 datasets, the number of cycles to diagonal cracking N_{cr} are documented.

As two different cracking loads are reported in right and left shear spans in some references, the shear database was checked to make sure that no dataset belongs to a single shear test and the first critical diagonal cracking is considered. This criterion can be justified with the fact that after a critical diagonal cracking in one shear span, the load redistribution might result in inaccurate determination of diagonal cracking load from applied load magnitude by hydraulic jacks. This condition reduced the number of cRC datasets

to 39 tests documented in [Cha-a1958], [Zan-2008], [Koh-2014]. For 15 tests, details could be found on shape and location of critical diagonal crack.

The number of tests in the mRC-V, mPC and cRC datasets are illustrated in Figure 5-1 with regard to influencing factors such as shear span to depth ratio a/d , longitudinal reinforcement ratio ρ_l , compressive strength f_c and relative effective depth d/d_0 . For the evaluation of relative effective depth, the reference value $d_0 = 200$ mm is chosen in conformity with DIN EN 1992-1-1.

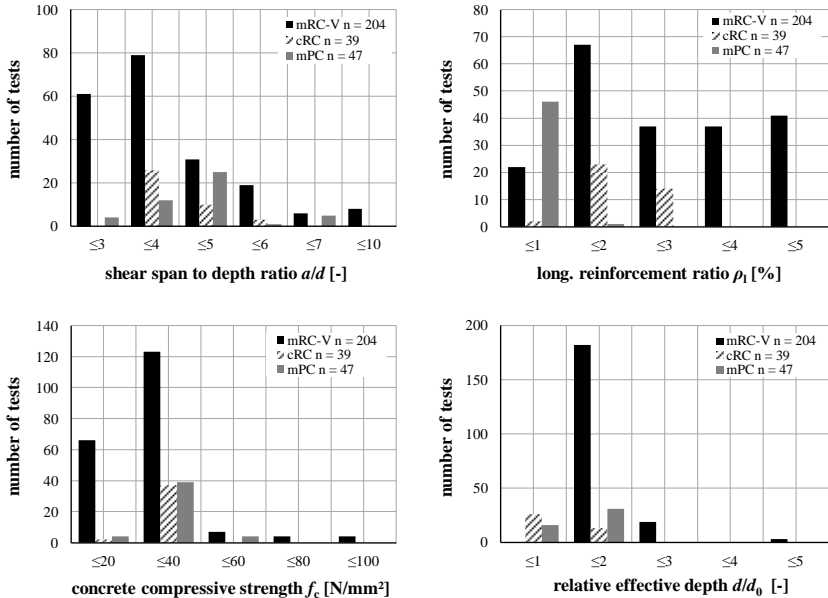


Figure 5-1: Number of tests with regard to shear span to depth ratio a/d (up, left), longitudinal reinforcement ratio ρ_l (up, right), concrete compressive strength f_c (down, left) and relative effective depth d/d_0 (down, right)

Based on the distribution of major influencing parameters of datasets, it can be noted that in mRC-V subset the major proportion of tests are conducted with a shear span to depth ratio between 2 and 4 on normal concrete beams. A meaningful statement about the effects of beam depth on diagonal cracking load is not possible based on available datasets, as the effective depth of most tests is limited to 400 mm. For cRC database, the effect of concrete strength cannot be thoroughly evaluated as all beams have a compressive strength between 30 and 40 N/mm². The longitudinal reinforcement ratios of mRC-V and cRC beams are also higher than 2% for almost the half of available datasets and therefore higher than the practical value of longitudinal reinforcement ratio. This tendency is common in shear tests, in order to avoid an unfavourable flexural failure within cyclic shear

tests. In mPC subset, generally higher shear span to depth ratios are investigated in comparison to RC beams. Additionally, the type of prestressing (post-tensioned or prestressed) and relative prestressing force (σ_{cp}/f_c) are further significant parameters for such members, which are provided in Figure 5-2.

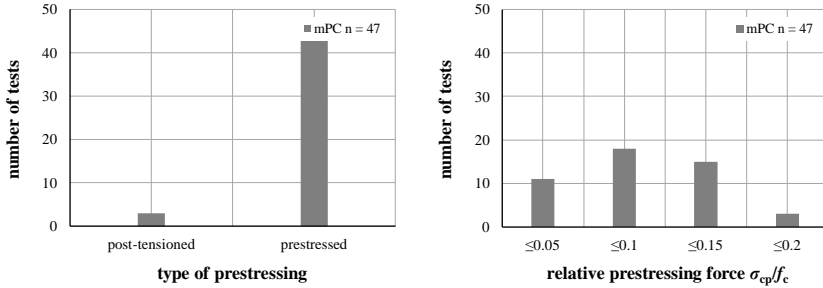


Figure 5-2: Number of mPC tests with regard to type of prestressing (left) and relative prestressing force σ_{cp}/f_c (right)

Most of the tests are conducted on prestressed members and with the maximum prestressing ratio of 20 % of the concrete compressive strength f_c .

For members in cRC subset, further decisive parameters are upper and lower tensile stress levels $\sigma_{1,sup}/f_{ct}$ and $\sigma_{1,inf}/f_{ct}$ during the cyclic loading. These values are determined using the calculated principal tensile stress σ_1 calculated based on the mechanical approach that will be proposed in chapter 6. The distribution of these two parameters is illustrated in Figure 5-3 for the sake of completeness.

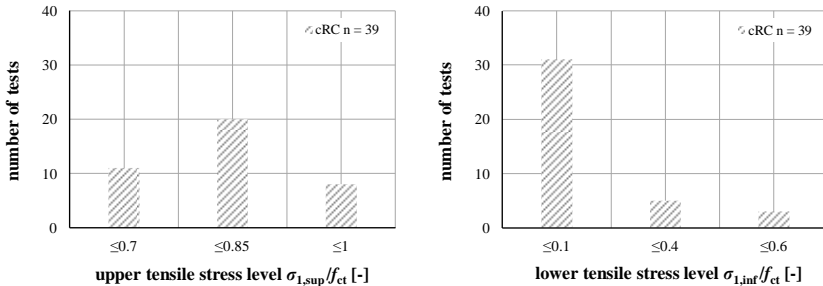


Figure 5-3: Number of cRC tests with regard to upper $\sigma_{1,sup}/f_{ct}$ (left) and lower tensile stress level $\sigma_{1,inf}/f_{ct}$ (right)

Based on this overview, a major part of tests (~78 %) in this subset were conducted with a $\sigma_{1,inf}/f_{ct}$ smaller than 10 % of concrete tensile strength and the upper stress levels ratios cover a range between 70 % and 93 %.

5.3 Location and shape of critical diagonal crack

Location of the critical diagonal crack is provided as the distance of diagonal crack from support axis $x_{cr,exp}$ [Rei-2012]. This value is determined as the distance of a characteristic point M, where the critical diagonal crack crosses the centreline of the member (CL).

According to mechanical considerations based on principal tensile stress σ_1 , the theoretical depth of maximum shear stress locates at the neutral axis of the specimen with the depth h_c . If the assumptions of TB are regarded as valid in the state of diagonal cracking, the point with a crack inclination equal to 45° comply with the experimental depth of maximum shear stress h_λ . This point was also evaluated by HOLZ in a crack database [Hol-2014]. The location of two characteristic points as illustrated in Figure 5-4 are documented in mRC-D subset.

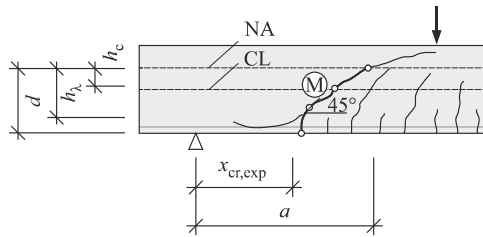


Figure 5-4: Characteristic points defining the shape and location of critical diagonal crack

The location of critical crack is evaluated as relative value in comparison to effective depth of the member. The correlation of the relative location of diagonal crack $x_{cr,exp} / d$ and shear span to depth ratio as well as longitudinal reinforcement ratio were evaluated by means of Figure 5-5.

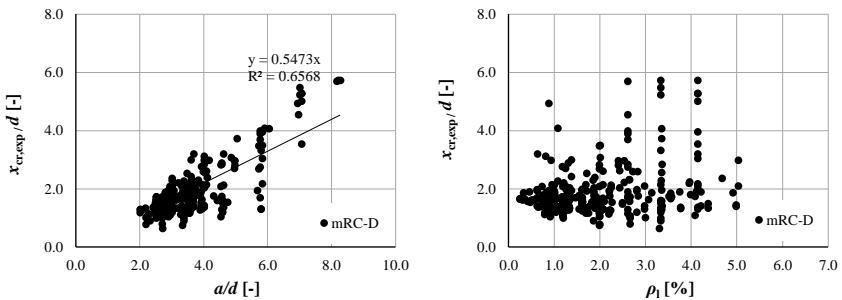


Figure 5-5: Correlation between x_{cr} shear span to depth ratio a/d (left) as well as longitudinal reinforcement ratio ρ_l (right)

It is apparent from the comparison that the location of critical diagonal crack is mainly influenced by shear span to depth ratio and can be approximated using a linear correlation. Similar results are also obtained in [Rei-2012], in which the crack distance from support axis is approximated as $0.5 \cdot a$. This value is also adapted for further calculation in chapter 6.

$$x_{cr,appr,RC} = 0.5 \cdot a \tag{Eq. 5-1}$$

It is worth noting, that the regression-based approximation of x_{cr} according to Eq. 5-1 is only possible with a coefficient of determination $R^2 = 0.65$. The high scatter is justified by other secondary influencing parameters such as concrete inhomogeneity, concrete resistance to splitting at level of flexural tensile reinforcement (combination of dowel action forces and concrete strength) as well as beam depth.

The experimental depth of maximum shear stress h_λ (depth, where primary cracks rotate toward an inclination of 45°) is calculated relative to calculated depth of neutral axis h_c . The correlation between h_λ/h_c and shear span to depth ratio as well as longitudinal reinforcement ratio are illustrated in Figure 5-6.

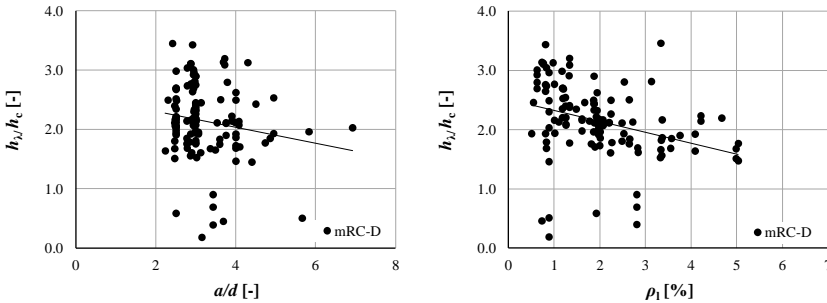


Figure 5-6: Correlation between h_λ and shear span to depth ratio a/d (left) as well as longitudinal reinforcement ratio ρ_l (right)

Based on the comparison of existing correlations, it can be concluded that h_λ correlates with both longitudinal reinforcement ratio and shear span to depth ratio. The experimental depth of maximum shear stresses h_λ is larger than the calculated depth of neutral axis h_c in almost all cases. It confirms also the common experimental observations, which points out that the stress state at diagonal cracking is affected by the primary cracks [Kan-1979], [Rei-1990].

It is worth noting that provided sketches of the shape of diagonal crack illustrate often the failure crack profiles, which is affected by formation of splitting cracks in the vicinity of longitudinal reinforcement due to bond loss shortly before failure (compare Figure 5-4). So, the first point from tensile extreme fibre of the beam cannot be regarded as the point at which the diagonal crack initiates. A reliable evaluation of shape of critical

diagonal crack is only possible under consideration of cracking sequence. The shear tests of CAVAGNIS [Cav-2017], [Cav-2017] can be regarded as detailed documented tests with regard to cracking sequence, which were conducted on cantilever beams with a constant longitudinal reinforcement ratio and variable shear span to depth ratios. A sample beam of this test series with a shear span to depth ratio $a/d = 5.7$ is depicted in Figure 5-7.

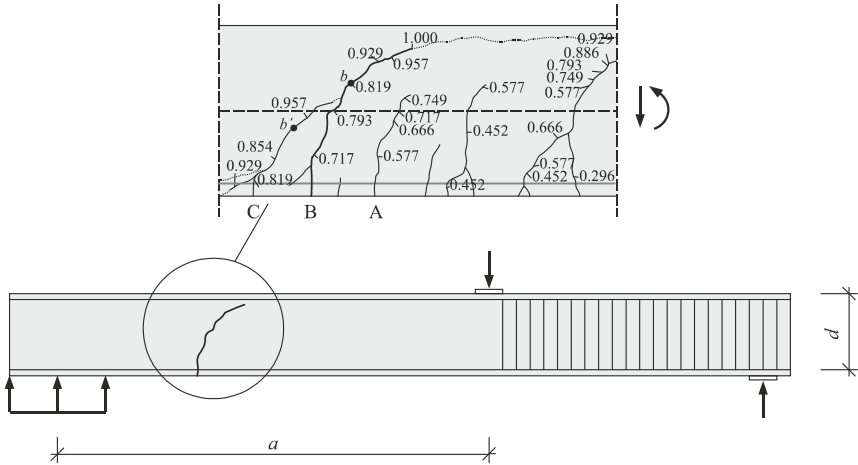


Figure 5-7: Crack propagation provided as relative load V/V_u during shear test SC 69 conducted by CAVAGNIS [Cav-2017]

It can be observed that primary crack B reaches the level of longitudinal reinforcement after a full development of antecedent crack (A) under a shear load corresponding to $0.717 \cdot V_u$. A gradual development of the crack toward point M is documented until $0.793 \cdot V_u$. Shortly before the crack reaches the neutral axis of the beam, a subsequent crack (C) forms and propagates toward the mid-depth of the beam under shear load of $0.819 \cdot V_u$. This crack forms with the crack B the failure shear crack with a significant crack opening. With regard to cracking sequence, the first point of the critical diagonal crack reaching an inclination of 45° is hence point b , which is almost equal to depth of concrete compression zone h_c , whereas an evaluation of shape of failure crack results in a higher value of h_λ from point b' .

Based on this example, it is evident that an evaluation of h_λ based on the shape of failure crack is not appropriate and further detailed crack documentations are needed for a better understanding about the mechanisms governing the critical diagonal cracking and experimental depth of maximum shear stress.

5.4 Evaluation of diagonal cracking load

The documented experimental values of diagonal cracking load $V_{cr,exp}$ in subset mRC-V are evaluated based on main influencing parameters shear span to depth ratio a/d , longitudinal reinforcement ratio ρ_l , compressive strength f_c and relative effective depth d/d_0 . The ratio between diagonal cracking load and the theoretical calculated value according to TB (Eq. 4-8) are used for the evaluation. Figure 5-8 illustrates the dependency between $V_{cr,exp}/V_{cr,TB}$ and the major influencing parameters.

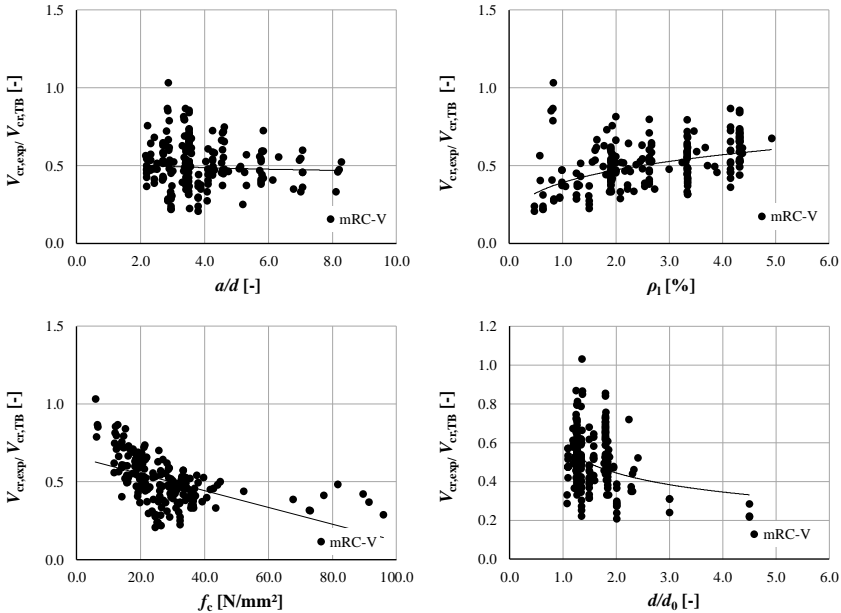


Figure 5-8: Correlation between experimental and theoretical diagonal cracking load with regard to shear span to depth ratio a/d (up, left), longitudinal reinforcement ratio ρ_l (up, right), concrete compressive strength f_c (down, left) and relative effective depth d/d_0 (down, right)

Based on the observations, a clear tendency can be figured out between $V_{cr,exp} / V_{cr,TB}$ and the longitudinal reinforcement ratio ρ_l as well as concrete tensile strength f_{ct} . This means that for derivation of a mechanical approach based on the assumption of technical bending theory, a modification with respect to these two parameters is necessary.

The difference between diagonal cracking load and ultimate shear load can be used as a criterion to quantify the prior notice of the shear critical members. The correlations between major influencing parameters and the ratio between diagonal cracking load and ultimate shear load are depicted in Figure 5-9.

Based on this evaluation, it can be concluded that a sudden failure at the state of diagonal cracking depends on the shear span to depth ratio and beam depth, whereas the lack of experimental evidence on cracking of deep beams make a reliable statement difficult. However, it gets apparent that beams with a shear span to depth ratio $a/d > 4.0$ fail after an insignificant increase of applied shear load due to diagonal cracking. This can be reasoned by likely formation of a direct compressive strut in case of smaller a/d , which prohibits a sudden failure direct after critical diagonal cracking.

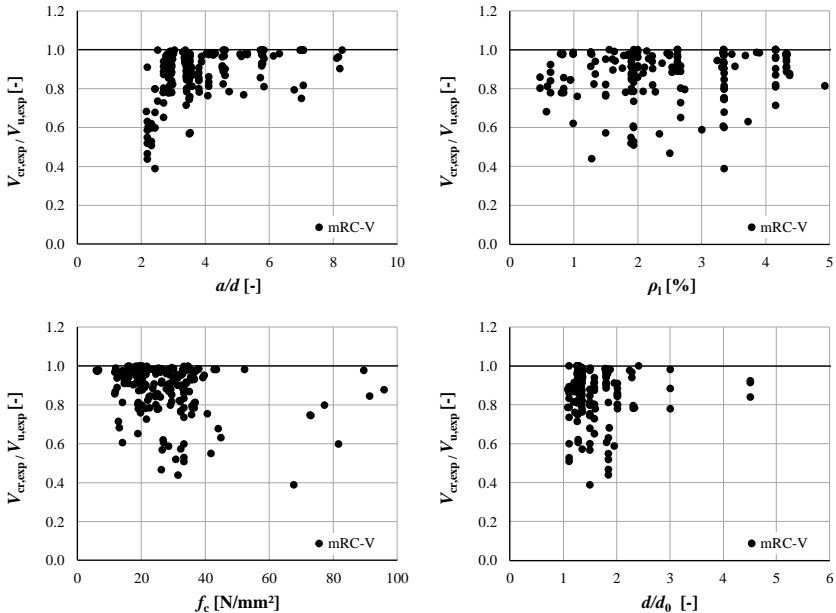


Figure 5-9: Correlation between experimental diagonal cracking load and ultimate shear load with regard to shear span to depth ratio a/d (up, left), longitudinal reinforcement ratio ρ_l (up, right), concrete compressive strength f_c (down, left) and relative effective depth d/d_0 (down, right)

5.5 Concluding remarks

A shear database was compiled to evaluate the available mechanical approaches as introduced in chapter 4. Selection criteria and an overview of the distribution of datasets regarding major influencing parameters in shear database was given in this chapter. It could be seen that the number of tests on RC members under monotonic load mRC with provided diagonal cracking load and information on shape and location of critical diagonal cracks are comparably limited. Following conclusions can be made based on evaluation of existing datasets:

- Comparison of experimental diagonal cracking loads with the approach according to TB showed that for an appropriate mechanically based model, an adaption of basic equation of TB with regard to concrete strength and longitudinal reinforcement ratio is required.
- Comparing diagonal cracking loads and ultimate shear loads, it is evident that a failure short after diagonal cracking is more probable for members with higher shear slenderness than $a/d = 4.0$.
- The proposed correlation in [Rei-2012] between the distance of failure crack from support axis $x_{cr,exp}$ and shear slenderness was confirmed.
- To evaluate the shape of the critical diagonal crack, the point with a crack inclination equal to 45° was evaluated as experimental depth of maximum shear stresses h_λ and compared with the calculated value h_c . It could be shown that an evaluation of h_λ based on failure crack profiles can be misleading.

6 Diagonal cracking load under monotonic and cyclic shear

6.1 General remarks

In this chapter, an analytical approach for the investigation of diagonal cracking load under monotonic and cyclic loading is proposed. In a first step, the introduced mechanical models in section 4.1.5 are evaluated using monotonic tests of shear database on reinforced concrete members (mRC). Based on the evaluations, an appropriate model is selected and modified for a better prediction of the diagonal cracking load. The modified model is afterwards adjusted for the evaluation of the diagonal cracking load of pre-stressed members under monotonic loading and for diagonal cracking under cyclic loads. The adapted models would be verified using shear tests in mPC and cRC subsets of shear database, respectively.

6.2 Monotonic diagonal cracking load of RC members

6.2.1 General approach

Experimental verification of the introduced mechanical approaches in chapter 4 is based on documented monotonic shear tests in mRC-V subset of the shear database. For this aim, the calculated and experimental values of the diagonal cracking load are compared. To quantify the prediction accuracy of each model, a model safety factor γ_{mod} is calculated for each test using the following equation:

$$\gamma_{\text{mod}} = \frac{V_{\text{cr,exp}}}{V_{\text{cr,cal}}} \quad \text{Eq. 6-1}$$

The values of γ_{mod} are considered as logarithmic-normally distributed for calculation of median m , variance v and standard deviation s .

As the experimental tensile strength values are not provided for all datasets, the considered concrete tensile strength $f_{\text{ct,cal}}$ is calculated based on provided concrete compressive strength f_c . This enables a uniform evaluation of test results disregarding the detail level of provided experimental data.

The originally assumed concrete tensile strength in each model was considered for the calculations. In the model according to HONG / HA [Hon-2012], the concrete tensile strength is assumed equal to the splitting tensile strength, which is calculated according to the proposed correlation by NIELSEN [Nie-1999]:

$$f_{\text{ct,sp}} = \sqrt{0.1 \cdot f_c} = 0.316 \cdot \sqrt{f_c} \quad \text{Eq. 6-2}$$

The value of concrete compressive strength in this equation is the mean value of concrete compressive strength.

Diagonal cracking load under monotonic and cyclic shear

According to GALLEGO et al. [Gal-2014], the failure criterion should be defined based on concrete flexural tensile strength $f_{ct,fl}$ under consideration of lateral compressive stress σ_2 as follows:

$$f_{ct,fl} = f_{ct} \cdot \left(1.6 - \frac{h}{1000}\right) \cdot \left(1 - \frac{\sigma_2}{f_c}\right) \quad \text{Eq. 6-3}$$

For the calculation according to Eq. 6-3, an isotropic stress state is considered ($\sigma_1 = \sigma_2$) at the state of diagonal cracking.

In the model of TRAN et al. and TUE et al., the value of concrete tensile strength is determined using the correlation of DIN EN 1992-1-1 as:

$$f_{ct,cal} = \begin{cases} 0.3 \cdot (f_c - 4)^{2/3} & \text{for } f_c \leq 54 \\ 2.12 \cdot \ln\left(1 + \frac{f_c}{10}\right) & \text{for } f_c > 54 \end{cases} \quad \text{Eq. 6-4}$$

In Eq. 6-4 is the characteristic value of concrete compressive strength f_{ck} is replaced by $f_c - 4$ as recommended in [Rei-2012] for tests in laboratory condition.

From the discussed approaches in section 4.1.5, the model according to TUE et al. is not considered as a mechanical approach, since the critical shear band width needs to be calculated based on an empirical equation.

In the model according to GALLEGO et al., no equation is provided for the calculation of σ_c , which considers the effect of bending moment M on the depth of primary cracks and the effective depth of the member h_{ef} . To determine σ_c , the simplified Eq. 6-5 (according to [Zil-2010]) is considered.

$$\sigma_c = \frac{M}{b \cdot d^2 \cdot \xi/2 \cdot (1 - \xi/3)} \quad \text{Eq. 6-5}$$

The value ξ determines the relative depth of flexural compression zone h_c , which can be evaluated using Eq. 4-16.

In the model proposed by TRAN, the strain of tensile bending reinforcement (Eq. 4-21) is calculated based on the curvature of the beam κ . The proposed correlation for determining beam curvature κ is based on the same equilibrium condition of normal sectional forces and corresponds to:

$$\kappa = \frac{2 \cdot M}{E_c \cdot b \cdot d^3 \cdot \xi^2/2 \cdot (1 - \xi/3)} \quad \text{Eq. 6-6}$$

The value of bending moment is calculated at the critical section. The critical section is considered to be at the site of critical diagonal crack with the distance x_{cr} from support axis (compare point M in Figure 5-4), which is provided for 82 tests in mRC-V, no tests in mPC and 15 tests in cRC subsets. In other cases, the location of critical diagonal crack

is calculated based on Eq. 5-1 for RC members. For datasets in mPC subset, the proposed correlation in [Rei-2012] is implemented for an approximation of critical section.

$$x_{cr,apr,PC} = 0.65 \cdot a \tag{Eq. 6-7}$$

6.2.2 Evaluation of mechanical approaches

Using mRC-V subset, the calculated values of diagonal cracking loads $V_{cr,cal}$ are compared with experimental values $V_{cr,exp}$ for the basic theoretical value according to TB and the models according to HONG / HA, GALLEGO et al. and the model according to TRAN et al.. The results are illustrated in Figure 6-1.

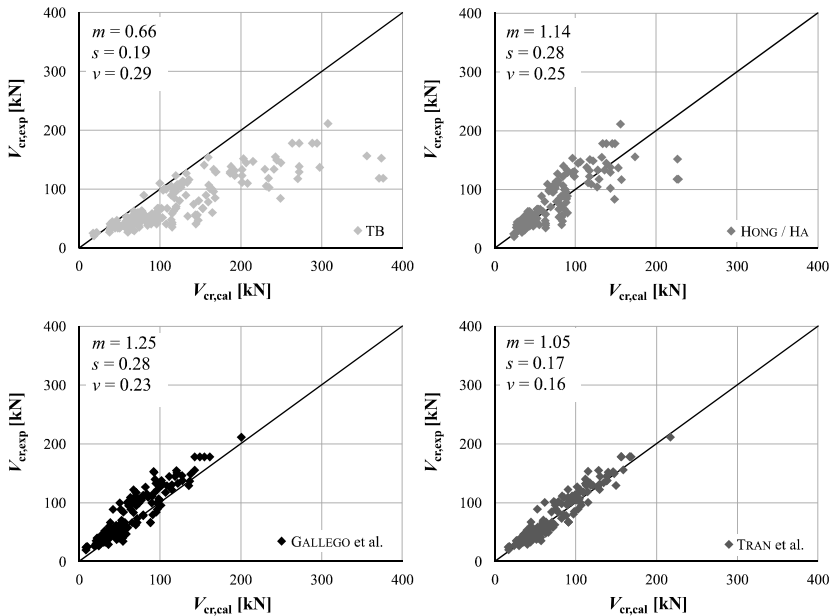


Figure 6-1: Comparison of experimental diagonal cracking loads with calculated values using models according to TB, HONG / HA [Hon-2012], GALLEGO et al. [Gal-2014] and TRAN et al. [Tra-2015]

Results of the evaluation show that as mentioned before, the basic equation of TB overestimates the diagonal cracking load and should be adapted to consider the primary cracks. An adjustment based on the model of HONG / HA provides a good approximation in terms of the mean value of the model safety factors. However, the relative high variation coefficient of 25% and a larger scatter for higher values of diagonal cracking load are observed. The same can be concluded for the model according to GALLEGO et al., although this model shows a better prediction for all ranges of diagonal cracking load. The model according to TRAN et al. provides the best prediction. For a more detailed

evaluation of approaches, the level of integrity of major influencing parameters (shear span to depth ratio a/d , longitudinal reinforcement ratio ρ_l and concrete compressive strength f_c) in each model is evaluated based on the correlation between model safety factors γ_{mod} and the corresponding influencing parameter of each dataset. Figure 6 2 depicts the level of integrity of a/d in the models. As shown in chapter 5, the value of a/d affects the distance of critical section from the support axis. In order to distinguish between detail level of each dataset with regard to the location of critical section x_{cr} , the γ_{mod} values datasets with experimental measured x_{cr} and approximated values of x_{cr} are marked differently.

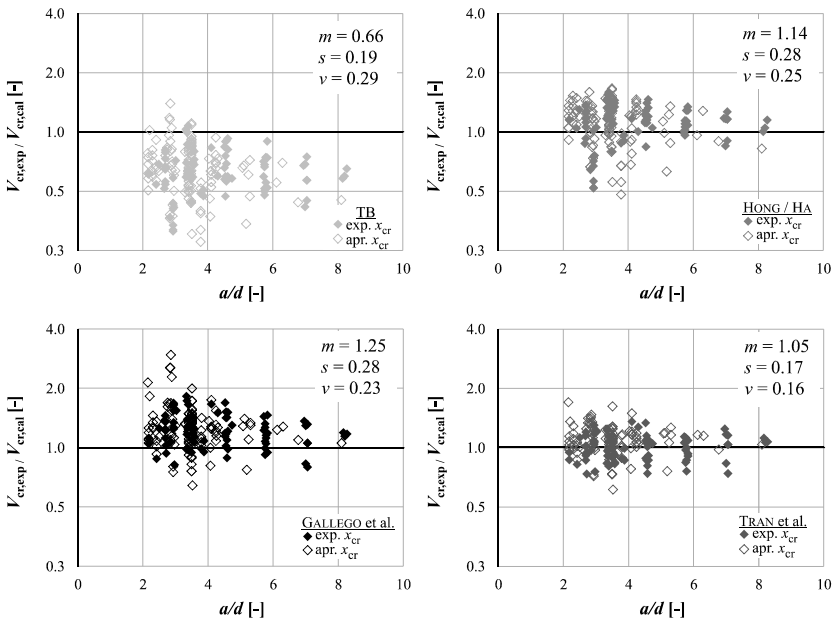


Figure 6 2: Correlation between shear span to depth ratio a/d and safety factors of models according to TB, HONG / HA [Hon-2012], GALLEGO et al. [Gal-2014] and TRAN et al. [Tra-2015]

Except for the models according to TB and HONG / HA, other models include the effect of shear span to depth ratio due to defined critical section x_{cr} . The model safety factors show a lower scatter for datasets with approximated x_{cr} values. However, inclusion of critical section in the model does not necessarily enhance the prediction accuracy of the model (compare model according to GALLEGO et al. with Model according to TRAN).

Comparing the integrity level of longitudinal reinforcement ratio ρ_l according to Figure 6-3, it is evident that the model according to HONG / HA does not include the effects

of longitudinal reinforcement ratio, as the effective depth h_{ef} is kept constant (equal to effective depth of longitudinal tensile reinforcement d) for different values of ρ_l .

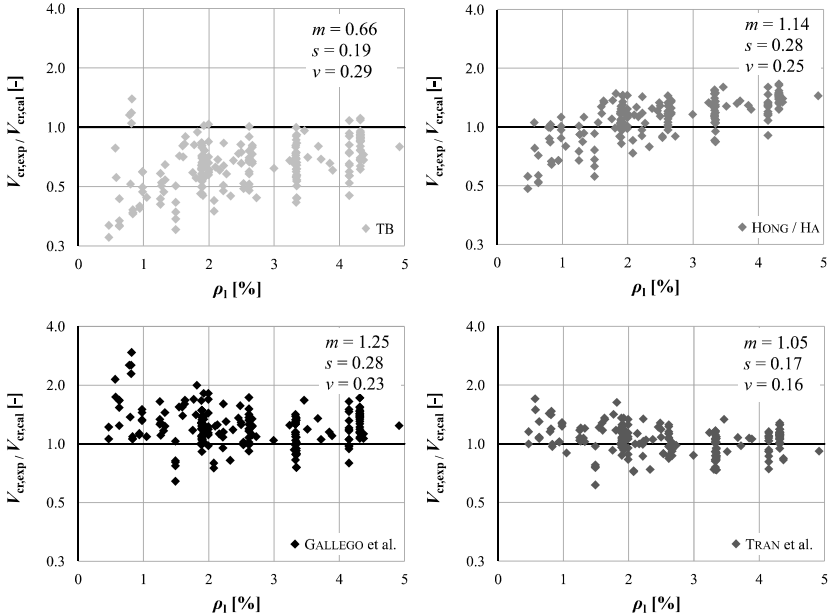


Figure 6-3: Correlation between longitudinal reinforcement ratio ρ_l and safety factors of models according to TB, HONG / HA [Hon-2012], GALLEGO et al. [Gal-2014] and TRAN et al. [Tra-2015]

To capture the influence of concrete tensile strength, the model safety factor is illustrated in Figure 6-4 depending on the concrete compressive strength f_c used for determination of $f_{ct,cal}$.

A more evident tendency between concrete strength and model safety factor can be observed especially for low values of concrete compressive strength for models, which consider a correlation according to uniaxial or flexural concrete tensile strength according to DIN EN 1992-1-1. For high-strength concrete beams, except for calculation according to TB, no correlation exists between the model safety factor and concrete strength: Due to this fact, it can be concluded that the calculated tensile strength corresponds in such cases with the available concrete tensile strength. This observation can also be made for the model according to HONG / HA with implemented splitting concrete tensile strength.

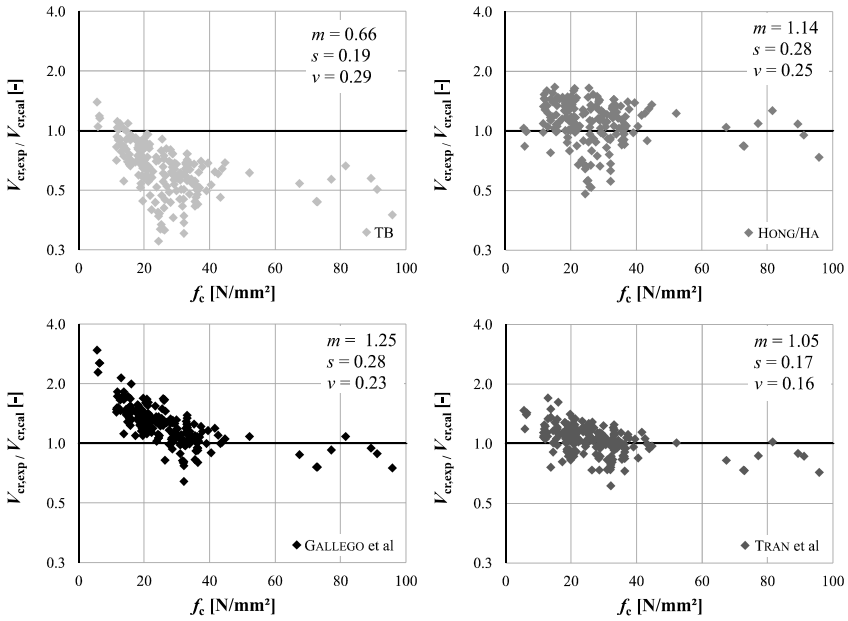


Figure 6-4: Correlation between concrete compressive strength f_c and safety factors of models according to TB, HONG / HA [Hon-2012], GALLEGO et al. [Gal-2014] and TRAN et al. [Tra-2015]

6.2.3 Modified mechanical model

Based on the previous investigations, a mechanical approach is selected and modified for a better prediction of diagonal cracking load under monotonic loads. For the selection of the model, the following criteria are considered:

- Adequate prediction accuracy for all ranges of diagonal cracking load
- Adequate consideration of major influencing parameters
- Clear mechanical parameters, which make the approach adaptable to PC members as well as to cyclically loaded members

The first two criteria are fulfilled by both approaches of GALLEGO et al. and TRAN et al.. However, due to existing knowledge gap on the effects of cyclic loading and prestressing on the tensile crack width $w_{cr,1}$ and the fracture energy G_F , the proposed model by GALLEGO et al. is selected for further modification. Based on the observed correlation between model safety factor and concrete compressive strength, the proposed equation for tensile strength calculation was kept constant for normal and high-strength concrete taking the proposed correlation of REINECK [Rei-2012] into account:

$$f_{ct,cal} = 1.115 \cdot (f_c - 4)^{1/3} \tag{Eq. 6-8}$$

Based on the main equation of model according to GALLEGO et al. and the selected correlation for determination of σ_c (Eq. 6-5) a closed-form solution can be proposed for determination of diagonal cracking load as follows:

$$V_{cr,cal} = \frac{2}{3} \cdot b \cdot h_{ef,mRC} \cdot f_{ct,cal} \tag{Eq. 6-9}$$

The value of effective depth for mRC members corresponds to:

$$h_{ef,mRC} = \frac{\xi \cdot d}{2} + \left(\frac{\xi^2 \cdot d^2}{4} + \frac{\xi^2 \cdot \left(1 - \frac{\xi}{3}\right) \cdot d^3}{\frac{2}{3} \cdot x_{cr}} \right)^{0.5} \tag{Eq. 6-10}$$

The resulting calculated diagonal cracking load $V_{cr,cal}$ with the modified proposed model (Eq. 6-9) is depicted in Figure 6-5. It is evident that the proposed model provides a more accurate prediction with a median value of γ_{mod} equal to $m = 1.01$ and a low variation coefficient $v = 0.13$. The agreement between calculated and experimental values can be justified by the integrity of major influencing parameters as illustrated in Figure 6-5. It is observed that the influence of shear span to depth ratio, longitudinal reinforcement ratio and concrete strength is considered adequately in the model.

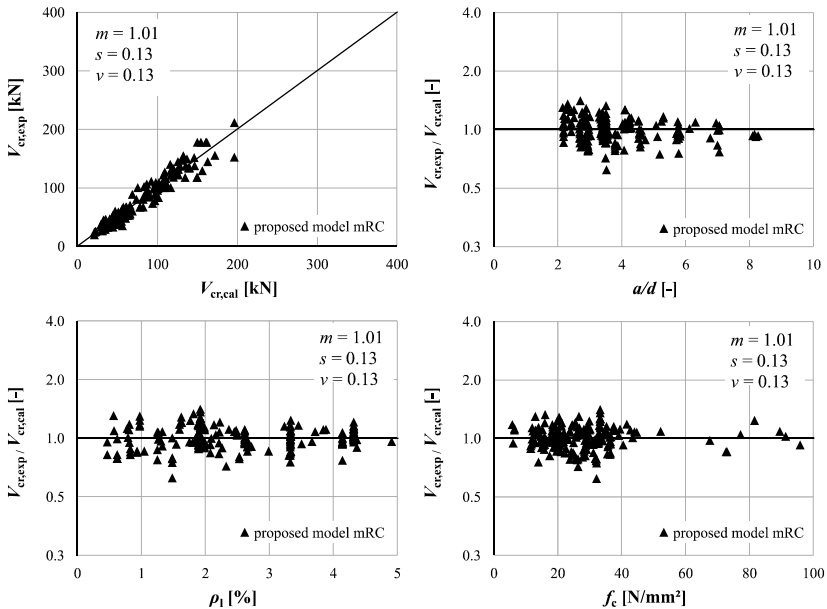


Figure 6-5: Comparison of experimental diagonal cracking loads with calculated values using proposed modification (up, left) and the correlation between model safety factors and a/d (up, right), ρ_l (down, left) as well as f_c (down, right)

6.3 Derived model for diagonal cracking of prestressed members

The modified model is adjusted for prestressed members under consideration of normal stresses caused by prestressing, which is superposed with the flexural normal stresses. Due to this superposition, the effective depth of the member $h_{ef,PC}$ is modified, which affects the calculated diagonal cracking load. The prestressing influences further the tensile failure criterion (compare 2.1.3) at the theoretical depth of maximum shear stress (assumed to remain at depth of neutral axis of the section), causing a significant change in concrete tensile strength (compare section 2.1.3). Additionally, the basic equation of proposed model should also consider the effects of lateral compressive stress using MOHR's circle of stresses (compare section 4.1.1).

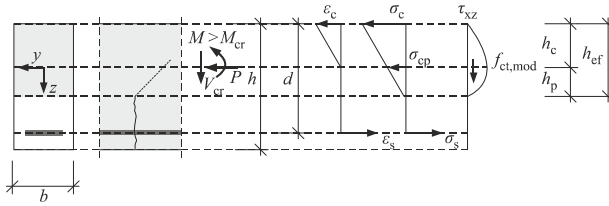


Figure 6-6: Normal and shear stress distribution over the cross-section of PC members according to proposed model

Accordingly, the calculated diagonal cracking load of a PC member with rectangular cross-section can be determined as follows:

$$V_{cr,cal} = \frac{2}{3} \cdot b \cdot h_{ef,mPC} \cdot f_{ct,mod} \cdot \sqrt{1 + \frac{|\sigma_{cp}|}{f_{ct,mod}}} \quad \text{Eq. 6-11}$$

The effective depth $h_{ef,mPC}$ consists of depth of compression zone of an equivalent non-prestressed member and an additional term due to prestressing represented as h_p . The influence of tensile zone h_{ct} is assumed negligible for prestressed members, since σ_{cp} is significantly higher than the concrete tensile strength.

$$h_{ef,mPC} = \xi \cdot d + h_p \quad \text{Eq. 6-12}$$

To account for the influence of lateral compressive stress on failure criterion for concrete, the modified tensile strength according to Eq. 2-16 was used considering a σ_2 equal to σ_{cp} for the sake of simplicity.

$$f_{ct,mod} = \frac{1 - \frac{|\sigma_{cp}|}{f_c}}{1 - \frac{f_{ct}}{f_c}} \cdot f_{ct,cal} \quad \text{Eq. 6-13}$$

The terms σ_{cp} corresponds to:

$$\sigma_{cp} = \frac{P}{b \cdot h_{ef,mPC}} \quad \text{Eq. 6-14}$$

The additional depth h_p can be calculated iteratively using the following equation:

$$\xi \cdot d \cdot |\sigma_{cp}| + \frac{\frac{2}{3} \cdot h_p \cdot (\xi \cdot d + h_p) \cdot x_{cr} \cdot \sqrt{f_{ct,mod}^2 + |\sigma_{cp}| \cdot f_{ct,mod}}}{d^2 \cdot \frac{\xi}{2} \cdot \left(1 - \frac{\xi}{3}\right)} = 0 \quad \text{Eq. 6-15}$$

To verify this model, the experimental diagonal cracking loads of members in mPC subset are compared with the calculated values $V_{cr,cal}$ according to Eq. 6-11 (compare Figure 6-7).

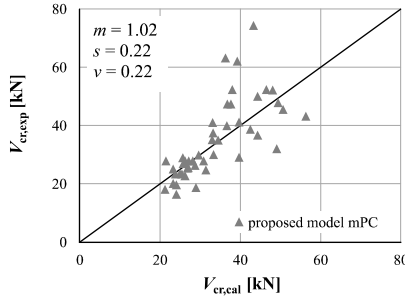


Figure 6-7: Comparison of experimental diagonal cracking loads with calculated values using the proposed model for mPC members

Based on the results, an estimation of the diagonal cracking load is possible for mPC datasets with the suggested model. However, in single cases, the diagonal cracking load is underestimated significantly. To figure out the origin of this deviation and for a better justification of comparably large scatter of results, the correlation between model safety factors and major influencing parameters for PC members (shear span to depth ratio a/d , longitudinal reinforcement ratio ρ_l , concrete compressive strength f_c and relative prestressing σ_{cp}/f_c) is depicted in Figure 6-8.

The comparison shows that except for the influence of shear span to depth ratio, further major influencing parameters are integrated satisfactorily in the model. The general underestimation of diagonal cracking load for low shear span to depth ratios $a/d < 3.0$ can be caused by the activation of arching action due to prestressing, which enables formation of a direct compressive strut between the loading point and the beam supports. Furthermore, the effect of a/d is considered in the model using the crack distance from support

axis x_{cr} , which is approximated for all mPC datasets. A better approximation of x_{cr} could probably improve the prediction accuracy of the new model for mPC members.

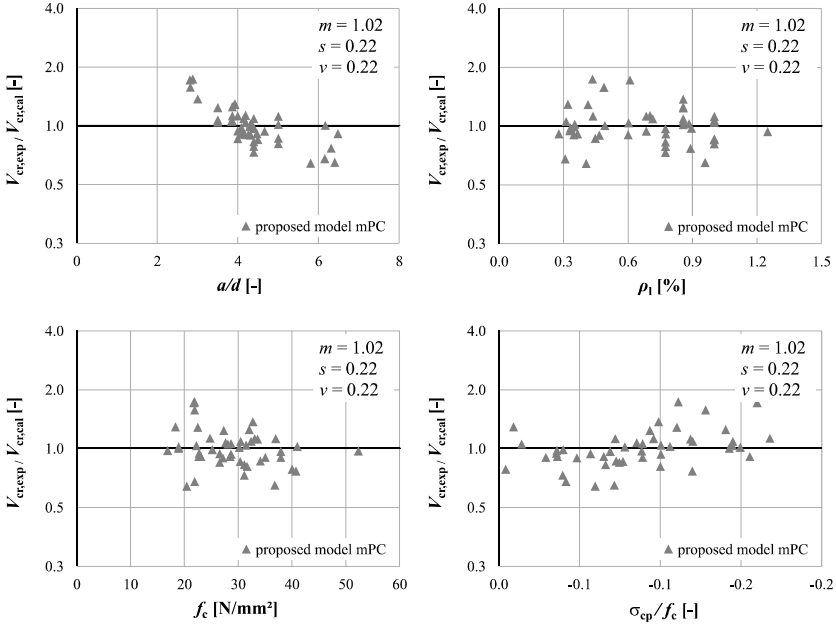


Figure 6-8: Correlation between safety factor of proposed model for mPC members and a/d (up, left), ρ_1 (up, right), f_c (down, left) as well as σ_{cp} / f_c (down, right)

6.4 Derived model for cyclic diagonal cracking

The proposed model for mRC members is adapted in this section for diagonal cracking under cyclic loading based on the phenomenological aspects of fatigue as discussed in chapters 2.2,3 and 4.2. The number of cycles to diagonal cracking is provided in cRC dataset. To consider the cyclic damage at the state of diagonal cracking $N = N_{cr}$, an unknown change of normal stress distribution is defined using a new relative depth of concrete compression zone $\xi_{N_{cr}}$. In the first loading cycle, the relative depth of compression zone ξ_1 can be calculated based on Eq. 4-16. At the state of cyclic diagonal cracking, the value of V_{sup} corresponds to diagonal cracking load, which is unknown and influences the compressive stress at the extreme fibre of the section.

$$\sigma_{c,sup,1} = \frac{V_{sup} \cdot x_{cr}}{b \cdot d^2 \cdot \xi_1 / 2 \cdot (1 - \xi_1 / 3)} \quad \text{Eq. 6-16}$$

Using the relative depth of compression zone under monotonic loading $\xi_1 = \xi$ at $N = 1$, the effective depth at the beginning of cyclic loading is equal to:

$$h_{ef,1} = \xi_1 \cdot d \cdot \left(1 + \frac{f_{ct}}{\sigma_{c,sup}} \right) \quad \text{Eq. 6-17}$$

Due to the cyclic normal stresses, the cyclic creep phenomenon causes a change in beam stiffness, which results in a modified effective depth $h_{ef,cRC}$. For a stationary evaluation of state of critical diagonal cracking, the damage effects should be integrated using a modified relative depth of concrete compression zone at diagonal cracking ξ_{Ncr} ($N = N_{cr}$). The stress distribution over the depth of cross-section is assumed to remain linear.

$$\xi_{Ncr} = \frac{h_{ef,cRC}}{d} \quad \text{Eq. 6-18}$$

Using $h_{ef,cRC}$, the lower principal tensile stress level can be calculated using:

$$\sigma_{1,inf,Ncr} = \frac{V_{inf}}{\frac{2}{3} \cdot b \cdot h_{ef,cRC}} \quad \text{Eq. 6-19}$$

With the lower principal tensile stress $\sigma_{1,inf,Ncr}$, the upper principal tensile stress $\sigma_{1,sup,Ncr}$ at the depth of neutral axis corresponds to fatigue tensile strength $f_{ct,fat}$, which is calculated using the proposed correlation by CORNELISSEN (Eq. 2-23). The diagonal cracking load of cRC members can hence be determined using the following equation:

$$V_{cr,cycl,cal} = \frac{2}{3} \cdot b \cdot h_{ef,cRC} \cdot f_{ct,fat} \quad \text{Eq. 6-20}$$

Furthermore, the effective depth $h_{ef,cRC}$ should fulfil the following equation:

$$h_{ef,cRC} = \xi_{Ncr} \cdot d \cdot \left(1 + \frac{f_{ct}}{\sigma_{c,sup,Ncr}} \right) \quad \text{Eq. 6-21}$$

It should be noted that the concrete tensile strength at the tip of flexural crack is not affected by cyclic loading, since the damage processes at this depth can be dissipated as macrocrack propagation.

$$\sigma_{c,sup,Ncr} = \frac{V_{cr,cycl,cal} \cdot x_{cr}}{b \cdot d^2 \cdot \xi_{Ncr} / 2 \cdot (1 - \xi_{Ncr} / 3)} \quad \text{Eq. 6-22}$$

With $\sigma_{c,sup,Ncr}$ determined in accordance with Eq. 6-22, the effective depth can be calculated by combining Eq. 6-21 and Eq. 6-22 into:

$$h_{ef,cRC} = \xi_{Ncr} \cdot d \cdot \left(1 + \frac{f_{ct} \cdot b \cdot d \cdot \xi_{Ncr} / 2 \cdot (1 - \xi_{Ncr} / 3)}{V_{cr,cycl,cal}} \right) \quad \text{Eq. 6-23}$$

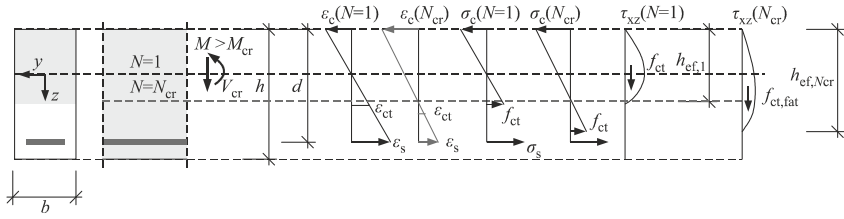


Figure 6-9: Normal and shear stress distribution over cross-section of member according to proposed model for RC members under cyclic shear loads

To find the unknown variable $V_{cr,cycl,cal}$, the value of $h_{ef,Ncr}$ is changed iteratively to satisfy Eq. 6-19, Eq. 6-20, Eq. 6-21 and Eq. 6-18 concurrently. A schematic view of the iterative procedure is depicted in Figure 6-10.

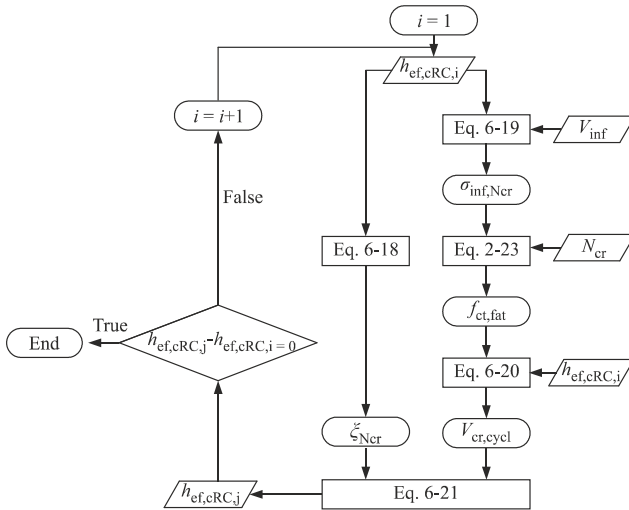


Figure 6-10: Iterative solution procedure for determination of cyclic diagonal cracking load $V_{cr,cycl}$

Due to the fact that the experimental diagonal cracking load $V_{cr,cycl,exp}$ at $N = N_{cr}$ equals the experimental upper shear load $V_{sup,exp}$, the prediction accuracy of the model is evaluated using the upper shear load level of documented tests in cRC subset of shear database. Figure 6-11 enables a comparison between experimental and calculated values of cyclic diagonal cracking load.

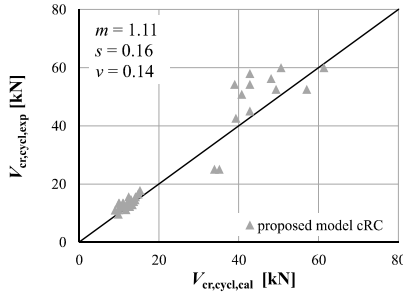


Figure 6-11: Comparison of experimental diagonal cracking loads with calculated values using proposed model for cRC members

Based on the median of model safety factors $m = 1.11$, a good prediction of the cyclic diagonal cracking load is possible using the model. To understand the background of the comparably large scatter of results ($v = 0.14$), the integrity level of different major parameters in the model are assessed and depicted in Figure 6-12.

The points with an unsafe prediction of cyclic diagonal cracking are two tests with relatively low longitudinal tensile reinforcement ratio (0.6%) conducted by ZANUY [ZAN-2008] with a failure due to fatigue of longitudinal tensile reinforcement. Although diagonal cracking occurs before fatigue failure, the stress state can be affected by the yielding of reinforcement, which makes the assumptions of proposed model invalid. Disregarding the tests with a fatigue failure of longitudinal tensile reinforcement (4 tests), the variation coefficient of the safety factor of proposed model would be $v = 0.11$ for the filtered dataset.

Other results show a satisfactory consideration of all major influencing parameters. Due to this fact as well as the visible slight dependency between model safety factor and number of applied cycles to diagonal cracking, it can be concluded that the general scatter in the predicted values of fatigue tensile strength $f_{ct,fat}$ causes the large scatter of results.

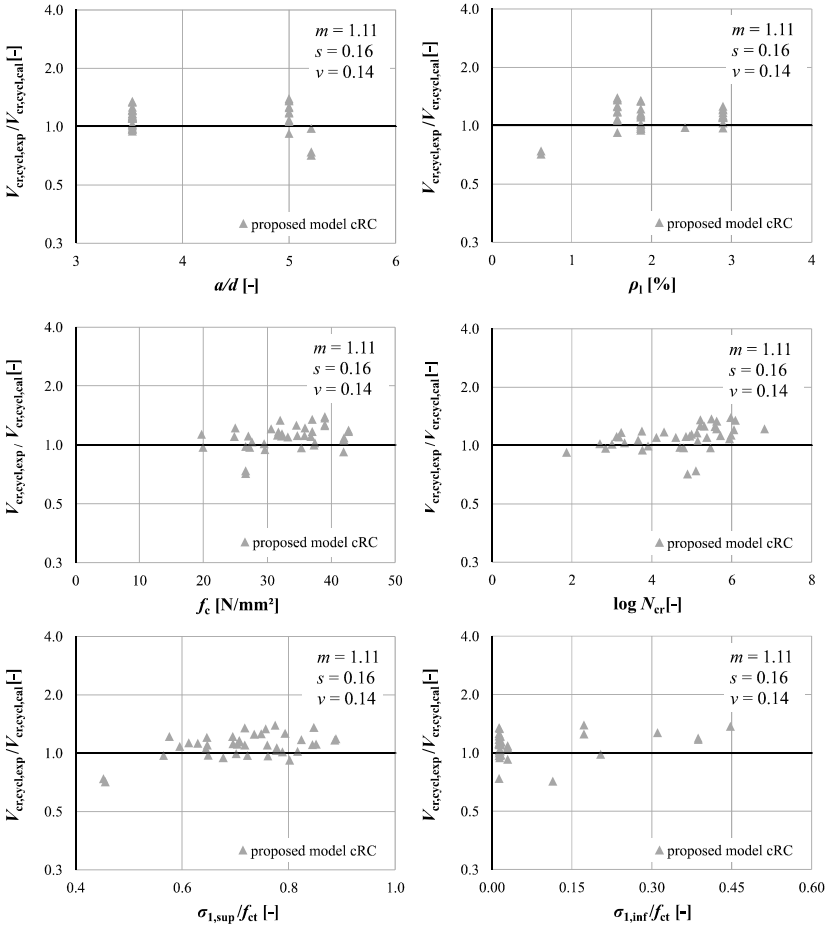


Figure 6-12: Correlation between model safety factor of the proposed model for cRC members and a/d (up, left), ρ_l (up, right), f_c (middle, left), $\log N_{cr}$ (middle, right), $\sigma_{1,sup} / f_{ct}$ (down, left) as well as $\sigma_{1,inf} / f_{ct}$ (down, right)

Seeking the value of $h_{ef,Ncr}$, further variables such as ξ_{Ncr} and $f_{ct,fat}$ are determined as by-product of the iterative calculation. Based on the value of ξ_{Ncr} , the influence of cyclic creep on stiffness of the concrete can be determined using the factor α_{Ncr} .

$$\alpha_{Ncr} = \frac{\xi_{Ncr}^2}{2(1 - \xi_{Ncr})} \quad \text{Eq. 6-24}$$

With the factor $\alpha_{N_{cr}}$ and assuming a non-variant stiffness for steel reinforcement E_s , the stiffness of cyclically damaged concrete after N_{cr} applied cycles $E_{c,N_{cr}}$ is determined as follows:

$$E_{c,N_{cr}} = \frac{E_s}{\alpha_{N_{cr}}} \quad \text{Eq. 6-25}$$

This enables a simplified assessment of cyclic creep coefficient $\varphi_{\text{cycl,al}}$ corresponding to:

$$\varphi_{\text{cycl,cal}} = \frac{E_{c,1}}{E_{c,N_{cr}}} - 1 \quad \text{Eq. 6-26}$$

Based on a data fitting, it is evident that a linear correlation exists between the calculated value of the cyclic creep coefficient and the number of applied cycles until diagonal cracking (s. Figure 6-13).

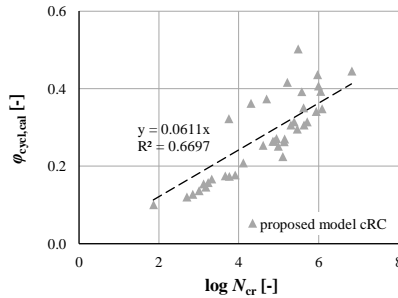


Figure 6-13: Correlation between cyclic creep coefficient and the number of applied cycles

Based on the illustrated linear approximation of cyclic creep coefficient in Figure 6-13, Eq. 3-6 can be simplified to determine the equivalent stress caused by cyclic damage $\sigma_{\varphi,\text{res}}(N_{cr})$ as follows:

$$\sigma_{\varphi,\text{res}}(N_{cr}) = 0.0611 \cdot f_{ct} \cdot (\log N_{cr}) \quad \text{Eq. 6-27}$$

6.5 Concluding remarks

The compiled shear database was used in this chapter to evaluate existing mechanical models in the technical literature. According to the evaluation results, the proposed model by GALLEG0 et al. was selected, since it adequately accounts for the existing primary cracks before diagonal cracking and is better adaptable to evaluate the diagonal cracking load of prestressed members and cyclically loaded members. With a modification of concrete tensile strength, a good accordance was reached between the experimental values of diagonal cracking load of mRC dataset and the calculated values. The modified model

was adapted to account for prestressing and cyclic loads. With the model for PC members, a good approximation was achieved, which, however, does not adequately account for effects of shear span to depth ratio. A reason could be the lack of experimental values of critical section x_{cr} for mPC members. A satisfactory prediction of cyclic diagonal cracking loads was possible using the proposed model for cRC members of shear database. A further optimization of this model with a better correlation between number of applied loads and concrete tensile strength could conceivably enhance the obtained results. A general improvement of diagonal cracking load prediction can be reached, if the location of the diagonal cracks were provided for the members. This is a prerequisite for a safe but economical application of the mechanical approaches (including the proposed models).

7 Nonlinear finite element evaluation of diagonal cracking

7.1 Scope and objectives

The development of commercial finite element (FE) programmes make nonlinear finite element evaluations to state of the art and easily accessible for the engineering practice. With the introduction of Model Code 2010 [fib-2010], structural analyses can be performed alternatively using numerical simulations. Also, some assessment guidelines and previous investigation of existing structures suggest nonlinear FE analysis as a way to find the underestimated or neglected load-bearing mechanisms to avoid over-conservative assessments [Heg-2016], [Mut-2012], [fib-2010], [NRR-2011], [Emp-2013].

The objectivity of models should, however, be critically verified using suggested tests including basic material tests, structural tests and mesh sensitivity tests [fib-2010]. A common material test for modelling of shear critical members is the simulation of biaxial tests of KUPFER / GERSTLE [Kup-1973] or the shear panels of VECCHIO / COLLINS [Vec-1986]. The mesh sensitivity is relatively uncomplicated to conduct. The more challenging test is proving the model objectivity using structural tests, which should be done on benchmark tests to check the uniqueness of response and the sensitivity of the model to major influencing parameters on shear capacity. Especially for simulation of members that fail as a reason of tensile cracking (mode I cracking), the brittle characteristics of failure can cause a premature numerical ultimate load mainly instigated by convergence problems. In such cases, the meaningfulness of the ultimate loads resulted in nonlinear FE analyses should be critically evaluated.

The present chapter focuses on structural tests for numerical simulation of monotonic shear tests on simply supported RC beams without shear reinforcement. The main objective is to investigate the dependency of numerically reached ultimate loads on characteristics of softening behaviour of model due to cracking. The focus is on influence of the selected crack model and the settings of iterative-incremental approach used for the nonlinear FE analysis.

To investigate the softening behaviour coupled with iterative-incremental procedure, six benchmark shear tests with similar test configurations and different shear span to depth ratios are investigated. The aim of this investigation is to find out a suitable crack model applicable for evaluation of softening behaviour caused by diagonal cracking and to minimize the effects of numerical iterative-incremental procedure on numerically predicted diagonal cracking loads.

The nonlinear finite element simulations in this work are performed using the FE-programme DIANA FEA [DIA-2017] (release 10.2), as it includes the required crack modelling and iterative-incremental concepts.

7.2 Modelling orthotropic damage in shear critical members

Several approaches are available for numerical simulation of the damage and the softening behaviour of the shear critical members. These approaches include discrete crack modelling, smeared cracking with total or decomposed strain models, plasticity-based approaches etc.. In contrast to discrete cracking approach, smeared cracking and plasticity approaches enable formation of cracks and are therefore appropriate for estimation of the cracking pattern. The smeared approaches are based on fictitious crack model and its further development to crack band approach as introduced in section 2.1.1. Both of former approaches can be found in previous numerical evaluations in [Heg-2016], [Hen-2017], [Mau-2012], [Hub-2014b], [Bel-2013], [Vec-1986], [Bel-2017a], [Bel-2017b]. The utilization of this approach for prediction of cracking pattern or even crack widths for shear critical members has not been validated so far [Mal-2006], [Hub-2014b]. For the state upon diagonal cracking, smeared total strain-based crack approach developed based on “modified compression field theory” in [Vec-1986] is suitable, which has been employed and evaluated in this thesis.

For undamaged concrete elements, the constitutive law for linear elastic isotropic materials can be written for uncracked concrete elements as:

$$\begin{bmatrix} \sigma_{nn} \\ \sigma_{tt} \\ \sigma_{nt} \end{bmatrix} = \frac{E_c}{1-\nu^2} \cdot \begin{bmatrix} 1 & \nu & 0 \\ \nu & 1 & 0 \\ 0 & 0 & \frac{1-\nu}{2} \end{bmatrix} \begin{bmatrix} \varepsilon_{nn} \\ \varepsilon_{tt} \\ \gamma_{nt} \end{bmatrix} \quad \text{Eq. 7-1}$$

For E_c being the concrete elasticity modulus and ν POISSON’S ratio. As soon as the principal tensile stress at an integration point violates concrete tensile failure criterion, the stiffness matrix is modified using damage factors μ and β to reduce the normal stiffness (mode I) and the tangential stiffness (mode II), respectively.

$$\begin{bmatrix} \sigma_{nn} \\ \sigma_{tt} \\ \sigma_{nt} \end{bmatrix} = \begin{bmatrix} \frac{\mu \cdot E_c}{1-\nu^2\mu} & \frac{\nu \cdot \mu \cdot E_c}{1-\nu^2\mu} & 0 \\ \frac{\nu \cdot \mu \cdot E_c}{1-\nu^2\mu} & \frac{\mu \cdot E_c}{1-\nu^2\mu} & 0 \\ 0 & 0 & \frac{\beta E_c}{2 \cdot (1+\nu)} \end{bmatrix} \begin{bmatrix} \varepsilon_{nn} \\ \varepsilon_{tt} \\ \gamma_{nt} \end{bmatrix} \quad \text{Eq. 7-2}$$

The factor μ can be determined using the tension softening behaviour described in chapter 2 and β is the so-called shear retention factor.

Different terms of stiffness matrix in Eq. 7-2 can be activated or deactivated by the selected constitutive model of concrete and crack model (compare Figure 7-1). Assuming a brittle tensile behaviour (no tensile softening) for instance, results in a term $\mu = 0$. Under this assumption and considering no shear stiffness for the cracked elements ($\beta = 0$), simulation of a flexure shear crack is impossible, since the first flexural cracking causes a significant reduction of stiffness and numerical failure of the model. Using a concrete

tensile curve with a softening branch, a further rotation of principal stresses after cracking results in diagonal cracks. In this case, either the shear stiffness of the cracked element can be ignored ($\beta = 0$), which is the basic assumption of the rotating crack model (R crack model) or change with a constant or variable value of shear retention factor in a fixed crack model (F crack model).

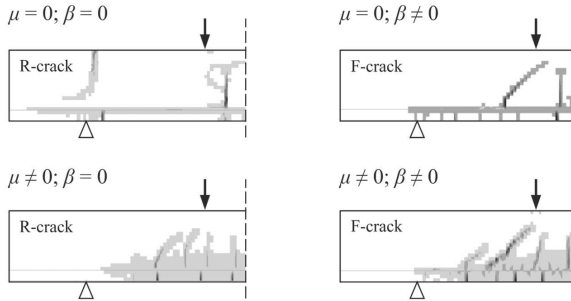


Figure 7-1: Influence of terms in stiffness matrix of damaged concrete and the resulted numerical crack patterns

Assuming no stiffness in cracks, no shear stresses are transmitted parallel to cracks and the cracks rotate with the rotation of principal stress trajectories. Thereafter, a small shear strain increment $\Delta\gamma$ causes a rotation of principal stress trajectories $\Delta\theta_\varepsilon$ in a way that no shear stress emerges in the crack (compare Figure 7-2). Due to the assumed coaxial stresses and strains, the same correlation applies also for the stresses in the R crack model. Therefore, the R crack model enables a calculation of global shear stresses τ and shear strains γ based on MOHR's circle.

$$\tan 2\Delta\theta_\varepsilon = \frac{\Delta\gamma}{2(\varepsilon_1 - \varepsilon_2)} = \frac{\Delta\sigma}{2(\sigma_1 - \sigma_2)} = \tan 2\Delta\theta_\sigma \quad \text{Eq. 7-3}$$

For the initiation of a crack in the R crack model, a predefined threshold angle α_R is also defined in DIANA FEA. Based on this definition, the principal tensile stress σ_1 should exceed the concrete tensile strength f_{ct} at the state of crack initiation and simultaneously, the angle between the existing crack and the initiated crack should exceed the value of α_R .

In contrast to R crack model, the F cracks can transfer shear stresses. Different F crack models can be defined based on assumed shear retention factor. According to existing numerical guidelines such as in [Hen-2017], a variable shear retention factor is often recommended, which can be defined based on crack width, aggregate size etc.. Due to existing shear stresses in F cracks, the crack inclination α_{cr} and the inclination of stress trajectories θ are not identical (compare Figure 7-2).

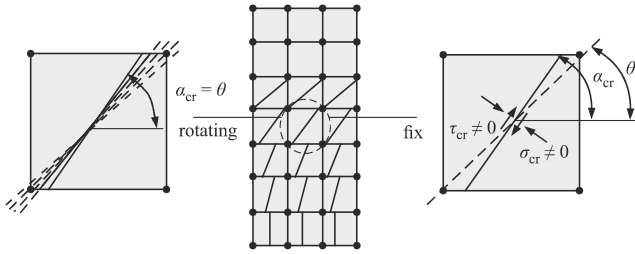


Figure 7-2: Concept of rotating and fixed crack models based on [Kau-2010]

Another possibility for modelling cracks is changing the crack model from rotating to fixed after a certain total normal strain threshold $\varepsilon_{nn,lim}$. The so-called rotating to fixed crack model (RF crack model) enables a shear transfer in cracks from a certain crack width.

It is worth noting that the orthotropic material behaviour of concrete is not fully included in the total strain-based crack models [Baž-1983]. Several considerations are included in this model in programme DIANA FEA. These include a reduction of POISSON's ratio and reduction of concrete compressive strength due to lateral cracking [Vec-1993]. However, the effects of biaxial loading on compressive and tensile failure criteria (strength reduction due to lateral compression or tension) are not included. However, the total strain-based crack model is quite beneficial due to its stability and enhanced convergence behaviour. For shear critical members without shear reinforcement, this advantageous convergence behaviour was approved by own primary numerical investigations and is the basis of selected crack models, which are evaluated in the ensuing chapter.

7.3 Element size and crack band width

A significant step in FE modelling and evaluation of mesh sensitivity is the selection of element size. From a numerical point of view, the size of elements should be reduced to an optimized element size avoiding unnecessary high numerical effort (computation time). From a mechanical point of view, the element size should be selected wisely to reach mesh-independent results using smeared crack approaches. Several mechanical aspects are available for the selection of element size. One aspect originates from a multiscale consideration signifying that for a homogenized modelling of material, the element size must be limited to a representative element size h_E . The value of h_E is selected based on the largest inhomogeneity in concrete, which equals for normal concrete the maximum aggregate size d_g . Available suggestions include $2.5 - 3.0 \cdot d_g$ according to [Sch-1986], $8.0 \cdot d_g$ according to [van-2013], [van-2007] and $5.0 \cdot d_g$ as proposed in [Tru-1999]. Another aspect considers an upper bound for element size based on stability considerations as proposed in [Hen-2017]. The size of element is limited accordingly to characteristic length

l_{ch} of concrete (Eq. 2-5). A further criterion in structural scale is based on reasonability of resulted crack patterns using finite element models. Based on that, element size should be selected in a way that the expected crack distance s_r is larger than the element size [Mal-2006].

Estimation of the crack band width h_{cb} is a crucial step in smeared crack modelling. The above-mentioned multiscale consideration is also one of the physical backgrounds of the proposed crack band width in [Baž-b1983]. Therefore, most crack band width estimators are based on the element size (h_E) [Sl0-2015]. Using this crack band width, the material parameters are also adjusted to element size in order to achieve mesh-independent results (such as for fracture energy in Figure 2-4).

The suggested numerical crack band width approaches in the literature can be mainly divided in approaches depending just on element size (e.g. approximation according to ROTS [Rot-1988]) or methods considering additionally crack alignment (e.g. the band width approximation according to GORVINJEE [6or-1995]). In this work, the commonly used crack band width estimator according to ROTS is implemented.

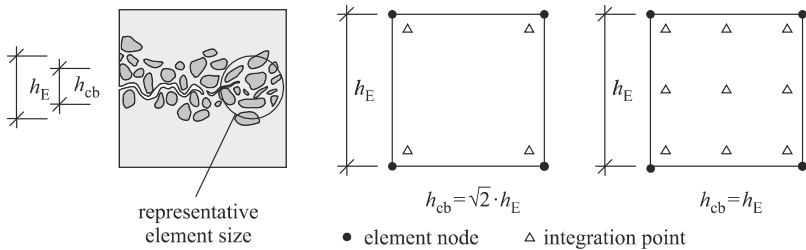


Figure 7-3: Physical background of element size and crack band width (left) and numerical crack band width approximations according to ROTS (right) (according to [Rot-1988])

7.4 Loading and analysis procedure

For the simulation of cracking, a reduction of applied load is enabled with a displacement-controlled loading scheme. Using the displacement alteration Δu_i and tangential stiffness matrix K_i , internal forces f_{int} and energy ($u_i \cdot f_{int}$) are calculated and compared with the external ones. The out of balance force w is calculated using this comparison (compare Figure 7-5).

$$\Delta u_i = K_i^{-1} \cdot w_i \tag{Eq. 7-4}$$

The iteration procedure is continued until the convergence criteria are fulfilled or a maximum number of iteration steps is reached. As convergence criterion, force criterion, en-

ergy criterion and also displacement criterion can be selected. For a displacement-controlled loading, force and energy criteria are often recommended. Based on that, the force criteria is fulfilled if the following ratio is smaller than a selected convergence norm:

$$\frac{\sqrt{w_i^T \cdot w_i}}{\sqrt{w_0^T \cdot w_0}} \leq \text{force convergence norm} \tag{Eq. 7-5}$$

The energy convergence norm is controlled by:

$$\left| \frac{\Delta u_i^T (f_{int,i+1} - f_{int,i})}{\Delta u_0^T (f_{int,1} - f_{int,0})} \right| \leq \text{energy convergence norm} \tag{Eq. 7-6}$$

For the incremental procedure of analysis, explicit load steps can be used alongside different adaptive loading procedures provided in DIANA FEA. An adaption of the applied increment sizes to stiffness is possible using an arc-length control, which can be combined with a refined energy-based adaption method. The application of method of energy-based adaption of increment sizes is already investigated for shear critical members in [Bel-2017a].

Within the arc-length method, the step size is adapted during the iteration based on a load factor $\Delta\lambda_i$. Combined with energy-based adaption, the next step size is chosen in a way, that the energy of the initial prediction equals the energy of first iteration of subsequent load step (compare Figure 7-4, right).

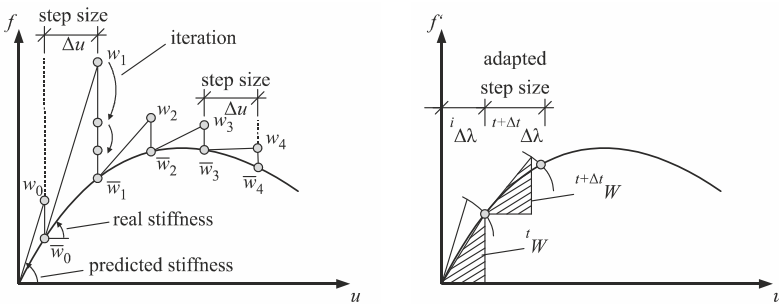


Figure 7-4: Incremental iterative procedures provided in DIANA FEA (according to [Göd-2012] and [DIA-2017])

7.5 Description of numerical models

7.5.1 Geometry and model discretization

To limit the numerical effort, 2D models are used for simulation of in-plane shear response of the beams. Previous studies in [Cla-2009] indicate that the stiffness and hence the response of the beams modelled by means of symmetry (half-beam models) is different

from that of full models. In order to have comparable models in case of asymmetrical loading, the RC beams are modelled as full models disregarding the symmetry.

Quadratic elements with a nearly 1:1 aspect ratio are used to generate element mesh. In this case, triangular elements are avoided deliberately, as previous studies in [Slo-2015], [Cla-2009] show that the resulted crack patterns are significantly influenced by mesh alignment in case of triangular elements. To refine the strain field and obtained crack patterns, 8-node quadrilateral isoparametric plane-stress elements CQ16M with a higher order integration scheme (3 x 3 Gauss integration) are implemented.

For the available shear tests with normal concrete with average beam depth values around 300 mm, the available recommendations for aggregate size based representative element size exceeds the beam depth and are not practical. Besides, the characteristic length for normal concrete is often more than a meter and the maximum element size criteria is fulfilled for laboratory tests. To have a fine crack path, the element size should be smaller than crack distance. However, to remain in macroscale the element size h_E is limited to maximum aggregate size d_g . The element size was defined using the beam depth h and aggregate size as follows:

$$h_E = \max \left\{ \begin{array}{l} d_g \\ h/20 \end{array} \right. \quad \text{Eq. 7-7}$$

For tests without documented d_g , $h/20$ is used for mesh size determination. To avoid stress concentrations at loading and support points elastic steel plates are modelled.

A schematic view of the model geometry and discretization is provided in Figure 7-5.

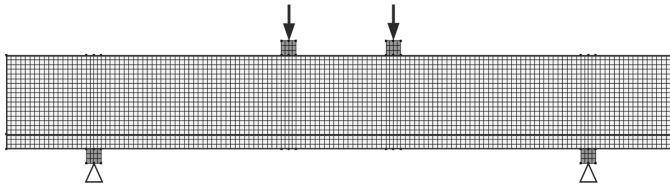


Figure 7-5: General set up of numerical models

7.5.2 Material parameters

The concrete is modelled using on total strain based cracks. The uniaxial stress-strain curve of concrete is defined according to Figure 7-6, left. For the tensile curve, the ascending branch is considered linear and the residual concrete tensile strength is defined using the exponential softening curve of HORDIJK [HOR-1992] (Eq. 2-15). The ascending branch under compression is simulated as a parabolic curve. The descending branch of the parabolic curve in DIANA FEA 10.2 is also adopted as illustrated in Figure 7-6, right.

For the modelling of longitudinal reinforcement (Figure 7-6, right), the tensile stiffening is considered by strain hardening according to VON MISES. A bilinear curve is assumed for the elastic and plastic regions. The longitudinal reinforcement is modelled as fully bonded embedded reinforcement.

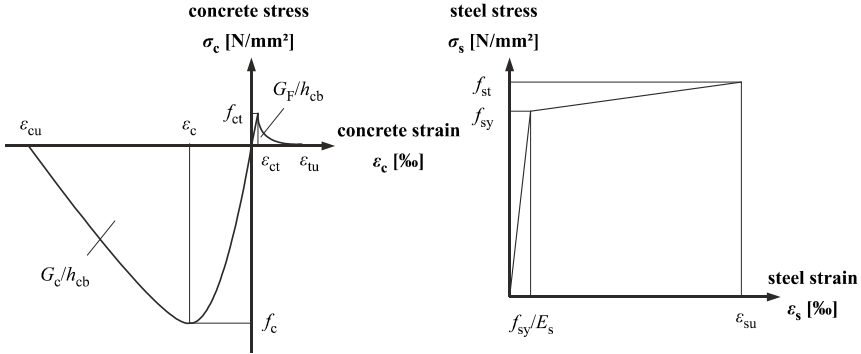


Figure 7-6: Tensile and compressive curve of concrete (left) and steel reinforcement curve (right)

In the reference evaluations of benchmark shear tests, an R crack model and an F crack model is defined and implemented for simulation of orthotropic damage. The R crack model was defined with a threshold angle $\alpha_R = 10^\circ$. The main parameter of the F crack model is the shear retention factor β , which was set as variable. Several methods exist for adaption of shear retention factor such as aggregate size based approaches (as suggested in [Hen-2017]) or approaches based on crack opening. In the present thesis, a variable shear retention factor, which is proposed by AL-MAHAIDI [Al-1978] is used (compare Eq. 7-8). In this model, the shear stiffness of cracked concrete is reduced toward a minimum lower bound β_{min} (which is set equal to 0.01 as basic setting) considering tensile parameters of concrete (f_{ct} and E_c) and the numerically calculated total normal strain ϵ_{nn} .

$$\beta = 0.4 \cdot \frac{f_{ct}}{E_c \cdot \epsilon_{nn}} \geq 0.01 \quad \text{Eq. 7-8}$$

7.5.3 Analysis procedure

For RC members without shear reinforcement, as it will be shown later, the brittle nature of failure under diagonal tension results in convergence problems during the numerical calculation process. However, after a short instable cracking phase, a new equilibrium condition and a convergence are still probable. Therefore, it is important to continue the iteration process even after a short-term violation of convergence criteria, which is also suggested in [Hen-2017].

For the iterative calculation, the equilibrium is sought using regular NEWTON-RAPHSON method. In each load step, a maximum number of 50 iterations is allowed. For the reference analysis, the beams are investigated with energy and force convergence criteria with convergence tolerances equal to $1 \cdot 10^{-2}$ and $1 \cdot 10^{-4}$, respectively.

The incremental setting of reference investigation was using an explicit incremental approach with constant load step sizes $\Delta u = 0.01$ mm (compare Figure 7-4, left) applied as a vertical displacement. The constant step sizes enhance tracing of changes caused by incremental procedure. The load step size is kept small in order to minimize the probability of premature failure caused by convergence problems. The incremental procedure is continued until a maximum number of load steps was reached, which varies based on the total displacement of models at failure. Within the variational investigations, further possibilities of load step adaption using arc-length control and energy-based adaption are investigated.

7.6 Scope of reference investigations

Six shear tests on simply supported beams with a rectangular cross-section are modelled in FE programme DIANA FEA. The selected beams are configured with constant material properties and longitudinal reinforcement ratio. The variable parameter of test configurations is only the shear span to depth ratio, which varies in a range of 2.0 - 5.8. Table 7-1 shows an overview of the evaluated beams.

Table 7-1: Benchmark experiments of LEONHARD / WALTHER [Leo-1962]

Test	Label	b	h	d	a/d	f_c	ρ_l	$V_{u,exp}$	$x_{cr,exp}$
		[mm]	[mm]	[mm]	[-]	[N/mm ²]	[%]	[kN]	[mm]
3	L3	190	320	270	2.00	29.0	2.07	147.7	350
4	L4	190	320	270	2.5	29.0	2.07	86.6	355
5	L5	190	320	270	3.00	29.0	2.07	75.8	355
6	L6	190	320	270	4.1	29.0	2.07	67.1	707
7/1	L7	190	320	278	4.9	29.0	2.01	60.8	856
8/1	L8	190	320	278	5.8	32.0	2.01	64.0	972

For the calculation of material parameters, the suggested correlations in [fib-2010], [DIN-1992 1-1] and [Hen-2017] (compare Table 7-2) are implemented to calculate further material parameters based on concrete compressive strength f_c . The effects of lateral cracking are considered on concrete compressive strength based on the proposed correction by VECCHIO / COLLINS [Vec-1993], with a limited reduction factor to 0.6. Each beam is evaluated once with the R crack model and once with the F crack model (compare 7.5.2).

Table 7-2: Material parameters of concrete for reference FE models

Material parameters of concrete	Parameter
Elasticity modulus [N/mm ²]	$E_c = 21500 \cdot (f_c/10)^{1/3}$
Concrete tensile strength [N/mm ²]	$f_{ct} = 0.3 \cdot (f_c - 4)^{2/3}$
Tensile fracture energy G_F [N/mm]	$G_F = 0.073 \cdot (f_c)^{0.18}$
Compressive fracture energy [N/mm]	$G_{F,c} = 250 \cdot G_F$
POISSON'S ratio	$\nu = 0.2$
reduction of concrete compressive strength due to lateral cracking	VECCHIO / COLLINS 1993 (lower bound 0.6)

7.6.1 Models with rotating cracks (R)

For beam L3 with a shear span to depth ratio of $a/d = 2$, a very good agreement could be reached between numerical results and the experimental value of ultimate shear load V_u . Based on the numerical load-deflection curve, a short-term instable crack growth was noticeable from a drop in applied shear load at $V = 69.8$ kN. Using the proposed mechanical model in chapter 6 (Eq. 6-9), the diagonal cracking load is determined as $V_{cr,cal} = 62$ kN, which shows a good accordance with the numerical shear load at the short-term instable load steps. The width of the critical diagonal crack is at this point equal to 0.3 mm. A comparison between numerical and experimental crack patterns at the state of failure is depicted in Figure 7-8. The experimental crack pattern is illustrated as fine lines and the numerically achieved crack pattern is scaled in the way that cracks with a width over 0.1 mm are illustrated in black.

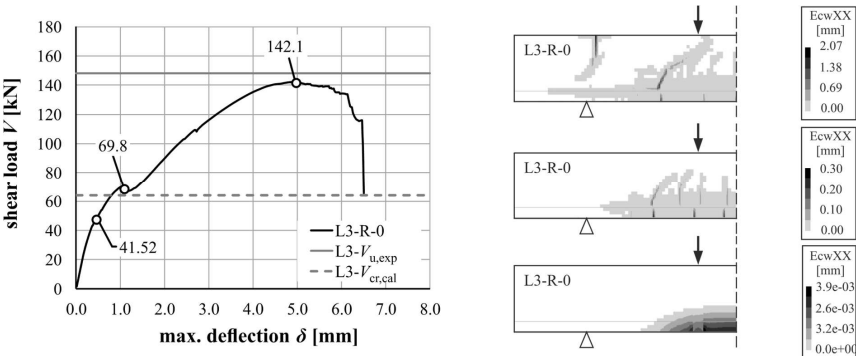


Figure 7-7: Load-deflection curve of beam L3-R-0 (left) and flexural (right, down), diagonal (right, middle) and failure (right, up) cracking stages

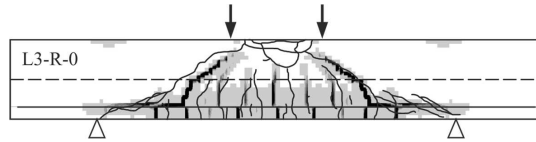


Figure 7-8: Comparison of experimental and numerical crack patterns of beam L3-R-0 (cracks with a crack width > 0.1 illustrated in black)

A comparison between equilibrium tolerances (force and energy) and the out of balance energy and forces in each load step is illustrated in Figure 7-9. At the state of diagonal cracking, a short-term grow in out of balance force is discernible. The results show that almost all steps are converged based on the selected force norm and the energy norm is violated after few load steps.

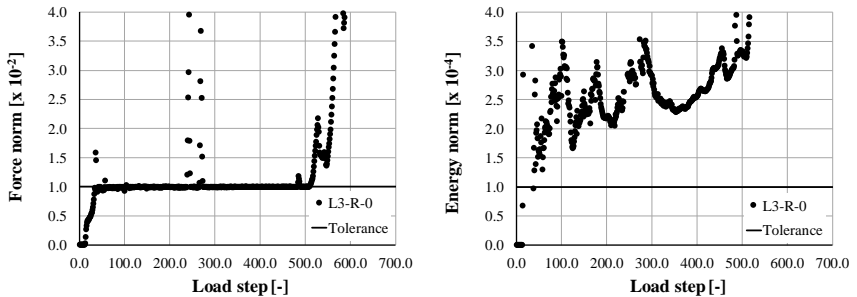


Figure 7-9: Force and energy norm compared to out of balance force (left) and energy (right) in each load step for model L3-R-0

The same evaluations are illustrated exemplarily for beams L6 in Figure 7-10. The gradual development of diagonal cracks for the beam with a shear span to depth ratio of $a/d = 4.1$ leads to a sudden shear load drop at the state of diagonal cracking.

The experimental and numerical crack patterns deviate to a larger extent compared to beam L3. An assessment of out of balance force and energy in the steps after the diagonal cracking (step 355) shows that no convergence could be achieved until a shear load of 36.9 kN (step 460) and the convergence criteria were violated again after a few steps.

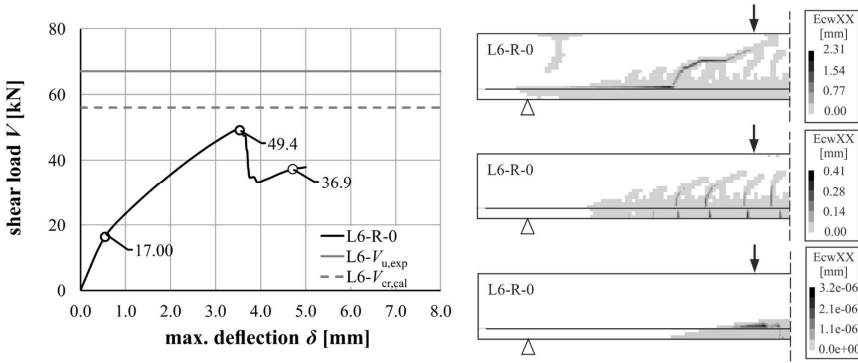


Figure 7-10: Load-deflection curve of beam L6-R-0 (left) and flexural (right, down), diagonal (right, middle) and failure (right, up) cracking stages

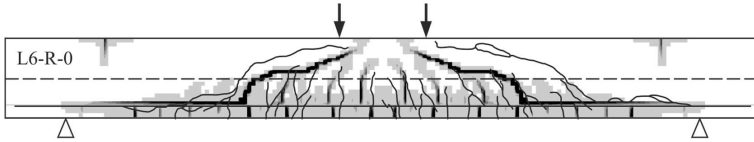


Figure 7-11: Comparison of experimental and numerical crack patterns of beam L6-R-0 (cracks with a crack width > 0.1 illustrated in black)

In general, an important difference between the numerical response of beams L3 and L6 is the cracking behaviour, which is visible in the evolution of out of balance energy. For beam model L6-R-0 (Figure 7-12), the out of balance energy grows in a more stable and gentle way and the energy release rate during flexural cracking is smaller in comparison to beam L3-R-0. However, at the state of diagonal cracking, a rather unpredicted jump can be seen in Figure 7-12. This comparison highlights the influence of shear slenderness on brittleness of diagonal crack propagation and specifically on the prior notice of critical diagonal cracking.

A prediction of maximum failure load was possible using the FE model of beam L3, whereas an over-rotating of critical shear crack in L6-R-0 leads to a premature failure of the model (compare Figure 7-11). For both beams, the numerically achieved distance of critical shear crack from the support axis $x_{cr,FE}$ is overestimated. A tendency between the shear span to depth ratio a/d and deviation between numerical and experimental diagonal crack paths was observed, according to which the ratio $x_{cr,exp} / x_{cr,FE}$ decreases with the increasing of a/d .

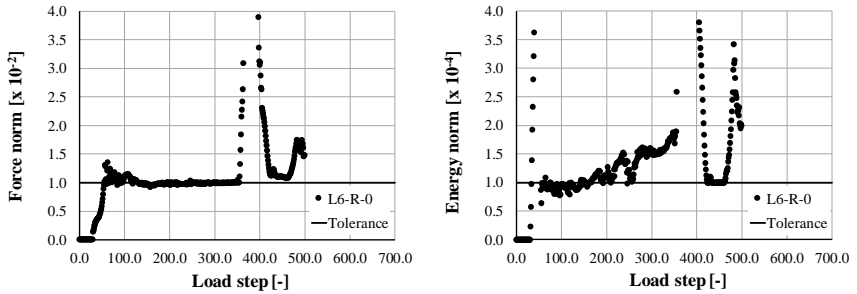


Figure 7-12: Force and energy norm compared to out of balance force (left) and energy (right) in each load step for model L6-R-0

7.6.2 Models with fixed cracks (F)

Beams L3 to L8 are modelled additionally with a fixed crack orientation (F) as introduced in chapter 7.5.2. The numerical results of L3 and L6 are discussed exemplarily and further results are documented in appendix D. A comparison between different cracking states and the load-deflection curve of beam L3 with a fixed crack model (L3-F-0) show that the flexural cracking state and a global stiffness reduction is occurring at significantly higher load (42.2 kN), which is also higher than the calculated flexural cracking load of $2 \cdot M_{cr,cal} / l = 10.2 \text{ kN}$ ($M_{cr,cal} = W \cdot f_{ct}$). The same applies also for the instable crack growth due to a critical diagonal cracking, which happens under a higher load than $V_{cr,cal}$. Comparing experimental and numerical ultimate failure loads, it can be perceived that the ultimate load is underestimated using a fixed crack model for beam L3.

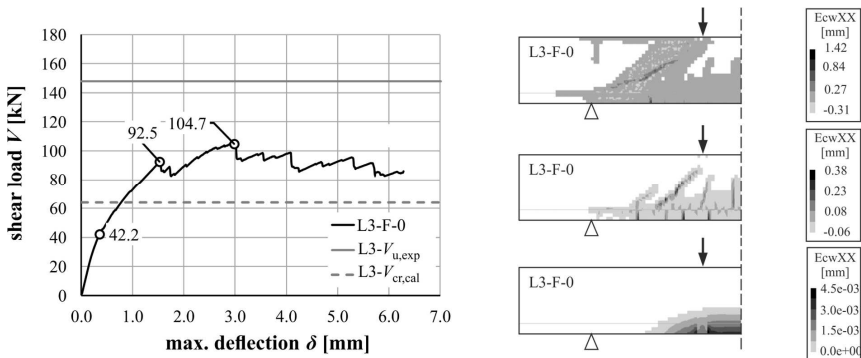


Figure 7-13: Load-deflection curve of beam L3-F-0 (left) and flexural (right, down), diagonal (right, middle) and failure (right, up) cracking stages

Comparing the failure crack path with the experimental one, it is evident that despite the good accordance between crack paths, the failure mode deviates from the experimentally observed one. Whereas in the shear tests, a compression failure between two loading

points results in ultimate failure, in the FE model, a crushing failure along the diagonal cracks causes a model failure at significantly high crack widths (max. value of 1.42 mm, compare Figure 7-13). This deviation correlates with the stress locking, which is a known aspect for fixed crack models [Rot-1988]. However, it can be concluded that this stress-locking does not necessarily overestimate the ultimate loads in contrast to observations of ROTS.

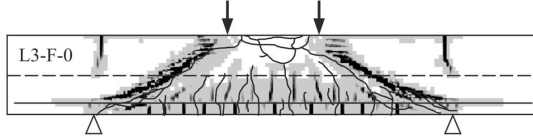


Figure 7-14: Comparison of experimental and numerical crack patterns of beam L3-F-0 (cracks with a crack width > 0.1 illustrated in black)

The out of balance energy and forces during the incremental nonlinear analysis of beam L3 show a more oscillating behaviour, as a new system equilibrium is found due to activation of shear stresses in cracks after a few load steps.

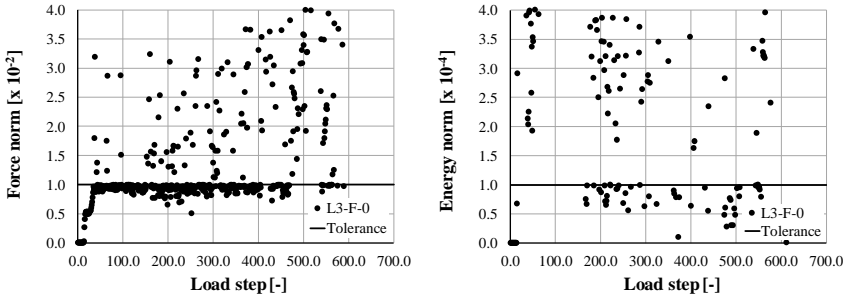


Figure 7-15: Force and energy norm compared to out of balance force (left) and energy (right) in each load step for model L3-F-0

The beam model L6-F-0 shows that in this case, the fixed crack model can provide a better approximation of the ultimate load. However, the state of critical diagonal cracking cannot be recognized from the load-displacement curve. Under the same load level, higher numerical cracks widths can be observed. It is worth noting that due to the shear stresses parallel to crack caused by fixation, numerical crack widths can have negative values, which makes a direct physical interpretation of crack widths incorrect.

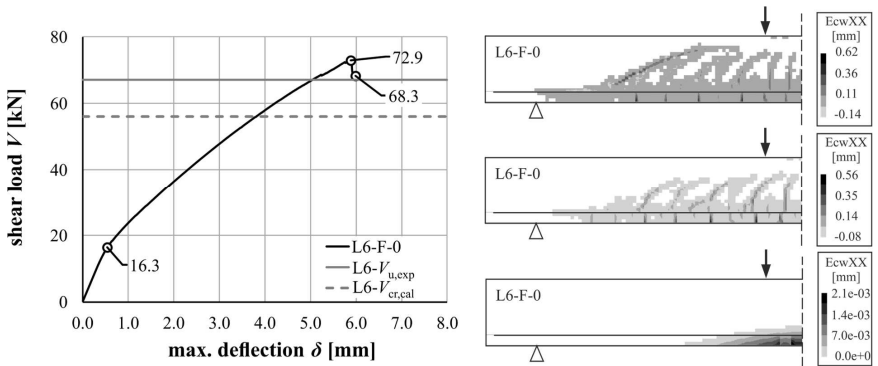


Figure 7-16: Load-deflection curve of beam L36-F-0 (left) and flexural (right, down), diagonal (right, middle) and failure (right, up) cracking stages

The failure crack path obtained from analysis of beam L6 with a fixed crack model suits the crack path of the beam captured at failure.

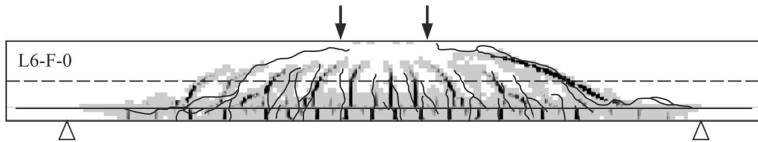


Figure 7-17: Comparison of experimental and numerical crack patterns of beam L6-F-0 (cracks with a crack width > 0.1 illustrated in black)

In contrast to other models, the convergence tolerances were fulfilled for some steps even after the excessive diagonal cracking, which are converged based on the energy criterion as depicted in Figure 7-18, right.

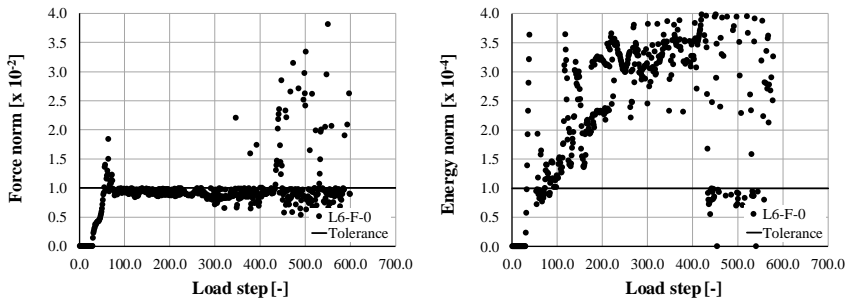


Figure 7-18: Force and energy norm compared to out of balance force (left) and energy (right) in each load step for model L6-F-0

7.6.3 Comparison of results and provisional conclusion

In general, it can be postulated the prediction accuracy of the models depend on the crack model and the shear span to depth ratio of the beam. The results of such variational evaluations can be used to get insight into the real shear load-bearing mechanisms of the beam. For instance, for a low shear span to depth ratio ($2.0 < a/d < 3.0$), both diagonal cracking load and experimental shear failure load can be determined using a rotating crack model. This shows that the concrete tensile capacity before diagonal cracking and the formed direct compressive strut after diagonal cracking are the main load-bearing mechanisms for such beams and are adequately simulated using the R cracks. Activation of shear stresses in cracks in the F crack model represents numerically the physical mechanism of aggregate interlock. For simulated beams, this load-bearing mechanism was not activated in the shear tests or overestimated by the applied F crack model; hence, the models with F cracks overestimated the experimental ultimate shear load. A comparison between numerically resulted failure loads with the R crack model and the F crack model are depicted in Figure 7-19.

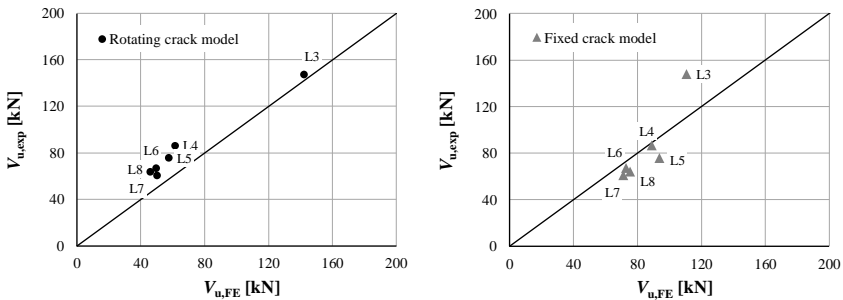


Figure 7-19: Comparison of experimental and numerical ultimate shear load V_u for rotating (left) and fixed (right) crack models

Based on the results, a safe prediction of ultimate load was possible using the R crack model in all cases. Since the R cracks are capable of simulating both diagonal tension and arching action, for shear span to depth ratios ($2.0 < a/d < 3.0$), the numerical ultimate loads correspond to experimental ultimate loads. The diagonal cracking was noticeable for such beams by a short-term violation of force convergence criterion. Since the arching action is not activated for higher shear span to depth ratios than 3.0, the numerical ultimate load for such beams represent the diagonal cracking load.

To check the validity of estimated diagonal cracking loads using the models with R cracks, the calculated diagonal cracking loads $V_{cr,cal}$ are determined using the validated proposed approach in chapter 6. For beams L3 and L4, the numerical diagonal cracking load is the point with a short-term instable cracking. A comparison between $V_{cr,FE}$ and

$V_{cr,cal}$ is illustrated in Figure 7-20, right and shows good agreement between numerical and calculated values of V_{cr} .

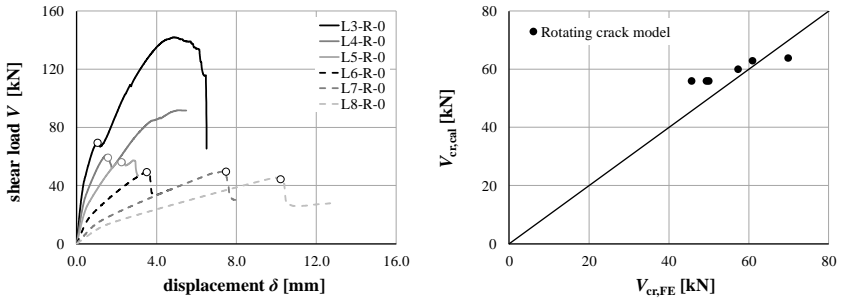


Figure 7-20: Comparison between numerical shear load-displacement diagrams (left) as well as between calculated and numerical diagonal cracking loads (right)

Comparing the experimental crack paths with the predicted critical section with models with the R cracks (Figure 7-21, left) and the F cracks (Figure 7-21, right), a visible tendency with the shear span to depth ratio is visible. For a certain range of shear span to depth ratio a/d , the F crack model leads to a better prediction of failure crack path and the critical section. According to existing tendencies, increasing shear span to depth ratio leads to overestimated distances of critical section from support axis for models with the R cracks. For F cracks, the opposite tendency is observed.

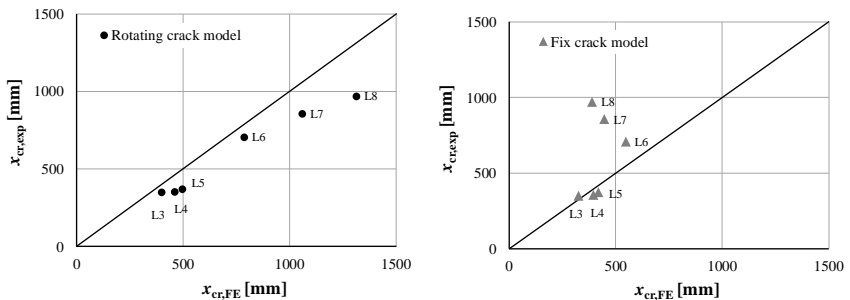


Figure 7-21: Comparison between experimental and numerical crack distances from support axis x_{cr} for rotating (left) and fixed (right) crack approaches

The coupled effects of convergence problem and crack model on numerically attained ultimate loads with the R crack model were also observed during reference evaluations. Based on that, especially with increasing shear span to depth ratio, a premature numerical failure was observed due to over-rotation of diagonal cracks or the abrupt violation of convergence criteria observed by evolution of out of balance energy. This different cracking behaviour coupled with characteristics of the R crack model is the reason for most convergence problems and a premature numerical failure.

To solve the former problem, defining the cracks as rotating to fixed (RF) can be a good method. The latter numerical problem will be studied also in further parts of this chapter using adaptive incremental methods.

7.7 Proposed iterative-incremental approach

Reference evaluations show a dependency between the energy release due to softening in each load step and ultimate loads of the numerical models. The out of balance energy changes with the selection of convergence norm as well as load incrementation approach. Hence, an explicit loading can cause inefficient convergence behaviour, underestimated diagonal cracking loads using R crack model due to convergence problems and also different cracking patterns [Jov-2018b]. A further disadvantage of explicit loads is the high computational effort due to a high number of required load steps.

For the adaption of the incremental approach, a load step size based on flexural stiffness of the beam can be advantageous and reduces the total number of required load steps (especially for test configurations with large shear spans). For this aim, an initial load step size is proposed based on the beam deflection under flexural cracking moment $M_{cr,cal}$ ($W \cdot f_{ct}$) for a more differentiated incremental setting. The initial load step u_{in} corresponds to:

$$u_{in} = \frac{f_{ct} \cdot l^2}{12 \cdot E_c \cdot h} \quad \text{Eq. 7-9}$$

As the calculated flexural cracking moment $M_{cr,cal}$ is lower than the numerical one, the beam models remain uncracked at the initial loading. To adapt the size of applied load increments as vertical displacement (after several variational evaluations), three representative incremental setting combinations I1 to I3 are selected and presented in this section.

The adaptive incremental methods include arc-length method (I1 and I2) and a combination of arc-length method and energy based adaption of load increment size (I3). The arc-length control was performed in each load step on the vertical translation of attached beam nodes to the loading plates.

Furthermore, the iterative setting is also adjusted slightly. The evaluated reference models show that the energy norm was violated for almost every load step. For this reason, the energy convergence norm was increased to $1 \cdot 10^{-3}$, which is also a recommended value according to [Bel- a2017].

The three incremental setting combinations I1 to I3 correspond to:

- arc-length control with an initial step size of u_{in} (I1)
- arc-length control with an initial step size of 0.01 mm (I2)
- combined arc-length control and the energy-based adaption of load steps (I3)

A comparison between resulted shear load-deflection curves and the reference simulation is possible with Figure 7-22. It is worth noting, that the curves are illustrated until the last converged load step.

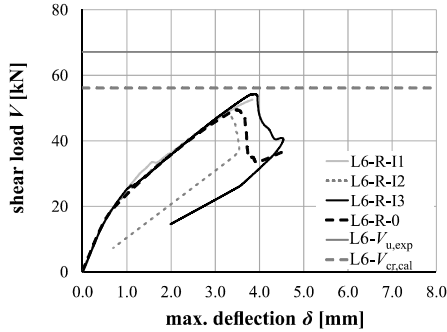


Figure 7-22: Load-deflection curves of beam L6 for the reference model and different configurations of incremental and iterative simulation settings

In the first model L6-R-I1, load steps are adapted during the incrementation using arc-length method. The initial load step is set according to Eq. 7-8. It could be observed that resulted ultimate load increases for this model (toward 52.6 kN), however, this load step implies also the last converged step of the model and the adaptive mechanism of arc-length method can not lead to further converged steps.

Using a smaller initial load step size of 0.01 mm (same value as reference simulations), the ultimate load was underestimated by model L6-R-I2, which shows that smaller step sizes are not necessarily beneficial for a prediction of ultimate load. In a third variational evaluation I3, the available energy-based adaptive loading in DIANA FEA is applied in combination with arc-length method. The initial step size was set as u_{in} and the minimum step size is selected as 0.01 mm. A maximum number of 500 load steps is chosen. Using this adjusted incremental iterative process, the value of $V_{cr,cal}$ is better approximated using the FE-simulation (compare Figure 7-23).

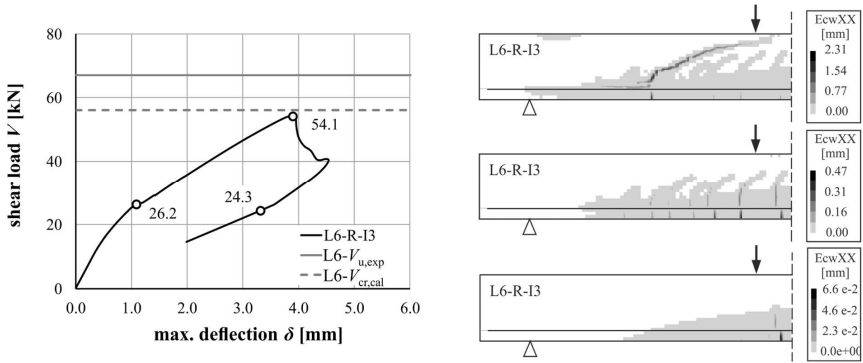


Figure 7-23: Load-deflection curve of beam L6-R-I3 (left) and flexural (right, down), diagonal (right, middle) and failure (right, up) cracking stages

A comparison between the achieved crack paths for the different model configurations is illustrated in Figure 7-24. It points out the influence of incremental procedure on the obtained numerical critical sections and shows a good agreement between the experimental and numerical diagonal crack paths for the model with small increment size (I2) or an adaptive incremental approach (I3). It adverts additionally the reason of lower predicted numerical ultimate loads with incremental setting I2. Comparing the critical crack path in I2 and I3, it gets evident that the smaller load increments in I2 enable a higher crack rotation from the mid-depth of the beam, which might be the reason for the premature numerical failure.

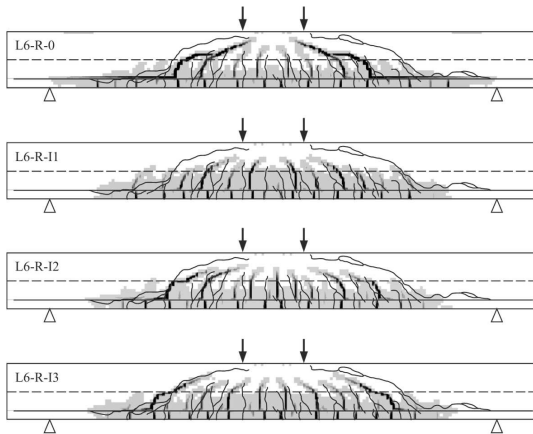


Figure 7-24: Failure crack path of the reference calculation (L6-R-0) and models with different incremental approaches I1-I3

Based on the out of balance energy in each load step, the difference between the iteration procedure with arc-length method (I2) and in combination with energy-based adaption of increment size (I3) is shown in Figure 7-25.

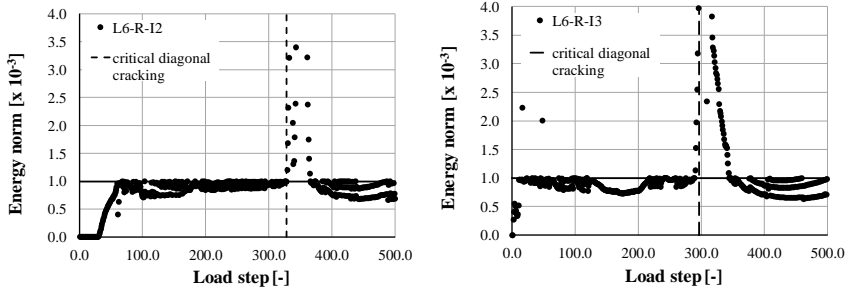


Figure 7-25: Out of balance energy of parameter combination I2 (left) and I3 (right)

Comparison of approaches I2 and I3 shows that despite the faster calculation in I3, convergence is reached after the short unstable diagonal cracking phase using the energy-based adaption of the load step size. Furthermore, the required number of applied load increments to capture the diagonal cracking is reduced. Due to this adaption of load increment, higher numerical ultimate loads are reached, which agree better with the analytical diagonal cracking loads and lead to a more realistic crack pattern.

7.8 Proposed rotating to fixed crack model (RF)

To counteract the over-rotation of R cracks, which impedes a meaningful prediction of diagonal cracking load using R crack for high shear span to depth ratios, a rotating to fixed crack model is proposed in this section.

To define this crack model, the concrete model must be provided with a threshold value, from which the existing cracks are set as fixed. This threshold value is defined using the analogy between uniaxial tensile cracking of concrete (chapter 2.1) and critical diagonal cracking (chapter 4.1). Based on this assumption, the critical diagonal crack emerges as the crack width exceeds the value $w_{cr,1}$ and a tensile instable cracking begins (similar to the assumption of the mechanical model proposed by TRAN et al.). With this mechanically sound assumption, a threshold total strain $\varepsilon_{nn,lim}$ is defined according to:

$$\varepsilon_{nn,lim} = \varepsilon_{el} + \frac{w_{cr,1}}{h_{cb}} \quad \text{Eq. 7-10}$$

As the cracks change to fixed cracks, a shear retention factor β should be defined for reduction of lateral stiffness (compare chapter 7.2). Here, the variable β proposed by AL-MAHAIDI (Eq. 7-8) is used in conformity with previous models with the F crack model.

Using the suggested RF crack model, beam L6 is modelled and the numerical response is compared with that of the R crack model in Figure 7-26.

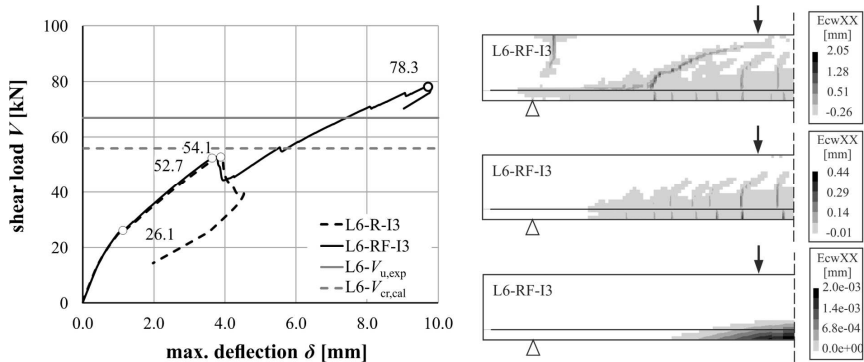


Figure 7-26: Load-deflection curve of beam L6-RF-I3 (left) and flexural (right, down), diagonal (right, middle) and failure (right, up) cracking stages

The comparison shows that the two shear load-deflection curves deviate from each other from a point, which corresponds to the diagonal cracking load. This observations confirmed the reasonability of the defined threshold value $\epsilon_{nn,lim}$. After this point, the critical diagonal crack is set as fixed and the shear stress transfer over the cracked elements is activated. Although the failure load is slightly over-estimated, a good approximation was possible using the proposed shear-retention factor. The failure crack path is not significantly changed by the RF cracks and is almost similar to the predicted failure crack path by model L6-R-I3. This crack path shows also a very good accordance with the experimental location of the critical section.

The application of RF crack model will be shown in the next chapter on different shear span to depth ratios and material and beam configurations to validate the defined threshold value $\epsilon_{nn,lim}$.

7.9 Concluding remarks

The dependency of numerically reached ultimate loads on characteristics of softening behaviour of model due to cracking was investigated in this chapter using six benchmark shear tests. The beams with different shear span to depth ratios were modelled once with rotating cracks (R crack model) and afterwards with a selected fixed crack model (F crack model). The resulted numerical ultimate loads of each model were compared with experimental ultimate loads and analytically determined diagonal cracking loads using the proposed mechanical model in chapter 6.

Based on this comparison, following conclusions are made:

- The numerical ultimate load reached by FE models with the R crack model signifies the ultimate failure load for beams with $2.0 \leq a/d \leq 3.0$ and the diagonal cracking load for beams with $a/d > 3.0$.
- With the F crack model, the ultimate loads are almost overestimated for all simulated beams (except for L3) but a better approximation of critical section was reached for beams with $a/d > 3.0$.
- Based on the fixed crack model, load-bearing mechanism caused by aggregate interlock can be simulated, whereas the R crack model simulates the shear capacity under diagonal tension and the formed direct compression strut after diagonal cracking.
- Critical diagonal cracking occurs in a more brittle manner for high shear span to depth ratios, which can cause a premature failure of models due to convergence problems.
- Over-rotation of R cracks can lead to premature failure of FE models with high shear span to depth ratios.

To provide solutions for premature numerical failure of models, a refined incremental-iterative approach was proposed to adapt the load incrementation on brittleness of diagonal cracking. To solve the problem of over-rotation of cracks, a new rotating to fixed crack model (the RF crack model) was developed using the analogy between uniaxial tensile cracking and critical diagonal cracking.

The proposed iterative-incremental approach should enable a prediction of diagonal cracking for different energy release rates during critical diagonal cracking i.e. different shear span to depth ratios. Furthermore, for beams with possible over-rotation of cracks (high a/d), the diagonal cracking loads should be better predictable.

The suggested iterative-incremental approach as well as the new RF crack model should be validated using further investigations (see chapter 8).

8 Numerical simulation of experiments in shear database

8.1 Outline

The present chapter extends the application of suggested model and incremental iterative configuration with a rotating crack model (R model) to different test setups, beam configurations and loading regimes. To this end, the objectivity of FE models is assessed using the tests in the shear database.

Furthermore, the proposed rotating to fixed crack model (RF crack model) is applied for evaluation of representative shear tests in the database. The results are compared with the results obtained using R model and limitations and potentials of RF model are emphasized. The influence of material input parameters on the response of models with the RF crack model will be further evaluated within a parametric study.

The adapted concrete tensile curve (see chapter 3) is applied for nonlinear FE evaluation of cyclically damaged reinforced concrete beams (selected tests of cRC database).

The finding of numerical investigations will be used to propose conceptual methods for evaluation of shear safety of reinforced concrete members under shear loads.

8.2 General approach

To evaluate the applicability of suggested incremental-iterative approach and the R crack model for evaluation of diagonal cracking load, 82 shear tests in mRC-V subset of shear database with documented $\chi_{cr,exp}$ and diagonal cracking loads $V_{cr,exp}$ are simulated in FE programme DIANA FEA. To enhance the modelling of different tests with various geometries and material properties, a parametric modelling script was developed (in Python), which is provided in appendix D.

The FE models are developed similar to the described reference models in chapter 7. The incremental refined approach with a combined arc-length control and energy-based adaptation of load increment size is implemented (variation I3). The concrete is simulated using a total strain based crack model. The material properties of concrete are calculated (similar to reference investigations in chapter 7 based on concrete compressive strength f_c). An overview of material and analysis set is given in Table 8-1.

Necessary changes of material or analysis parameters for evaluation of cRC models and the settings of the RF crack model will be described in the corresponding chapters.

The models are evaluated first with a rotating crack orientation (threshold angle $\alpha_R = 10^\circ$) to assess the prediction accuracy of models regarding numerical diagonal cracking load $V_{cr,FE}$. The results are going to be analysed with regard to numerically reached diagonal cracking loads $V_{cr,FE}$ and ultimate shear loads $V_{u,FE}$, the maximum deflections of the beams

at the state of diagonal cracking $\delta_{cr,FE}$ as well as numerically estimated critical sections $x_{cr,FE}$. The significant findings of evaluations are shown exemplarily for representative models in this chapter. Further results of the numerical evaluations are documented in appendix D.

Table 8-1: Material and analysis parameter settings of FE models

Material parameters of concrete	setting
Elasticity modulus [N/mm ²]	$E_c = 21500 \cdot (f_c/10)^{1/3}$
Concrete tensile strength [N/mm ²]	$f_{ct} = 0.3 \cdot (f_c - 4)^{2/3}$
Tensile fracture energy [N/mm]	$G_F = 0.073 \cdot (f_c)^{0.18}$
Compressive fracture energy [N/mm]	$G_{F,c} = 250 \cdot G_F$
Poisson's ratio ν	$\nu = 0.2$
Material parameters of steel reinforcement	setting
Elasticity modulus [N/mm ²]	210000 N/mm ²
Poisson's ratio	$\nu = 0.3$
Yield stress	as provided
Max. strain	as provided or $\epsilon_{su} = 0.05$
Plastic strain	$\epsilon_u - f_{sy}/E_s$
Analysis procedure	setting
Iteration method	regular NEWTON-RAPHSON
Solution method	parallel direct sparse
Load incrementation approach	energy-based adaption and arc-length control
Initial step size	$u_{in} = f_{ct} \cdot l^2 / (12 \cdot E_c \cdot h)$
Minimum step size	0.01 mm
Maximum number of load steps	500
Maximum iteration per load step	50
Energy convergence tolerance	$1 \cdot 10^{-3}$
Force convergence tolerance	$1 \cdot 10^{-2}$

8.3 Diagonal cracking of RC members under monotonic shear loads

8.3.1 Diagonal cracking and failure loads

The shear tests in the mRC subset are simulated with the R crack model and the proposed iterative-incremental approach. The resulted diagonal cracking loads are determined using the short-term instable cracking for shear span to depth ratios smaller than 3.0 and correspond to the ultimate numerical loads attained in FE simulations of members with higher a/d values.

The resulted values of diagonal cracking loads $V_{cr,FE}$ and ultimate shear loads $V_{u,FE}$ are compared with experimental values (compare Figure 8-1). The prediction accuracy is

calculated based on median value m , standard deviation s and variation coefficient v of model safety factors, as introduced in chapter 6.

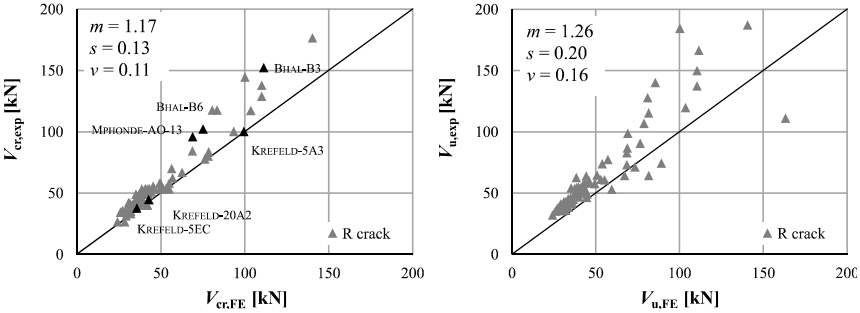


Figure 8-1: Comparison between the prediction accuracy of models with a rotating crack model regarding diagonal cracking load V_{cr} (left) and ultimate shear load V_u (right)

Whereas the diagonal cracking load can be predicted satisfactorily with a good prediction accuracy ($m = 1.17$) and relatively small scatter ($v = 0.11$), the ultimate load is underestimated for most of the tests ($m = 1.27$). Based on the results, the path of failure crack signifies if an immediate failure follows after diagonal cracking or not. A comparison between the model safety factor and the shear span to depth ratio shows that the ultimate load is mainly underestimated for members with shear span to depth ratios between 2 and 4.

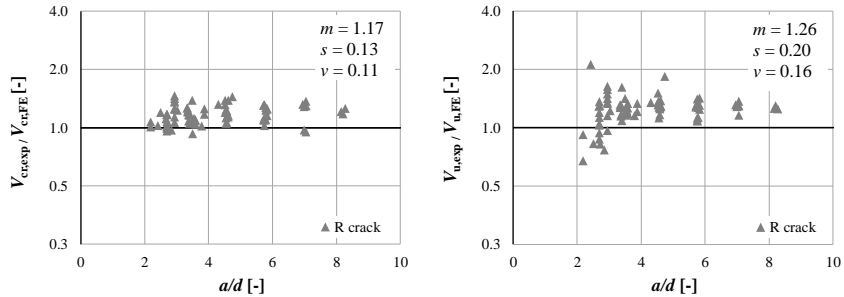


Figure 8-2: Correlation between prediction accuracy of the model regarding $V_{cr,FE}$ (left) as well as $V_{u,FE}$ (right) and the shear span to depth ratio

Results of selected tests (shown in black and labelled in Figure 8-1) would be discussed in detail to give a better insight on performance of the R crack model for simulation of different beam and test configurations. For the evaluation, the numerical shear load - deflection curves and the cracking states of beams are compared with the experimental diagonal and failure loads as well as experimental critical sections.

8.3.2 Load-displacement curves and crack propagation

An example of a nearly exact approximation of both diagonal cracking load and ultimate shear load ($\gamma_{\text{mod,cr}} = 1.0$ and $\gamma_{\text{mod,u}} = 0.92$) is the FE model corresponding to beam 5A3 with a beam depth of $h = 457.2$ mm, a shear span to depth ratio of $a/d = 2.18$ and a $\rho_1 = 3.0$ % tested by KREFELD.

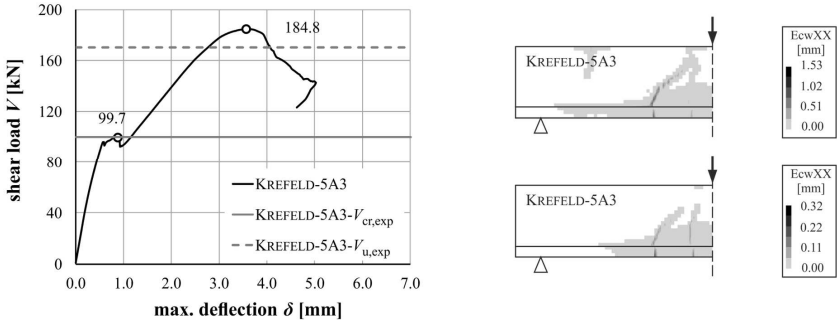


Figure 8-3: Load-deflection curve of beam 5A3 (left) as well as diagonal (right, down) and failure (right, up) cracking stages

However, the high prediction accuracy of the model is not accompanied by a good approximation of critical section. The resulted $x_{\text{cr,FE}}$ is larger than the experimental value as illustrated in Figure 8-4.

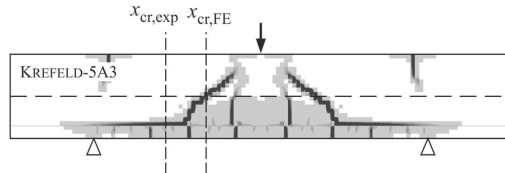


Figure 8-4: Comparison of the experimental and numerical critical section of beam 5A3 (cracks with a crack width > 0.1 illustrated in black)

For a beam with the same shear span length, a lower beam depth of $h = 308.8$ mm and hence a higher shear span to depth ratio of $a/d = 3.6$ tested by KREFELD, direct after the critical diagonal cracking, an instable crack opening proceeds and no convergence under a higher load level can be reached. This leads to equal numerically obtained diagonal cracking and ultimate loads. This model predicted the experimental diagonal cracking load almost exactly (a deviation of of 4 % from experimental value) but underestimated the ultimate shear load by 18 %.

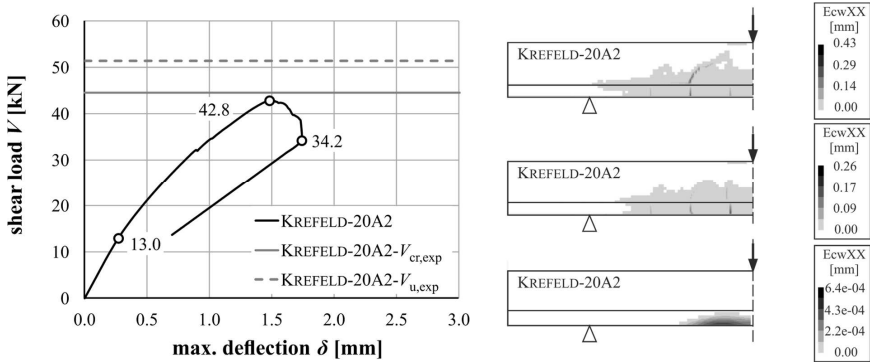


Figure 8-5: Load-deflection curve of beam 20A2 (left) and flexural (right, down), diagonal (right, middle) and failure (right, up) cracking stages

Similar to beam 5A3, the experimental and numerical critical sections do not agree with each other. In contrast to usual observations during shear tests, the failure crack is not the next emerged primary crack to support axis.

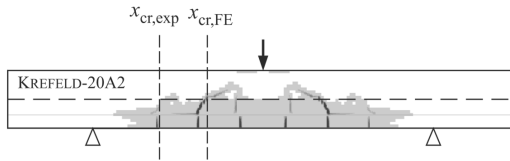


Figure 8-6: Comparison of experimental and numerical critical section of beam 20A2 (cracks with a crack width > 0.1 illustrated in black)

For shear test 5EC conducted by KREFELD with considering higher shear span to depth ratio of 6.99 and the same beam depth as beam 20A2, it can be seen that also for long shear spans, a reliable approximation of diagonal cracking load can be reached for beams with small depths ($d/d_0 = 1.54$) using the proposed incremental method.

In contrast to beams with low and intermediate shear span to depth ratios, the numerically obtained critical crack path and the critical section is closer to support axis and underestimated the experimental critical section. Using the numerical value $x_{cr,FE}$ for the analytical determination of diagonal cracking load $V_{cr,cal}$ with the proposed mechanical model (Eq. 6-8-Eq. 6-10) leads to an overestimated calculated diagonal cracking load.

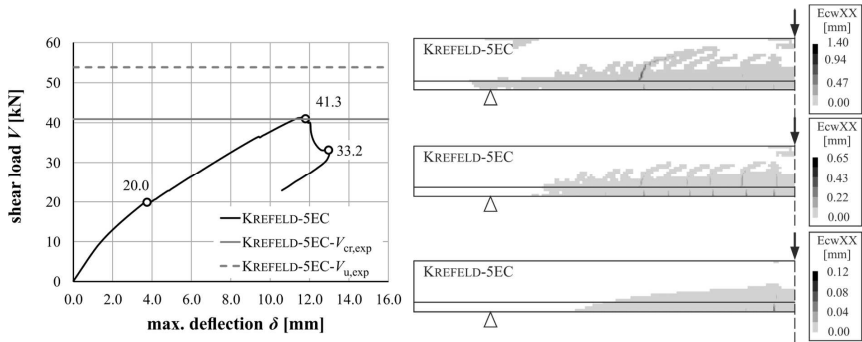


Figure 8-7: Load-deflection curve of beam 5EC (left) and flexural (right, down), diagonal (right, middle) and failure (right, up) cracking stages)

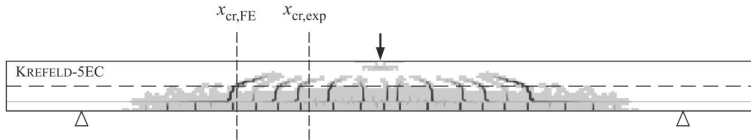


Figure 8-8: Comparison of experimental and numerical critical section of beam 5EC (cracks with a crack width > 0.1 illustrated in black)

A high strength concrete beam tested by MPHONDE et al. with an intermediate shear span to depth ratio of $a/d = 3.49$ and a concrete compressive strength of 94 N/mm^2 belongs to the few tests conducted on high strength concrete beams with documented experimental diagonal cracking loads. The resulted shear load-deflection curve and crack patterns at different load levels are depicted in Figure 8-9.

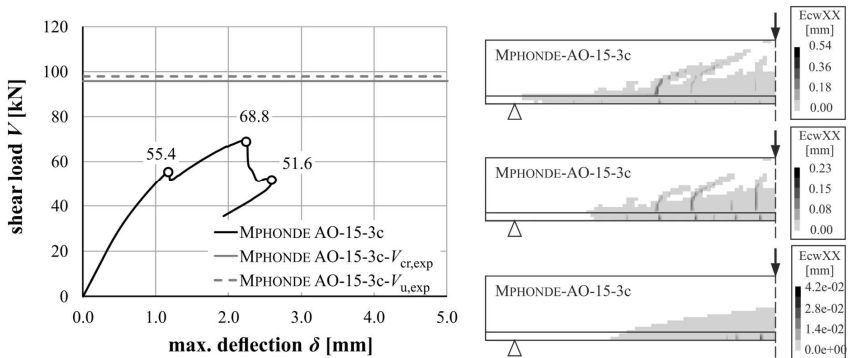


Figure 8-9: Load-deflection curve of beam AO-15-3c (left) and flexural (right, down), diagonal (right, middle) and failure (right, up) cracking stages

The diagonal cracking load of this member is numerically underestimated by 39 %. The failure crack path achieved numerically for the beam deviates also significantly from the experimental crack path. The brittleness of crack propagation can be a reason for the premature numerical failure of the model. This beam shows the limitations of proposed incremental model for an appropriate adaption of loading increment to released energy even at load levels beneath the experimental critical diagonal cracking.

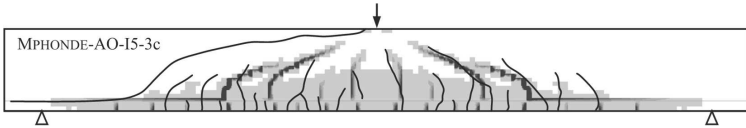


Figure 8-10: Comparison of experimental and numerical critical section of beam AO-15-3c (cracks with a crack width > 0.1 illustrated in black)

Diagonal cracking load of deep beams tested by BHAL belong to numerically underestimated diagonal cracking loads using a rotating crack approach. A comparison between experimental and numerical results of beam B3 with a beam depth of $h = 950$ mm, a shear span to depth ratio of $a/d = 2.94$ and a $\rho_1 = 1.26$ % are presented in Figure 8-11. The numerical diagonal cracking load underestimated the experimental value by 36 %.

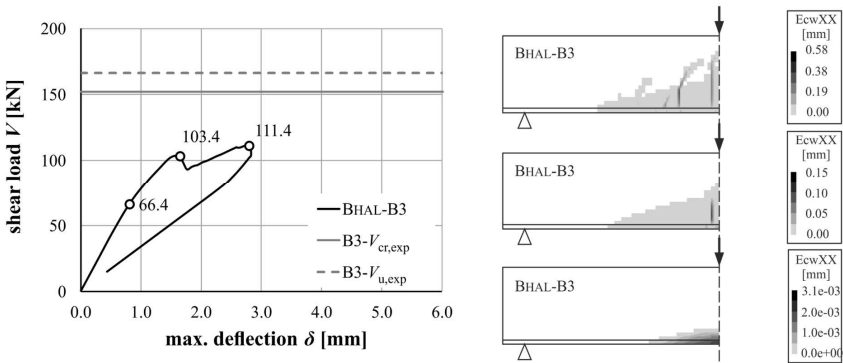


Figure 8-11: Load-deflection curve of beam B3 (left) and flexural (right, down), diagonal (right, middle) and failure (right, up) cracking stages

After new primary cracks appear in sections closer to support axis, an adjacent crack to a diagonal crack starts to over-rotate. This crack is marked in crack pattern short before failure (Figure 8-12). A change of incremental method (for instance initial or minimum load step size) could possibly influence this crack rotation and cause a better prediction of critical section based on failure crack. This is, however, not a useful method, as long as the incremental method cannot be applied to other beam configurations.

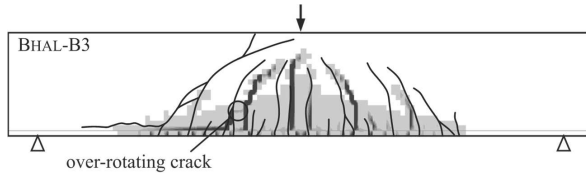


Figure 8-12: Comparison of experimental and numerical crack patterns of beam B3 (cracks with a crack width > 0.1 illustrated in black)

Same model response is observed in FE results of beam B6 with $h = 650$ mm, same shear span to depth ratio and a lower longitudinal reinforcement ratio of $\rho_l = 0.63\%$. The FE model underestimated the diagonal cracking load and ultimate shear load of this beam by 35 % and 41 %, respectively.

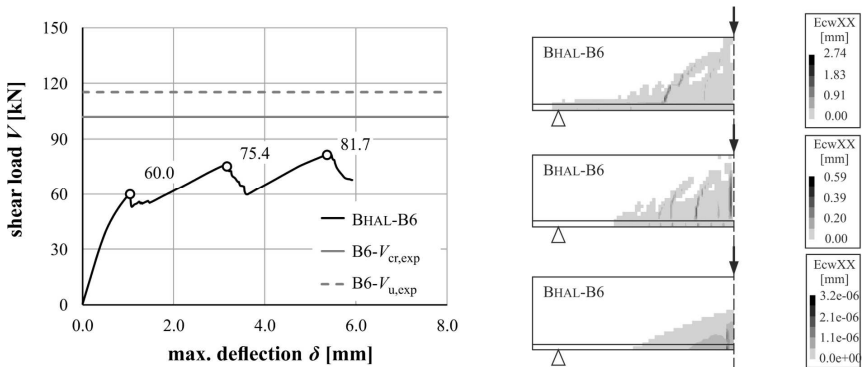


Figure 8-13: Load-deflection curve of beam B6 (left) and flexural (right, down), diagonal (right, middle) and failure (right, up) cracking stages

Based on short instable phases after each cracking state, it can be concluded that a convergence problems after diagonal cracking ($V_{cr,FE} = 75.4$) results in the numerical premature failure of the model. Based on the numerical crack path in Figure 8-14, the over-rotating R cracks (marked) is spotted as the main reason for convergence problems after cracking. Changing the crack model to a rotating to fixed crack model (RF) prevents the illustrated over-rotation and causes higher stability of FE response.

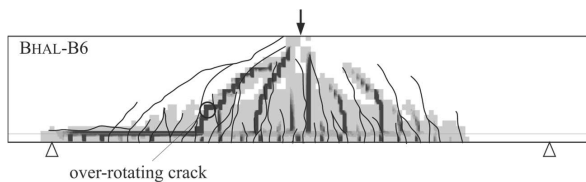


Figure 8-14: Comparison of experimental and numerical crack patterns of beam B6 (cracks with a crack width > 0.1 illustrated in black)

8.3.3 Brittleness of critical diagonal cracking and prior notice

For the observed rather brittle behaviour of diagonal cracking of concrete members without shear reinforcement, a numerical approximation of the prior notice is beneficial for definition of a safety concept and assessment purposes. For an objective evaluation of brittleness of diagonal cracking and subsequent shear failure, parameters are required for the quantification of prior notice.

As pointed out during the reference evaluations in chapter 7 and section 8.3.2, following criteria are suggested for evaluation of prior notice:

- diagonal cracking before ultimate shear failure
- maximum deflection at state of critical diagonal cracking
- energy release at the state of critical diagonal cracking

To define a scale using prior notice of failure with such criteria, a factor between zero and one is derived. A brittle failure is designated with a brittleness factor $\eta = 1$ and a higher value of η shows some kind of prior notice.

The first criterion was evaluated in chapter 5 based on experimental results in mRC-V dataset (Figure 5-8) and is difficult to quantify using the experimental datasets due to the existing large scatter. With the numerical evaluations using the R crack model, the relative difference between $V_{cr,FE}$ and $V_{u,FE}$ was more significant for members with a lower shear span to depth ratio than 3.0. The higher ultimate shear load caused by the activation of direct compressive strut after diagonal cracking for such models (compare Figure 8-15, left) can be quantified in correlation to shear span to depth ratio.

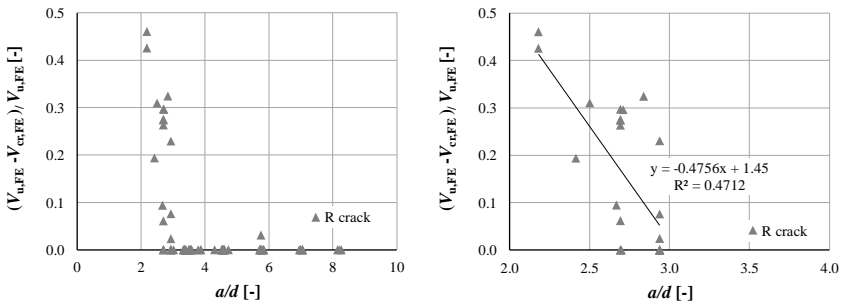


Figure 8-15: Correlation between the difference between diagonal cracking loads and ultimate shear loads with shear span to depth ratio a/d for all models (left) and for models with $2.0 \leq a/d \leq 3.0$ (right)

For the 23 beams with shear span to depth ratios $2.0 \leq a/d \leq 3.0$ (Figure 8-15, right), a correlation based on shear span to depth ratio can be used for approximation of a brittleness factor defined as

$$\eta_{cr} = 0.33 \cdot \left(\frac{a}{d}\right) \quad \text{for } 2.0 \leq a/d \leq 3.0 \quad \text{Eq. 8-1}$$

To determine a factor for higher shear span to depth ratios, the results of R crack models are not suitable, since the influence of further load-bearing mechanisms such as aggregate interlock on ultimate shear load is not computable using the R cracks. The proposed RF crack model is more appropriate for evaluation of ultimate loads of such beams.

The first criterion is evaluated based on FE results using the numerical value of beam maximum deflection at the state of diagonal cracking $\delta_{cr,FE}$ and the calculated beam deflection at the state of flexural failure $\delta_{u,cal}$ according to Eq. 8-2.

$$\delta_{u,cal} = \frac{F_u \cdot l^3}{48 \cdot E_c \cdot I^{II}} \quad \text{Eq. 8-2}$$

Where F_u equals:

$$F_u = \frac{A_s \cdot f_{sy} \cdot z}{l/4} \quad \text{Eq. 8-3}$$

With

$$z = d - h_c/3 \quad \text{Eq. 8-4}$$

The moment of inertia of the cracked section I^{II} is calculated using the following equation according to [Zil-2010]:

$$I^{II} = \frac{b \cdot h_c^3}{3} + \alpha \cdot A_s \cdot (d - h_c)^2 \quad \text{Eq. 8-5}$$

The value of α is calculated based on Eq. 4-17 and the depth of concrete compression zone h_c according to Eq. 4-16. The ratio between $\delta_{cr,FE}$ and $\delta_{u,cal}$ was evaluated in correlation with shear span to depth ratio and longitudinal reinforcement ratio (compare Figure 8-16).

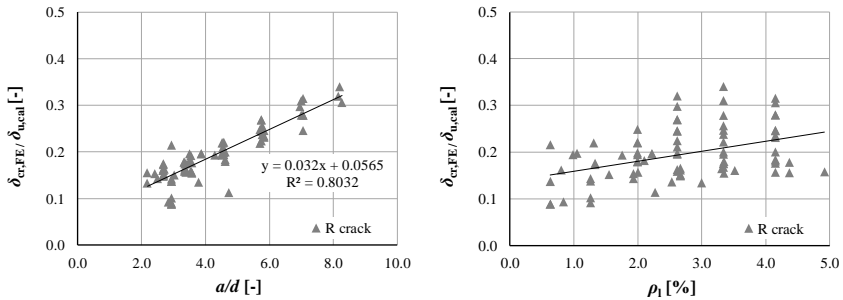


Figure 8-16: Correlation between the ratio $\delta_{cr,FE} / \delta_{u,cal}$ with shear span to depth ratio a/d (left) and longitudinal reinforcement ratio ρ_l (right)

It is evident that the maximum deflection at the state of diagonal cracking is in a range much lower than the deflection due to flexural cracking (between $0.1 - 0.3 \cdot \delta_{u,cal}$). A clear tendency is also observed between shear slenderness and the ratio $\delta_{cr,FE} / \delta_{u,cal}$. As a result, a parameter based on shear span to depth ratio can be proposed to quantify the prior notice.

$$\eta_{\delta} = 0.94 - 0.032 \cdot \left(\frac{a}{d}\right) \quad \text{Eq. 8-6}$$

Using Eq. 8-5 and Eq. 8-6, for beams with shear span to depth ratios $2.0 \leq a/d \leq 3.0$, an increasing brittleness factor as a function of a/d based on difference between the ultimate and the diagonal cracking loads η_{cr} and a decreasing brittleness factor based on beam deflection at diagonal cracking η_{δ} are acting. The total brittleness factor for such beams corresponds to:

$$\eta = 0.31 \cdot \left(\frac{a}{d}\right) - 0.01 \cdot \left(\frac{a}{d}\right)^2 \quad \text{for } 2.0 \leq a/d \leq 3.0 \quad \text{Eq. 8-7}$$

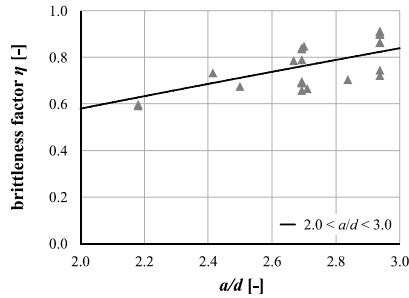


Figure 8-17: Total brittleness factor for beams with shear span to depth ratios $2.0 \leq a/d \leq 3.0$

The combination between displacement based brittleness factor and energy release evolution is more relevant for beams with high shear span to depth ratios. For such beams higher beam deflections are also affecting the energy release factor g during diagonal cracking. This factor is calculated as a ratio between out of balance energy norm and the energy convergence norm. A comparison between energy release of two beams 5A3 ($a/d = 2.18$) and 5EC ($a/d = 6.99$) are illustrated in Figure 8-18.

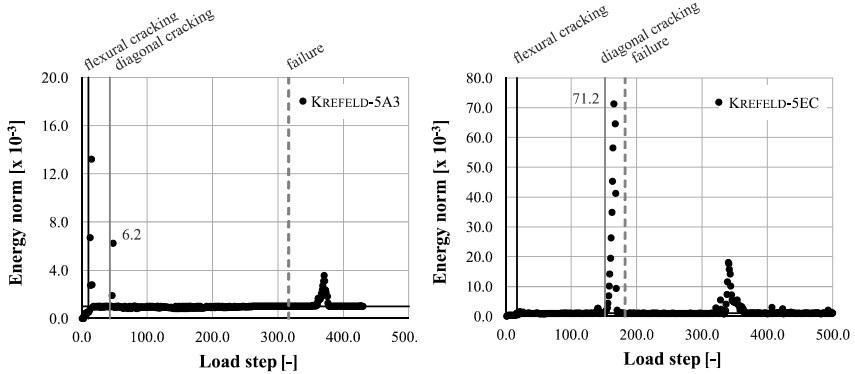


Figure 8-18: Comparison of energy release during cracking for beams 5A3 (left) and 5EC (right)

A relative sudden increase in released energy at the state of diagonal cracking for model 5EC shows a rather brittle formation of critical diagonal crack, which makes finding a new equilibrium condition impossible for the model with the R cracks. In contrast, the smaller out of balance energy at the state of diagonal cracking for model 5A3 is settled within four load steps.

The evolution of out of balance energy is a powerful criterion, as it also accounts for brittleness of cracking in members casted with high-strength concrete. For instance, for beam AO-15-3c (compare Figure 8-19), the out of balance energy at the state of diagonal cracking is higher than a comparable test on a normal-strength concrete beam 19A2 tested by KREFELD.

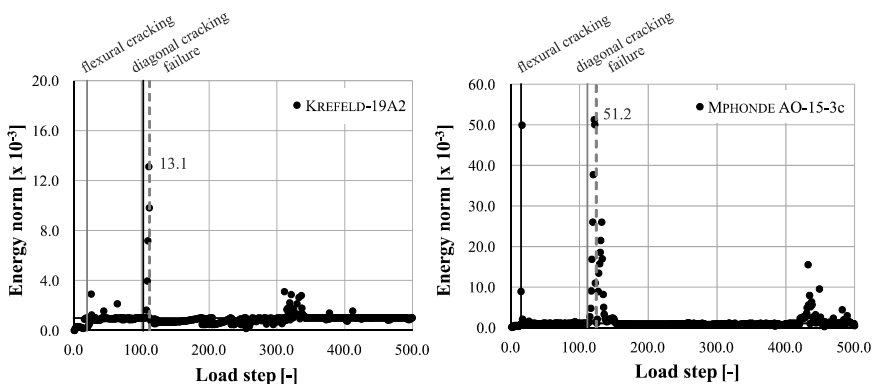


Figure 8-19: Energy release during cracking for beams 19A2 (left) and AO-15-3c (right)

Using a scaling method with peak value of 20 for relative out of balance energy g , the brittleness based on energy release is defined as follows:

$$\eta_g = \frac{(g - 1)}{20} \leq 1.0 \quad \text{Eq. 8-8}$$

For beam 5A3 is the energy based brittleness factor equal to $\eta_g = 0.26$ and for beam model 5EC, a factor equal to $\eta_g = 1.0$ can be determined. Based on that, the overall brittleness factor of beam 5EC corresponds to

$$\eta = \eta_g \cdot \eta_\delta = 0.72 \quad \text{Eq. 8-9}$$

It must be noted that the introduced factors intend to propose a conceptual method for quantification of prior notice and should be improved using more refined numerical approaches for evaluation of both diagonal cracking load and ultimate shear load.

8.4 Evaluation of the rotating to fixed crack model (RF crack model)

8.4.1 Diagonal cracking and failure loads

Six representative beams in the chapter 8.3.2 are modelled with a rotating to fixed cracking approach. Based on the proposed model, the cracks are set as fixed cracks from a threshold total strain $\varepsilon_{nn,lim}$ according to Eq. 7-10. The shear stiffness reduction was adapted for cracked concrete with a variable shear retention factor (β) proposed by AL-MAHAIDI with a minimum shear retention factor of 0.01 (see chapter 7.8). The threshold total strain proposed for the new RF crack model is assessed for different material and tests configurations. The benefits and limitations of the F model will be evaluated using the simulations.

The obtained results using the RF crack model do not change significantly for beam 5A3. This is a desired output, since the good accordance between experimental and numerical results for this beam shows that the main load-bearing mechanisms are adequately considered in the R crack model and aggregate interlock was not a governing load-bearing mechanism during the test. The numerical results of the model 5A3-RF show merely a reduction of failure crack width (from 1.53 to 1.19) and a reduced beam deflection at failure state.

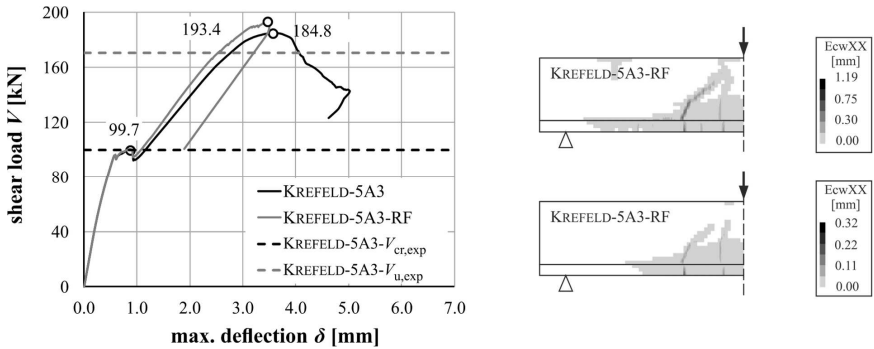


Figure 8-20: Load-deflection curve of the model of beam 5A3 with R and RF crack model (left) and crack pattern at the state of diagonal cracking (right, down) and under ultimate load (right, up) of the model 5A3-RF

Similar to beam 5A3, the crack pattern and obtained ultimate load with the RF crack model is not significantly changed for beam 20A2. The shear-load-deflection curve and cracking states are illustrated in Figure 8-21. The ultimate crack width equals 0.32 mm, which is lower than the resulted value by the rotating crack model (0.43 mm).

The results are less apt, as the crack over-rotation after diagonal cracking had to be counteracted by activation of shear stresses along cracks. The activation of shear stiffness of the cracked elements could have enabled the prediction of ultimate shear loads as well. A comparison between model of beam 5EC with a rotating crack model and the proposed RF model is presented in Figure 8-22.

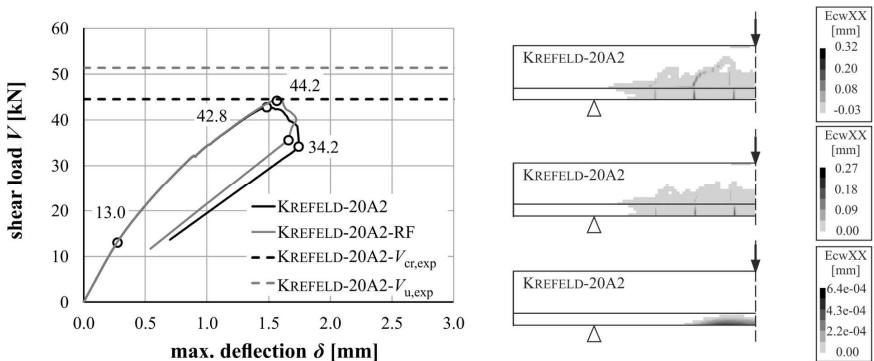


Figure 8-21: Load-deflection curve of the model of beam 20A2 with R and RF crack model (left) and crack pattern at the state of flexural cracking (right, down), diagonal cracking (right, middle) and under ultimate load (right, up) of the model 20A2-RF

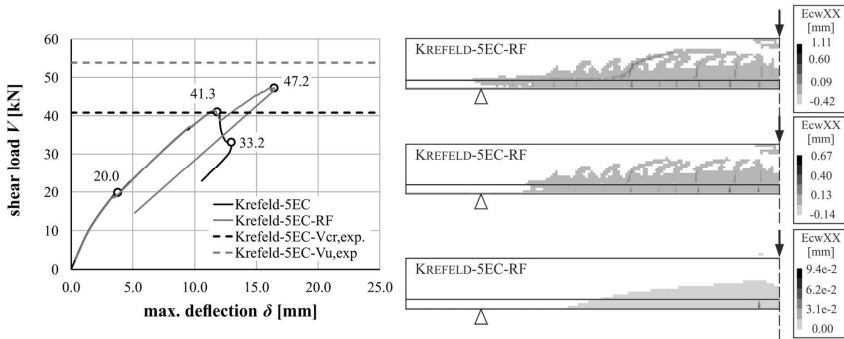


Figure 8-22: Load-deflection curve of the model of beam 5EC with R and RF crack model (left) and crack pattern at the state of flexural cracking (right, down), diagonal cracking (right, middle) and under ultimate load (right, up) of the model 5EC-RF

For beam 5EC, the shear-load displacement curves of the models with the R cracks and the RF cracks deviate as looked-for from a point corresponding to critical diagonal cracking. Although the activated shear stiffness in cracks in the RF model is not adequate for a satisfactory prediction of ultimate shear load, the numerically predicted ultimate load is higher than the models with the R cracks.

The path of the critical diagonal crack does not change significantly from the resulted critical cession using the R crack model (compare Figure 8-8 and Figure 8-23).

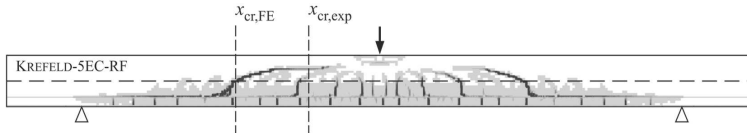


Figure 8-23: Comparison of experimental and numerical crack patterns of beam 5EC with the proposed rotating to fixed cracking approach (cracks with a crack width > 0.1 illustrated in black)

Using the RF crack model, a better prediction of the ultimate shear load is possible for the high-strength concrete beam tested by MPHONDE et al.. The brittle behaviour of this beam at failure is reasonably reproduced using the applied incremental method (even after variation of minimum step size values in a variational approach). The numerical diagonal cracking load was slightly higher than for the corresponding rotating crack model with a lower maximum crack width. The failure occurred however at crack widths significantly higher than in R model variation. The predicted critical section did not change with the RF crack model.

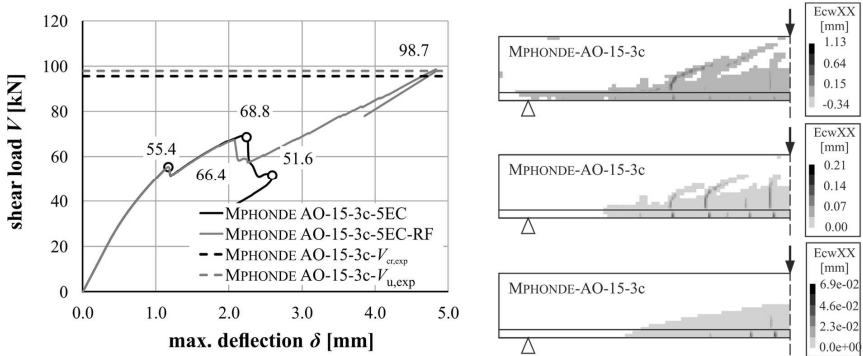


Figure 8-24: Load-deflection curve of the model of beam AO-15-3c with R and RF crack model (left) and crack pattern at the state of flexural cracking (right, down), diagonal cracking (right, middle) and under ultimate load (right, up) of the model AO-15-3c-RF

For beam B3 simulated with the proposed rotating to fixed crack model, the resulted ultimate load is significantly higher than the experimental failure shear load. A point with a stiffness change is detected in nonlinear path of shear load-deflection curve, at which no new cracks were formed and the main change in beam response was due to increasing crack widths. In general, the resulted crack widths were larger in comparison to calculated ones using the model with R cracks. The two load-deflection curves of R and RF model deviate not at a point corresponding to diagonal cracking load. The R crack model caused a premature failure, which prohibited the prediction of diagonal cracking load. Based on crack propagation sequence of the RF crack, the critical diagonal crack emerged at $V = 139.3$. The load-deflection curve get steeper at this point, which is based on the activated shear stiffness in the critical diagonal crack. The ultimate shear load is overestimate using the RF crack model for beam B3. The reason for the overestimation is an overvalued shear retention factor. A modification of lower bound for shear retention factor would rescind this problem (will be discussed in chapter 8.4.2).

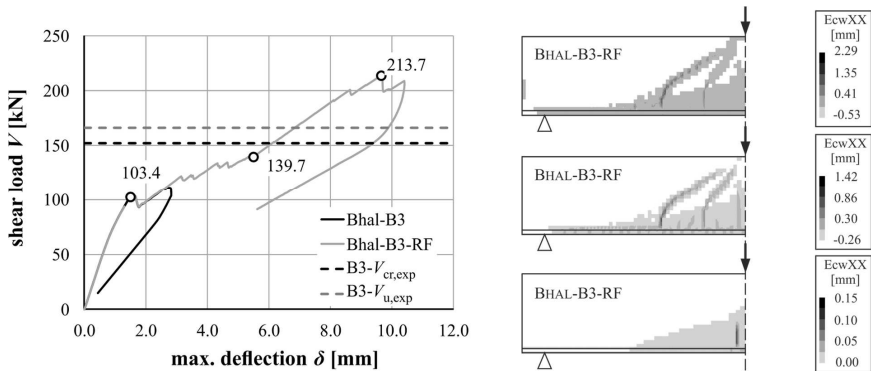


Figure 8-25: Load-deflection curve of the model of beam B3 with R and RF crack model (left) and crack pattern at the state of flexural cracking (right, down), diagonal cracking (right, middle) and under ultimate load (right, up) of the model B3-RF

As depicted in Figure 8-26, a very good accordance between numerical and experimental crack pattern is reached using the adjustment of the crack model to RF.

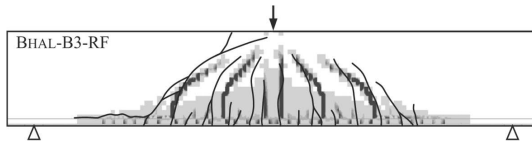


Figure 8-26: Comparison of experimental and numerical crack patterns of beam B3 with the proposed rotating to fixed cracking approach (cracks with a crack width > 0.1 illustrated in black)

In contrast to model B3, the adaption of the crack model to RF provides a good prediction of the numerical diagonal cracking load as well as ultimate load possible for model B6. The results are illustrated in comparison to numerical shear load-displacement curve obtained with a rotating crack model in Figure 8-27.

The load-deflection curves of R model and RF model deviate also diverge also at the point corresponding to critical diagonal cracking. A comparison between ultimate crack widths (compare Figure 8-13 and Figure 8-27) show that in contrast to B3, the cracks widths with RF model at ultimate load were lower than the resulted values using a rotating crack model. The failure crack path is also better approximated for beam B6 with the new RF crack model (see Figure 8-28).

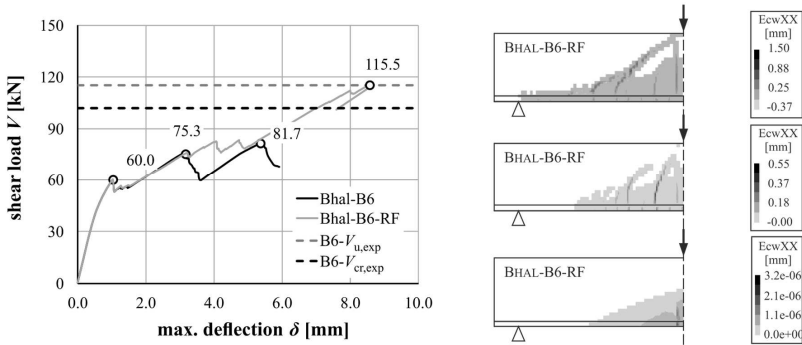


Figure 8-27: Load-deflection curve of the model of beam B6 with R and RF crack model (left) and crack pattern at the state of flexural cracking (right, down), diagonal cracking (right, middle) and under ultimate load (right, up) of the model B6-RF

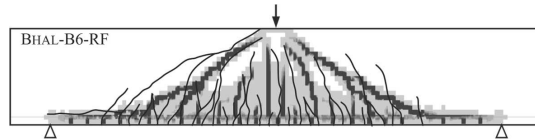


Figure 8-28: Comparison of experimental and numerical crack patterns of beam B6 with the proposed rotating to fixed cracking approach

For deep members, experimental observations e.g. in [Bha-1968] show that the positive effects of longitudinal tensile reinforcement decrease with a growing beam depth. The numerical results for deep beams show that the width of primary cracks in such beams overstep the critical crack width $w_{cr,1}$ and further consideration of relative displacement of crack faces influence the general load-deflection behaviour. This is also in accordance with the observations made during experimental investigations (e.g. [Pla-1969], [Rei-1990]). Therefore, a modification of shear retention factor might lead to a better approximation of ultimate shear loads for deep beams.

8.4.2 Parametric study

Using the RF model, the influence of input parameters including concrete tensile parameters (concrete tensile fracture energy G_F and concrete tensile strength f_{ct}) can be evaluated on the response of the numerical models. Until the fixation of cracks from the threshold total strain value $\epsilon_{nn,lim}$, the effects of parameter variation of the softening behaviour of model with R cracks is traced. The effects of tensile parameters is also considered on the value of threshold total strain value $\epsilon_{nn,lim}$. As the crack model switches to the fixed crack model, the same variable shear retention factor according to AL-MAHAIDI is considered. The reduction of the shear retention factor β depends also on concrete tensile

strength (compare Eq. 7-8). A further variable parameter is the value of minimum shear retention factor β_{\min} , toward which the shear retention along cracks reduces.

Within the parametric study, three representative beams B6 (deep beam), 20A2 (beam with intermediate a/d) and 5EC (beam with high a/d) are simulated with two different tensile fracture energy values G1 and G2 and two different concrete tensile strength values T1 and T2. Furthermore, the effects of the defined minimum shear retention factor (β_{\min}) is assessed for two values C1 and C2. An overview of designations is given in Table 8-2. The variable parameters are defined based on previously introduced equations in section 2.1.2.

Both fracture energy values G1 (according to CEP *fib* 90) and G2 (according to BAŽANT / BECQ-GIRAUDON) are lower than the basic value of fracture energy according to Model Code 2010. These suggestions consider further properties of concrete such as aggregate size (G1) and a combination of aggregate size and w/c ratio ($G2 < G1$).

Table 8-2: Overview of variable parameters

Tensile fracture energy	setting
Basic setting	Model Code 2010 (Eq. 2-14)
G1	CEP FIP 90 (Eq. 2-12)
G2	BAŽANT / BECQ-GIRAUDON (Eq. 2-11)
Tensile strength	
Basic setting	f_{ct} according to DIN EN 1992-1-1 (Eq. 6-4)
T1	$f_{ctk,0.05}$ ($0.7 \cdot f_{ct}$) according to DIN EN 1992-1-1
T2	f_{ct} according to REINECK (Eq. 6-8)
Min. shear retention factor	
Basic setting	0.010
C1	0.050
C2	0.001

For beam B6 the required concrete properties are available, whereas an approximation of these properties is needed for beams 20A2 and 5EC (assumed as $d_g = 30$ mm and $w/c = 0.5$). Since the value of fracture energy is also implemented in the correlation for determination of threshold strain of the RF model $\varepsilon_{nn,lim}$, the effects of this variation are also considered on the fixation state of the critical diagonal crack. The results are illustrated for beam models 20A2 and 5EC in Figure 8-29.

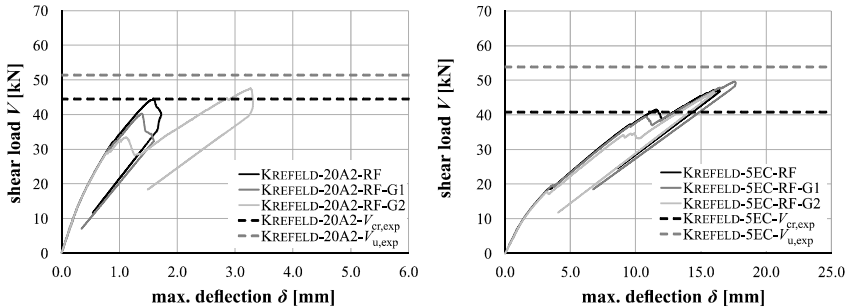


Figure 8-29: Shear load-deflection curve of the model of beam 20A2 (left) and 5EC (right) under variation of fracture energy

Using this comparison, a lower value of fracture energy reduces the ultimate shear load and the activation point of shear stresses along cracks in model 20A2. For the fracture energy value G1, no further increase in shear load is possible due to fixation of cracks, whereas for the model with G2, the activation of shear stiffness for cracked elements increases the numerical ultimate load. These results can be discussed using the depicted curve of shear retention factor in Figure 8-30.

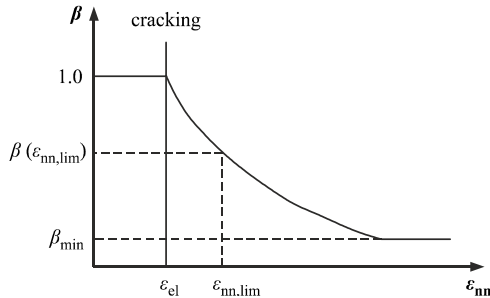


Figure 8-30: Shear retention factor upon cracking for the RF crack model

A reduction of fracture energy in model 20A2-RF-G1 causes a value of $\epsilon_{nn,lim} = 0.003$, which corresponds to a shear retention value of 0.009 being lower than the minimum value of shear retention factor. Therefore, a constant shear retention factor of 0.01 (basic value) is activated after cracking of elements. This value is apparently not adequate to reinstate a new equilibrium condition after critical diagonal cracking. In contrast, the corresponding value of threshold strain for 20A2-RF-G2 equals $\epsilon_{nn,lim} = 0.002$, which corresponds to a shear retention factor of $\beta = 0.013$ (higher than the minimum shear retention factor). Consequently, a strain dependent tangential stiffness in cracked elements is activated.

For beam model 5EC, the fracture energy influences the activation points of tangential shear stiffness in cracked elements, which are marked in Figure 8-29, right. Since the widths of primary cracks increase with the lower value of fracture energy, the shear stiffness of cracked elements is activated for beam 5EC-RF-G2 during the flexural cracking (beam deflection of 5.5 mm). For 5EC-RF-G1, the crack model translation from rotating to fixed occurs at the state of diagonal cracking (beam deflection of 10.5 mm). The results signify that an activation of shear stiffness in cracked elements upon the state of critical diagonal cracking leads to better prediction of ultimate shear loads. At the same time, flexibility of the proposed RF crack model is shown, which makes activation of shear stiffness possible in cracks in different cracking states.

The value of concrete tensile strength influences the diagonal cracking load, which is not significant for small alterations as in case of T1 and T2. The results are depicted for beam models 20A2 and 5EC in Figure 8-31. In general, higher concrete tensile strength decreases the threshold value $\epsilon_{mn,lim}$, increases the shear retention factor at the state of cracking and also increases the cracking loads.

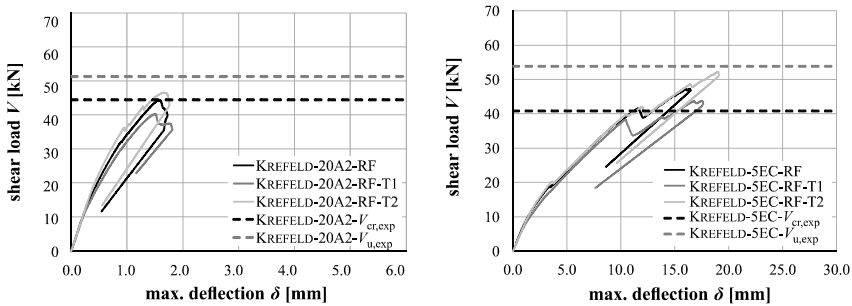


Figure 8-31: Shear load-deflection curve of the model of beam 20A2 (left) and 5EC (right) under variation of concrete tensile strength

The influence of variation of concrete tensile strength is however not so significant for beam models 20A2-RF-T1 and 20A2-RF-T2. According to Figure 8-31, the higher value T2 causes for both models 20A2 and 5EC a higher diagonal cracking load. Due to the increase in shear retention factor, the model 5EC-RF-T1 can also better approximate the ultimate shear load. The results point out also the sensibility of results to slight changes in input parameters, which causes for certain parameter sets a premature numerical failure caused by convergence problems in case of 5EC-RF.

For all beam models, the role of minimum value of the shear retention factor β_{min} is perceptible on predicted ultimate shear loads.

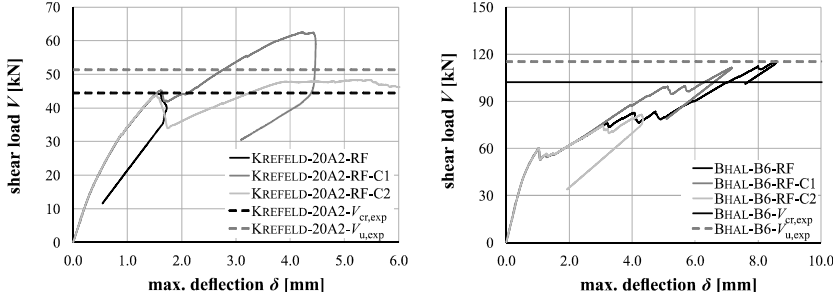


Figure 8-32: Shear load-deflection curve of the model of beam 20A2 (left) and B6 (right) under variation of minimum shear retention factor

The modification of β_{\min} for beam 20A2 shows that for the highest value, higher ultimate shear load is resulted. In contrast, the higher value of minimum shear retention factor causes for beam model B6-RF-C1 an over-stiff beam response, which does not increase the resulted numerical ultimate load. The C2 values of β_{\min} cause an increased softening behaviour, which leads in the cause of simulated deep beam B6 to a premature numerical failure.

Based on the parametric study and the characteristic points marked in Figure 8-30, it was observed that the minimum value of shear retention factor should be selected smaller than 10% of the value $\beta(\varepsilon_{nn,lim})$. Thereafter, following criterion should be fulfilled by the selected minimum shear retention factor:

$$\beta_{\min} \leq 0.1 \cdot \left(0.4 \cdot \frac{f_{ct}}{E_c \cdot \varepsilon_{nn,lim}} \right) \quad \text{Eq. 8-10}$$

8.5 FE simulation of RC members under cyclic loading

To determine the cyclic diagonal cracking, selected cRC tests are simulated with similar geometry and boundary conditions. The models are evaluated using a stationary analysis of a damaged beam through the adjustment of constitutive law of concrete under tension as proposed in chapter 3. Nonlinear analysis of models under incremental loading is conducted to determine the cyclic diagonal cracking load of the members. In the incremental-iterative approach, the minimum load step size is reduced to enhance finding of an initial equilibrium condition. For this aim, the initial size of load step was set as 0.1 mm and not according to the proposed value of u_{in} .

To account for effects of cyclic loading in a stationary numerical analysis, the existing damage should be considered in constitutive material laws and model configurations. In this part, cyclic effects on tensile behaviour of concrete is investigated. Further effects caused by bond loss of longitudinal reinforcement or compression failure of concrete due

to fatigue are not the topic of this investigation. The observations within fatigue tensile tests and the proposed tensile model using cyclic creep phenomenon is used to adapt the tensile curve of concrete. Two documented beams in cRC subset (V3 and V5 tested by KOHL) are modelled and compared with the reference monotonic test V1 with a diagonal cracking load of 60 kN. Both beams have similar cross-section, a longitudinal reinforcement ratio of 1.571 % and a shear span to depth ratio of $a/d = 5.0$.

The cracking pattern of the reference monotonic test V1 is illustrated in Figure 8-33 in comparison to the experimental crack path. The failure crack path of the beam tested under monotonic shear loading concurs with the numerically predicted crack path. The numerically predicted ultimate shear load $V_{cr,FE} = 56.3$ kN agrees with the experimental value.

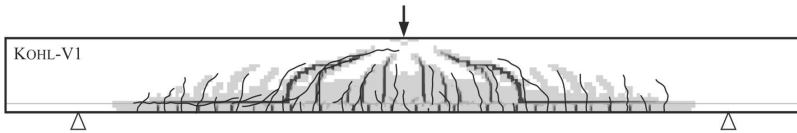


Figure 8-33: Comparison of experimental and numerical crack patterns of monotonically tested beam V1 (cracks with a crack width > 0.1 illustrated in black)

For adaption of tensile curve, two parameters are changed. One value corresponds to the modified fracture energy G_F calculated based on proposed equation of KESSLER-KRAMER (Eq. 2-25) and the other value is the internal stress caused by cyclic damage $\sigma_{\phi,cr}$ as proposed in chapter 3 (Eq. 3-6).

The diagonal cracking occurred for beam V3 after 73 load cycles with lower load level of 5 kN and an upper load level of 52.5 kN. The calculated initial stress for tensile curve of this beam corresponds to 0.47 N/mm² using the cyclic creep coefficient $\phi_{cycl,cal} = 0.1$. The resulted numerical load-deflection curve is illustrated in Figure 8-34.

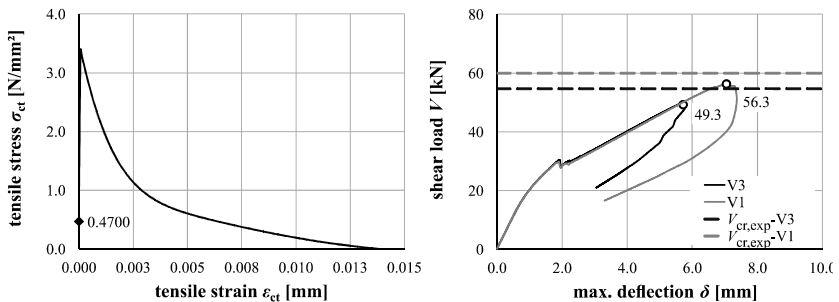


Figure 8-34: Adapted tensile curve for beam V3 (left) and diagonal cracking load predicted with the numerical model (right)

A reduction of the diagonal cracking load was reached numerically using the introduced damage. Based on results, the ratio of $V_{cr,cycl,exp} / V_{cr,exp} = 0.875$ was approximated numerically as $V_{cr,cycl,FE} / V_{cr,FE} = 0.877$. The failure crack pattern of beam V3 is illustrated in Figure 8-35. The comparably steeper failure crack within the cyclic test could also be reached using the proposed numerical adjustment of the concrete tensile curve.

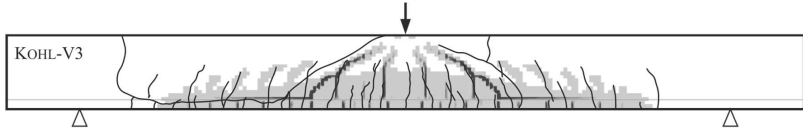


Figure 8-35: Comparison of experimental and numerical crack patterns of monotonically tested beam V3 (cracks with a crack width > 0.1 illustrated in black)

The shear test V5 was conducted under a lower loading amplitude $\Delta V = 40$ kN with an upper shear load of $V_{sup} = 45$ kN. Based on this number of load cycles and the corresponding creep value, an initial stress level of 1.01 kN was calculated for adaption of the concrete tensile curve (compare Figure 2-12, left).

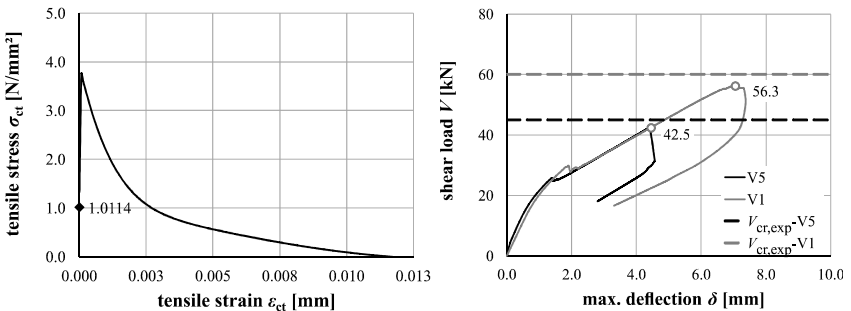


Figure 8-36: Adapted tensile curve for beam V5 (left) and diagonal cracking load predicted with the numerical model (right)

Due to the higher cyclic creep coefficient, a lower diagonal cracking load was obtained numerically. Furthermore, the ratio of $V_{cr,cycl,exp} / V_{cr,exp} = 0.750$ was approximated numerically as $V_{cr,cycl,FE} / V_{cr,FE} = 0.755$.

A comparison between the numerical and experimental cracking pattern of beam V5 is also depicted in Figure 8-37. The predicted critical section does not coincide with the experimental location of the critical crack; however, the profile of failure crack has some similarities with the experimental one.

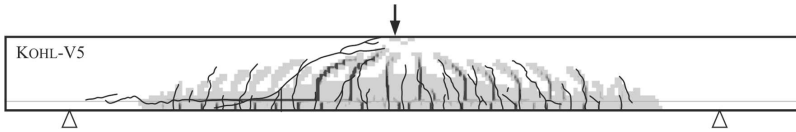


Figure 8-37: Comparison of experimental and numerical crack patterns of monotonically tested beam V5 (cracks with a crack width > 0.1 illustrated in black)

8.6 Concluding remarks

In this chapter, the suitability of the R crack model and the proposed incremental-iterative approach in chapter 7 was evaluated for the prediction of diagonal cracking load of mRC members in shear database. Additionally, the numerically determined critical sections (distance of failure crack from support axis) and beam model deflections at the state of diagonal cracking were documented. Using the rotating crack approach, an adequate prediction of the diagonal cracking load was achieved with a median of model safety factor equal to 1.17 and a variation coefficient of 0.11 (compare Figure 8-1). The prediction accuracy of results regarding diagonal cracking load and failure crack paths were analysed for four categories of tests exemplarily based on six selected mRC tests: beams with an intermediate shear span to depth ratio, beams with a high shear span to depth ratio, high-strength concrete beams and deep beams.

For beams with the intermediate shear span to depth ratio, a very good prediction of diagonal cracking load was possible. For shear tests with a shear span to depth ratio $2.0 \leq a/d \leq 3.0$, the ultimate shear load was also predicted with adequate accuracy with the R crack model. For large a/d values, a good approximation of the diagonal cracking was possible, but the ultimate load and $x_{cr,FE}$ was underestimated. The high-strength beam was inadequately simulated with the R crack model and the numerical ultimate loads underestimated the experimental values considerably. For the category of deep beams, the diagonal cracking loads were underestimated and $x_{cr,FE}$ were higher than the experimental values. During the evaluation of reasonability of numerically resulted ultimate loads, an over-rotation of diagonal cracks for deep beams caused a premature numerical failure. Based on evaluations, three sorts of brittleness were detected and used to derive a conceptual approach for evaluation of prior notice and quantify the shear failure brittleness. Three different brittleness factors based on difference between diagonal cracking and ultimate shear load η_{cr} , maximum beam deflection at state of diagonal cracking η_{δ} and energy release at the state of diagonal cracking η_g were defined and used in a multiplicative approach to define a total brittleness factor η .

To enhance the conceptual approach in terms of η_{cr} , refined numerical models are required, which enable approximation of both V_{cr} and V_u . The new RF model is supposed to be able of such approximation and was investigated using six representative tests. With

the RF model, the diagonal cracking load and ultimate shear load of the high-strength beam and deep beams were better predicted. A prediction of ultimate shear load of intermediate beams and the beam with high a/d was not enhanced using the RF crack model.

To better understand the effects of input model parameters on the response of the models with the new RF model, a parametric study was conducted. Based on the parametric study, recommendations are made for calculative determination of minimum shear retention factor based on input tensile parameters of concrete.

For simulation of diagonal cracking under cyclic loading, the adjusted concrete tensile curve was implemented for two cyclic tests in shear database V3 and V5 and compared with the reference monotonic tests V1. Based on the results with a rotating crack configuration, a reduces cyclic diagonal cracking load $V_{cr,cycl}$ was attained as assumed based on experimental results. The reduction ratio $V_{cr,cycl} / V_{cr}$ of numerical simulation and test showed very good accordance for the beams V3 and V5. Also, the cracking pattern could be approximated numerically. However, for a general application of the proposed tensile curve, further justifications are required.

9 Proposals for evaluation of shear capacity under monotonic and cyclic loading

9.1 General

Based on the investigation in this dissertation, analytical approaches (mechanical models) and numerical approaches are proposed for the calculation of diagonal cracking load of members with a flexure shear crack. Keeping safety in mind for structures subjected to cyclic loads such as traffic loads, the effects of cyclic damage on concrete tensile strength and its influence on diagonal cracking load (shear capacity provided by concrete tensile strength) was quantified using tensile tests and implemented in the analytical and the numerical approaches. For existing structural members without shear reinforcement, a further important criterion can be based on prior notice defined using both diagonal cracking load and ultimate shear load. A robust shear critical structural member is hence a member with sufficient prior notice. To quantify the prior notice (brittleness) of the shear failure, a new numerical crack model was proposed to enable a prediction of ultimate shear load and crack path. Furthermore, concepts are suggested to distinguish shear critical members with sufficient prior notice.

This chapter gives a brief outline of the proposed analytical, numerical and conceptual approaches.

9.2 Analytical approach

A mechanical model was suggested for the calculation of diagonal cracking load of members with a rectangular section and without longitudinal steel reinforcement in compression zone. Based on the assumed stress-distribution over the depth of cross-section originally proposed by GALLEG0 et al. [60-2014], the following closed-form solution was developed for determination of diagonal cracking load $V_{cr,cal}$ of monotonically loaded reinforced concrete beams:

$$V_{cr,cal} = \frac{2}{3} \cdot b \cdot h_{ef,mRC} \cdot f_{ct,cal} \quad \text{Eq. 9-1}$$

The effective depth h_{ef} consists of a compression and a tensile part (compare Figure 4-9) and corresponds to:

$$h_{ef,mRC} = \frac{\xi \cdot d}{2} + \left(\frac{\xi^2 \cdot d^2}{4} + \frac{\frac{\xi^2}{2} \cdot \left(1 - \frac{\xi}{3}\right) \cdot d^3}{\frac{2}{3} \cdot \chi_{cr}} \right)^{0.5} \quad \text{Eq. 9-2}$$

In this equation, the value of relative compression zone ξ is determined as:

$$\xi = \left(-\alpha \cdot \rho_1 + \sqrt{(\alpha \cdot \rho_1)^2 + 2 \cdot \alpha \cdot \rho_1} \right) \cdot d \quad \text{Eq. 9-3}$$

Where the coefficient α is equal to:

$$\alpha = E_s/E_c \quad \text{Eq. 9-4}$$

The longitudinal reinforcement ratio ρ_1 is determined based on the cross-section of longitudinal steel reinforcement A_s and the concrete cross-section with the effective depth of longitudinal tensile reinforcement d :

$$\rho_1 = \frac{A_s}{b \cdot d} \quad \text{Eq. 9-5}$$

The location of the (critical) diagonal crack x_{cr} should be provided for the evaluation of experimental results ($x_{cr,exp}$) or should be approximated using the length of shear span a with the following expression:

$$x_{cr,appr,RC} = 0.5 \cdot a \quad \text{Eq. 9-6}$$

The value of concrete tensile strength is defined in correlation with the concrete compressive strength f_c as:

$$f_{ct,cal} = 1.115 \cdot (f_c - 4)^{1/3} \quad \text{Eq. 9-7}$$

To apply the proposed mechanical model for the prediction of diagonal cracking load of prestressed members, some adjustments were made. These include

- adjustment of basic expression. (Eq. 9-1) with regard to MOHR's failure criteria with existing lateral compression,
- adjustment of effective depth to $h_{ef,mPC}$ to account for prestressing and
- modification of calculated concrete tensile strength $f_{ct,cal}$ to a modified value $f_{ct,mod}$ considering the effects of lateral compression.

As a result, the expression for the calculation of diagonal cracking load for monotonically loaded PC members corresponds to:

$$V_{cr,cal} = \frac{2}{3} \cdot b \cdot h_{ef,mPC} \cdot f_{ct,mod} \cdot \sqrt{1 + \frac{|\sigma_{cp}|}{f_{ct,mod}}} \quad \text{Eq. 9-8}$$

The effective depth $h_{ef,mPC}$ consists of depth of compression zone of an equivalent non-prestressed member $\xi \cdot d$ and an additional term h_p due to prestressing.

$$h_{ef,mPC} = \xi \cdot d + h_p \quad \text{Eq. 9-9}$$

The modified concrete tensile strength $f_{c,mod}$ should be calculated using the following expression:

$$f_{ct,mod} = \frac{1 - \frac{|\sigma_{cp}|}{f_c}}{1 - \frac{f_{ct}}{f_c}} \cdot f_{ct} \quad \text{Eq. 9-10}$$

The following terms σ_{cp} defines the correlation between h_p and $f_{ct,mod}$:

$$\sigma_{cp} = \frac{P}{b \cdot h_{ef,mPC}} \quad \text{Eq. 9-11}$$

For the determination of these terms, h_p should be determined, which is calculated using the iterative solution of following equation:

$$\xi \cdot d \cdot |\sigma_{cp}| + \frac{\frac{2}{3} \cdot h_p \cdot (\xi \cdot d + h_p) \cdot x_{cr} \cdot \sqrt{f_{ct,mod}^2 + |\sigma_{cp}| \cdot f_{ct,mod}}}{d^2 \cdot \frac{\xi}{2} \cdot \left(1 - \frac{\xi}{3}\right)} = 0 \quad \text{Eq. 9-12}$$

The proposed mechanical model is also applicable to predict the diagonal cracking load after a significant number of applied loads with following adaptations:

- Changing the effective depth to $h_{ef,cRC}$ to account for cyclic creep
- Modification of calculated concrete tensile strength $f_{ct,cal}$ to the fatigue tensile strength $f_{ct,fat}$ at the depth of neural axis

The cyclic effective depth $h_{ef,cRC}$ is determined iteratively, until the initial guess ($h_{ef,cRC,i}$) equals the latter one ($h_{ef,cRC,j}$) by fulfilling following equations:

$$\sigma_{inf} = \frac{V_{inf}}{\frac{2}{3} \cdot b \cdot h_{ef,cRC,i}} \quad \text{Eq. 9-13}$$

With this lower principal stress, the fatigue tensile stress is determined as:

$$f_{ct,fat} = \frac{f_{ct,ref}}{14.52} \cdot \left(14.81 + 2.79 \cdot \frac{\sigma_{inf}}{f_{ct,ref}} - \log N_{cr} \right) \quad \text{Eq. 9-14}$$

The diagonal cracking load $V_{cr,cycl}$ is determined using:

$$V_{cr,cycl} = \frac{2}{3} \cdot b \cdot h_{ef,cRC,i} \cdot f_{ct,fat} \quad \text{Eq. 9-15}$$

With the initial guess for $h_{ef,cRC}$, the relative depth of compression zone ξ_{Ncr} is simply calculated as:

$$\xi_{Ncr} = \frac{h_{ef,cRC,i}}{d} \quad \text{Eq. 9-16}$$

With the initial guess for $\xi_{N_{cr}}$ and $V_{cr,cycl}$, the latter value of $h_{ef,cRC,j}$ is resulted using:

$$h_{ef,cRC,j} = \xi_{N_{cr}} \cdot d \cdot \left(1 + \frac{f_{ct} \cdot b \cdot d^2 \cdot \frac{\xi_{N_{cr}}}{2} \cdot \left(1 - \frac{\xi_{N_{cr}}}{3} \right)}{V_{cr,cycl} \cdot x_{cr}} \right) \quad \text{Eq. 9-17}$$

Using the final value of $h_{ef,cRC}$, secondary parameters such as cyclic creep coefficient $\varphi_{cycl,cal}$ can be determined as follows:

$$\varphi_{cycl,cal} = \frac{E_{c,1} \cdot \xi_{N_{cr}}^2}{2 \cdot E_s \cdot (1 - \xi_{N_{cr}})} - 1 \quad \text{Eq. 9-18}$$

The value of cyclic creep coefficient is a useful parameter to consider the cyclic damage in the structural scale.

9.3 Numerical approach

To propose a unified FE-modelling approach for numerical evaluation of diagonal cracking under shear loads, the influence of assumed crack models and selected incremental-iterative procedure are accentuated in the benchmark evaluations in chapter 7. Based on parameter variations, a refined iterative approach was suggested. The shear load applied as displacement increments is adapted using arc-length control and energy based adaption provided in DIANA FEA. The lower bound of the step size was set as 0.01 mm and the initial load increment was set based on flexural cracking displacement according to:

$$u_{in} = \frac{f_{ct} \cdot l^2}{12 \cdot E_c \cdot h} \quad \text{Eq. 9-19}$$

The maximum number of load steps was limited to 500. Using this refined iteration process, instable cracking state at critical diagonal cracking was detectable from the numerical load-deflection curve, even in the case of deviating $V_{cr,FE}$ and $V_{u,FE}$ determined with the R crack model. Based on numerically evaluated mRC tests, it was shown that FE models with the rotating crack model provides a good approximation of diagonal cracking load in most cases. However, the over-rotation of the rotating cracks caused a premature numerical failure for deep beams, which made the prediction of diagonal cracking load inaccurate. To solve this problem and enable prediction of ultimate shear loads, a new crack model was proposed based on the analogy between the uniaxial tensile behaviour of concrete and the critical diagonal cracking as well as observation during benchmark evaluations. In this model, the crack width causing an instable tensile crack propagation $w_{cr,1}$ was assumed to correspond with the width of diagonal crack at the state of critical diagonal cracking. Hence, the critical diagonal crack initiates as the total normal strain ε_{nn} exceeds the following threshold value:

$$\varepsilon_{nn,lim} = \varepsilon_{el} + \frac{w_{cr,1}}{h_{cb}} \quad \text{Eq. 9-20}$$

Here, the elastic strain is calculated using:

$$\varepsilon_{el} = \frac{f_{ct}}{E_c} \quad \text{Eq. 9-21}$$

The value of $w_{cr,1}$ corresponds to the crack width causing an instable uniaxial tensile cracking, which was approximated as:

$$w_{cr,1} = \frac{G_F}{f_{ct}} \quad \text{Eq. 9-22}$$

With this threshold value, it was shown that in most cases, the numerical load-deflection curves obtained with the RF crack models deviate at a point corresponding to experimental diagonal cracking load from those achieved with the R crack model. Justifications for the RF crack model was sought using a parametric study. A significant influencing parameter for all models were found out to be the minimum shear retention factor β_{min} . Based on tensile parameters of concrete f_{ct} and G_F , following criteria should be fulfilled for the appropriate selection of β_{min} :

$$\beta_{min} \leq 0.1 \cdot \left(0.4 \cdot \frac{f_{ct}}{E_c \cdot \varepsilon_{nn,lim}} \right) \quad \text{Eq. 9-23}$$

After evaluation of cRC tests, a cyclic creep coefficient φ_{cycl} was determined, which was used to calculate the modified stiffness of the beam at the state of diagonal cracking $E_{c,N}$. Based on the modified stiffness, an equivalent stress $\sigma_{\varphi,res}$ was calculated as:

$$\sigma_{\varphi,res}(N) = f_{ct} \cdot \left(\frac{E_c}{E_{c,N}} - 1 \right) \quad \text{Eq. 9-24}$$

Furthermore, the fracture energy was also modified according to:

$$G_F(N) = G_F - 0.0214 \cdot \log N \quad \text{Eq. 9-25}$$

With the above-mention adjustments, the new modified concrete tensile curve was suggested (compare Figure 9-1). Using the new tensile curve for the displacement-controlled numerical evaluation of selected cRC tests showed that the effects of cyclic damage were considered adequately on the diagonal cracking loads with the modifications.

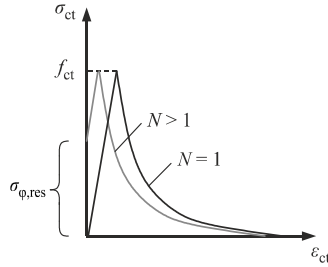


Figure 9-1: Proposed modified tensile curve

The possibility of predicting critical section using nonlinear FE evaluations was investigated. In general, the numerically approximated path of the critical diagonal crack showed a good accordance in some cases and deviated from the experimental one in some other cases. A good approximation of the critical section was not necessarily leading to better numerical prediction of diagonal shear cracks. Based on the crack path of the models with the R crack model, a premature numerically caused failure due to over-rotation of the R cracks was discernible. However, the critical section predicted using the smeared crack models are too sensible to the iterative-incremental approach and input material parameters. A possible solution is to combine the smeared cracks with crack propagation algorithms such as the proposed one in [Slo-2015].

9.4 Conceptual approach Conceptual approach and recommendations

For development of safety concepts for shear critical members, an objective quantification of brittleness of shear failure is required. The analytical and numerical observations within this thesis were used to define a concept for quantification of prior notice. For this aim, a brittleness factor η is defined based on three criteria:

- diagonal cracking before ultimate shear failure η_{cr}
- maximum deflection at state of critical diagonal cracking η_{δ}
- energy release at the state of critical diagonal cracking η_g

The overall brittleness factor η was defined using a multiplicative approach as:

$$\eta = \eta_{cr} \cdot \eta_g \cdot \eta_{\delta} \tag{Eq. 9-26}$$

The first criterion plays a significant role according to database evaluation and numerical investigations for beams with shear span to depth ratios $2.0 \leq a/d \leq 3.0$. The derived brittleness factor η_{cr} was determined using a correlation between shear span to depth ratio and the ratio $(V_u - V_{cr}) / V_u$.

$$\eta_{cr} = 0.33 \cdot \left(\frac{a}{d}\right) \quad \text{for } 2.0 \leq a/d \leq 3.0 \tag{Eq. 9-27}$$

Proposals for evaluation of shear capacity under monotonic and cyclic loading

The ratio between $\delta_{cr,FE}$ and $\delta_{u,cal}$ was evaluated in correlation with shear span to depth ratio and longitudinal reinforcement ratio. A clear tendency was also observed between shear slenderness and the ratio $\delta_{cr,FE} / \delta_{u,cal}$. As a result, a parameter based on shear span to depth ratio was proposed to quantify the brittleness as follows:

$$\eta_{\delta} = 0.94 - 0.032 \cdot \left(\frac{a}{d}\right) \quad \text{Eq. 9-28}$$

Using a scaling method, the brittleness factor based on relative out of balance energy (g) would be defined as follows:

$$\eta_g = \frac{(g - 1)}{20} \leq 1.0 \quad \text{Eq. 9-29}$$

The first and second brittleness factors depend mainly on shear span to depth ratio. The factor based on out of balance energy however, considers also the effects of concrete strength on brittleness of failure.

10 Conclusions and outlook

10.1 Conclusion

The major aim of this thesis was to derive new models and make proposals for a detailed investigation of diagonal cracking of concrete members with a potential flexure shear crack. The load-bearing mechanism attributed to concrete tensile strength was analysed theoretically, experimentally and numerically. The analogy between uniaxial tensile cracking of concrete and diagonal cracking caused by shear loads is used in this thesis to derive new models.

In the first step, the uniaxial tensile cracking and strength was evaluated theoretically and experimentally. A tensile database of uniaxial tensile tests under cyclic loading (fatigue tensile tests) and monotonic tests on cyclically preloaded specimens (residual tensile tests) were compared to understand the cyclic damage on macroscopic tensile parameters of concrete. Although fatigue tensile tests in the database showed a reduction of peak stress with the number of applied load cycles, the residual tensile strength of cyclically preloaded specimens in the database remained unchanged. To understand the cyclic damage phenomena and justify this discrepancy, an experimental programme of residual tensile tests was conducted on cyclically preloaded specimens. The results of database evaluation were affirmed using own tensile tests. Using the cyclic creep during tests and stiffness of the preloaded specimens in the monotonic loading phase, a new concrete tensile curve (Figure 3-12) was proposed for a displacement-controlled numerical evaluation of cyclically preloaded specimens.

Diagonal tension caused by shear loads has been evaluated theoretically for beams with a rectangular cross-section and without shear reinforcement. Influencing parameters affecting the primary cracking and the stress state at the diagonal cracking were figured out to be the shear span to depth ratio, longitudinal reinforcement ratio, and depth of the member. Provided mechanical models for prediction of diagonal cracking load using a limitation of principal tensile stress to concrete tensile strength were introduced. To evaluate and adjust the available mechanical models, the shear database was compiled, which includes shear tests on members with a rectangular cross-section and without shear reinforcement with a documented diagonal cracking loads under monotonic loads (mRC and mPC) and cyclic (cRC) loads. Using the comparison between mechanical models, a selected model was modified (Eq. 6-8 - Eq. 6-10) and adjusted for a consistent evaluation of diagonal cracking load of PC members (chapter 6.3) as well as for cyclically loaded RC members (chapter 6.4). The new models were applied to calculate the diagonal cracking load of the corresponding tests in the shear database and showed a very good to good agreement with the experimental values. It could be seen, however, that for an appropriate application of models, the location of the critical section should be provided. This fact

limits the applicability of the provided model for the existing structures, as the critical section is also not a priori during the assessment of existing concrete members.

For prediction of the critical section as well as to enable prediction of diagonal cracking load in a higher approximation level, the accuracy of nonlinear FE models regarding prediction of diagonal cracking loads, critical section and ultimate shear loads was investigated. In a first step, the applicability of nonlinear FE analysis is investigated using benchmark shear tests of LEONHARDT / WALTHER. A total strain-based crack model was used for the simulations. A rotating crack model (R model) and a fixed crack model (F model) were applied for the simulation of the benchmark tests. With the R crack model, a prediction of diagonal cracking load was confirmed. The accuracy of prediction depends on the shear span to depth ratio. Using the simulations, two sorts of premature numerical failure, one based on high energy release at the state of cracking and convergence difficulties and one based on over-rotation of R cracks were figured out. Two solutions, a refined energy based adaptive incremental-iterative approach and a new rotating to fixed crack model (RF model) was proposed.

Combining R crack model and the refined energy-based adaptive incremental-iterative approach leads to good numerical prediction of diagonal cracking loads, which was verified using simulation of 82 mRC tests in the shear database. For deep beams and high-strength beams, the results were not suitable and the diagonal cracking loads were considerably underestimated. Furthermore, a conceptual approach for the quantification of shear failure brittleness was developed based on numerical investigations with the R crack model.

The new RF crack model was applied to selected mRC tests and proved to provide better prediction of diagonal cracking loads and ultimate loads for deep beams and high-strength concrete beams. Within a parametric study, the influence of input tensile parameters of concrete and shear retention factor on response of the RF model are evaluated. Based on the results, a high sensitivity of the response of RF crack models was detected to the input value of concrete tensile fracture energy. Furthermore, suggestions were made to determine tensile parameters of concrete with respect to the threshold parameters of the RF crack model.

Finally, the proposed modification of concrete tensile curve was used for stationary nonlinear FE evaluation of some tests in cRC database. The tensile curves were adapted using the cyclic creep coefficient determined during database evaluation and were implemented in FE models with a rotating crack model. The numerical analyses were able to reproduce the reduction of diagonal cracking load due to cyclic damage. However, further investigations are required to validate this approach.

Based on the theoretical, experimental and numerical investigations in this work, a mechanical model was proposed for calculation of diagonal cracking load of RC members

under monotonic and cyclic loads as well as for PC members. Although this model calculates the diagonal cracking with a good to very good prediction accuracy, prediction of critical section is necessary to obtain realistic results. Applicability of nonlinear FE models for numerical prediction of the diagonal cracking load was confirmed. The predicted critical sections were proved to be quite sensible to input parameters and iterative-incremental approach.

10.2 Outlook

Although the residual tensile tests often show no reduction of peak tensile stress of cyclically preloaded members, these observations are only valid up to a certain state of damage. For the experimental determination of a critical damage state for cyclically preloaded members, new measurement methods are required such as computer tomography or ultrasonic measurements, which visualize the microcrack development during cyclic tests. Using the cracking intensity and the length of microcracks, the residual tensile strength of critically damaged concrete specimens should be determined.

Application of mechanical models for the analytical determination of diagonal cracking loads can be generalized and enhanced. This requires reliable methods for the prediction of the critical section. The numerical investigations showed that such prediction is not possible using available smeared crack models. For future evaluations, the combination of crack models with crack propagation algorithms should be studied.

To further refine the new RF crack model, experimental backgrounds are required for determination of crack width (threshold strain value for fixation of cracks) and the activated aggregate interlock upon the crack fixation.

The proposed modified concrete tensile curve accounts only for constant amplitude applications and should be generalized to variable amplitude loading for a practical application. The proposed modified concrete tensile curve on cyclically preloaded members should be also further evaluated and generalized for such applications. Furthermore, investigations regarding the influence of cyclic damage on softening behaviour of concrete and crack width development, specifically under lateral compression due to prestressing, are still missing.

The rotating crack model with the proposed model configuration and the new rotating to fixed crack model should be validated or extended further for evaluation of diagonal cracking as well as ultimate shear load of prestressed members and cyclically damaged members.

With reliable numerical approaches for the assessment of shear critical members, costly experimental investigations can be replaced by numerical investigations. Using such approaches, new datasets can be generated to rectify the statistical bias in shear databases.

11 References

- [Ahm-1986] Ahmad, S. H.; Khaloo, A. R.; Poveda, A.: Shear Capacity of Reinforced High-Strength Concrete Beams. *ACI Journal Proceedings* 83 (1986), No. 2, P. 297–305.
- [Al-1978] Al Mahaidi, R. S. H.: Nonlinear finite element analysis of reinforced concrete deep beams. Doctoral thesis, Cornell University, 1978.
- [Bal-1991] Balázs, G. L.: Fatigue of bond. *ACI Materials Journal* 88 (1991), No. 6, P. 620–629.
- [Baž- a1983] Bažant, Z. P.: Comment on orthotropic models for concrete and geomaterials. *ASCE* 109 (1983), No. 3, P. 849–865.
- [Baž- b1983] Bažant, Z. P.; Oh, B. H.: Crack band theory for fracture of concrete. *Matériaux et Constructions* 16 (1983), No. 3, P. 155–177. doi: 10.1007/BF02486267.
- [Baž-1984] Bažant, Z. P.; Kim, W.: Size effect in shear failure of longitudinally reinforced beams. *ACI Journal* 81 (1984), P. 456–468.
- [Baž-1991] Bažant, Z. P.; Xu, K.: Size effect in fatigue fracture of concrete. *ACI Material Journal* 88 (1991), No. 4, P. 390–399.
- [Baž-2002] Bažant, Z. P.; Becq-Giraudon, E.: Statistical prediction of fracture parameters of concrete and implications for choice of testing standard. *Cement and Concrete Research* 32 (2002), No. 4, P. 529–556. doi: 10.1016/S0008-8846(01)00723-2.
- [Baž-2014] Bažant, Z. P.; Hubler, M. H.: Theory of cyclic creep of concrete based on Paris law for fatigue growth of subcritical microcracks. *Journal of Mechanics and Physics of Solids* 63 (2014), P. 187–200.
- [Bel-2013] Belletti, B.; Damoni, C.; den Uijl, J. A.; Hendriks, M. A. N.; Walraven, J. C.: Shear resistance evaluation of prestressed concrete bridge beams: fib Model Code 2010 guidelines for level IV approximations. *Structural Concrete* 14 (2013), No. 3, P. 242–249. doi: 10.1002/suco.201200046.
- [Bel- a2017] Belletti, B.; Damoni, C.; Hendriks, M. A. N.; Boer, A. de: Validation of the Guideine for Nonlinear Finite Element Analysis of Concrete Structures. Part: Reinforced Beams, 2017.
- [Bel- b2017] Belletti, B.; Damoni, C.; Hendriks, M. A. N.; Boer, A. de: Validation of the Guidelines for Nonlinear Finite Element Analysis of Concrete Structures, 2017.
- [Bha-1968] Bhal, N. S.: Über den Einfluß der Balkenhöhe auf die Schubtragfähigkeit von einfeldrigen Stahlbetonbalken mit und ohne Schubbewehrung. Doctoral thesis, Universität Stuttgart, Stuttgart, 1968.
- [Bla-1993] Blaschke, F.; Losekamp, C.; Mehlhorn, G.: Zugtragvermögen nach langandauernder statischer sowie schwellender Zugvorbelastung von Beton. Research report No. 20, Kassel, 1993.
- [Bre-1963] Bresler, B.; Scordelis, A. C.: Shear strength of reinforced concrete beams. *ACI Journal Proceedings* 60 (1963), No. 1, P. 51–74.
- [Bus-2019] Busse, D.: Querkrafttragverhalten von dünnwandigen, mikrobewehrten Betonbauteilen. Doctoral Thesis, Technische Universität Braunschweig, Braunschweig, Schriftreihe des iBMB, Heft 236, 2019.
- [Cam-2013] Campana, S.; Fernández Ruiz, M.; Anastasi, A.; Muttoni, A.: Analysis of shear-transfer actions on one-way RC members based on measured cracking pattern and failure kinematics. *Magazine of Concrete Research* 65 (2013), No. 6, P. 386–404. doi: 10.1680/macr.12.00142.
- [Cao-2001] Cao, S.: Size effect and the influence of longitudinal reinforcement on the shear response of large reinforced concrete members. Doctoral thesis, University of Toronto, 2001.
- [Car-1982] Carpinteri, A.: Notch sensitivity in fracture testing of aggregate materials. *Engineering Fracture Mechanics* 16 (1982), No. 4, P. 467–481.

- [Cav-2017] Cavagnis, F.: Shear in reinforced concrete without transverse reinforcement: from refined experimental measurements to mechanical models. Doctoral thesis, École Polytechnique Fédérale de Lausanne, Lausanne, 2017.
- [Cha-a1958] Chang, T. S.; Kesler, C. E.: Fatigue Behavior of Reinforced Concrete Beams. *ACI Journal Proceedings* 30 (1958), No. 2, P. 245–254.
- [Cha-b1958] Chang, T. S.; Kesler, C. E.: Static and Fatigue Strength in Shear of Beams with Tensile Reinforcement. *ACI Journal Proceedings* 54 (1958), No. 6, P. 1033–1057. doi: 10.14359/11493.
- [Che-2016] Chen, X.; Bu, J.: Experimental Study on Direct Tensile Behavior of Concrete under Various Loading Regimes. *ACI Materials Journal* 113 (2016), No. 4, P. 513–522. doi: 10.14359/51688932.
- [Che-2017] Chen, X.; Bu, J.; Xu, L.: Experimental Study on Cyclic Tensile Behavior of Concrete under High Stress Level. *ACI Materials Journal* 114 (2017), No. 5, P. 775–781. doi: 10.14359/51700796.
- [Cho-2007] Choi, K. K.; Kim, J. C.; Park, H. G.: Shear strength model of concrete beams based on compression zone failure mechanism. *ACI Structural Journal* 104 (2007), No. 2, P. 142–152.
- [Cla-2005] Cladera, A.; Marí, A.: Experimental Study on high-strength concrete beams failing in shear. *Engineering Structures* 27 (2005), P. 1519–1527.
- [Cla-2009] Claus, T. T. B.: Non-linear finite element analysis of shear critical reinforced concrete beams. Master Thesis, Delft University of Technology, 2009.
- [Col-1999] Collins, M. P.; Kuchma, D. A.: How safe are our large, lightly reinforced concrete beams, slabs and footings? *ACI Structural Journal* 96 (1999), No. 4, P. 482–490.
- [Col-2008] Collins, M. P.; Bentz, E. C.; Sherwood, E. G.: Where is Shear Reinforcement Required? Review of Research Results and Design Procedures. *Structural Journal* 105 (2008), No. 5, P. 590–600. doi: 10.14359/19942.
- [Coo-1981] Cook, D. J.; Chindapasirt, P.: Influence of loading history upon the tensile properties of concrete. *Magazine of Concrete Research* 33 (1981), No. 116, P. 154–160. doi: 10.1680/mac.1981.33.116.154.
- [Cor-1981] Cornelissen, H. A. W.; Timmers, G.: Fatigue of plain concrete in uniaxial tension and in alternating tension-compression experiment and results. Report Stevin Laboratory, Concrete Structures 5-81-7. Report, Delft University of Technology, Faculty Civil Engineering and Geosciences, 1981.
- [Cor-1984] Cornelissen, H. A. W.: Fatigue failure of concrete in tension, Delft University of Technology; Stevin Laboratory, Heron vol. 29, no. 4, Delft, 1984.
- [Cor-1986] Cornelissen, H. A. W.; Hordijk, D. A.; Reinhardt, H. W.: Experimental determination of crack softening characteristics of normalweight and lightweight concrete, 1986.
- [DIA-2017] DIANA FEA BV: User's Manual, DIANA FEA, 2017.
- [Dia-1960] Diaz de Casio, R.; Seiss, C. P.: Behavior and strength in shear of beams and frames without web reinforcement. *ACI Journal* 56 (1960), P. 695–735.
- [DIN-1992-1-1] DIN EN 1992-1-1: Eurocode 2: Bemessung und Konstruktion von Stahlbeton- und Spannbetontragwerken – Teil 1-1: Allgemeine Bemessungsregeln und Regeln für den Hochbau; Deutsche Fassung EN 1992-1-1:2004 + AC:20102011.
- [Dud-1991] Duda, H.: Bruchmechanische Verhalten von Beton unter monotoner und zyklischer Zugbeanspruchung, DAFStb, Berlin, 1991.
- [Dun-2018] Dunkelberg, D.; Sneed, L. H.; Zilch, K.; Reineck, K.-H.: The 2015 ACI-DAFStb database of shear tests on slender prestressed concrete beams without stirrups-Overview and evaluation of current design approaches. *Structural Concrete* 100 (2018), No. 2, P. 240. doi: 10.1002/suco.201700216.

References

- [Emp-1995] Empelmann, M.: Zum nichtlinearen Trag- und Verformungsverhalten von Stabtragwerken aus Konstruktionsbeton unter besonderer Berücksichtigung von Betriebsbeanspruchungen. Doctoral Thesis, Aachen, 1995.
- [Emp-2013] Empelmann, M.; Wichers, M.; Unger, C.: Brücken im Bestand - Herausforderungen und Lösungsansätze. In: Nothnagel, R. und Twelmeier, H. (Eds.). Festschrift zum 60. Geburtstag von Harald Budelmann, Springer Berlin Heidelberg, 2013. ISBN: 978-3-642-29572-0.
- [fib-2008] fib Bulletin 42: Constitutive modelling of high strength/high performance concrete, International Federation for Structural Concrete, Lausanne, 2008.
- [fib-90] fib comité Euro-international du Béton: CEB-FIP model code 1990, Thomas Telford; Telford, London.
- [fib-2010] fib fédération internationale du béton: fib Model Code for Concrete Structures 2010, Ernst Sohn, Lausanne, Switzerland.
- [Fis-2014] Fischer, O.; Müller, A.; Lechner, T.; Wild, M.; Kessner, K.: Ergebnisse und Erkenntnisse zu durchgeführten Nachrechnungen von Betonbrücken in Deutschland, 2014.
- [Fis-2017] Fischer, O.; Schramm, N.; Gehrlein, S.: Labor- und Feldversuche zur realitätsnahen Beurteilung der Querkrafttragfähigkeit von bestehenden Spannbetonbrücken. Bauingenieur 92 (2017), No. 11, P. 455–463.
- [Fro-2000] Frosch, R. J.: Behavior of Large-Scale Reinforced Concrete Beams with Minimum Shear Reinforcement. Structural Journal 97 (2000), No. 6, P. 814–820. doi: 10.14359/9626.
- [Fuj-2013] Fujiyama, C.; Tang, X. J.; Maekawa, K.; An, X. H.: Pseudo cracking approach to fatigue life assessment of RC bridge decks in service. Journal of Advanced Concrete Technology 11 (2013), P. 7–21.
- [Fus-2017] Fust, C.: Zum Tragverhalten von gering querkraftbewehrten Stahlbetonbalken. Doctoral thesis, Ruhr Universität Bochum, 2017.
- [Gal-2014] Gallego, J. M.; Zanuy, C.; Albajar, L.: Shear fatigue behaviour of reinforced concrete elements without shear reinforcement. Engineering Structures 79 (2014), P. 45–57. doi: 10.1016/j.engstruct.2014.08.005.
- [Geb-2008] Gebreyouhannes, E.; Chijiwa, N.; Fujiyama, C.; Maekawa, K.: Shear fatigue simulation of RC beams subjected to fixed pulsating and moving loads. Journal of Advanced Concrete Technology 6 (2008), No. 1, P. 215–226.
- [Gha-1998] Ghannoum, W. M.: Size effect on shear strength of reinforced concrete beams. Master Thesis, McGill University, Montreal, Canada, 1998.
- [Gil-2010] Gilbert, R. I.; Ranzi, G.: Time-dependent behaviour of concrete structures, London, New York, Spon Press/Taylor & Francis Group, 2010. ISBN: 9780415493840.
- [Gil-2011] Gilbert, R. I.: The Serviceability Limit States in Reinforced Concrete Design. Procedia Engineering 14 (2011), P. 385–395. doi: 10.1016/j.proeng.2011.07.048.
- [Göd-2012] Gödde, L.: Numerische Simulation und Bemessung von Flächentragwerken aus Stahlfaserbeton sowie stahlfaserverstärktem Stahl- und Spannbeton. Doctoral Thesis, Ruhr-Universität Bochum, Bochum, 2012.
- [Gop-1987] Gopalaratnam, V. S.; Shah, S. P.: Tensile Failure of Steel Fiber-Reinforced Mortar. Journal of Engineering Mechanics 113 (1987), No. 5, P. 635–652. doi: 10.1061/(ASCE)0733-9399(1987)113:5(635).
- [Gör-2004] Görtz, S.: Zum Schubrisserverhalten von Stahlbeton- und Spannbetonbalken aus Normal- und Hochleistungsbeton. Doctoral thesis, RWTH Aachen, Aachen, 2004.
- [Gor-1995] Gorvindjee, S.; Kay, G. J.; Simo, J. C.: Anisotropic modelling and numerical simulation of brittle damage in concrete. International Journal of numerical Methods in Engineering 38 (1995), P. 3611–3633.

- [Gri-1997] Grimm, R.: Einfluß bruchmechanischer Kenngrößen auf das Biege- und Schubverhalten hochfester Betone, 1997.
- [Gro-2014] Gross, D.; Hauger, W.; Schröder, J.; Wall, W. A.: Technische Mechanik 2. Elastostatik, Berlin, Springer Vieweg, 2014. ISBN: 978-3-642-40966-0.
- [Ham-2006] Hampel, T.: Experimentelle Analyse des Tragverhaltens von Hochleistungsbeton unter mehraxialer Beanspruchung. Doctoral thesis, Technische Universität Dresden, Dresden, 2006.
- [Han-1958] Hanson, J. A.: Shear strength of lightweight reinforced concrete beams. *ACI Journal* 55 (1958), P. 387–403.
- [Han-1961] Hanson, J. A.: Tensile strength and diagonal tension resistance of structural lightweight concrete. *ACI Journal Proceedings* 58 (1961), No. 1, P. 1–40.
- [Heg-2016] Hegger, J.; Herbrand, M.: Erweiterte Nachweiskonzepte nach Stufe 4 der Nachrechnungsrichtlinie: Proceedings of 2. Brückenkolloquium Beurteilung, Instandsetzung und Ertüchtigung von Brücken, 21.-22. June, Esslingen, 2016.
- [Hei-1969] Heilmann, H. G.; Hilsdorf, H.; Finsterwalder, K.: Festigkeit und Verformung von Beton unter Zugspannungen, Berlin, 1969.
- [Hen-2017] Hendriks, M. A. N.; de Boer, A.; Belletti, B.: Guidelines for nonlinear finite element analysis, 2017.
- [Her-2016] Herbrand, M.; Kueres, D.; Claßen, M.; Hegger, J.: Einheitliches Querkraftmodell zur Bemessung von Stahl- und Spannbetonbrücken im Bestand. *Beton- und Stahlbetonbau* 111 (2016), No. 2, P. 58–67. doi: 10.1002/best.201500055.
- [Her-2017] Herbrand, M.: Shear Strength Models for Reinforced and Prestressed Concrete Members. Doctoral thesis, RWTH Aachen, Aachen, 2017.
- [Hig-1978] Higai, T.: Fundamental Study of Shear Failure of Reinforced Concrete Beams. *JSCE Proceedings* 279 (1978), No. 1, P. 113–126.
- [Hil-1976] Hillerborg, A.; Modéer, M.; Petersson, P.-E.: Analysis of crack formation and crack growth in concrete by means of fracture mechanics and finite elements. *Cement and Concrete Research* (1976), P. 773–782.
- [Hol-2014] Holz, K.: Untersuchung der schrägen Rissentwicklung im Stahlbeton. Project report, Technische Universität Dresden, Dresden, 2014.
- [Hon-2012] Hong, S. G.; Ha, T.: Effective capacity of diagonal strut for shear strength of reinforced concrete beams without shear reinforcement. *ACI Structural Journal* 109 (2012), No. 2, P. 139–148.
- [Hor-1992] Hordijk, D. A.: Tensile and tensile fatigue behaviour of concrete; experiments, modelling and analysis, Delft University of Technology, 1992.
- [Hub- 2014a] Huber, P.; Kolleger, J.; Nguyen, V. T.; Nguyen, D. T.: Mechanisch konsistentes Schubfeldmodell für Bestandsbrücken ohne bzw. mit geringer Querkraftbewehrung, Technische Universität Wien; Technische Universität Graz, 2014.
- [Hub- 2014b] Huber, P.; Kolleger, J.: Numerical simulation of shear behavior of reinforced concrete beams with and without flanges. In: Bicanic, N., et al. (Eds.): Proceedings of EURO-C 2014: Computational Modelling of Concrete Structures, 24-27 March, Arlberg, Austria, 2014.
- [Hub-2016] Huber, P.: Beurteilung der Querkrafttragfähigkeit bestehender Stahlbeton- und Spannbetonbrücken. Doctoral thesis, Technische Universität Wien, Wien, 2016.
- [Hus-2006] Hussein, A. A.: Behavior of high-strength concrete under biaxial loading conditions. Doctoral thesis, Memorial University of Newfoundland, 2006.
- [Hyo-2013] Hyodo, H.; Sato, R.; Kawai, K.; Nakayama, H.: Effects of drying shrinkage on shear tension strength of reinforced concrete beams. In: Ruiz, Miguel Fernández, Toledo (Spain), 2013.
- [Jav-2017] Javidmehr, S.; Empelmann, M.: Zugtragwirkung von Beton bei der Querkrafttragfähigkeit von Bestandsbrücken. Bestimmung der Schrägrisslasten unter Querkraftbeanspruchung. In: Breit W.,

References

- et al.: Proceedings of 5. DAFStb-Jahrestagung mit 58. Forschungskolloquium, 20.-21. September, Kaiserslautern, 2017.
- [Jav-2018a] Javidmehr, S.; Oettel, V.; Empelmann, M.: Schrägrissbildung von Stahlbetonbalken unter Querkraftbeanspruchung. *Bauingenieur* 93 (2018), No. 6, S. 248-254, Spriger-VDI Verlag, 2018.
- [Jav-2018b] Javidmehr, S.; Empelmann, M.: Diagonal cracking load of concrete members without shear reinforcement. In: Kohoutková, A., et al (Eds.): Proceedings of 12th fib International PhD Symposium in Civil Engineering, 29.-31. August, Prague, 2018.
- [Kan-1979] Kani, G. N.; Huggings, M. W.; Wittkopp, R. R.: Kani on shear in reinforced concrete. Report, University of Toronto, Toronto, Canada, 1979.
- [Kan-1968] Kani, G. N. J.: Was wissen wir heute über die Schubbruchsicherheit? *Bauingenieur* 43 (1968), No. 5, P. 67–174.
- [Kar-1969] Kar, J. N.: Shear strength of prestressed concrete beams without web reinforcement. *Magazine of Concrete Research* 21 (1969), No. 68, P. 159–170.
- [Kau-2010] Kautsch, R.: Beitrag zur Nachweisführung von querkraftbewehrten Stahlbeton- und Spannbetonquerschnitten unter kombinierter Biege- und Schubbeanspruchung auf Grundlage der Erweiterten Technischen Biegelehre. Doctoral thesis, Technische Universität Kaiserslautern, Kaiserslautern, 2010.
- [Kes-2002] Kessler-Kramer, C.: Zugtragverhalten vom Beton unter Ermüdungsbeanspruchung. Dissertation, TH, Karlsruhe, 2002.
- [Kha-2013] Khaja, M. N.; Sherwood, E. G.: Does the shear strength of reinforced concrete beams and slabs depend upon the flexural reinforcement ratio or the reinforcement strain? *Canadian Journal of Civil Engineering* 40 (2013), No. 11, P. 1068–1081. doi: 10.1139/cjce-2012-0459.
- [Kim-1991] Kim, W.; White, R. N.: Initiation of Shear Cracking in Reinforced Concrete Beams with No Web Reinforcement. *ACI Structural Journal* 88 (1991), No. 3, P. 301–308. doi: 10.14359/9447.
- [Kle-2016] Kley, C.; Mark, P.: Zur Mindestquerkraftbewehrung von Stahlbetonbalken. *Beton- und Stahlbetonbau* 111 (2016), No. 11, P. 728–737. doi: 10.1002/best.201500063.
- [Koh-2014] Kohl, M.: Tragverhalten von Stahlbetontragwerken ohne Querkraftbewehrung unter Ermüdungsbeanspruchung. Doctoral thesis, Technische Universität Hamburg-Harburg, 2014.
- [Kre-1966] Krefeld, W. J.; Thurston, C. W.: Contribution of Longitudinal Steel to Shear Resistance of Reinforced Concrete Beams. *ACI Journal Proceedings* 63 (1966), No. 3, P. 325–344.
- [Kup- a1973] Kupfer, H.; Gerstle, K. H.: Behavior of concrete under biaxial stresses. *Journal of the Engineering Mechanics Division, ASCE* 99 (1973), No. 4, P. 853–866.
- [Kup- b1973] Kupfer, H.: Das Verhalten des Betons unter mehrachsiger Kurzzeitbelastung unter besonderer Berücksichtigung der zweiachsigen Beanspruchung. *Bau und Erprobung einer Versuchseinrichtung für zweiachsige Belastung*, Technische Universität München, Berlin, 1973.
- [Leo-1962] Leonhardt, F.; Walther, R.: Schubversuche an einfeldrigen Stahlbetonbalken mit und ohne Schubbewehrung zur Ermittlung der Schubtragfähigkeit und der oberen Schubspannungsgrenze, DAFStb, Berlin, 1962.
- [Mae-2006] Maekawa, K.; Toongoenthong, K.; Gebreyouhannes, E.; Kishi, T.: Direct path-integral scheme for fatigue simulation of reinforced concrete in shear. *Journal of Advanced Concrete Technology* 4 (2006), No. 1, P. 159–177.
- [Mal-2006] Malm, R.: Shear cracks in concrete structures subjected to in-plane stresses, KTH, Stockholm, Sweden, 2006.
- [Mar-2014] Marí, A.; Bairán, J.; Cladera, A.; Oller, E.; Ribas, C.: Shear-flexural strength mechanical model for the design and assessment of reinforced concrete beams. *Structure and Infrastructure Engineering* 11 (2014), No. 11, P. 1399–1419. doi: 10.1080/15732479.2014.964735.

- [Mar-1985] Marti, P.: Basic Tools of Reinforced Concrete Beam Design. *ACI Journal Proceedings* 82 (1985), No. 1, P. 46–56. doi: 10.14359/10314.
- [Mar-2015] Marzahn, G.; Hegger, J.; Maurer, R.; Zilch, K.; Dunkelberg, D.; Kolodziejczyk, A.; Teworte, F.: Die Nachrechnung von Betonbrücken - Fortschreibung der Nachrechnungsrichtlinie. In: Bergmeister, K.; Fingerloos, F.; Wörner, J.-D., Ernst & Sohn, 2015.
- [Mat-1963] Mathey, R. C.; Watstein, D.: Shear Strength of Beams Without Web Reinforcement Containing Deformed Bars of Different Yield Strengths. *ACI Journal* 60 (1963), No. 2, P. 183–208.
- [Mau-2012] Maurer, R., Heeke, G., Kiziltan, H., Kolodziejczyk, A., Zilch, K., Dunkelberg, D.: Nachrechnung von Betonbrücken zur Bewertung der Tragfähigkeit bestehender Bauwerke. Bericht zum Forschungsprojekt FE 15.0490/2010/FRB, Bundesanstalt für Straßenwesen, Hannover, Bremerhaven, 2012.
- [Men-2007] Meng, X.; Song, Y.: Residual tensile strength of plain concrete under tensile fatigue loading. *Journal of Wuhan University of Technology-Mater. Sci. Ed.* 22 (2007), No. 3, P. 564–568. doi: 10.1007/s11595-006-3564-6.
- [Moo-1954] Moody, K. G.; Viest, I. M.; Elstner, R. C.; Hodgson, T.: Shear Strength of Reinforced Concrete Beams. Part I-Test of Simple Beams. *Journal of American Concrete Institute* 26 (1954), No. 4, P. 317–332.
- [Mor-1956] Morrow, J.; Viest, I. M.: Shear strength of reinforced concrete frame members without web reinforcement. *ACI Journal Proceedings* 28 (1956), No. 9, P. 833–869.
- [Mör-1907] Mörsch, E.: *Der Eisenbetonbau. Seine Theorie und Anwendung*, Stuttgart, Konrad Wittwer, 1907.
- [Mph-1984] Mphonde, A. G.; Frantz, G. C.: Shear Tests of High- and Low-Strength Concrete Beams Without Stirrups. *ACI Journal* 81 (1984), No. 4, P. 350–357.
- [Mut-2012] Muttoni, A.; Ruiz, M. F.: Level-of-Approximation Approach in Codes of Practice. *Structural Engineering International* 22 (2012), P. 190–194.
- [Nie-1999] Nielsen, M. P.: *Limit Analysis and Concrete Plasticity*, Boca Raton, FL, CRC Press, 1999.
- [NRR-2011] NRR: Richtlinie zur Nachrechnung von Straßenbrücken im Bestand (Nachrechnungsrichtlinie), Bundesministerium für Verkehr, Bau und Stadtentwicklung, Abteilung Straßenbau, 2011.
- [Pfa-2003] Pfanner, D.: Zur Degradation von Stahlbetonbauteilen unter Ermüdungsbeanspruchung. Zugl.: Bochum, Ruhr-Universität, Diss., 2002, Düsseldorf, VDI-Verl., 2003. ISBN: 3-18-318904-6.
- [Pla-1969] Placas, A.: *Shear Strength of Reinforced Concrete Beams*. Doctoral thesis, Imperial College, London, 1969.
- [Pod-1998] Podgorniak-Stanik, B. A.: *The influence of Concrete Strength, Distribution of Longitudinal Reinforcement, Amount of Transverse Reinforcement and Member Size on Shear Strength of Reinforced Concrete Members*. Doctoral thesis, University of Toronto, Toronto, 1998.
- [Rei-1990] Reineck, K.-H.: Ein mechanisches Modell für den Querkraftbereich von Stahlbetonbauteilen. Doctoral thesis, Universität Stuttgart, Stuttgart, 1990.
- [Rei-1991] Reineck, K.-H.: Ultimate shear force of structural concrete members without transverse reinforcement derived from a mechanical model. *ACI Structural Journal* 88 (1991), No. 5, P. 592–602.
- [Rei-2012] Reineck, K.-H.; Kuchma, D. A.; Fitik, B.: *Erweiterte Datenbanken zur Überprüfung der Querkraftbemessung für Konstruktionsbetonbauteile mit und ohne Bügel*, Berlin, Beuth, 2012. ISBN: 978-3-410-65215-1.
- [Rei-1981] Reinhardt, H. W.: *Similitude of brittle fracture of structural concrete*, 1981.
- [Rei-1986] Reinhardt, H. W.; Cornelissen, H. A. W.; Hordijk, D. A.: Tensile tests and failure analysis of concrete. *ASCE Journal of Structural Division* 112 (1986), No. 11, P. 2462–2477.
- [Rei-2013] Reinhardt, H. W.: *Understanding the Tensile Properties of Concrete - Factors affecting the tensile properties of concrete*. In: Reinhardt, H. W., Elsevier, 2013. ISBN: 9780857090454.

References

- [Rem-1994] Rimmel, G.: Zum Zug- und Schubtragverhalten von Bauteilen aus hochfestem Beton, Beuth, Berlin, 1994.
- [Roo-2018] Roosen, M.; van der Veen, C.; Hordijk, D. A.: Sustainability of Shear Tension Code Requirements for the Assessment of Existing Structures Build-Up with Prestresses I- and T-Shape Girders. In: Hordijk, D. A.; Luković, M., Springer International Publishing, 2018.
- [Rot-1988] Rots, J. G.: Computational modeling of concrete fracture. Doctoral thesis, Technische Universiteit Delft, Delft, 1988.
- [Rui-2015] Ruiz, M. F.; Zanuy, C.; Natário, F.; Gallego, J. M.; Albajar, L.; Muttoni, A.: Influence of Fatigue Loading in Shear Failures of Reinforced Concrete Members without Transverse Reinforcement. *Journal of Advanced Concrete Technology* 13 (2015), No. 5, P. 263–274. doi: 10.3151/jact.13.263.
- [Rüs-1967] Rüschi, H.; Mayer, H.: 5 Versuche zum Studium der Verformung im Querkraftbereich eines Stahlbetonbalken, Berlin, Wilhelm Ernst & Sohn, 1967.
- [Sch-2014] Schacht, G.: Experimentelle Bewertung der Schubtragsicherheit von Stahlbetonbauteilen. Doctoral thesis, Technische Universität Dresden, Dresden, 2014.
- [Sch-1986] Schäfer, K.; Baumann, P.: Ausbreitung von Druckkräften in Betonscheiben - Vergleichende Versuche mit Lasteinleitung über Lastplatten, Bewehrungsstabumlenkung und Bewehrungsknoten. Test report, Universität Stuttgart, Stuttgart, 1986.
- [Sch-1987] Schlaich, J.; Schafer, K.; Jennewein, M.: Toward a Consistent Design of Structural Concrete. *Journal of Precast Concrete Institute (PCI)* 32 (1987), No. 3, P. 74–150.
- [Ska-2017] Skar, A.; Poulsen, P. N.; Oelsen, J. F.: Cyclic cohesive model for fatigue crack growth in concrete: Proceedings of 2nd International Symposium on Multiscale Experimental Mechanics (ISMEM), 8.-9. November, Lyngby, Denmark, 2017.
- [Slo-2015] Slobbe, A. T.: Propagation and band width of smeared cracks. Doctoral thesis, Delft University of Technology, Faculty Civil Engineering and Geosciences, Delft, 2015.
- [Slo-2014] Slowik, M.: Shear failure mechanism in concrete beams. *Procedia Materials Science* 3 (2014), P. 1977–1982.
- [Soz-1957] Sozen, M. A.: Strength in shear of prestressed concrete beams without web reinforcement, University of Illinois, 1957.
- [Tew-2014] Teworte, F.: Zum Querkrafttragverhalten von Spannbetonträgern unter Ermüdungsbeanspruchung. Doctoral thesis, RWTH Aachen, Aachen, 2014.
- [Thu-2011] Thun, H.; Ohlsson, U.; Elfgrén, L.: A deformation criterion for fatigue of concrete in tension. *Structural Concrete* 12 (2011), No. 3, P. 187–197. doi: 10.1002/suco.201100013.
- [Tra-2015] Tran, N. L.; Kohoutek, J.; Graubner, C.-A.: Querkrafttragfähigkeit von Stahlbetonbauteilen ohne Querkraftbewehrung. *Beton- und Stahlbetonbau* 110 (2015), No. 4, P. 244–253. doi: 10.1002/best.201400063.
- [Tra-2017] Tran, N. L.: A new shear model for fibre-reinforced concrete members without shear reinforcement. In: Hordijk, D. A.; Luković (Eds.), *High Tech Concrete: Where Technology and Engineering Meet* (Proceedings of fib Symposium 2017, 12.-14.06.2017 in Maastricht, Niederlande), P. 727–739. doi: 10.1007/978-3-319-59471-2_86.
- [Tru-1999] Trunk, B. G.: Einfluss der Bauteilgröße auf die Bruchenergie von Beton. Doctoral Thesis, Eidgenössischen Technischen Hochschule Zürich, Zürich, 1999.
- [Tue-2014] Tue, N. V.; Theiler, W.; Tung, N. D.: Schubverhalten von Biegebauteilen ohne Querkraftbewehrung. *Beton- und Stahlbetonbau* 109 (2014), No. 10, P. 666–677. doi: 10.1002/best.201400058.
- [Tue-2015] Tue, N. V.; Ehmman, R.; Tung, N. D.: Schubversuche an Stahlbetonbalken unterschiedlicher M/V-Kombinationen. *Beton- und Stahlbetonbau* 110 (2015), No. 7, P. 446–457. doi: 10.1002/best.201500005.

- [Tun-2016] Tung, N. D.; Tue, N. V.: Effect of support condition and load arrangement on the shear response of reinforced concrete beams without transverse reinforcement. *Engineering Structures* 111 (2016), P. 370–382. doi: 10.1016/j.engstruct.2015.12.022.
- [Ued-1982] Ueda, T.: Behavior in Shear of Reinforced Concrete Beams under Fatigue Loading. Doctoral thesis, University of Tokyo, Tokyo, 1982.
- [Van-1962] Van den Berg, F. J.: Shear Strength of Reinforced Concrete Beams Without Web Reinforcement. Part 2 - Factors Affecting Load at Diagonal Cracking. *Journal of American Concrete Institute* 59 (1962), No. 11, P. 1587–1600.
- [van-2007] van Mier, J. G. M.; Mechtcherine, V.: Experimental determination of the stress-crack opening curve for concrete in tension. Chapter 2: Minimum demands for deformation controlled uniaxial tensile tests, RILEM, 2007.
- [van-2013] van Mier, J. G. M.: A solution to the parameter-identification conundrum. Multi-scale interaction potentials. *International Journal of Fracture* 184 (2013), No. 1-2, P. 171–183. doi: 10.1007/s10704-013-9858-8.
- [Vec-1986] Vecchio, F. J.; Collins, M. P.: The modified compression field theory for reinforced concrete elements subjected to shear. *ACI Journal* 83 (1986), No. 22, P. 219–231.
- [Vec-1993] Vecchio, F. J.; Collins, M. P.: Compression Response of Cracked Reinforced Concrete. *Journal of Structural Engineering* (1993), No. 119, P. 3590–3610.
- [Wal-1981] Walraven, J. C.; Reinhardt, H. W.: Theory and experiments on the mechanical behaviour of cracks in plain and reinforced concrete subjected to shear loading, Heron Vol. 26, no. 1A, Stevin Laboratory, Delft, 1981.
- [Wal-1980] Walraven, J. C.: Aggregate interlock: A theoretical and experimental analysis. Doctoral Thesis, Technische Universiteit Delft, Delft, 1980.
- [Wei-1987] Weigler, H.; Rings, K.-H.: Unbewehrter und bewehrter Beton unter Wechselbeanspruchung, Berlin, Ernst, 1987. ISBN: 3-433-01383-7.
- [Wit-1983] Wittmann, F. H.: *Fracture Mechanics of Concrete // Fracture mechanics of concrete*, Amsterdam, Elsevier Science Publishers B. V., 1983. ISBN: 9780444421999.
- [Xie-1994] Xie, Y.; Ahmad, S. A.; Yu, T., Hino, S.; Chung, W.: Shear Ductility of Reinforced Concrete Beams of Normal and High-Strength Concrete. *ACI Structural Journal* 91 (1994), No. 2, P. 140–149.
- [Yan-2014] Yang, Y. A.: New Look at an Old Problem: Shear Behaviour of Reinforced Concrete Members without Shear Reinforcement. Doctoral thesis, Technische Universiteit Delft, Delft, 2014.
- [Yan-2016] Yang, Y.; den Uijl, J.; Walraven, J.: Critical shear displacement theory. On the way to extending the scope of shear design and assessment for members without shear reinforcement. *Structural Concrete* 17 (2016), No. 5, P. 790–798. doi: 10.1002/suco.201500135.
- [Yan-1989] Yankelevsky, D. Z.; Reinhardt, H. W.: Uniaxial behaviour of concrete in cyclic tension. *ASCE Journal of Structural Engineering* 115 (1989), No. 1, P. 166–182.
- [Zan-2008] Zanuy Sanchez, C.: Analisis Seccional de elementos de hormigon armado sometidos a fatiga, incluyendo secciones entre fisuras. Doctoral thesis, Universidad politecnico de madrid, Madrid, 2008.
- [Zar-2003] Zararis, P. D.: Shear Strength and Minimum Shear Reinforcement of Reinforced Concrete Slender Beams. *ACI Structural Journal* 100 (2003), No. 2, P. 203–214. doi: 10.14359/12484.
- [Zil-2010] Zilch, K.; Zehetmaier, G.: Bemessung im konstruktiven Betonbau. Nach DIN 1045-1 (Fassung 2008) und EN 1992-1-1 (Eurocode 2), Berlin, Heidelberg, Springer-Verlag Berlin Heidelberg, 2010. ISBN: 978-3-540-70637-3.
- [Zin-2000] Zink, M.: Zum Biegeschubversagen schlanker Bauteile aus Hochleistungsbeton mit und ohne Vorspannung. Doctoral thesis, Universität Leipzig, Leipzig, 2000.

Appendix A: Database of cyclic tensile tests

1	3	2	4	5					6	7	8	9	10			11			12	13	14	15	16	17
No.	reference	label	type	cross-section	Geometry					$f_{t,aver}$ [N/mm ²]	d_g [mm]	state	S_{sup} [-]	S_{int} [-]	$\log N$ [-]	f [Hz]	$f_{c,cyc}$	$f_{c,ext}$						
					b [mm]	t [mm]	\emptyset [mm]	h [mm]	concrete										cyclic loading					
65		Cornelissen-65	FT	cylinder (dogbone)	-	-	-	120	175	2.92	16	wet	0.74	0.4	3.37	6	-							
66		Cornelissen-66	FT	cylinder (dogbone)	-	-	-	120	175	2.92	16	wet	0.80	0.4	3.42	6	-							
67		Cornelissen-67	FT	cylinder (dogbone)	-	-	-	120	175	2.92	16	wet	0.74	0.4	3.85	6	-							
68		Cornelissen-68	FT	cylinder (dogbone)	-	-	-	120	175	2.92	16	wet	0.70	0.4	4.24	6	-							
69		Cornelissen-69	FT	cylinder (dogbone)	-	-	-	120	175	2.92	16	wet	0.70	0.4	4.71	6	-							
70		Cornelissen-70	FT	cylinder (dogbone)	-	-	-	120	175	2.92	16	wet	0.63	0.4	4.71	6	-							
71		Cornelissen-71	FT	cylinder (dogbone)	-	-	-	120	175	2.46	16	dry	0.85	0.2	1.02	6	-							
72		Cornelissen-72	FT	cylinder (dogbone)	-	-	-	120	175	2.46	16	dry	0.90	0.2	1.31	6	-							
73		Cornelissen-73	FT	cylinder (dogbone)	-	-	-	120	175	2.46	16	dry	0.90	0.2	1.43	6	-							
74		Cornelissen-74	FT	cylinder (dogbone)	-	-	-	120	175	2.46	16	dry	0.80	0.2	1.92	6	-							
75		Cornelissen-75	FT	cylinder (dogbone)	-	-	-	120	175	2.46	16	dry	0.76	0.2	1.95	6	-							
76		Cornelissen-76	FT	cylinder (dogbone)	-	-	-	120	175	2.46	16	dry	0.80	0.2	2.02	6	-							
77		Cornelissen-77	FT	cylinder (dogbone)	-	-	-	120	175	2.46	16	dry	0.91	0.2	2.09	6	-							
78		Cornelissen-78	FT	cylinder (dogbone)	-	-	-	120	175	2.46	16	dry	0.86	0.2	2.19	6	-							
79		Cornelissen-79	FT	cylinder (dogbone)	-	-	-	120	175	2.46	16	dry	0.80	0.2	2.21	6	-							
80		Cornelissen-80	FT	cylinder (dogbone)	-	-	-	120	175	2.46	16	dry	0.80	0.2	2.34	6	-							
81		Cornelissen-81	FT	cylinder (dogbone)	-	-	-	120	175	2.46	16	dry	0.80	0.2	2.52	6	-							
82		Cornelissen-82	FT	cylinder (dogbone)	-	-	-	120	175	2.46	16	dry	0.86	0.2	2.62	6	-							
83		Cornelissen-83	FT	cylinder (dogbone)	-	-	-	120	175	2.46	16	dry	0.91	0.2	2.62	6	-							
84		Cornelissen-84	FT	cylinder (dogbone)	-	-	-	120	175	2.46	16	dry	0.91	0.2	2.93	6	-							
85		Cornelissen-85	FT	cylinder (dogbone)	-	-	-	120	175	2.46	16	dry	0.80	0.2	3.36	6	-							
86	[Cor-1981]	Cornelissen-86	FT	cylinder (dogbone)	-	-	-	120	175	2.46	16	dry	0.80	0.2	3.46	6	-							
87	[Cor-1984]	Cornelissen-87	FT	cylinder (dogbone)	-	-	-	120	175	2.46	16	dry	0.80	0.2	3.54	6	-							
88	[Cor-1986]	Cornelissen-88	FT	cylinder (dogbone)	-	-	-	120	175	2.46	16	dry	0.75	0.2	3.59	6	-							
89		Cornelissen-89	FT	cylinder (dogbone)	-	-	-	120	175	2.46	16	dry	0.76	0.2	3.89	6	-							
90		Cornelissen-90	FT	cylinder (dogbone)	-	-	-	120	175	2.46	16	dry	0.80	0.2	4.35	6	-							
91		Cornelissen-91	FT	cylinder (dogbone)	-	-	-	120	175	2.46	16	dry	0.70	0.2	4.86	6	-							
92		Cornelissen-92	FT	cylinder (dogbone)	-	-	-	120	175	2.46	16	dry	0.70	0.2	5.00	6	-							
93		Cornelissen-93	FT	cylinder (dogbone)	-	-	-	120	175	2.46	16	dry	0.65	0.2	5.11	6	-							
94		Cornelissen-94	FT	cylinder (dogbone)	-	-	-	120	175	2.46	16	dry	0.71	0.2	5.90	6	-							
95		Cornelissen-95	FT	cylinder (dogbone)	-	-	-	120	175	2.92	16	wet	0.75	0.2	1.81	6	-							
96		Cornelissen-96	FT	cylinder (dogbone)	-	-	-	120	175	2.92	16	wet	0.90	0.2	1.95	6	-							
97		Cornelissen-97	FT	cylinder (dogbone)	-	-	-	120	175	2.92	16	wet	0.85	0.2	1.96	6	-							
98		Cornelissen-98	FT	cylinder (dogbone)	-	-	-	120	175	2.92	16	wet	0.90	0.2	2.39	6	-							
99		Cornelissen-99	FT	cylinder (dogbone)	-	-	-	120	175	2.92	16	wet	0.85	0.2	2.50	6	-							
100		Cornelissen-100	FT	cylinder (dogbone)	-	-	-	120	175	2.92	16	wet	0.75	0.2	2.66	6	-							
101		Cornelissen-101	FT	cylinder (dogbone)	-	-	-	120	175	2.92	16	wet	0.75	0.2	3.04	6	-							
102		Cornelissen-102	FT	cylinder (dogbone)	-	-	-	120	175	2.92	16	wet	0.80	0.2	3.06	6	-							
103		Cornelissen-103	FT	cylinder (dogbone)	-	-	-	120	175	2.92	16	wet	0.70	0.2	3.11	6	-							
104		Cornelissen-104	FT	cylinder (dogbone)	-	-	-	120	175	2.92	16	wet	0.65	0.2	3.65	6	-							
105		Cornelissen-105	FT	cylinder (dogbone)	-	-	-	120	175	2.92	16	wet	0.75	0.2	3.78	6	-							
106		Cornelissen-106	FT	cylinder (dogbone)	-	-	-	120	175	2.92	16	wet	0.70	0.2	4.00	6	-							
107		Cornelissen-107	FT	cylinder (dogbone)	-	-	-	120	175	2.92	16	wet	0.71	0.2	4.14	6	-							
108		Cornelissen-108	FT	cylinder (dogbone)	-	-	-	120	175	2.92	16	wet	0.65	0.2	4.67	6	-							
109		Cornelissen-109	FT	cylinder (dogbone)	-	-	-	120	175	2.92	16	wet	0.65	0.2	6.30	6	-							
110		HSC-1-2	FT	prism (dogbone)	100	60	-	220	536	16	sealed	0.90	0	1.32	10	-								
111		HSC-1-3	FT	prism (dogbone)	100	60	-	220	536	16	sealed	0.80	0	4.13	10	-								
112		HSC-1-4	FT	prism (dogbone)	100	60	-	220	536	16	sealed	0.70	0	4.68	10	-								
113		NSC-1-1	FT	prism (dogbone)	100	60	-	220	349	16	unsealed	0.90	0	3.35	10	-								
114		NSC-1-2	FT	prism (dogbone)	100	60	-	220	349	16	unsealed	0.80	0	4.74	10	-								
115	[Kes-2002]	NSC-1-3	FT	prism (dogbone)	100	60	-	220	349	16	sealed	0.91	0	3.68	1	-								
116		NSC-1-5	FT	prism (dogbone)	100	60	-	220	349	16	sealed	0.82	0	4.33	1	-								
117		NSC-1-6	FT	prism (dogbone)	100	60	-	220	349	16	sealed	0.91	0	1.08	10	-								
118		NSC-1-8	FT	prism (dogbone)	100	60	-	220	449	16	sealed	0.62	0	2.33	10	-								
119		NSC-1-9	FT	prism (dogbone)	100	60	-	220	549	16	sealed	0.45	0	5.44	10	-								
120		Chen-1	FT	cylinder	73	-	-	146	359	16	-	0.95	0	1.23	4	-								
121		Chen-2	FT	cylinder	73	-	-	146	359	16	-	0.95	0	1.73	4	-								
122		Chen-3	FT	cylinder	73	-	-	146	359	16	-	0.95	0	1.78	4	-								
123		Chen-4	FT	cylinder	73	-	-	146	359	16	-	0.95	0	1.99	4	-								
124		Chen-5	FT	cylinder	73	-	-	146	359	16	-	0.95	0	2.01	4	-								
125	[Che-2017]	Chen-6	FT	cylinder	73	-	-	146	359	16	-	0.95	0	2.13	4	-								
126		Chen-7	FT	cylinder	73	-	-	146	359	16	-	0.95	0	2.34	4	-								
127		Chen-8	FT	cylinder	73	-	-	146	359	16	-	0.95	0	2.38	4	-								
128		Chen-9	FT	cylinder	73	-	-	146	359	16	-	0.95	0	2.58	4	-								
129		Chen-10	FT	cylinder	73	-	-	146	359	16	-	0.95	0	2.65	4	-								
130		Chen-11	FT	cylinder	73	-	-	146	359	16	-	0.95	0	2.95	4	-								

Appendix A: Database of cyclic tensile tests

3	2	4	5	6	7	8	9	10	11	12	13	14	15	16	17	
reference	label	type	cross-section	Geometry				$f_{t,ref}$ [N/mm ²]	concrete	state	S_{sup} [-]	S_{inf} [-]	log N [-]	cyclic loading	f [Hz]	f_{durs}/f_{cyc} [-]
				h [mm]	t [mm]	\emptyset [mm]	h [mm]									
[Che-2017]	Chen-12	FT	cylinder	73	-	-	146	3.59	16	-	0.9	0	2.15	4	-	
	Chen-13	FT	cylinder	73	-	-	146	3.59	16	-	0.9	0	2.32	4	-	
	Chen-14	FT	cylinder	73	-	-	146	3.59	16	-	0.9	0	2.45	4	-	
	Chen-15	FT	cylinder	73	-	-	146	3.59	16	-	0.9	0	2.52	4	-	
	Chen-16	FT	cylinder	73	-	-	146	3.59	16	-	0.9	0	2.61	4	-	
	Chen-17	FT	cylinder	73	-	-	146	3.59	16	-	0.9	0	2.68	4	-	
	Chen-18	FT	cylinder	73	-	-	146	3.59	16	-	0.9	0	2.74	4	-	
	Chen-19	FT	cylinder	73	-	-	146	3.59	16	-	0.9	0	2.76	4	-	
	Chen-20	FT	cylinder	73	-	-	146	3.59	16	-	0.9	0	3.02	4	-	
	Chen-21	FT	cylinder	73	-	-	146	3.59	16	-	0.9	0	3.39	4	-	
	Chen-22	FT	cylinder	73	-	-	146	3.59	16	-	0.9	0	3.51	4	-	
	Chen-23	FT	cylinder	73	-	-	146	3.59	16	-	0.9	0	3.63	4	-	
	Chen-24	FT	cylinder	73	-	-	146	3.59	16	-	0.85	0	2.98	4	-	
	Chen-25	FT	cylinder	73	-	-	146	3.59	16	-	0.85	0	3.11	4	-	
	Chen-26	FT	cylinder	73	-	-	146	3.59	16	-	0.85	0	3.39	4	-	
	Chen-27	FT	cylinder	73	-	-	146	3.59	16	-	0.85	0	3.54	4	-	
	Chen-28	FT	cylinder	73	-	-	146	3.59	16	-	0.85	0	3.63	4	-	
	Chen-29	FT	cylinder	73	-	-	146	3.59	16	-	0.85	0	3.74	4	-	
	Chen-30	FT	cylinder	73	-	-	146	3.59	16	-	0.85	0	3.80	4	-	
	Chen-31	FT	cylinder	73	-	-	146	3.59	16	-	0.85	0	3.87	4	-	
	Chen-32	FT	cylinder	73	-	-	146	3.59	16	-	0.85	0	3.97	4	-	
	Chen-33	FT	cylinder	73	-	-	146	3.59	16	-	0.85	0	4.02	4	-	
	Chen-34	FT	cylinder	73	-	-	146	3.59	16	-	0.85	0	4.08	4	-	
	Chen-35	FT	cylinder	73	-	-	146	3.59	16	-	0.85	0	4.24	4	-	
	Chen-36	FT	cylinder	73	-	-	146	3.59	16	-	0.85	0	4.32	4	-	
	Chen-37	FT	cylinder	73	-	-	146	3.59	16	-	0.85	0	4.59	4	-	
	Chen-38	FT	cylinder	73	-	-	146	3.59	16	-	0.85	0	4.68	4	-	
	Chen-39	FT	cylinder	73	-	-	146	3.59	16	-	0.8	0	3.38	4	-	
	Chen-40	FT	cylinder	73	-	-	146	3.59	16	-	0.8	0	3.57	4	-	
	Chen-41	FT	cylinder	73	-	-	146	3.59	16	-	0.8	0	3.67	4	-	
	Chen-42	FT	cylinder	73	-	-	146	3.59	16	-	0.8	0	3.72	4	-	
Chen-43	FT	cylinder	73	-	-	146	3.59	16	-	0.8	0	4.01	4	-		
Chen-44	FT	cylinder	73	-	-	146	3.59	16	-	0.8	0	4.20	4	-		
Chen-45	FT	cylinder	73	-	-	146	3.59	16	-	0.8	0	4.26	4	-		
Chen-46	FT	cylinder	73	-	-	146	3.59	16	-	0.8	0	4.39	4	-		
Chen-47	FT	cylinder	73	-	-	146	3.59	16	-	0.8	0	4.77	4	-		
Chen-48	FT	cylinder	73	-	-	146	3.59	16	-	0.8	0	4.89	4	-		
Chen-49	FT	cylinder	73	-	-	146	3.59	16	-	0.8	0	5.12	4	-		
Chen-50	FT	cylinder	73	-	-	146	3.59	16	-	0.8	0	5.37	4	-		
Chen-51	FT	cylinder	73	-	-	146	3.59	16	-	0.8	0	5.48	4	-		
[Cor-1984]	111-06	RT	cylinder (dogbone)		120	175	2.45	16	wet	0.7	0.4	5.6	6	1.05		
	117-06	RT	cylinder (dogbone)		120	175	2.45	16	wet	0.7	0.4	5.6	6	1.2		
	111-09	RT	cylinder (dogbone)		120	175	2.45	16	wet	0.7	0.4	5.3	6	1.01		
	112-10	RT	cylinder (dogbone)		120	175	2.45	16	wet	0.7	0.4	5.3	6	0.89		
	111-10	RT	cylinder (dogbone)		120	175	2.45	16	wet	0.7	0.4	5.0	6	1.08		
	114-09	RT	cylinder (dogbone)		120	175	2.45	16	wet	0.7	0.4	5.0	6	1.17		
	116-12	RT	cylinder (dogbone)		120	175	2.45	16	dry	0.6	0.4	5.6	6	1.06		
	116-11	RT	cylinder (dogbone)		120	175	2.45	16	dry	0.6	0.4	5.3	6	1.22		
	116-09	RT	cylinder (dogbone)		120	175	2.45	16	dry	0.6	0.4	5.0	6	1		
	106-05a	RT	cylinder (dogbone)		120	175	2.88	16	sealed-dry	0.6	0.4	5.6	6	0.94		
	121-06a	RT	cylinder (dogbone)		120	175	2.88	16	sealed-dry	0.6	0.4	5.6	6	1.02		
	121-07a	RT	cylinder (dogbone)		120	175	2.88	16	sealed-dry	0.6	0.4	5.3	6	0.95		
	122-14a	RT	cylinder (dogbone)		120	175	2.88	16	sealed-dry	0.6	0.4	5.3	6	0.94		
	107-05a	RT	cylinder (dogbone)		120	175	2.88	16	sealed-dry	0.6	0.4	5.0	6	1		
	108-08a	RT	cylinder (dogbone)		120	175	2.88	16	sealed-dry	0.6	0.4	5.0	6	1.04		
	107-06	RT	cylinder (dogbone)		120	175	2.45	16	dry	0.4	0.1	6.3	6	1.01		
	108-06	RT	cylinder (dogbone)		120	175	2.45	16	dry	0.5	0.1	6.3	6	1.09		
	101-13	RT	cylinder (dogbone)		120	175	2.45	16	dry	0.5	0	6.3	6	0.81		
	109-11	RT	cylinder (dogbone)		120	175	2.45	16	dry	0.6	0	6.3	6	1.06		
	111-11	RT	cylinder (dogbone)		120	175	2.45	16	dry	0.6	0	6.3	6	1.06		
	95-15	RT	cylinder (dogbone)		120	175	2.45	16	dry	0.7	0	6.3	6	1.12		
	97-05	RT	cylinder (dogbone)		120	175	2.45	16	dry	0.7	0	6.3	6	1.08		
	110-12	RT	cylinder (dogbone)		120	175	2.45	16	dry	0.6	0.2	6.3	6	1.16		
	112-12	RT	cylinder (dogbone)		120	175	2.45	16	dry	0.6	0.2	6.3	6	1.12		
	114-12	RT	cylinder (dogbone)		120	175	2.45	16	dry	0.6	0.2	6.3	6	1.21		
	97-01	RT	cylinder (dogbone)		120	175	2.45	16	dry	0.7	0.2	6.3	6	1.19		

Appendix A: Database of cyclic tensile tests

1	3	2	4	5					6	7	8	9	10			11	12	13	14	15	16	17
No.	reference	label	type	cross-section	Geometry				$f_{t,axial}$ [N/mm ²]	d_f [mm]	state	concrete			S_{sup} [-]	S_{inf} [-]	log N [-]	f [Hz]	$f_{t,axial}/f_{t,axial}$ [-]			
					b [mm]	t [mm]	\varnothing [mm]	h [mm]				S_{sup} [-]	S_{inf} [-]	log N [-]						f [Hz]	$f_{t,axial}/f_{t,axial}$ [-]	
197	[Cor-1984]	111-12	RT	cylinder (dogbone)				120	175	2.45	16	dry	0.7	0.2	6.3	6	1.33					
198		106-10	RT	cylinder (dogbone)				120	175	2.45	16	dry	0.65	0.4	6.3	6	1.07					
199	[Bla-1993]	II-232	RT	prism	200	200	-	1000	1.56	16	sealed-dry	0.75	0.1	4.0	0.1	0.97						
200		II-242	RT	prism	200	200	-	1000	1.56	16	sealed-dry	0.75	0.1	4.0	0.1	0.97						
201		II-254	RT	prism	200	200	-	1000	1.56	16	sealed-dry	0.75	0.1	4.0	0.1	1.23						
202		III-249	RT	prism	200	200	-	1000	1.56	16	sealed-dry	0.75	0.3	4.0	0.1	1.20						
203		III-250	RT	prism	200	200	-	1000	1.56	16	sealed-dry	0.75	0.3	4.0	0.1	1.14						
204		III-251	RT	prism	200	200	-	1000	1.56	16	sealed-dry	0.75	0.3	4.0	0.1	1.28						
205		III-252	RT	prism	200	200	-	1000	1.56	16	sealed-dry	0.75	0.3	4.0	0.1	1.23						
206		III-296	RT	prism	200	200	-	1000	1.56	16	sealed-dry	0.75	0.3	4.0	0.1	1.21						
207		III-286	RT	prism	200	200	-	1000	1.56	16	sealed-dry	0.75	0.3	4.0	0.1	1.26						
208		IVa-245	RT	prism	200	200	-	1000	1.56	16	sealed-dry	0.75	0.1	4.0	1	0.97						
209		IVa-246	RT	prism	200	200	-	1000	1.56	16	sealed-dry	0.75	0.1	4.0	1	0.92						
210		IVa-297	RT	prism	200	200	-	1000	1.56	16	sealed-dry	0.75	0.1	4.0	1	0.87						
211		IVb-291	RT	prism	200	200	-	1000	1.56	16	sealed-dry	0.75	0.1	4.0	0	1.08						
212		IVb-283	RT	prism	200	200	-	1000	1.56	16	sealed-dry	0.75	0.1	4.0	0	1.19						
213		IVb-281	RT	prism	200	200	-	1000	1.56	16	sealed-dry	0.75	0.1	4.0	0	1.22						
214		V-271	RT	prism	200	200	-	1000	1.56	16	sealed-dry	0.75	0.1	5.0	0.1	1.12						
215		V-295	RT	prism	200	200	-	1000	1.56	16	sealed-dry	0.75	0.1	5.0	0.1	1.12						
216		V-290	RT	prism	200	200	-	1000	1.56	16	sealed-dry	0.75	0.1	5.0	0.1	1.12						
217		VIa-282	RT	prism	200	200	-	1000	1.56	16	sealed-dry	0.6	0.1	4.0	0.1	1.03						
218		VIa-268	RT	prism	200	200	-	1000	1.56	16	sealed-dry	0.6	0.1	4.0	0.1	1.09						
219	VIa-253	RT	prism	200	200	-	1000	1.56	16	sealed-dry	0.6	0.1	4.0	0.1	1.09							
220	VIb-265	RT	prism	200	200	-	1000	1.56	16	sealed-dry	0.5	0.1	4.0	0.1	0.90							
221	VIb-268	RT	prism	200	200	-	1000	1.56	16	sealed-dry	0.5	0.1	4.0	0.1	1.12							
222	VIb-253	RT	prism	200	200	-	1000	1.56	16	sealed-dry	0.5	0.1	4.0	0.1	0.97							
223	VII-284	RT	prism	200	200	-	1000	1.56	16	sealed-dry	0.75	0.1	4.0	0.1	1.11							
224	VII-285	RT	prism	200	200	-	1000	1.56	16	sealed-dry	0.75	0.1	4.0	0.1	1.08							
225	VII-288	RT	prism	200	200	-	1000	1.56	16	sealed-dry	0.75	0.1	4.0	0.1	1.16							
226	[Men-2007]	1	RT	prism (dogbone)	100	100	-	110	2.7	-	dry	0.75	0	4.0	-	0.8						
227		2	RT	prism (dogbone)	100	100	-	110	2.7	-	dry	0.75	0	4.0	-	0.9						
228		3	RT	prism (dogbone)	100	100	-	110	2.7	-	dry	0.75	0	1.3	-	0.9						
229		4	RT	prism (dogbone)	100	100	-	110	2.7	-	dry	0.75	0	4.3	-	0.7						
230		5	RT	prism (dogbone)	100	100	-	110	2.7	-	dry	0.75	0	4.2	-	0.9						
231		6	RT	prism (dogbone)	100	100	-	110	2.7	-	dry	0.75	0	4.0	-	1.0						
232		7	RT	prism (dogbone)	100	100	-	110	2.7	-	dry	0.75	0	1.5	-	1.0						
233		8	RT	prism (dogbone)	100	100	-	110	2.7	-	dry	0.75	0	4.5	-	0.8						
234		9	RT	prism (dogbone)	100	100	-	110	2.7	-	dry	0.75	0	4.2	-	1.0						
235		10	RT	prism (dogbone)	100	100	-	110	2.7	-	dry	0.75	0	4.0	-	1.0						
236		11	RT	prism (dogbone)	100	100	-	110	2.7	-	dry	0.75	0	1.7	-	1.1						
237		12	RT	prism (dogbone)	100	100	-	110	2.7	-	dry	0.85	0	3.1	-	0.9						
238		13	RT	prism (dogbone)	100	100	-	110	2.7	-	dry	0.85	0	3.0	-	0.9						
239		14	RT	prism (dogbone)	100	100	-	110	2.7	-	dry	0.85	0	3.4	-	0.8						
240		15	RT	prism (dogbone)	100	100	-	110	2.7	-	dry	0.85	0	3.3	-	0.9						
241		16	RT	prism (dogbone)	100	100	-	110	2.7	-	dry	0.85	0	3.0	-	1.0						
242		17	RT	prism (dogbone)	100	100	-	110	2.7	-	dry	0.85	0	3.8	-	0.9						
243		18	RT	prism (dogbone)	100	100	-	110	2.7	-	dry	0.85	0	3.3	-	1.0						
244		19	RT	prism (dogbone)	100	100	-	110	2.7	-	dry	0.85	0	3.0	-	1.1						

Appendix B: Documentation of cyclic tensile tests

B-1 Concrete mixture

Specimens ZP1-ZP6 were casted using the concrete mixed in the first batch and the rest of specimens (Z1-Z5 and ZO1-ZO10) were casted with the concrete mixed in the second batch. Both mixtures were identical with a target compressive strength $f_{dry,cube} = 37 \text{ N/mm}^2$.

Table B-1: Concrete mixture composition

component		batch 1	batch 2
volume	[litre]	76	396
cement content	[kg/m ³]	350	350
cement type	[-]	CEM I/42.5R	CEM I/42.5R
aggregate content	[kg/m ³]	1854	1854
max. aggregate size d_g	[mm]	16	16
water-cement ratio w / c	[-]	0.5	0.5
aggregate type	[-]	sand and gravel stone	sand and gravel stone
air content	[vol-%]	1.5	1.5

Table B-2: Aggregate grading for batch 1 and 2

sieve no.	aggregate size	relative mass [%]
01/13	0/1	0
02/15	0/2	35
03/15	2/8	30
04/14	8/16	35

B-2 Concrete properties

Fresh concrete

Table B-3: Fresh concrete properties

property		Batch 1	Batch 2
slump	[mm]	46/46	44/45
temperature	[°c]	20.1	18.9

Hardened concrete

The first tests (ZP) were conducted on ZP1 to ZP6 at the age of 41-42 days on specimens casted with batch 1. Second test group (Z) was conducted at an age of 118-120 days on specimens casted with batch 2. The last testing interval was 254-336 days after casting of specimens Z1-Z10 with batch 2. The reference mean values of concrete properties at different ages are provided for age of concrete at three different testing intervals.

Table B-4: Hardened concrete properties

Propetry / test group		ZP	Z	ZO
concrete compressive strength f_c	[N/mm ²]	42.2	43.3	47.2
elasticity modulus E_c	[N/mm ²]	35600	35000	28883
splitting tensile strength $f_{ct,sp}$	[N/mm ²]	-	2.94	-
flexural tensile strength $f_{ct,l}$	[N/mm ²]	-	-	6.26



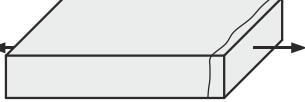







B-3 Overview of results

Table B-4: Specimen properties and test results



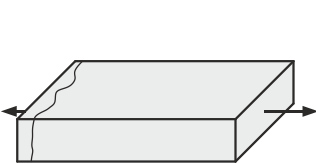
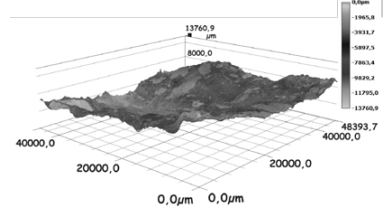
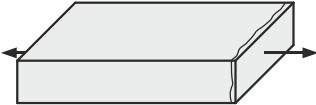

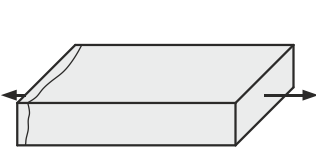
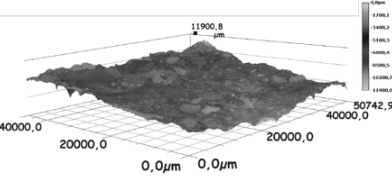
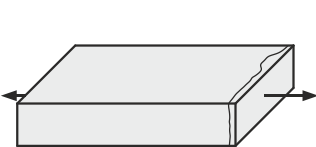
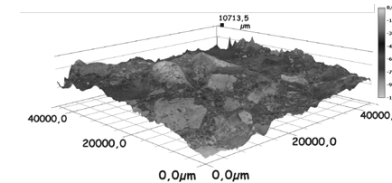
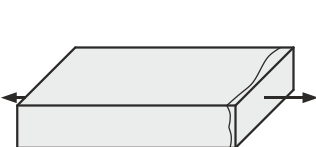
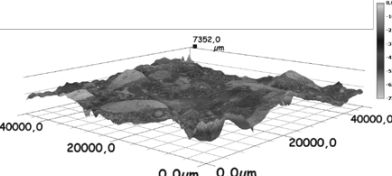
Specimen	Mass [kg]	A [mm ²]	F_{max} [kN]	N [-]	F_{sup} [kN]	F_{inf} [kN]	ϵ_{max} [μm/m]	$\epsilon_{sup,1}$ [μm/m]	$\epsilon_{sup,N}$ [μm/m]
ZP1	31.3	20180	44	1	-	-	76.7	-	
ZP2	31.3	20180	45.8	1	-	-	73.8	-	
ZP3	31.3	19910	46.1	1000	30.0	15.0	-	-	
ZP4	31.3	20511	50.6	2460	30.0	18.0	-	-	
ZP5	31.3	20000	46.3	1	-	-	68.4	-	
ZP6	31.3	20220	40.8	1	-	-	104.3	-	
Z1	31.4	20180	46.5	1	-	-	-	-	
Z2	31.4	19910	46.6	10336	32.0	20.0	95.6	-	
Z3	31.4	20511	51.3	10124	36.0	20.0	166.9	70.5	131.0
Z4	31.4	20000	46.7	31053	36.0	20.0	165.1	69.2	120.6
Z5	31.4	20220	46.3	1	-	-	116.1	70.4	97.7
ZO1	31.3	20000	-(52.0)	10	52.0	31.0	107.3	-	-
ZO2	30.9	20000	-(46.0)	3	46.0	31.0	-	-	-
ZO3	31.1	23400	50.5	16182	39.0	27.0	-	92.3	147.9
ZO4	31.3	24676	48.4	1	-	-	168.5	-	-
ZO5	31.4	23115	50.8	43200	43.0	27.0	145.8	71.4	142.2
ZO6	31.5	20341	51.8	86400	43.0	27.0	151.0	91.4	136.6
ZO7	31.4	20241	43	3530	43.0	17.0	173.0	87.5	173.0
ZO8	31.3	20210	49.7	129600	43.0	27.0	257.3	106.5	251.5
ZO9	31.0	20331	53.7	129600	33.0	17.0	232.4	67.5	219.6
ZO10	31.4	20140	49.1	86400	33.0	17.0	114.7	58.5	73.4

B-4 Failure sections and surfaces

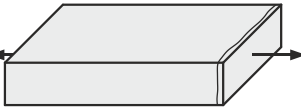
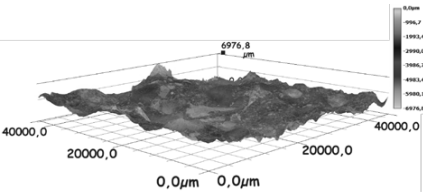

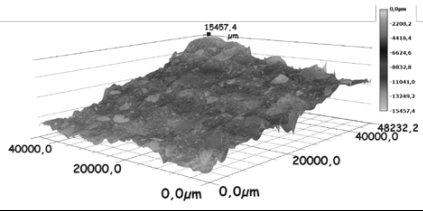

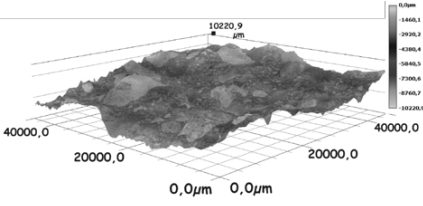
Table B-5: Failure sections and surfaces of tensile specimens

specimen	failure section	failure surface
ZP1		-
ZP2		-
ZP3		-
ZP4		-
ZP5		-
ZP6		-
Z1		-
Z2		-
Z3		-
Z4		-

Appendix B: Documentation of cyclic tensile tests

specimen	failure section	failure surface
Z5		-
Z01		-
Z02		
Z03		-
Z04		-
Z05		
Z06		
Z07		

Appendix B: Documentation of cyclic tensile tests

specimen	failure section	failure surface
ZO8		
ZO9		
ZO10		

Appendix C: Shear database

C-1 Calculation of concrete properties

The provided concrete compressive strength in ACI-DAfStb database correspond to uni-axial concrete compressive strength f_{1c} . However, to use the correlations for a calculative determination of f_{ct} , E_c and G_F , mean value of cylinder compressive strength f_c (cylinder Ø150/300 mm) is required, which was calculated according to [Rei-2012] based on the following equation and documented in the database.

$$f_c = f_{1c}/0.95 \quad \text{Eq. C-1-1}$$

Based on applied test type for determination of concrete compressive strength, the provided mean values are calculated to cylinder compressive strength according to [Rei-2012]:

$$f_c = 0.789 \cdot f_{c,cu150} \quad \text{Eq. C-1-2}$$

The cube compressive strength $f_{c,cu150}$ (150 x 150 x 150 mm) equals:

$$f_{c,cu150} = 1.05 \cdot f_{c,cu200} \quad \text{Eq. C-1-3}$$

$$f_{c,cu150} = 0.90 \cdot f_{c,cu100} \quad \text{Eq. C-1-4}$$

Conversion to SI-Units

1.0 in = 25.4 mm

1.0 lbf = 4.4482 N

1.0 kip = 4.4482 N

1.0 kp/cm² =

1.0 kgf/cm² = 1.0 kp/cm² = 0.0981 N/mm²

1.0 psi = 1 lbf/in² = 6.8948 · 10⁻³ N/mm²

C-2 Shear tests on RC members with diagonal cracking load (mRC-V)

1	3	2	4	5				6		9	10		11	12
				4	5	6	7	Geometry	8		longitudinal reinforcement			
No.	reference	label	type	b [mm]	h [mm]	d [mm]	a [mm]	A_s [mm ²]	ϕ_s [mm]	ρ_l [%]	f_{s_y} [N/mm ²]	f_{s_t} [N/mm ²]		
1	[Bha-1968]	B1	3-point	240.0	350.0	300.0	300.0	905	24.0	1.26	425.8	513.1		
2		B2	3-point	240.0	650.0	600.0	600.0	1810	24.0	1.26	425.8	513.1		
3		B3	3-point	240.0	950.0	900.0	900.0	2714	24.0	1.26	425.8	513.1		
4		B5	3-point	240.0	650.0	600.0	600.0	905	24.0	0.63	425.8	513.1		
5		B6	3-point	240.0	650.0	600.0	600.0	905	12.0	0.63	421.8	522.4		
6		B7	3-point	240.0	950.0	900.0	900.0	1357	24.0	0.63	425.8	513.1		
7		B8	3-point	240.0	950.0	900.0	900.0	1357	12.0	0.63	421.8	522.4		
8		0A-1	3-point	309.9	556.3	461.0	461.0	2579	28.7	1.81	555.2	957.9		
9	[Bre-1963]	0A-2	3-point	304.8	561.3	466.1	466.1	3224	28.7	2.27	555.2	957.9		
10		0A-3	3-point	307.3	556.3	461.5	461.5	3868	28.7	2.73	552.4	933.1		
11		A-1	3-point	152.4	304.8	254.0	254.0	380	12.7	0.98	458.6	834.5		
12		A-2	3-point	152.4	304.8	254.0	254.0	380	12.7	0.98	469.0	834.5		
13		A-3	3-point	152.4	304.8	254.0	254.0	380	12.7	0.98	452.4	834.5		
14		A-4	3-point	152.4	304.8	254.0	254.0	380	12.7	0.98	459.3	834.5		
15		A-11	3-point	152.4	304.8	254.0	254.0	1289	28.7	3.33	341.4	519.3		
16		A-12	3-point	152.4	304.8	254.0	254.0	1289	28.7	3.33	313.8	519.3		
17		A-13	3-point	152.4	304.8	254.0	254.0	1289	28.7	3.33	393.1	519.3		
18		A-14	3-point	152.4	304.8	254.0	254.0	1289	28.7	3.33	364.1	519.3		
19		A-15	3-point	152.4	304.8	254.0	254.0	1289	28.7	3.33	331.7	519.3		
20		II-4A3	3-point	203.2	457.2	390.1	390.1	1583	31.8	2.00	364.8			
21		5A3	3-point	203.2	457.2	390.1	390.1	2375	31.8	3.00	364.8			
22		11A2	3-point	152.4	381.0	313.9	313.9	1583	31.8	3.31	364.8			
23		12A2	3-point	152.4	304.8	237.7	237.7	1583	31.8	4.37	364.8			
24		III-18A2	3-point	152.4	381.0	316.0	316.0	1283	28.6	2.66	370.3			
25			18B2	3-point	152.4	381.0	316.0	316.0	1283	28.6	2.66	370.3		
26			18C2	3-point	152.4	381.0	316.0	316.0	1283	28.6	2.66	370.3		
27		18D2	3-point	152.4	381.0	316.0	316.0	1283	28.6	2.66	370.3			
28	IV-13A2	3-point	152.4	381.0	319.0	319.0	388	22.2	0.80	378.6				
29		14A2	3-point	152.4	304.8	242.8	242.8	388	22.2	1.05	378.6			
30	15A2	3-point	152.4	381.0	316.0	316.0	641	28.6	1.33	370.3				
31	15B2	3-point	152.4	381.0	316.0	316.0	641	28.6	1.33	370.3				
32	16A2	3-point	152.4	304.8	239.8	239.8	641	28.6	1.75	370.3				
33	17A2	3-point	152.4	304.8	242.8	242.8	776	22.2	2.10	378.6				
34	18E2	3-point	152.4	381.0	316.0	316.0	1283	28.6	2.66	370.3				
35	19A2	3-point	152.4	304.8	239.8	239.8	1283	28.6	3.51	370.3				
36	20A2	3-point	152.4	304.8	237.7	237.7	1583	31.8	4.37	364.8				
37	21A2	3-point	203.2	304.8	237.7	237.7	2375	31.8	4.92	364.8				
38	2AC	3-point	152.4	304.8	254.0	254.0	507	25.4	1.31	393.8				
39	3AC	3-point	152.4	304.8	255.5	255.5	776	22.2	1.99	378.6				
40	4AC	3-point	152.4	304.8	254.0	254.0	1013	25.4	2.62	393.8				
41	5AC	3-point	152.4	304.8	252.5	252.5	1283	28.6	3.33	370.3				
42	6AC	3-point	152.4	304.8	250.4	250.4	1583	31.8	4.15	364.8				
43	7CC	3-point	152.4	304.8	255.5	255.5	776	22.2	1.99	378.6				
44	4CC	3-point	152.4	304.8	254.0	254.0	1013	25.4	2.62	393.8				
45	5CC	3-point	152.4	304.8	252.5	252.5	1283	28.6	3.33	370.3				
46	6CC	3-point	152.4	304.8	250.4	250.4	1583	31.8	4.15	364.8				
47	4EC	3-point	152.4	304.8	254.0	254.0	1013	25.4	2.62	393.8				
48	5EC	3-point	152.4	304.8	252.5	252.5	1283	28.6	3.33	370.3				
49	6EC	3-point	152.4	304.8	250.4	250.4	1583	31.8	4.15	364.8				
50	4GC	3-point	152.4	304.8	254.0	254.0	1013	25.4	2.62	393.8				
51	5GC	3-point	152.4	304.8	252.5	252.5	1283	28.6	3.33	370.3				
52	6GC	3-point	152.4	304.8	250.4	250.4	1583	31.8	4.15	364.8				
53	VII-6C	3-point	152.4	304.8	252.5	252.5	1283	28.6	3.33	370.3				
54	VIII-3AAC	3-point	152.4	304.8	255.5	255.5	776	22.2	1.99	378.6				
55		4AAC	3-point	152.4	304.8	254.0	254.0	1013	25.4	2.62	393.8			
56		5AAC	3-point	152.4	304.8	252.5	252.5	1283	28.6	3.33	370.3			
57		6AAC	3-point	152.4	304.8	250.4	250.4	1583	31.8	4.15	364.8			
58		3AC	3-point	152.4	304.8	255.5	255.5	776	22.2	1.99	378.6			
59		4AC	3-point	152.4	304.8	254.0	254.0	1013	25.4	2.62	393.8			
60		5AC	3-point	152.4	304.8	252.5	252.5	1283	28.6	3.33	370.3			
61		6AC	3-point	152.4	304.8	250.4	250.4	1583	31.8	4.15	364.8			
62	4CC	3-point	152.4	304.8	254.0	254.0	1013	25.4	2.62	393.8				
63	5CC	3-point	152.4	304.8	252.5	252.5	1283	28.6	3.33	370.3				
64	6CC	3-point	152.4	304.8	250.4	250.4	1583	31.8	4.15	364.8				

Appendix C: Shear database

13	14	15	16	17	18	19	20	
concrete			diagonal cracking and failure state				def. V_c	
f_c [N/mm ²]	test type	d_{ef} [mm]	V_{cr} [kN]	V_{cr} [kN]	b_w [mm]	$x_{cr,exp}$ [mm]		
23.2	cu	30.0	70.14	70.99	227.0	480	applied shear load at major diagonal cracking	
29.6	cu	30.0	117.23	119.48	415.4	1200		
27.5	cu	30.0	152.06	166.38	632.3	1875		
26.6	cu	30.0	83.39	106.90	446.0	1022		
24.7	cu	30.0	102.02	115.38	462.8	853		
27.2	cu	30.0	117.72	140.05	613.4	1757		
27.7	cu	30.0	117.72	127.63	635.0	1785		
22.6	cyl	19.1	133.44	170.38				diagonal tension cracking load
23.7	cyl	19.1	144.56	184.37	356.3	716		
37.6	cyl	19.1	155.68	195.12				
28.1	cyl	25.4	45.81	73.77				
31.5	cyl	25.4	41.81	42.32				
19.4	cyl	25.4	34.25	35.05	252.7	449		
26.8	cyl	25.4	35.14	35.90				
28.3	cyl	25.4	62.94	103.79				
26.7	cyl	25.4	58.94	59.44				
22.1	cyl	25.4	46.93	47.56				
27.5	cyl	25.4	54.71	55.47				
25.0	cyl	25.4	49.37	50.26				
30.3	cyl	0.0	100.08	109.87		305	critical state of diagonal crack, as the crack extends a short distance into the compression zone	
29.9	cyl	0.0	100.08	170.36		394		
30.2	cyl	0.0	66.72	73.39		203		
30.1	cyl	0.0	55.60	64.05		318		
19.3	cyl	0.0	57.82	63.16		330		
19.9	cyl	0.0	57.82	72.06		254		
22.6	cyl	0.0	53.38	73.39		546		
22.1	cyl	0.0	53.38	60.05		318		
19.9	cyl	0.0	37.81	48.48		381		
20.7	cyl	0.0	26.69	35.14		343		
20.1	cyl	0.0	40.03	45.81		445		
20.7	cyl	0.0	48.93	52.04		406		
22.2	cyl	0.0	37.81	41.81		279		
22.0	cyl	0.0	40.03	44.04		381		
19.8	cyl	0.0	53.38	81.84		343		
20.6	cyl	0.0	42.26	46.26		419		
21.0	cyl	0.0	44.48	50.71		356		
19.9	cyl	0.0	62.27	76.51		445		
23.0	cyl	0.0	31.14	37.81		737		
20.8	cyl	0.0	40.03	44.04		267		
16.5	cyl	0.0	37.81	37.81		724		
18.3	cyl	0.0	37.81	41.81		381		
22.8	cyl	0.0	53.38	53.38		343		
20.5	cyl	0.0	35.58	35.58		686		
20.6	cyl	0.0	40.03	40.03		699		
20.3	cyl	0.0	44.48	44.48		330		
20.6	cyl	0.0	44.48	44.48		546		
21.2	cyl	0.0	41.81	41.81		1156		
19.5	cyl	0.0	39.59	39.59		1321		
19.1	cyl	0.0	42.26	42.26		1257		
21.0	cyl	0.0	35.58	36.92		1448		
21.9	cyl	0.0	37.81	41.81		1448		
21.4	cyl	0.0	40.48	40.48		1435		
20.1	cyl	0.0	51.15	51.15		254		
34.6	cyl	0.0	53.38	55.60		191		
29.2	cyl	0.0	55.60	57.82		292		
32.8	cyl	0.0	53.38	56.93		330		
34.4	cyl	0.0	57.82	60.05		330		
31.9	cyl	0.0	48.93	53.38		533		
30.5	cyl	0.0	48.93	53.82		330		
32.8	cyl	0.0	48.93	54.27		305		
34.1	cyl	0.0	53.38	59.16		533		
38.4	cyl	0.0	48.93	52.49		432		
37.4	cyl	0.0	53.38	57.38		838		
38.4	cyl	0.0	51.15	63.16		991		

Appendix C: Shear database

1	3	2	4	4	5	6	7	8	9	10	11	12		
No.	reference	label	type	Geometry				longitudinal reinforcement						
				b [mm]	h [mm]	d [mm]	a [mm]	A_s [mm ²]	ϕ_s [mm]	ρ_s [%]	f_y [N/mm ²]	f_{ct} [N/mm ²]		
65	[Kre-1966]	5EC	3-point	152.4	304.8	252.5	252.5	1283	28.6	3.33		370.3		
66		6EC	3-point	152.4	304.8	250.4	250.4	1583	31.8	4.15		364.8		
67		IX-3AAC	3-point	152.4	304.8	255.5	255.5	776	22.2	1.99		378.6		
68		4AAC	3-point	152.4	304.8	254.0	254.0	1013	25.4	2.62		393.8		
69		5AAC	3-point	152.4	304.8	252.5	252.5	1283	28.6	3.33		370.3		
70		6AAC	3-point	152.4	304.8	250.4	250.4	1583	31.8	4.15		364.8		
71		3AC	3-point	152.4	304.8	255.5	255.5	776	22.2	1.99		378.6		
72		4AC	3-point	152.4	304.8	254.0	254.0	1013	25.4	2.62		393.8		
73		5AC	3-point	152.4	304.8	252.5	252.5	1283	28.6	3.33		370.3		
74		6AC	3-point	152.4	304.8	250.4	250.4	1583	31.8	4.15		364.8		
75		3CC	3-point	152.4	304.8	255.5	255.5	776	22.2	1.99		378.6		
76		4CC	3-point	152.4	304.8	254.0	254.0	1013	25.4	2.62		393.8		
77		5CC	3-point	152.4	304.8	252.5	252.5	1283	28.6	3.33		370.3		
78		6CC	3-point	152.4	304.8	250.4	250.4	1583	31.8	4.15		364.8		
79		X-C	3-point	203.2	533.4	482.6	482.6	1520	25.4	1.55		393.8		
80		XI-PCA	3-point	152.4	304.8	250.4	250.4	1583	31.8	4.15		364.8		
81		PCB	3-point	152.4	304.8	250.4	250.4	1583	31.8	4.15		364.8		
82		s-I-Oca	3-point	152.4	304.8	254.0	254.0	1013	25.4	2.62		393.8		
83		Ocb	3-point	152.4	304.8	254.0	254.0	1013	25.4	2.62		393.8		
84		s-II-Oca	3-point	254.0	508.0	455.7	455.7	2565	28.6	2.22		370.3		
85		Ocb	3-point	254.0	508.0	455.7	455.7	2565	28.6	2.22		370.3		
86		IIIa-17	4-point	203.2	457.2	402.8	402.8	2074	29.7	2.53		506.7	568.0	
87		IIIa-18	4-point	203.2	457.2	402.8	402.8	2074	29.7	2.53		506.7	568.0	
88		Va-19	4-point	203.2	457.2	402.8	402.8	768	18.1	0.94		684.7	850.6	
89		Va-20	4-point	203.2	457.2	402.8	402.8	768	18.1	0.94		684.7	850.6	
90		[Mat-1963]	VIIb-21	4-point	203.2	457.2	402.8	402.8	681	17.0	0.83		714.4	849.4
91			VIIb-22	4-point	203.2	457.2	402.8	402.8	681	17.0	0.83		714.4	849.4
92	VIIb-23		4-point	203.2	457.2	402.8	402.8	681	17.0	0.83		714.4	849.4	
93	VIIa-24		4-point	203.2	457.2	402.8	402.8	383	12.7	0.47		695.9	915.9	
94	VIIa-25		4-point	203.2	457.2	402.8	402.8	383	12.7	0.47		695.9	915.9	
95	A1		3-point	177.8	304.8	261.6	261.6	1007	35.8	2.17		310.3	510.3	
96	A2		3-point	177.8	304.8	266.7	266.7	1013	25.4	2.14		310.3	510.3	
97	A3		3-point	177.8	304.8	268.0	268.0	1061	21.2	2.23		310.3	510.3	
98	A4		3-point	177.8	304.8	270.0	270.0	1140	19.1	2.37		310.3	510.3	
99	B1		3-point	177.8	304.8	266.7	266.7	760	18.0	1.60		310.3	510.3	
100	B2	3-point	177.8	304.8	268.0	268.0	776	22.2	1.63		310.3	510.3		
101	B3	3-point	177.8	304.8	270.0	270.0	768	18.1	1.60		310.3	510.3		
102	B4	3-point	177.8	304.8	271.5	271.5	792	15.9	1.64		310.3	510.3		
103	C1	3-point	177.8	304.8	268.0	268.0	388	22.2	0.81		310.3	510.3		
104	C2	3-point	177.8	304.8	271.8	271.8	396	15.9	0.82		310.3	510.3		
105	C3	3-point	177.8	304.8	273.1	273.1	380	12.7	0.78		310.3	510.3		
106	C4	3-point	177.8	304.8	274.3	274.3	396	11.2	0.81		310.3	510.3		
107	[Moo-1954]	1	4-point	152.4	304.8	268.2	268.2	776	22.2	1.90		310.3	510.3	
108		2	4-point	152.4	304.8	268.2	268.2	776	22.2	1.90		310.3	510.3	
109		3	4-point	152.4	304.8	268.2	268.2	776	22.2	1.90		310.3	510.3	
110		4	4-point	152.4	304.8	268.2	268.2	776	22.2	1.90		310.3	510.3	
111		5	4-point	152.4	304.8	268.2	268.2	776	22.2	1.90		310.3	510.3	
112		6	4-point	152.4	304.8	268.2	268.2	776	22.2	1.90		310.3	510.3	
113		7	4-point	152.4	304.8	268.2	268.2	776	22.2	1.90		310.3	510.3	
114		8	4-point	152.4	304.8	268.2	268.2	776	22.2	1.90		310.3	510.3	
115		9	4-point	152.4	304.8	268.2	268.2	776	22.2	1.90		310.3	510.3	
116		10	4-point	152.4	304.8	268.2	268.2	776	22.2	1.90		310.3	510.3	
117		11	4-point	152.4	304.8	268.2	268.2	776	22.2	1.90		310.3	510.3	
118		12	4-point	152.4	304.8	268.2	268.2	776	22.2	1.90		310.3	510.3	
119		13	4-point	152.4	304.8	268.2	268.2	776	22.2	1.90		310.3	510.3	
120		14	4-point	152.4	304.8	268.2	268.2	776	22.2	1.90		310.3	510.3	
121		15	4-point	152.4	304.8	268.2	268.2	776	22.2	1.90		310.3	510.3	
122		16	4-point	152.4	304.8	268.2	268.2	776	22.2	1.90		310.3	510.3	
123	[Mor-1956]	B28 B2	3-point	304.8	406.4	362.0	362.0	2122	21.2	1.92		471.0	867.6	
124		B28 E2	3-point	308.1	406.4	371.6	371.6	649	14.4	0.57		463.4	846.2	
125		B28 A4	3-point	304.8	406.4	368.3	368.3	2803	24.4	2.50		332.4	584.1	
126		B28 B4	3-point	304.8	406.4	368.3	368.3	2122	21.2	1.89		441.4	833.1	
127		B28 E4	3-point	304.8	406.4	368.3	368.3	1425	19.1	1.27		429.0	777.2	
128		B28 A6	3-point	308.1	406.4	368.3	368.3	4220	27.7	3.72		455.2	880.7	
129		B28 B6	3-point	304.8	406.4	368.3	368.3	2122	21.2	1.89		451.7	877.2	
130		B40 B4	3-point	304.8	406.4	368.3	368.3	2122	21.2	1.89		377.9	677.9	

Appendix C: Shear database

13	14	15	16	17	18	19	20
concrete			diagonal cracking and failure state				def. V_c
f_c [N/mm ²]	test type	d_{eff} [mm]	V_{cr} [kN]	V_{cr} [kN]	h_w [mm]	$x_{cr,exp}$ [mm]	
37.4	cyl	0.0	40.03	53.38			1384
33.8	cyl	0.0	40.03	48.93			889
12.6	cyl	0.0	40.03	40.48			356
12.9	cyl	0.0	40.03	42.70			483
15.4	cyl	0.0	46.70	50.26			229
13.4	cyl	0.0	44.48	62.27			508
13.7	cyl	0.0	35.58	36.92			724
12.9	cyl	0.0	35.58	40.03			445
15.4	cyl	0.0	42.26	43.59			406
12.4	cyl	0.0	35.58	40.92			800
12.2	cyl	0.0	26.69	31.14			889
17.1	cyl	0.0	35.14	35.14			940
14.7	cyl	0.0	33.36	34.25			330
13.7	cyl	0.0	37.81	39.59			762
16.8	cyl	0.0	84.51	84.51			635
36.3	cyl	0.0	53.38	53.38			1321
36.3	cyl	0.0	53.38	53.38			1321
35.7	cyl	0.0	44.48	48.48			991
39.0	cyl	0.0	51.15	52.49			1016
38.3	cyl	0.0	137.89	146.78			800
38.3	cyl	0.0	128.99	133.44			584
29.2	eyl	25.4	77.84	88.07	325.9		896
25.2	eyl	25.4	73.39	80.73			
23.5	eyl	25.4	53.38	63.27			
25.6	eyl	25.4	55.60	65.94			
26.1	eyl	25.4	55.60	71.39			
25.8	eyl	25.4	53.38	62.38			
30.6	eyl	25.4	60.05	75.06	323.9	645	
26.3	eyl	25.4	46.70	54.49			
25.8	eyl	25.4	40.03	49.93			
30.3	eyl	25.4	57.82	60.53			
31.0	eyl	25.4	66.72	67.21			
31.0	eyl	25.4	62.27	76.10			
31.5	eyl	25.4	66.72	71.65			
21.2	eyl	25.4	50.93	56.75			
21.6	eyl	25.4	60.05	60.53			
19.2	eyl	25.4	53.38	56.09			
16.8	eyl	25.4	52.93	56.09			
6.3	eyl	25.4	20.02	20.50			
6.1	eyl	25.4	24.46	24.95			
6.9	eyl	25.4	25.35	25.84			
6.8	eyl	25.4	25.13	25.62			
36.7	eyl	25.4	51.15	58.79			
16.7	eyl	25.4	33.36	36.55			
25.8	eyl	25.4	51.15	53.23			
15.4	eyl	25.4	37.81	41.45			
30.7	eyl	25.4	46.70	53.01			
15.8	eyl	25.4	33.36	35.44			
30.9	eyl	25.4	44.48	52.12			
12.2	eyl	25.4	31.14	32.10			
41.2	eyl	25.4	51.15	54.34			
23.9	eyl	25.4	42.26	49.90			
38.1	eyl	25.4	48.93	61.02			
20.2	eyl	25.4	46.70	48.12			
37.8	eyl	25.4	44.48	56.57			
22.6	eyl	25.4	42.26	44.11			
37.4	eyl	25.4	51.15	52.12			
16.3	eyl	25.4	35.58	38.78			
14.7	eyl	25.4	122.32	201.49			
13.7	eyl	25.4	88.96	130.34			
27.5	eyl	25.4	151.23	323.81			
32.3	eyl	25.4	133.44	257.09			
33.1	eyl	25.4	117.87	268.21			
47.2	eyl	25.4	211.28	334.95			
43.9	eyl	25.4	177.92	323.81			
34.8	eyl	25.4	154.57	157.42			

Appendix C: Shear database

1	3	2	4	Geometry				8	9	10		11	12
				4	5	6	7			longitudinal reinforcement			
No.	reference	label	type	b [mm]	h [mm]	d [mm]	a [mm]	A_s [mm ²]	\emptyset_s [mm]	ρ_s [%]	f_y [N/mm ²]	f_{ct} [N/mm ²]	
				131	[Mor-1956]	B56 B2	3-point	304.8	406.4	368.3	368.3	2122	21.2
132	B56 E2	3-point	304.8	406.4		368.3	368.3	649	14.4	0.58	462.1	839.3	
133	B56 A4	3-point	304.8	406.4		374.7	374.7	2803	24.4	2.45	329.7	578.6	
134	B56 B4	3-point	304.8	406.4		368.3	368.3	2122	21.2	1.89	440.7	850.3	
135	B56 E4	3-point	304.8	406.4		368.3	368.3	1425	19.1	1.27	429.0	777.2	
136	B56 A6	3-point	308.1	406.4		355.6	355.6	4220	27.7	3.85	438.6	889.7	
137	B56 B6	3-point	304.8	406.4		371.6	371.6	2122	21.2	1.87	466.2	881.4	
138	B70 B2	3-point	304.8	406.4		365.3	365.3	2122	21.2	1.91	462.1	871.0	
139	B70 A4	3-point	304.8	406.4		368.3	368.3	2803	24.4	2.50	435.9	856.6	
140	B70 A6	3-point	304.8	406.4		355.6	355.6	4220	27.7	3.89	435.2	872.4	
141	B84 B4	3-point	304.8	406.4		363.5	363.5	2122	21.2	1.92	464.8	873.8	
142	B113 B4	3-point	304.8	406.4		365.3	365.3	2122	21.2	1.91	469.0	874.5	
143	AO-3-3b	3-point	152.4	336.6		298.5	298.5	1520	25.4	3.34	413.8		
144	AO-3-3c	3-point	152.4	336.6		298.5	298.5	1061	21.2	2.33	413.8		
145	AO-7-3a	3-point	152.4	336.6		298.5	298.5	1520	25.4	3.34	413.8		
146	AO-7-3b	3-point	152.4	336.6		298.5	298.5	1520	25.4	3.34	413.8		
147	AO-11-3a	3-point	152.4	336.6		298.5	298.5	1520	25.4	3.34	413.8		
148	AO-11-3b	3-point	152.4	336.6		298.5	298.5	1520	25.4	3.34	413.8		
149	AO-15-3b	3-point	152.4	336.6		298.5	298.5	1520	25.4	3.34	413.8		
150	AO-15-3c	3-point	152.4	336.6		298.5	298.5	1520	25.4	3.34	413.8		
151	AO-3-2	3-point	152.4	336.6		298.5	298.5	1520	25.4	3.34	413.8		
152	AO-7-2	3-point	152.4	336.6		298.5	298.5	1520	25.4	3.34	413.8		
153	AO-11-2	3-point	152.4	336.6		298.5	298.5	1520	25.4	3.34	413.8		
154	AO-15-2a	3-point	152.4	336.6		298.5	298.5	1520	25.4	3.34	413.8		
155	AO-15-2b	3-point	152.4	336.6		298.5	298.5	1520	25.4	3.34	413.8		
156	[van-1962]	D-1	4-point	228.6		419.1	359.2	359.2	3547	25.4	4.32	275.9	469.0
157		D-2	4-point	228.6		419.1	359.2	359.2	3547	25.4	4.32	275.9	469.0
158		D-3	4-point	228.6		419.1	359.2	359.2	3547	25.4	4.32	275.9	469.0
159		D-4	4-point	228.6		419.1	359.2	359.2	3547	25.4	4.32	275.9	469.0
160		D-5	4-point	228.6		419.1	359.2	359.2	3547	25.4	4.32	275.9	469.0
161		D-6	4-point	228.6		419.1	359.2	359.2	3547	25.4	4.32	275.9	469.0
162		D-7	4-point	228.6	419.1	359.2	359.2	3547	25.4	4.32	275.9	469.0	
163		D-8	4-point	228.6	419.1	359.2	359.2	3547	25.4	4.32	275.9	469.0	
164		D-9	4-point	228.6	419.1	359.2	359.2	3547	25.4	4.32	275.9	469.0	
165		D-10	4-point	228.6	419.1	359.2	359.2	3547	25.4	4.32	275.9	469.0	
166		D-11	4-point	228.6	419.1	359.2	359.2	3547	25.4	4.32	275.9	469.0	
167		D-12	4-point	228.6	419.1	359.2	359.2	3547	25.4	4.32	275.9	469.0	
168		D-13	4-point	228.6	419.1	359.2	359.2	3547	25.4	4.32	275.9	469.0	
169		D-14	4-point	228.6	419.1	359.2	359.2	3547	25.4	4.32	275.9	469.0	
170		D-15	4-point	228.6	419.1	359.2	359.2	3547	25.4	4.32	275.9	469.0	
171		D-16	4-point	228.6	419.1	359.2	359.2	3547	25.4	4.32	275.9	469.0	
172		D-17	4-point	228.6	419.1	359.2	359.2	3547	25.4	4.32	275.9	469.0	
173		D-18	4-point	228.6	419.1	359.2	359.2	3547	25.4	4.32	275.9	469.0	
174		D-19	4-point	228.6	419.1	359.2	359.2	3547	25.4	4.32	275.9	469.0	
175	D-20	4-point	228.6	419.1	359.2	359.2	3547	25.4	4.32	275.9	469.0		
176	E-1	4-point	228.6	419.1	359.2	359.2	3547	25.4	4.32	275.9	469.0		
177	E-2	4-point	228.6	419.1	359.2	359.2	3547	25.4	4.32	275.9	469.0		
178	E-3	4-point	228.6	419.1	359.2	359.2	3547	25.4	4.32	275.9	469.0		
179	E-4	4-point	228.6	419.1	359.2	359.2	3547	25.4	4.32	275.9	469.0		
180	E-5	4-point	228.6	419.1	359.2	359.2	3547	25.4	4.32	275.9	469.0		
181	AS-1	4-point	304.8	419.1	359.2	359.2	3547	25.4	3.24	275.9	469.0		
182	AS-2	4-point	228.6	419.1	359.2	359.2	1496	14.5	1.82	269.0	0.0		
183	AS-3	4-point	228.6	419.1	359.2	359.2	3016	20.7	3.67	269.0	0.0		
184	AS-4	4-point	228.6	419.1	359.2	359.2	2043	16.1	2.49	269.0	0.0		
185	A -5	4-point	228.6	419.1	359.2	359.2	1457	14.4	1.77	269.0	0.0		
186	AS-6	4-point	228.6	419.1	359.2	359.2	1829	16.1	2.23	269.0	0.0		
187	AS-7	4-point	228.6	508.0	448.1	448.1	3547	25.4	3.46	275.9	469.0		
188	NNN-3	4-point	127.0	254.0	215.9	215.9	570	19.1	2.08	420.7	0.0		
189	NHN-3	4-point	127.0	254.0	215.9	215.9	570	19.1	2.08	420.7	0.0		

Appendix C: Shear database

13	14	15	16	17	18	19	20
concrete			diagonal cracking and failure state				def. V_x
f_c [N/mm ²]	test type	d_n [mm]	V_{cr} [kN]	V_u [kN]	b_w [mm]	$x_{cr,exp}$ [mm]	
14.7	cyl	25.4	100.08	102.21	279.0	883	first diagonal cracking load
14.7	cyl	25.4	66.72	81.91			
25.0	cyl	25.4	137.89	140.17			
27.2	cyl	25.4	122.32	124.61			
28.4	cyl	25.4	108.98	111.26			
39.9	cyl	25.4	177.92	180.23			
45.7	cyl	25.4	136.78	139.06			
16.3	cyl	25.4	88.96	91.72			
27.2	cyl	25.4	132.33	135.09			
45.0	cyl	25.4	177.92	180.68			
27.2	cyl	25.4	111.20	114.44			
32.6	cyl	25.4	104.31	108.53			
21.3	cyl	9.5	56.76	64.60			
27.8	cyl	9.5	37.94	66.79			
38.6	cyl	9.5	66.79	82.16			
42.7	cyl	9.5	62.40	82.79			
76.8	cyl	9.5	66.79	89.69			
76.5	cyl	9.5	66.79	89.37			
96.1	cyl	9.5	84.67	100.03			
94.2	cyl	9.5	95.64	97.84	216.9	409	
21.1	cyl	9.5	62.09	77.77			
46.3	cyl	9.5	79.96	117.91			
81.3	cyl	9.5	89.06	111.32			
85.9	cyl	9.5	106.62	177.80			
71.2	cyl	9.5	79.96	205.71	216.9	411	
41.7	cu	19.1	146.78	154.02			
35.9	cu	19.1	131.22	134.01			
30.2	cu	19.1	128.99	131.78			
29.7	cu	19.1	133.44	147.35			
35.9	cu	19.1	122.32	134.01			
34.5	cu	19.1	126.77	142.90			
27.0	cu	19.1	140.11	142.90			
21.3	cu	19.1	113.42	120.66			
12.6	cu	19.1	88.96	91.75			
22.3	cu	19.1	126.77	129.56			
16.0	cu	19.1	108.98	111.77			
19.5	cu	19.1	100.08	109.54			
17.4	cu	19.1	99.19	101.98			
20.0	cu	19.1	106.75	109.54			
18.7	cu	19.1	102.30	105.09			
21.7	cu	19.1	111.20	113.99			
18.5	cu	19.1	104.53	107.32			
20.4	cu	19.1	104.53	107.32			
22.9	cu	19.1	115.65	118.44			
20.2	cu	19.1	106.75	109.54			
55.0	cu	19.1	149.01	151.46			
39.5	cu	19.1	144.56	147.01			
34.6	cu	19.1	128.99	131.44			
30.3	cu	19.1	128.99	131.44			
16.7	cu	19.1	97.86	100.31			
37.2	cu	19.1	177.92	188.31			
17.0	cu	19.1	100.08	102.87			
19.6	cu	19.1	95.63	98.42			
19.1	cu	19.1	95.63	98.42			
20.9	cu	19.1	102.30	105.43			
22.5	cu	19.1	111.20	123.22			
22.1	cu	19.1	153.46	156.84			
38.5	cyl	19.1	29.00	36.91			
100.9	cyl	19.1	40.39	45.96			

Appendix C: Shear database

1	3	2	4	4	5	6	7	8	9	10	11	12
No.	reference	label	type	Geometry				longitudinal reinforcement				
				b [mm]	h [mm]	d [mm]	a [mm]	A_s [mm ²]	Φ_s [mm]	ρ [%]	f_{sy} [N/mm ²]	f_{st} [N/mm ²]
190	[Sch-2014] [Hol-2014]	BO01	4-point	200.0	300.0	270.0	270.0	804	16.0	1.49	525.0	0.0
191		BO02	4-point	200.0	300.0	270.0	270.0	804	16.0	1.49	525.0	0.0
192		BO03	4-point	200.0	300.0	270.0	270.0	804	16.0	1.49	525.0	0.0
193		BO04	4-point	200.0	300.0	270.0	270.0	804	16.0	1.49	525.0	0.0
194	[Slo-2014]	S4	4-point	120.0	250.0	220.0	220.0	509	18.0	1.93	453.0	698.0
195		S5	4-point	120.0	250.0	220.0	220.0	509	18.0	1.93	453.0	698.0
196		S3	4-point	120.0	250.0	220.0	220.0	509	18.0	1.93	453.0	698.0
197		S2	4-point	120.0	250.0	220.0	220.0	509	18.0	1.93	453.0	698.0
198		OI-2	4-point	120.0	250.0	220.0	220.0	509	18.0	1.93	453.0	698.0
199		OI-1	3-point	120.0	250.0	220.0	220.0	509	18.0	1.93	453.0	698.0
200		S1	3-point	120.0	250.0	220.0	220.0	509	18.0	1.93	453.0	698.0
201		S5k	3-point	120.0	250.0	220.0	220.0	509	18.0	1.93	453.0	698.0
202		S3k	3-point	120.0	250.0	220.0	220.0	509	18.0	1.93	453.0	698.0
203		PI-2	3-point	120.0	250.0	220.0	220.0	509	18.0	1.93	453.0	698.0
204		S2k	3-point	120.0	250.0	220.0	220.0	509	18.0	1.93	453.0	698.0

Appendix C: Shear database

13	14	15	16	17	18	19	20
concrete							diagonal cracking and failure state
f_c [N/mm ²]	test type	d_g [mm]	V_G [kN]	V_u [kN]	b_s [mm]	$x_{cr,exp}$ [mm]	def. V_G
33.9	cu	16.0	58.02	60.88			shear load, at which the failure diagonal crack is formed
33.9	cu	16.0	35.00	60.98			
33.9	cu	16.0	42.84	56.07			
33.9	cu	16.0	39.50	51.27			
35.0	cyl	0.0	42.00	82.50			
35.0	cyl	0.0	40.50	40.50		330	shear load causing first diagonal cracking
35.0	cyl	0.0	33.00	42.00		343	
35.0	cyl	0.0	37.50	42.00			
35.0	cyl	0.0	37.50	43.50			
35.0	cyl	0.0	37.50	45.00			
35.0	cyl	0.0	37.50	43.50			
35.0	cyl	0.0	45.00	51.00			
35.0	cyl	0.0	37.50	51.00			
35.0	cyl	0.0	37.50	71.00			
35.0	cyl	0.0	45.00	75.00			

Appendix C: Shear database

C-3 Shear tests on RC members with crack detail (mRC-D)

1	2	3	4	5	6	7	8	11	12	13	14	15	16	17	18	
No.	label	reference	type	Geometry				ρ_1 [%]	f_{c1} [N/mm ²]	f_{c2} [N/mm ²]	f_c [N/mm ²]	concrete	test type	d_g [mm]	h_c [mm]	x_c [mm]
				b [mm]	h [mm]	d [mm]	a [mm]									
1	B1	[Ahm-1986]	4-point	127.0	254.0	201.7	806.7	5.03	413.8	500.0	68.7	cyl	12.7	150.3	602	
2	B2		4-point	127.0	254.0	201.7	605.0	5.03	413.8	500.0	68.7	cyl	12.7	180.4	424	
3	B7		4-point	127.0	254.0	208.0	832.1	2.25	413.8	500.0	68.7	cyl	12.7	197.2	429	
4	B8		4-point	127.0	254.0	208.0	624.1	2.25	413.8	500.0	68.7	cyl	12.7	178.7	444	
5	2		4-point	1000.0	273.4	250.0	920.0	0.64	543.5	599.4	26.9	cu	30.0	-	801	
6	3		4-point	1000.0	278.4	250.0	920.0	0.91	524.8	581.7	27.3	cu	30.0	-	349	
7	11		4-point	1000.0	528.4	500.0	1825.0	0.46	524.8	581.7	24.6	pr	30.0	-	953	
9	12		4-point	1000.0	529.1	500.0	1825.0	0.65	524.8	581.7	27.3	cu	30.0	-	683	
10	16		4-point	1000.0	782.0	750.0	2750.0	0.42	525.8	600.4	30.4	pr	30.0	-	1176	
11	III-2.5-00		4-point	533.4	1066.8	980.4	2241.1	2.20	455.2	0.0	21.4	cyl	19.1	-	-	1113
12	OB28	4-point	304.8	406.4	368.3	800.1	1.89	519.3	942.8	37.6	cyl	25.4	-	-	493	
13	AT-1-East	4-point	2016.0	1005.0	916.0	2662.0	0.76	465.0	674.0	64.6	cyl	10.0	-	-	1399	
14	AT-1 West	4-point	2016.0	1005.0	916.0	2662.0	0.76	465.0	674.0	64.6	cyl	10.0	-	-	1273	
15	AT-2/250N	4-point	250.0	469.0	437.0	1262.0	0.92	465.0	618.0	37.7	cyl	10.0	-	-	459	
16	AT-2/250W	4-point	252.0	471.0	439.0	1262.0	0.90	465.0	618.0	38.5	cyl	10.0	-	-	674	
17	AT-2/1000W	4-point	1002.0	471.0	439.0	1262.0	0.91	465.0	618.0	39.0	cyl	10.0	-	-	527	
18	AT-2/1000N	4-point	1002.0	470.0	438.0	1262.0	0.91	465.0	618.0	37.9	cyl	10.0	-	-	555	
19	AT-2/3000	4-point	3005.0	472.0	439.0	1262.0	0.91	465.0	618.0	40.6	cyl	10.0	-	-	486	
20	AT-3/N1	4-point	697.0	339.0	307.0	1001.9	0.93	465.0	618.0	37.5	cyl	20.0	-	-	533	
21	AT-3/N2	4-point	706.0	339.0	306.0	1001.9	0.93	465.0	618.0	37.1	cyl	20.0	-	-	509	
22	AT-3/T1	4-point	700.0	338.0	306.0	1001.9	0.93	465.0	618.0	37.8	cyl	20.0	-	-	400	
23	AT-3/T2	4-point	706.0	339.0	307.0	1001.9	0.92	465.0	618.0	37.1	cyl	20.0	-	-	345	
24	B1	4-point	240.0	350.0	300.0	881.3	1.26	425.8	513.1	23.2	cu	30.0	227.0	480		
25	B2	4-point	240.0	650.0	600.0	1762.5	1.26	425.8	513.1	29.6	cu	30.0	415.4	1200		
26	B3	4-point	240.0	950.0	900.0	2643.8	1.26	425.8	513.1	27.5	cu	30.0	632.3	1875		
27	B4	4-point	240.0	1250.0	1200.0	3525.0	1.26	425.8	513.1	25.2	cu	30.0	-	2138		
28	B5	4-point	240.0	650.0	600.0	1762.5	0.63	425.8	513.1	26.6	cu	30.0	446.0	1022		
29	B6	4-point	240.0	650.0	600.0	1762.5	0.63	421.8	522.4	24.7	cu	30.0	462.8	853		
30	B7	4-point	240.0	950.0	900.0	2643.8	0.63	425.8	513.1	27.2	cu	30.0	613.4	1757		
31	B8	4-point	240.0	950.0	900.0	2643.8	0.63	421.8	522.4	27.7	cu	30.0	635.0	1785		
32	OA-2	[Bre-1963]	4-point	304.8	561.3	466.1	2209.8	2.27	555.2	957.9	23.7	cyl	19.1	356.3	716	
33	H 50/1	[Cla-2005]	4-point	200.0	400.0	360.0	1042.5	2.23	500.0	0.0	49.9	cyl	12.0	227.9	453	
34	B100	[Col-1999]	4-point	300.0	1000.0	925.0	2662.0	1.01	550.0	0.0	36.0	cyl	10.0	595.8	1496	
35	B100H	4-point	300.0	1000.0	925.0	2662.0	1.01	550.0	0.0	98.0	cyl	10.0	673.5	1727		
36	A-3	[Dia-1960]	4-point	152.4	304.8	254.0	1092.2	0.98	452.4	834.5	19.4	cyl	25.4	252.7	449	
37	F12	4-point	177.8	304.8	268.3	1073.2	2.44	434.5	578.3	20.7	cyl	12.7	-	707		
38	F1	4-point	177.8	304.8	269.9	1079.5	1.19	434.5	578.3	65.5	cyl	12.7	-	564		
39	F2	4-point	177.8	304.8	268.3	1073.2	2.44	434.5	578.3	65.5	cyl	12.7	-	547		
40	F3	4-point	177.8	304.8	269.9	839.8	1.19	434.5	578.3	69.0	cyl	12.7	-	320		
41	L-1	4-point	152.4	304.8	252.5	508.0	3.35	303.4	519.3	21.0	cyl	25.4	-	326		
42	L-2	4-point	152.4	304.8	252.5	762.0	3.33	310.3	519.3	21.5	cyl	25.4	191.4	544		
43	L-2A	4-point	152.4	304.8	252.5	762.0	3.35	282.8	519.3	36.7	cyl	25.4	-	497		
44	L-3	4-point	152.4	304.8	252.5	1016.0	3.35	310.3	519.3	28.0	cyl	25.4	-	648		
45	L-4	4-point	152.4	304.8	252.5	1270.0	3.35	303.4	519.3	25.8	cyl	25.4	-	940		
46	L-5	4-point	152.4	304.8	252.5	1524.0	3.35	331.0	519.3	27.9	cyl	25.4	-	1029		
47	L2R	4-point	152.4	304.8	252.5	723.9	3.35	310.3	519.3	21.5	cyl	25.4	195.7	401		
48	N90 (N)	4-point	400.0	90.0	65.0	162.5	1.92	477.0	670.0	34.2	cyl	20.0	55.9	88		
49	N485 (N)	4-point	400.0	485.0	440.0	1100.0	1.99	385.0	637.0	34.2	cyl	20.0	352.1	516		
50	N485 (S)	4-point	400.0	485.0	440.0	1100.0	1.19	385.0	637.0	34.2	cyl	20.0	357.0	477		
51	N960 (N)	4-point	400.0	960.0	889.0	2222.5	1.97	385.0	637.0	34.2	cyl	20.0	675.5	1449		
52	N960 (S)	4-point	400.0	960.0	889.0	2222.5	1.18	385.0	637.0	34.2	cyl	20.0	626.6	1542		
53	H155 (N)	4-point	400.0	155.0	127.5	318.8	1.96	444.0	667.0	58.6	cyl	10.0	93.2	193		
54	H155 (S)	4-point	400.0	155.0	127.5	318.8	1.18	444.0	667.0	58.6	cyl	10.0	113.9	164		
55	H220 (N)	4-point	400.0	220.0	190.0	475.0	1.97	433.0	686.0	58.6	cyl	10.0	133.7	286		
56	H220 (S)	4-point	400.0	220.0	190.0	475.0	1.18	433.0	686.0	58.6	cyl	10.0	153.9	230		
57	H350 (N)	4-point	400.0	350.0	312.5	781.3	2.00	436.0	675.0	58.6	cyl	10.0	236.9	332		
58	H350 (S)	4-point	400.0	350.0	312.5	781.3	1.20	436.0	675.0	58.6	cyl	10.0	252.8	315		
59	H485 (N)	4-point	400.0	485.0	440.0	1100.0	1.99	385.0	637.0	58.6	cyl	10.0	352.1	516		
60	H485 (S)	4-point	400.0	485.0	440.0	1100.0	1.19	385.0	637.0	58.6	cyl	10.0	357.0	477		
61	H960 (N)	4-point	400.0	960.0	889.0	2222.5	1.97	385.0	637.0	58.6	cyl	10.0	675.5	1449		
62	H960 (S)	4-point	400.0	960.0	889.0	2222.5	1.18	385.0	637.0	58.6	cyl	10.0	626.6	1542		
63	S 1.1	[Gri-1997]	4-point	300.0	200.0	153.0	570.0	1.34	660.0	739.0	90.1	cyl	16.0	141.6	273	
64	S 1.2	4-point	300.0	200.0	152.0	570.0	2.20	517.0	580.0	91.2	cyl	16.0	117.3	293		

Appendix C: Shear database

1	2	3	4	5			8	11	12	13	14	15		16	17		18
				b [mm]	h [mm]	d [mm]						α [mm]	ρ_l [%]		$f_{c,0}$ [N/mm ²]	$f_{c,s}$ [N/mm ²]	
No.	label	reference	type	Geometry								concrete			crack detail		
65	S.1.3	[Gri-1997]	4-point	300.0	200.0	146.0	570.0	4.22	487.0	624.0	613.0	93.7	cyl	16.0	150.7	277	
66	S.2.2		4-point	300.0	400.0	348.0	1230.0	1.88	469.0	570.0	91.3	cyl	16.0	252.1	615		
67	S.2.4		4-point	300.0	400.0	328.0	1230.0	3.75	487.0	624.0	94.1	cyl	16.0	276.7	625		
68	S.3.2		4-point	300.0	800.0	718.0	2630.0	1.72	487.0	624.0	93.7	cyl	16.0	-	1387		
69	S.3.3		4-point	300.0	800.0	746.0	2630.0	0.83	487.0	624.0	94.4	cyl	16.0	-	1063		
70	S.4.1		4-point	300.0	200.0	153.0	570.0	1.34	660.0	739.0	110.9	cyl	16.0	142.9	309		
71	S.4.2		4-point	300.0	200.0	152.0	570.0	2.20	517.0	580.0	110.9	cyl	16.0	114.3	293		
72	S.4.3		4-point	300.0	200.0	146.0	570.0	4.22	487.0	624.0	110.9	cyl	16.0	142.0	208		
73	B91SD1-4-61		[Rei-2012]	4-point	156.0	247.0	193.9	700.0	3.99	494.0	613.0	60.8	cyl	18.0	-	350	
74	B91SD2-4-61			4-point	156.0	248.0	195.0	700.0	3.96	494.0	613.0	60.8	cyl	18.0	-	438	
75	B91SD5-4-58	4-point		156.0	249.0	195.5	700.0	3.95	494.0	613.0	58.3	cyl	18.0	-	429		
76	B91SD6-4-58	4-point		150.0	249.0	195.5	700.0	4.11	494.0	613.0	58.3	cyl	18.0	-	375		
77	G1	4-point		100.0	400.0	370.0	1255.0	1.70	400.0	565.0	30.3	cu	20.0	-	795		
78	G2	4-point		100.0	400.0	372.0	1255.0	1.08	460.0	740.0	23.5	cu	20.0	-	843		
79	G4a	4-point		100.0	400.0	372.0	2195.0	1.08	800.0	888.0	22.0	cu	20.0	-	1520		
80	8A	4-point		152.4	304.8	266.7	660.4	2.49	333.1	0.0	27.7	cyl	0.0	210.4	394		
81	8B	4-point		152.4	304.8	266.7	660.4	2.49	333.1	0.0	37.1	cyl	0.0	238.4	409		
82	8C	4-point		152.4	304.8	266.7	660.4	4.99	333.1	0.0	58.0	cyl	0.0	207.2	374		
83	8D	[Han-1958], [Han-1961]	4-point	152.4	304.8	266.7	660.4	4.99	333.1	0.0	73.7	cyl	0.0	224.5	385		
84	8B4		4-point	152.4	304.8	266.7	1320.8	1.25	610.9	0.0	31.0	cyl	0.0	224.0	721		
85	8B2	4-point	152.4	304.8	266.7	1320.8	2.53	636.5	0.0	30.8	cyl	0.0	223.7	791			
86	8B3	4-point	152.4	304.8	266.7	660.4	1.25	334.1	0.0	30.1	cyl	0.0	212.5	335			
87	84	[Kan-1968]	4-point	151.1	304.8	271.0	1085.1	2.84	342.1	0.0	27.4	cyl	19.1	209.4	706		
88	74		4-point	152.4	609.6	523.2	1630.7	2.84	365.5	0.0	27.2	cyl	19.1	387.2	923		
89	3044		4-point	152.4	1219.2	1097.3	4363.7	2.72	375.9	0.0	29.5	cyl	19.1	-	2842		
90	CTL-2	[Kim-1991]	4-point	170.0	300.0	270.0	810.0	1.87	477.0	0.0	52.0	cyl	25.0	209.8	478		
91	P1.0-2		4-point	170.0	300.0	272.0	816.0	1.01	477.0	0.0	52.0	cyl	25.0	224.9	466		
92	P3.4-2		4-point	170.0	300.0	267.0	801.0	3.35	477.0	0.0	52.0	cyl	25.0	234.9	609		
93	P4.6-2		4-point	170.0	300.0	255.0	765.0	4.68	477.0	0.0	52.0	cyl	25.0	235.5	603		
94	A4.5-2		4-point	170.0	300.0	270.0	1215.0	1.87	477.0	0.0	52.0	cyl	25.0	216.3	440		
95	D50-2		4-point	300.0	620.0	550.0	1650.0	1.88	477.0	0.0	52.0	cyl	25.0	489.7	1038		
96	D915-2		4-point	300.0	1000.0	915.0	2745.0	1.87	477.0	0.0	52.0	cyl	25.0	780.4	1867		
97	II-4A3		4-point	203.2	457.2	390.1	850.9	2.00	364.8	0.0	30.3	cyl	0.0	-	305		
98	5A3		4-point	203.2	457.2	390.1	850.9	3.00	364.8	0.0	29.9	cyl	0.0	-	394		
99	11A2		4-point	152.4	381.0	313.9	850.9	3.31	364.8	0.0	30.2	cyl	0.0	-	203		
100	12A2	4-point	152.4	381.0	237.7	850.9	4.37	364.8	0.0	30.1	cyl	0.0	-	318			
101	III-18A2	4-point	152.4	381.0	316.0	850.9	2.66	370.3	0.0	19.3	cyl	0.0	-	330			
102	18B2	4-point	152.4	381.0	316.0	850.9	2.66	370.3	0.0	19.9	cyl	0.0	-	254			
103	18C2	4-point	152.4	381.0	316.0	850.9	2.66	370.3	0.0	22.6	cyl	0.0	-	546			
104	18D2	4-point	152.4	381.0	316.0	850.9	2.66	370.3	0.0	22.1	cyl	0.0	-	318			
105	IV-13A2	4-point	152.4	381.0	319.0	850.9	0.80	378.6	0.0	19.9	cyl	0.0	-	381			
106	14A2	4-point	152.4	304.8	242.8	850.9	1.05	378.6	0.0	20.7	cyl	0.0	-	343			
107	15A2	4-point	152.4	381.0	316.0	850.9	1.33	370.3	0.0	20.1	cyl	0.0	-	445			
108	15B2	4-point	152.4	381.0	316.0	850.9	1.33	370.3	0.0	20.7	cyl	0.0	-	406			
109	16A2	4-point	152.4	304.8	239.8	850.9	1.75	370.3	0.0	22.2	cyl	0.0	-	279			
110	17A2	4-point	152.4	304.8	242.8	850.9	2.10	378.6	0.0	22.0	cyl	0.0	-	381			
111	18E2	4-point	152.4	381.0	316.0	850.9	2.66	370.3	0.0	19.8	cyl	0.0	-	343			
112	19A2	4-point	152.4	304.8	239.8	850.9	3.51	370.3	0.0	20.6	cyl	0.0	-	419			
113	20A2	4-point	152.4	304.8	237.7	850.9	4.37	364.8	0.0	21.0	cyl	0.0	-	356			
114	21A2	[Kre-1966]	4-point	203.2	304.8	237.7	850.9	4.92	364.8	0.0	19.9	cyl	0.0	-	445		
115	2AC		4-point	152.4	304.8	254.0	1155.7	1.31	393.8	0.0	23.0	cyl	0.0	-	737		
116	3AC		4-point	152.4	304.8	255.5	1155.7	1.99	378.6	0.0	20.8	cyl	0.0	-	267		
117	4AC		4-point	152.4	304.8	254.0	1155.7	2.62	393.8	0.0	16.5	cyl	0.0	-	724		
118	5AC		4-point	152.4	304.8	252.5	1155.7	3.33	370.3	0.0	18.3	cyl	0.0	-	381		
119	6AC		4-point	152.4	304.8	250.4	1155.7	4.15	364.8	0.0	22.8	cyl	0.0	-	343		
120	3CC		4-point	152.4	304.8	255.5	1460.5	1.99	378.6	0.0	20.5	cyl	0.0	-	686		
121	4CC		4-point	152.4	304.8	254.0	1460.5	2.62	393.8	0.0	20.6	cyl	0.0	-	699		
122	5CC		4-point	152.4	304.8	252.5	1460.5	3.33	370.3	0.0	20.3	cyl	0.0	-	330		
123	6CC		4-point	152.4	304.8	250.4	1460.5	4.15	364.8	0.0	20.6	cyl	0.0	-	546		
124	4EC	4-point	152.4	304.8	254.0	1765.3	2.62	393.8	0.0	21.2	cyl	0.0	-	1156			
125	5EC	4-point	152.4	304.8	252.5	1765.3	3.33	370.3	0.0	19.5	cyl	0.0	-	1321			
126	6EC	4-point	152.4	304.8	250.4	1765.3	4.15	364.8	0.0	19.1	cyl	0.0	-	1257			
127	4GC	4-point	152.4	304.8	254.0	2070.1	2.62	393.8	0.0	21.0	cyl	0.0	-	1448			
128	5GC	4-point	152.4	304.8	252.5	2070.1	3.33	370.3	0.0	21.9	cyl	0.0	-	1448			
129	6GC	4-point	152.4	304.8	250.4	2070.1	4.15	364.8	0.0	21.4	cyl	0.0	-	1435			
130	VII-6C	4-point	152.4	304.8	252.5	850.9	3.33	370.3	0.0	20.1	cyl	0.0	-	254			

Appendix C: Shear database

1	2	3	4	5				7	8	11	12	13	14	15		16	17	18
				Geometry										concrete				
No.	label	reference	type	b [mm]	h [mm]	d [mm]	a [mm]	ρ_l [%]	$f_{c,1}$ [N/mm ²]	$f_{c,2}$ [N/mm ²]	$f_{c,3}$ [N/mm ²]	f_c [N/mm ²]	test type	d_{eq} [mm]	h_c [mm]	x_{cr} [mm]		
																	131	VIII-3AAC
132	4AAC	4-point	152.4	304.8	254.0	850.9	2.62	393.8	0.0	29.2	0.0	29.2	cyl	0.0	-	292		
133	5AAC	4-point	152.4	304.8	252.5	850.9	3.33	370.3	0.0	32.8	0.0	32.8	cyl	0.0	-	330		
134	6AAC	4-point	152.4	304.8	250.4	850.9	4.15	364.8	0.0	34.4	0.0	34.4	cyl	0.0	-	330		
135	3AC	4-point	152.4	304.8	255.5	1155.7	1.99	378.6	0.0	31.9	0.0	31.9	cyl	0.0	-	533		
136	4AC	4-point	152.4	304.8	254.0	1155.7	2.62	393.8	0.0	30.5	0.0	30.5	cyl	0.0	-	330		
137	5AC	4-point	152.4	304.8	252.5	1155.7	3.33	370.3	0.0	32.8	0.0	32.8	cyl	0.0	-	305		
138	6AC	4-point	152.4	304.8	250.4	1155.7	4.15	364.8	0.0	34.1	0.0	34.1	cyl	0.0	-	533		
139	4CC	4-point	152.4	304.8	254.0	1460.5	2.62	393.8	0.0	38.4	0.0	38.4	cyl	0.0	-	432		
140	5CC	4-point	152.4	304.8	252.5	1460.5	3.33	370.3	0.0	37.4	0.0	37.4	cyl	0.0	-	838		
141	6CC	4-point	152.4	304.8	250.4	1460.5	4.15	364.8	0.0	38.4	0.0	38.4	cyl	0.0	-	991		
142	5EC	4-point	152.4	304.8	252.5	1765.3	3.33	370.3	0.0	37.4	0.0	37.4	cyl	0.0	-	1384		
143	6EC	4-point	152.4	304.8	250.4	1765.3	4.15	364.8	0.0	33.8	0.0	33.8	cyl	0.0	-	889		
144	IX-3AAC	4-point	152.4	304.8	255.5	850.9	1.99	378.6	0.0	12.6	0.0	12.6	cyl	0.0	-	356		
145	4AAC	4-point	152.4	304.8	254.0	850.9	2.62	393.8	0.0	12.9	0.0	12.9	cyl	0.0	-	483		
146	5AAC	4-point	152.4	304.8	252.5	850.9	3.33	370.3	0.0	15.4	0.0	15.4	cyl	0.0	-	229		
147	6AAC	4-point	152.4	304.8	250.4	850.9	4.15	364.8	0.0	13.4	0.0	13.4	cyl	0.0	-	508		
148	3AC	4-point	152.4	304.8	255.5	1155.7	1.99	378.6	0.0	13.7	0.0	13.7	cyl	0.0	-	724		
149	4AC	4-point	152.4	304.8	254.0	1155.7	2.62	393.8	0.0	12.9	0.0	12.9	cyl	0.0	-	445		
150	5AC	4-point	152.4	304.8	252.5	1155.7	3.33	370.3	0.0	15.4	0.0	15.4	cyl	0.0	-	406		
151	6AC	4-point	152.4	304.8	250.4	1155.7	4.15	364.8	0.0	12.4	0.0	12.4	cyl	0.0	-	800		
152	3CC	4-point	152.4	304.8	255.5	1460.5	1.99	378.6	0.0	12.2	0.0	12.2	cyl	0.0	-	889		
153	4CC	4-point	152.4	304.8	254.0	1460.5	2.62	393.8	0.0	17.1	0.0	17.1	cyl	0.0	-	940		
154	5CC	4-point	152.4	304.8	252.5	1460.5	3.33	370.3	0.0	14.7	0.0	14.7	cyl	0.0	-	330		
155	6CC	4-point	152.4	304.8	250.4	1460.5	4.15	364.8	0.0	13.7	0.0	13.7	cyl	0.0	-	762		
156	X-C	4-point	203.2	533.4	482.6	1460.5	1.55	393.8	0.0	16.8	0.0	16.8	cyl	0.0	-	635		
157	XI-PCA	4-point	152.4	304.8	250.4	1765.3	4.15	364.8	0.0	36.3	0.0	36.3	cyl	0.0	-	1321		
158	PCB	4-point	152.4	304.8	250.4	1765.3	4.15	364.8	0.0	36.3	0.0	36.3	cyl	0.0	-	1321		
159	s-LOCa	4-point	152.4	304.8	254.0	1460.5	2.62	393.8	0.0	35.7	0.0	35.7	cyl	0.0	-	991		
160	Ocb	4-point	152.4	304.8	254.0	1460.5	2.62	393.8	0.0	39.0	0.0	39.0	cyl	0.0	-	1016		
161	s-II-Oca	4-point	254.0	508.0	455.7	1765.3	2.22	370.3	0.0	38.3	0.0	38.3	cyl	0.0	-	800		
162	Ocb	4-point	254.0	508.0	455.7	1765.3	2.22	370.3	0.0	38.3	0.0	38.3	cyl	0.0	-	584		
163	E	[Hol-2014]	4-point	140.0	230.0	200.0	500.0	1.10	491.8	659.2	18.9	cu	30.0	163.0	337			
164	P2	4-point	503.0	162.0	142.0	490.0	0.95	426.7	536.6	12.4	cu	30.0	-	306				
165	3	4-point	190.0	320.0	270.0	540.0	2.07	465.0	549.4	30.4	cyl	30.0	-	350				
166	4l	4-point	190.0	320.0	270.0	670.0	2.07	465.0	549.4	30.4	cyl	30.0	231.7	355				
167	4r	4-point	190.0	320.0	270.0	670.0	2.07	465.0	549.4	30.4	cyl	30.0	225.0	355				
168	5l	4-point	190.0	320.0	270.0	810.0	2.07	465.0	549.4	30.4	cyl	30.0	236.0	355				
169	5r	4-point	190.0	320.0	270.0	810.0	2.07	465.0	549.4	30.4	cyl	30.0	232.8	454				
170	6l	4-point	190.0	320.0	270.0	1100.0	2.07	465.0	549.4	30.4	cyl	30.0	226.3	707				
171	6r	4-point	190.0	320.0	270.0	1100.0	2.07	465.0	549.4	30.4	cyl	30.0	226.3	580				
172	7-1	4-point	190.0	320.0	278.0	1350.0	2.01	465.0	549.4	30.1	cyl	30.0	237.4	856				
173	8-1	4-point	190.0	320.0	278.0	1620.0	2.01	465.0	549.4	33.6	cyl	30.0	203.8	970				
174	EA1	4-point	190.0	320.0	270.0	750.0	1.82	439.8	555.2	20.4	cu	30.0	213.4	414				
175	EA2	4-point	190.0	320.0	270.0	750.0	1.78	429.7	590.7	20.4	cu	30.0	189.6	380				
176	D1/1	4-point	50.0	80.0	70.0	210.0	1.62	451.3	553.3	29.5	cu	15.0	55.4	140				
177	D2/2	4-point	100.0	160.0	140.0	420.0	1.62	426.7	536.6	31.3	cu	15.0	111.8	240				
178	D3/2r	4-point	150.0	240.0	210.0	630.0	1.62	413.0	526.8	33.8	cu	15.0	164.2	346				
179	D4/1	4-point	200.0	320.0	280.0	840.0	1.68	439.5	555.2	34.6	cu	15.0	203.2	380				
180	C1	4-point	100.0	180.0	150.0	450.0	1.33	424.8	529.7	38.3	cu	30.0	122.0	238				
181	C2	4-point	150.0	300.0	300.0	900.0	1.34	424.8	529.7	38.3	cu	30.0	289.8	404				
182	C3	4-point	200.0	500.0	450.0	1350.0	1.34	424.8	529.7	38.3	cu	30.0	359.2	914				
183	C4	4-point	225.0	670.0	600.0	1800.0	1.34	424.8	529.7	38.3	cu	30.0	473.2	1000				
184	E6	4-point	190.0	320.0	270.0	750.0	3.58	425.3	520.7	28.3	cu	30.0	236.8	466				
185	IIIa-17	[Mat-1963]	4-point	203.2	457.2	402.8	1524.0	2.53	506.7	568.0	29.2	cyl	25.4	325.9	896			
186	Vlb-22	4-point	203.2	457.2	402.8	1143.0	0.83	714.4	849.4	25.8	cyl	25.4	323.9	645				
187	B5E B2	[Mor-1956]	4-point	304.8	406.4	368.3	1511.3	1.89	471.0	869.7	14.7	cyl	25.4	279.0	883			
188	AO-15-3c	4-point	152.4	336.6	298.5	1041.4	3.34	413.8	0.0	94.2	cyl	9.5	216.9	409				
189	AO-15-2b	[Mph-1984]	4-point	152.4	336.6	298.5	720.7	3.34	413.8	0.0	71.2	cyl	9.5	216.9	411			
190	BRL100	4-point	300.0	1000.0	925.0	2662.5	0.51	550.0	0.0	94.0	cyl	10.0	626.3	1503				
191	BRH100	4-point	300.0	1000.0	895.0	2662.5	3.14	550.0	0.0	94.0	cyl	10.0	718.1	1670				
192	BN100	4-point	300.0	1000.0	925.0	2662.5	0.76	550.0	0.0	37.0	cyl	10.0	686.4	1504				
193	BH100	4-point	300.0	1000.0	925.0	2662.5	0.76	550.0	0.0	99.0	cyl	10.0	667.9	1444				
194	BN50	4-point	300.0	500.0	450.0	1312.5	0.81	486.2	677.0	37.0	cyl	10.0	381.2	690				
195	BH50	4-point	300.0	500.0	450.0	1312.5	0.81	486.2	677.0	37.0	cyl	10.0	370.0	785				
196	BN25	4-point	300.0	500.0	425.0	663.5	0.89	437.0	643.0	99.0	cyl	10.0	168.1	392				

Appendix C: Shear database

1	2	3	4	5				7	8	11	12	13	14	15		16	17		18
				Geometry										concrete			crack detail		
No.	label	reference	type	b [mm]	h [mm]	d [mm]	a [mm]	ρ_l [%]	f_{yk} [N/mm ²]	f_{yk} [N/mm ²]	f_{ctk} [N/mm ²]	f_{ctk} [N/mm ²]	test type	d_c [mm]	h_c [mm]	x_{cr} [mm]			
197	BH25	[Pod-1998]	4-point	300.0	250.0	225.0	665.5	0.89	437.0	643.0	99.0	cyl	10.0	166.3	249				
198	P 1	[Rei-1990]	4-point	900.0	340.0	313.0	1000.0	1.21	564.1	622.0	23.7	pr	30.0	-	690				
199	1	[Rem-1994]	4-point	150.0	200.0	165.0	381.0	1.87	523.0	0.0	85.1	cyl	16.0	130.9	149				
200	2		4-point	150.0	200.0	165.0	504.9	1.87	523.0	0.0	85.1	cyl	16.0	141.9	320				
201	4		4-point	150.0	200.0	160.0	358.0	4.09	554.0	0.0	84.5	cyl	16.0	145.1	175				
202	5		4-point	150.0	200.0	160.0	489.6	4.09	554.0	0.0	84.5	cyl	16.0	121.3	280				
203	1.2 / 1		[Hol-2014]	4-point	200.0	300.0	260.0	875.0	3.55	550.0	0.0	43.4	cu	0.0	236.3	435			
204	X	[Hol-2014]	4-point	90.0	134.0	111.0	400.0	2.65	480.7	0.0	23.0	cu	30.0	85.0	257				
205	Y		4-point	120.0	229.0	199.0	716.8	2.65	407.1	0.0	23.0	cu	30.0	159.2	313				
206	Z		4-point	180.0	301.0	262.0	947.2	2.64	412.0	0.0	24.2	cu	30.0	217.9	609				
207	A-2		4-point	200.0	400.0	372.0	1116.0	0.81	500.0	0.0	80.6	cyl	16.0	228.9	644				
208	A-3		4-point	200.0	400.0	372.0	1488.0	0.81	500.0	0.0	80.6	cyl	16.0	251.9	1165				
209	B-2	[Hol-2014]	4-point	200.0	400.0	368.0	1104.0	2.00	500.0	0.0	84.5	cyl	16.0	251.7	442				
210	B-3		4-point	200.0	400.0	368.0	1472.0	2.00	500.0	0.0	84.5	cyl	16.0	278.6	526				
211	C-2		4-point	200.0	400.0	366.0	1098.0	3.36	500.0	0.0	83.9	cyl	16.0	273.4	518				
212	C-3		4-point	200.0	400.0	366.0	1464.0	3.36	500.0	0.0	83.9	cyl	16.0	341.8	1039				
213	D-2		4-point	200.0	400.0	362.0	1086.0	1.94	500.0	0.0	96.8	cyl	16.0	232.8	571				
214	D-3	[Rei-2012]	4-point	200.0	400.0	362.0	1448.0	1.94	500.0	0.0	96.8	cyl	16.0	290.0	500				
215	MHB 2.5-0		4-point	125.0	250.0	215.0	526.3	3.77	410.1	0.0	52.0	cyl	19.0	-	285				
216	HB 2.5-0		4-point	125.0	250.0	215.0	526.3	3.77	410.1	0.0	73.0	cyl	13.0	-	297				
217	A2		4-point	200.0	450.0	420.0	1260.0	0.74	440.0	0.0	24.1	pr	16.0	-	751				
218	A3		4-point	200.0	750.0	720.0	2160.0	0.79	440.0	0.0	24.4	pr	16.0	-	1281				
219	YB2000/0	[Rei-2012]	4-point	300.0	2000.0	1890.0	5327.0	0.74	457.0	642.0	33.6	cyl	10.0	-	3013				
220	AW1		4-point	1170.0	590.0	538.0	1773.8	0.79	467.0	637.0	36.9	cyl	10.0	-	607				
221	AW4		4-point	1168.0	590.0	506.0	1773.8	1.69	467.0	637.0	39.9	cyl	10.0	-	590				
222	AW8		4-point	1169.0	591.0	507.0	1812.0	1.69	467.0	637.0	39.4	cyl	10.0	-	649				
223	AX6		4-point	703.0	338.0	288.0	1002.0	1.73	467.0	637.0	41.0	cyl	10.0	-	387				
224	AX7	[Hol-2014]	4-point	704.0	335.0	287.0	1002.0	1.04	413.0	598.0	41.0	cyl	10.0	-	375				
225	AX8		4-point	705.0	339.0	289.0	1002.0	1.72	467.0	637.0	41.0	cyl	10.0	-	732				
226	AY1		4-point	249.0	467.0	434.0	1262.0	0.33	900.0	1100.0	40.7	cyl	10.0	-	814				
227	L-10N1		4-point	300.0	1510.0	1400.0	4012.0	0.83	452.0	0.0	38.4	cyl	9.5	-	2073				
228	L-10N2		4-point	300.0	1510.0	1400.0	4012.0	0.83	452.0	0.0	40.3	cyl	9.5	-	2092				
229	L-10H	4-point	300.0	1510.0	1400.0	4012.0	0.83	452.0	0.0	73.6	cyl	9.5	-	2552					
230	L-20N1	[Hol-2014]	4-point	300.0	1510.0	1400.0	4012.0	0.83	452.0	0.0	31.4	cyl	19.0	-	2270				
231	L-20N2		4-point	300.0	1510.0	1400.0	4012.0	0.83	452.0	0.0	33.2	cyl	19.0	-	1939				
232	L-40N1		4-point	300.0	1510.0	1400.0	4012.0	0.83	452.0	0.0	28.1	cyl	38.0	-	2314				
233	L-40N2		4-point	300.0	1510.0	1400.0	4012.0	0.83	452.0	0.0	28.5	cyl	38.0	-	2342				
234	L-50N1		4-point	300.0	1510.0	1400.0	4012.0	0.83	452.0	0.0	41.0	cyl	51.0	-	2331				
235	L-50N2	4-point	300.0	1510.0	1400.0	4012.0	0.83	452.0	0.0	40.1	cyl	51.0	-	2483					
236	L-50N2R	[Hol-2014]	4-point	300.0	1510.0	1400.0	4012.0	0.83	452.0	0.0	40.1	cyl	51.0	-	1782				
237	S-10N1		4-point	122.0	330.0	280.0	779.5	0.83	494.0	0.0	41.9	cyl	9.5	-	396				
238	S-10N2		4-point	122.0	330.0	280.0	779.5	0.83	494.0	0.0	41.9	cyl	9.5	-	478				
239	S-10H		4-point	122.0	330.0	280.0	779.5	0.83	494.0	0.0	77.3	cyl	9.5	-	489				
240	S-20N1		4-point	122.0	330.0	280.0	779.5	0.83	494.0	0.0	39.2	cyl	19.0	200.6	458				
241	S-20N2	[Rei-2012]	4-point	122.0	330.0	280.0	779.5	0.83	494.0	0.0	38.1	cyl	19.0	-	458				
242	S-40N1		4-point	122.0	330.0	280.0	779.5	0.83	494.0	0.0	29.1	cyl	38.0	-	528				
243	S-40N2		4-point	122.0	330.0	280.0	779.5	0.83	494.0	0.0	29.1	cyl	38.0	217.2	408				
244	S-50N1		4-point	122.0	330.0	280.0	779.5	0.83	494.0	0.0	43.5	cyl	51.0	-	524				
245	S-50N2		4-point	122.0	330.0	280.0	779.5	0.83	494.0	0.0	43.5	cyl	51.0	229.5	486				
246	L-20L	[Rei-2012]	4-point	295.0	1510.0	1450.0	4012.0	0.25	880.0	1150.0	35.4	cyl	19.0	-	2428				
247	L-20LR		4-point	295.0	1510.0	1450.0	4012.0	0.25	880.0	1150.0	35.4	cyl	19.0	-	2396				
248	T1_ohne		4-point	400.0	300.0	248.0	1030.0	0.93	581.0	676.0	25.6	cu	16.0	-	740				
249	T7_70_oben		4-point	400.0	350.0	297.0	1030.0	1.35	580.0	652.0	24.6	cu	16.0	-	496				
250	T9_ohne		4-point	400.0	200.0	167.0	830.0	2.41	632.0	710.0	41.8	cu	16.0	-	470				
251	T13_ohne	[Rei-2012]	4-point	400.0	250.0	217.0	830.0	1.85	632.0	710.0	42.5	cu	16.0	-	500				
252	T10_40_oben		4-point	400.0	250.0	167.0	830.0	2.41	632.0	710.0	41.8	cu	16.0	-	495				
253	SB 2		4-point	150.0	240.0	200.0	781.8	1.19	572.7	645.7	35.1	cyl	16.0	-	305				
254	SB 3		4-point	150.0	345.0	300.0	1175.0	1.18	565.9	643.1	35.1	cyl	16.0	-	830				
255	SB 4		4-point	225.0	495.0	450.0	1768.8	1.20	566.5	646.7	35.1	cyl	16.0	-	965				
256	SB 5	4-point	300.0	647.0	600.0	2362.5	1.20	590.4	680.2	35.1	cyl	16.0	-	980					
257	SB 6	4-point	450.0	950.0	900.0	3550.0	1.20	570.8	673.1	35.1	cyl	16.0	-	1190					
258	1-1-1	[Rei-2012]	4-point	200.0	300.0	260.0	875.0	0.65	550.0	0.0	43.4	cu	16.0	-	435				
259	2-1-1		4-point	200.0	300.0	260.0	875.0	3.55	550.0	0.0	43.4	cu	16.0	-	480				
260	V-S-1		4-point	457.2	406.4	360.4	1181.1	0.96	524.1	627.6	40.9	cyl	19.1	-	650				
261	V-S-2		4-point	457.2	426.7	360.4	1181.1	1.92	524.1	627.6	41.4	cyl	19.1	-	623				
262	V-D-2		4-point	457.2	406.4	360.4	1181.1	0.36	744.8	1000.0	43.7	cyl	19.1	-	596				

Appendix C: Shear database

1	2	3	4	5	6	7	8	11	12	13	14	15	16	17	18	
No.	label	reference	type	Geometry				ρ [%]	$f_{c,y}$ [N/mm ²]	$f_{c,x}$ [N/mm ²]	f_c [N/mm ²]	concrete	test type	d_{eq} [mm]	h_c [mm]	crack detail
				b [mm]	h [mm]	d [mm]	a [mm]									
263	SBB1.1	[Rei-2012]	4-point	104.0	103.0	84.0	235.0	1.63	400.0	0.0	35.6	cyl	10.0	.	131	
264	SBB1.2		4-point	105.0	103.0	84.0	235.0	1.61	400.0	0.0	35.6	cyl	10.0	.	131	
265	SBB1.3		4-point	104.0	103.0	84.0	235.0	1.63	400.0	0.0	35.6	cyl	10.0	.	121	
266	SBB2.1		4-point	106.0	206.0	168.0	482.5	1.59	400.0	0.0	34.3	cyl	10.0	.	224	
267	SBB2.2		4-point	105.0	206.0	168.0	482.5	1.61	400.0	0.0	34.3	cyl	10.0	.	241	
268	SBB2.3		4-point	106.0	204.0	166.0	482.5	1.61	400.0	0.0	34.3	cyl	10.0	.	207	
269	SBB3.1		4-point	105.0	378.0	333.0	977.5	1.55	400.0	0.0	36.1	cyl	10.0	.	592	
270	SBB3.2		4-point	101.0	378.0	333.0	977.5	1.61	400.0	0.0	36.1	cyl	10.0	.	468	
271	SBB3.3		4-point	101.0	378.0	333.0	977.5	1.61	400.0	0.0	36.1	cyl	10.0	.	499	
272	1-1		4-point	304.8	306.3	233.3	679.5	1.20	431.0	669.0	64.0	cyl	9.5	.	330	
273	1-2		4-point	306.3	611.1	531.7	1536.7	1.24	453.1	687.6	64.0	cyl	9.5	.	739	
274	1-3		4-point	304.8	762.0	681.0	1965.3	1.24	473.8	696.6	63.0	cyl	9.5	.	1118	
275	1-4		4-point	306.3	914.4	822.1	2374.9	1.60	475.2	703.4	72.4	cyl	9.5	.	1361	
276	2-1		4-point	203.2	306.3	234.9	679.5	1.24	482.8	737.9	66.4	cyl	9.5	.	366	
277	2-2		4-point	407.9	608.1	527.1	1536.7	1.20	473.8	696.6	62.8	cyl	9.5	.	815	
278	2-3		4-point	508.0	762.0	684.2	1965.3	1.30	473.8	696.6	66.0	cyl	9.5	.	889	
279	2-4		4-point	612.9	914.4	820.3	2374.9	1.60	475.2	703.4	70.6	cyl	9.5	.	1608	
280	70-3.1-1-2P		4-point	500.0	700.0	650.0	1625.0	0.31	560.3	660.0	43.5	cyl	20.0	.	1050	
281	70-4.8-1-2P		4-point	500.0	700.0	650.0	1625.0	0.48	531.7	654.3	43.1	cyl	20.0	.	1000	
282	70-7.6-1-2P		4-point	500.0	700.0	650.0	1625.0	0.76	500.0	0.0	42.7	cyl	20.0	.	1000	
283	V18-0		4-point	228.6	485.8	425.5	1238.3	1.04	551.7	696.6	35.9	cyl	19.1	.	510	
284	III-1		4-point	203.2	485.8	406.4	1181.1	3.07	469.0	0.0	26.7	cyl	19.1	.	665	
285	BG-01		4-point	135.0	500.0	465.0	1550.0	1.00	580.0	0.0	81.0	cyl	10.0	.	800	
286	BG-02		4-point	135.0	500.0	465.0	1550.0	1.00	580.0	0.0	81.0	cyl	10.0	.	900	
287	BL-01		4-point	135.0	500.0	465.0	1550.0	1.00	580.0	0.0	69.2	cyl	10.0	.	990	
288	BL-02		4-point	135.0	500.0	465.0	1550.0	1.00	580.0	0.0	69.2	cyl	10.0	.	800	
289	A0		4-point	200.0	300.0	260.0	720.0	1.47	550.0	640.0	26.0	cyl	32.0	.	440	
290	A0		4-point	140.0	260.0	235.0	846.0	1.38	588.0	0.0	24.9	cyl	0.0	.	457	
291	A0.33		4-point	140.0	260.0	235.0	846.0	1.38	588.0	0.0	22.4	cyl	0.0	.	705	
292	B0.33		4-point	140.0	260.0	235.0	846.0	1.38	588.0	0.0	22.4	cyl	0.0	.	569	
293	VOCC	4-point	200.0	350.0	303.9	1000.0	2.98	620.7	825.9	40.2	cyl	25.0	.	398		
294	VOCCS	4-point	200.0	350.0	303.9	1000.0	2.98	620.7	825.9	46.8	cyl	25.0	.	638		
295	VORCS	4-point	200.0	350.0	303.9	1000.0	2.98	620.7	825.9	41.5	cyl	25.0	.	430		
296	SC70	3-point	250.0	600.0	556.0	3850.0	0.89	713.0	820.0	35.3	cyl	16.0	369.0	2739		
297	SC69	3-point	250.0	600.0	556.0	3150.0	0.89	713.0	820.0	32.9	cyl	16.0	323.0	1080		
298	SC61	3-point	250.0	600.0	556.0	2450.0	0.89	713.0	820.0	35.3	cyl	16.0	80.0	750		
299	SC64	3-point	250.0	600.0	556.0	1750.0	0.89	713.0	820.0	35.6	cyl	16.0	229.0	1079		
300	SC68	3-point	250.0	600.0	556.0	1400.0	0.89	713.0	820.0	32.6	cyl	16.0	29.0	750		
301	SC65	3-point	250.0	600.0	559.0	1750.0	0.54	760.0	920.0	35.5	cyl	16.0	320.0	911		
302	SV1-1	3-point	170.0	450.0	407.0	1500.0	0.74	670.0	800.0	26.3	cu	16.0	272.0	838		
303	SV1-2	3-point	170.0	450.0	407.0	1500.0	0.74	670.0	800.0	25.3	cu	16.0	349.0	700		
304	V0A	3-point	200.0	300.0	262.0	900.0	2.81	557.6	662.8	41.7	cyl	16.0	52.0	505		
305	V0B	3-point	200.0	300.0	262.0	900.0	2.81	557.6	662.8	41.7	cyl	16.0	45.0	517		
306	V0C	3-point	200.0	300.0	262.0	900.0	2.81	557.6	662.8	41.7	cyl	16.0	103.0	313		
307	S5	3-point	120.0	250.0	220.0	550.0	1.93	453.0	698.0	35.0	cyl	0.0	59.0	330		
308	S3	3-point	120.0	250.0	220.0	594.0	1.93	453.0	698.0	35.0	cyl	0.0	50.0	343		

Appendix C: Shear database

C-4 Shear tests on PC members with diagonal cracking load (mPC)

1	3	2	4	4	5	6	7	8	9	10	11	12
No.	reference	label	type	Geometry				prestressing steel				
				b [mm]	h [mm]	d [mm]	α [mm]	A_p [mm ²]	ρ_s [%]	f_{tp} [N/mm ²]	f_p [N/mm ²]	F_p [N/mm ²]
1	[Kar-1969]	A-1	4-point	127	254	178	889	101	0.45	1386	1559	186149
2		A-4	4-point	127	254	178	622	194	0.86	1476	1628	193044
3		A-5	4-point	127	254	178	533	194	0.86	1476	1628	193044
4		A-6	4-point	127	254	178	711	155	0.69	1476	1628	193044
5		A-7	4-point	127	254	178	686	194	0.86	1476	1628	193044
6		A-8	4-point	127	254	178	737	194	0.86	1476	1628	193044
7		A-9	4-point	127	254	178	686	194	0.86	1476	1628	193044
8		A-10	4-point	127	254	178	889	194	0.86	1476	1628	193044
9		A-12	4-point	127	254	178	711	155	0.69	1476	1628	193044
10		B-3	4-point	102	203	152	533	155	1.00	1476	1628	193044
11		B-4	4-point	102	203	152	610	155	1.00	1476	1628	193044
12		B-5	4-point	102	203	152	686	155	1.00	1476	1628	193044
13		B-6	4-point	102	203	152	711	194	1.25	1476	1628	193044
14		B-7	4-point	102	203	152	533	155	1.00	1476	1628	193044
15		B-9	4-point	102	203	152	762	155	1.00	1476	1628	193044
16		B-10	4-point	102	203	152	762	155	1.00	1476	1628	193044
17		A1143	4-point	152	305	209	1321	284	0.89	1434	1655	206897
18	A1151	4-point	152	305	214	1321	161	0.49	1503	1710	206897	
19	A1153	4-point	152	305	204	1321	241	0.78	1503	1710	206897	
20	A1223	4-point	155	305	237	914	161	0.44	1503	1710	206897	
21	A1231	4-point	152	305	219	914	201	0.60	1503	1710	206897	
22	A1234	4-point	152	305	208	914	284	0.89	1434	1655	206897	
23	A1236	4-point	155	305	233	914	150	0.41	1421	1697	206897	
24	A1242	4-point	152	305	211	914	284	0.88	1434	1655	206897	
25	A1246	4-point	152	305	208	914	227	0.72	1434	1655	206897	
26	A1253	4-point	152	305	218	914	201	0.60	1503	1710	206897	
27	A1256	4-point	152	305	218	914	234	0.70	1472	1759	206897	
28	A1439	4-point	152	305	212	610	141	0.44	1503	1710	206897	
29	A1444	4-point	152	305	216	610	161	0.49	1503	1710	206897	
30	A1455	4-point	152	305	217	610	201	0.61	1503	1710	206897	
31	A2129	4-point	152	305	215	1321	101	0.31	1503	1710	206897	
32	A2139	4-point	152	305	227	1321	141	0.41	1503	1710	206897	
33	A2151	4-point	152	305	206	1321	301	0.96	1503	1710	206897	
34	A2220	4-point	152	305	215	914	114	0.35	1434	1655	206897	
35	A2224	4-point	152	305	224	914	95	0.28	1434	1655	206897	
36	A2227	4-point	152	305	213	914	114	0.35	1434	1655	206897	
37	A2228	4-point	155	305	222	914	114	0.33	1434	1655	206897	
38	A2231	4-point	152	305	205	914	114	0.36	1434	1655	206897	
39	A2234	4-point	152	305	212	914	151	0.47	1434	1655	206897	
40	A2236	4-point	152	305	212	914	114	0.35	1434	1655	206897	
41	A2239	4-point	152	305	224	914	114	0.33	1434	1655	206897	
42	A2240	4-point	152	305	208	914	246	0.77	1434	1655	206897	
43	A2249	4-point	152	305	208	914	246	0.77	1434	1655	206897	
44	A3222	4-point	152	305	238	914	114	0.31	1434	1655	206897	
45	A3227	4-point	152	305	233	914	114	0.32	1434	1655	206897	
46	A3237	4-point	152	305	208	914	246	0.77	1434	1655	206897	
47	A3249	4-point	152	305	208	914	246	0.77	1434	1655	206897	

Appendix C: Shear database

13	14	15	16	17	18	19	20
concrete				Prestressing		diagonal cracking and failure state	
f_c [N/mm ²]	test type	d_g [mm]	type	P [kN]	V_G [kN]	V_o [kN]	def. V_G
35.9	cyl	19.05	Post	80.06	22.68	27.08	applied shear load at diagonal cracking
28.8	cyl	19.05	Post	82.69	40.89	55.56	
34.5	cyl	19.05	Post	104.79	52.20	69.30	
28.0	cyl	19.05	Post	48.93	25.20	38.90	
30.2	cyl	19.05	Post	82.60	34.99	45.76	
34.1	cyl	19.05	Post	125.88	39.87	43.79	
33.8	cyl	19.05	Post	145.76	47.24	54.61	
31.8	cyl	19.05	Post	145.76	34.91	40.78	
34.9	cyl	19.05	Post	102.75	37.43	44.28	
29.2	cyl	19.05	Post	48.93	24.91	28.83	
32.0	cyl	19.05	Post	48.31	19.99	29.29	
28.0	cyl	19.05	Post	41.19	18.02	25.85	
30.2	cyl	19.05	Post	59.60	23.39	27.32	
33.2	cyl	19.05	Post	65.47	26.86	38.58	
33.3	cyl	19.05	Post	65.47	19.48	26.33	
35.4	cyl	19.05	Post	82.69	28.78	33.65	
42.9	cyl	38.1	Post	227.03	43.05	54.84	
20.0	cyl	38.1	Post	126.26	29.70	31.60	
30.1	cyl	38.1	Post	206.56	38.60	42.20	
39.0	cyl	38.1	Post	126.37	52.19	60.82	
40.0	cyl	9.525	Pre	157.70	45.50	60.07	
55.1	cyl	38.1	Post	215.28	63.29	74.39	
23.7	cyl	38.1	Post	117.54	47.30	48.90	
43.2	cyl	38.1	Post	202.37	61.07	70.03	
32.1	cyl	38.1	Post	205.73	52.17	63.14	
23.4	cyl	9.525	Pre	149.81	41.05	54.75	
26.1	cyl	9.525	Pre	194.03	49.95	59.71	
23.1	cyl	38.1	Post	113.45	63.12	65.23	
23.1	cyl	38.1	Post	130.69	62.01	71.97	
22.9	cyl	38.1	Post	161.85	74.24	81.47	
23.1	cyl	38.1	Post	42.40	16.36	18.58	
21.6	cyl	38.1	Post	57.11	18.58	24.95	
38.8	cyl	38.1	Post	122.76	31.93	38.93	
36.9	cyl	38.1	Post	47.91	27.71	33.20	
23.9	cyl	38.1	Post	38.51	23.26	32.24	
26.6	cyl	38.1	Post	46.97	27.71	31.84	
24.0	cyl	38.1	Post	38.59	25.50	29.68	
24.3	cyl	38.1	Post	69.99	26.15	34.18	
28.6	cyl	38.1	Post	61.41	29.93	31.60	
19.9	cyl	38.1	Post	68.89	27.71	33.71	
17.8	cyl	38.1	Post	28.26	23.26	24.82	
39.9	cyl	38.1	Post	122.02	47.72	59.71	
32.8	cyl	38.1	Post	96.26	36.60	52.02	
29.6	cyl	38.1	Post	18.79	27.71	32.24	
19.3	cyl	38.1	Post	7.83	27.71	28.77	
42.2	cyl	38.1	Post	8.47	24.59	39.96	
32.8	cyl	38.1	Post	57.62	29.04	47.50	

Appendix C: Shear database

C-5 Shear tests on RC members under cyclic loading (cRC)

1	3	2	4	4	5	6	7	8	9	10	11	12
No.	reference	label	type	Geometry				Longitudinal reinforcement	ϕ_s [mm]	ρ [%]	f_{cy} [N/mm ²]	f_{ts} [N/mm ²]
				b [mm]	h [mm]	d [mm]	a [mm]					
1		1-5	4-point	101.6	152.4	136.7	482.6	401.38	16	2.89	327.6	500
2		2-5	4-point	101.6	152.4	136.7	482.6	401.38	16	2.89	327.6	500
3		3-5	4-point	101.6	152.4	136.7	482.6	401.38	16	2.89	327.6	500
4		4-3	4-point	101.6	152.4	136.7	482.6	258.33	12	1.86	327.6	500
5		4-8	4-point	101.6	152.4	136.7	482.6	258.33	12	1.86	327.6	500
6		4-9	4-point	101.6	152.4	136.7	482.6	258.33	12	1.86	327.6	500
7		4-11	4-point	101.6	152.4	136.7	482.6	258.33	12	1.86	327.6	500
8		4-12	4-point	101.6	152.4	136.7	482.6	258.33	12	1.86	327.6	500
9		4-14	4-point	101.6	152.4	136.7	482.6	258.33	12	1.86	327.6	500
10		4-19	4-point	101.6	152.4	136.7	482.6	258.33	12	1.86	327.6	500
11		4-24	4-point	101.6	152.4	136.7	482.6	258.33	12	1.86	327.6	500
12		4-25	4-point	101.6	152.4	136.7	482.6	258.33	12	1.86	327.6	500
13		4-26	4-point	101.6	152.4	136.7	482.6	258.33	12	1.86	327.6	500
14		4-27	4-point	101.6	152.4	136.7	482.6	258.33	12	1.86	327.6	500
15		4-28	4-point	101.6	152.4	136.7	482.6	258.33	12	1.86	327.6	500
16		4-29	4-point	101.6	152.4	136.7	482.6	258.33	12	1.86	327.6	500
17		5-4	4-point	101.6	152.4	136.7	482.6	401.38	16	2.89	327.6	500
18		5-5	4-point	101.6	152.4	136.7	482.6	401.38	16	2.89	327.6	500
19		5-6	4-point	101.6	152.4	136.7	482.6	401.38	16	2.89	327.6	500
20		5-8	4-point	101.6	152.4	136.7	482.6	401.38	16	2.89	327.6	500
21		5-11	4-point	101.6	152.4	136.7	482.6	401.38	16	2.89	327.6	500
22		5-13	4-point	101.6	152.4	136.7	482.6	401.38	16	2.89	327.6	500
23		5-14	4-point	101.6	152.4	136.7	482.6	401.38	16	2.89	327.6	500
24		5-15	4-point	101.6	152.4	136.7	482.6	401.38	16	2.89	327.6	500
25		5-16	4-point	101.6	152.4	136.7	482.6	401.38	16	2.89	327.6	500
26		5-17	4-point	101.6	152.4	136.7	482.6	401.38	16	2.89	327.6	500
27		VA1	4-point	300.0	300.0	260.0	1354.0	1884.96	20	2.42	327.6	500
28		VB1	4-point	300.0	300.0	260.0	1354.0	480.66	16-10	0.62	327.6	500
29		VB2	4-point	300.0	300.0	260.0	1354.0	480.66	16-10	0.62	327.6	500
30		V3	3-point	200.0	340.0	300.0	1500.0	942.48	20	1.57	327.6	500
31		V4	3-point	200.0	340.0	300.0	1500.0	942.48	20	1.57	327.6	500
32		V5	3-point	200.0	340.0	300.0	1500.0	942.48	20	1.57	327.6	500
33		V6	3-point	200.0	340.0	300.0	1500.0	942.48	20	1.57	327.6	500
34		V7b	3-point	200.0	340.0	300.0	1500.0	942.48	20	1.57	327.6	500
35		V8	3-point	200.0	340.0	300.0	1500.0	942.48	20	1.57	327.6	500
36		V13	3-point	200.0	340.0	300.0	1500.0	942.48	20	1.57	327.6	500
37		V14b	3-point	200.0	340.0	300.0	1500.0	942.48	20	1.57	327.6	500
38		V15a	3-point	200.0	340.0	300.0	1500.0	942.48	20	1.57	327.6	500
39		V18	3-point	200.0	340.0	300.0	1500.0	942.48	20	1.57	327.6	500

Appendix C: Shear database

13	14	15	16	17	18	19	20
concrete			V_{in} [kN]	cyclic loading			failure mode
f_c [N/mm ²]	test type	d_g [mm]		V_{sup} [kN]	N_c [-]	N_r [-]	
19.90	cyl	25.4	0.50	12.25	63400	1027200	concrete
19.70	cyl	25.4	0.50	11.10	976100	976100	concrete
25.00	cyl	25.4	0.50	13.35	418600	467200	concrete
32.00	cyl	25.4	0.50	11.10	519200	2114500	steel reinforcement
27.00	cyl	25.4	0.50	13.35	425000	557000	concrete
27.20	cyl	25.4	0.50	13.35	1500	16800	concrete
29.60	cyl	25.4	0.50	9.50	292800	1902000	concrete
37.30	cyl	25.4	0.50	11.10	5700	1142100	concrete
35.90	cyl	25.4	0.50	12.25	8000	19300	concrete
31.70	cyl	25.4	0.50	10.95	6690200	6690200	concrete
29.50	cyl	25.4	0.50	12.25	135100	4822400	concrete
35.30	cyl	25.4	0.50	12.70	1000	1097300	concrete
37.40	cyl	25.4	0.50	12.25	97500	1493600	steel reinforcement
37.00	cyl	25.4	0.50	12.80	700	1250400	concrete
37.00	cyl	25.4	0.50	13.90	500	578800	concrete
32.20	cyl	25.4	0.50	13.35	1207600	1207600	concrete
34.70	cyl	25.4	0.50	17.80	1700	1700	concrete
34.50	cyl	25.4	0.50	16.45	1300	402900	concrete
24.80	cyl	25.4	0.50	14.45	71200	15871700	concrete
30.60	cyl	25.4	0.50	15.55	202800	11217700	concrete
36.80	cyl	25.4	0.50	13.35	39800	39800	concrete
33.20	cyl	25.4	0.50	13.35	1133100	3666500	concrete
27.60	cyl	25.4	0.50	15.55	13000	13000	concrete
35.80	cyl	25.4	0.50	13.35	239000	239000	concrete
26.60	cyl	25.4	0.50	14.45	2100	4300	concrete
41.90	cyl	25.4	0.50	14.45	87800	87800	concrete
41.90	cyl	20	25.00	60.00	50000	56596	concrete
42.00	cyl	16	2.50	25.00	128000	166684	steel reinforcement
42.00	cyl	16	10.00	25.00	77000	170718	steel reinforcement
42.70	cyl	16	5.00	52.50	73	289	concrete
42.70	cyl	16	5.00	52.50	4500	7290	concrete
39.00	cyl	16	5.00	45.00	140000	153000	concrete
39.00	cyl	16	5.00	42.50	870000	986000	run out
39.00	cyl	16	30.00	60.00	5600	13500	concrete
39.00	cyl	16	30.00	56.25	19900	1000000	run out
39.00	cyl	16	16.40	50.85	379500	1000000	run out
0.00	cyl	16	16.40	54.15	940000	1000000	run out
0.00	cyl	16	24.90	54.15	164000	1000000	run out
0.00	cyl	16	32.80	57.45	307000	1000000	run out

Appendix D: Finite Element Models

The models are generated using parametrized commands in python scripts.

D-1 Input

Sample python code

```
### Shear test Krefeld 20A2 full-model
# Date: 2018-10-22
# Version: 1
# Units mm, N

#-----
# PROJECT INITIALIZATION
#-----
''' do not change!
### generic import of functions '''
import time, os, inspect, math
if "dirPath" in locals(): #if old name of dirPath is in memory it should be deleted.
    del dirPath

''' following line can be (un)commented '''
#dirPath="r"project path" #dirPath=r.....don't forget r before the working dirPath. If not specified it takes the dirPath of the script
location.

''' dictionaries for script, do not change'''
#soilLayer={}
#-----
# MODEL INITIALIZATION
#-----
newProject( "project path", 10000 )
setModelAnalysisAspects( [ "STRUCT" ] )
setModelDimension( "2D" )
setDefaultMeshOrder( "QUADRATIC" )
setDefaultMesherType( "HEXQUAD" )
setDefaultMidSideNodeLocation( "ONSHAP" )
setUnit( "MASS", "T" )
setUnit( "FORCE", "N" )
setUnit( "ANGLE", "DEGREE" )
setUnit( "LENGTH", "MM" )

# Geometry (should be defined)

b = 152.4      # beam width
h = 304.8      # beam height
#l = 3200      # beam length
love = 457.2   # bA beam overstand
llp = 2*127    # 2*aF length of load plate
hlp = 63.5     # height of load plate
lsp = 190.5    # aA length of support plate
hsp = 63.5     # height of support plate
leff = 1828.8  # beam effective length
a = leff/2     # length of shear span
l = leff+2*love # beam total length
d = 237.7     # effective depth
c = h-d       # cover of reinforcement from bar centreline
```


Appendix D: Finite Element Models

Concrete compressive strength (should be provided)

fc = 21.03 # mean value of uniaxial concrete compressive strength in MPA
dg = 30 # max. aggregate size
CGamma = 2.5e-09 # density of concrete T/m³
Cnu = 0. # poisson's ratio concrete

Reinforcement properties (should be provided)

Es = 210000 # E-modulus steel reinforcement
Snu = 0.3 # poissions ratio steel
fsy = 364.83 # yield strength N/mm²
fsu = 512 # ultimate strength N/mm²
tsh = 0.05 # total strain at fsu
psh = tsh-(fsy/Es) # plastic stain hardening
ds = 31.75 # bar diameter mm
As = 1583.46 # total area of reinforcement mm²

Element size

selem = h/20 # element size

#-----
GEOMETRY
#-----

x1 = 0
x2 = love-(lsp/2)
x3 = love
x4 = love+(lsp/2)
x5 = love+a-(llp/2)
x6 = love+a
x7 = love+a+(llp/2)
x8 = love+2*a-(lsp/2)
x9 = love+2*a
x10 = love+2*a+(lsp/2)
x11 = l

shapes

createPolyline("Beam", [[x1, 0, 0],[x2, 0, 0],[x3, 0, 0],[x4, 0, 0],[x5, 0, 0],[x6, 0, 0],[x7, 0, 0],[x8, 0, 0],[x9, 0, 0],[x10, 0, 0],[x11, 0, 0]], False)
extrudeProfile(["Beam"], [0, h, 0])
createPolyline("Support Plate 1", [[x2, 0, 0],[x3, 0, 0],[x4, 0, 0]], False)
extrudeProfile(["Support Plate 1"], [0, -hsp, 0])
createPolyline("Load Plate", [[x5, h, 0],[x6, h, 0],[x7, h, 0]], False)
extrudeProfile(["Load Plate"], [0, hlp, 0])
createPolyline("Support Plate 2", [[x8, 0, 0],[x9, 0, 0],[x10, 0, 0]], False)
extrudeProfile(["Support Plate 2"], [0, -hsp, 0])
createPolyline("Reinforcement", [[x1, c, 0],[x11, c, 0]], False)

#-----
MATERIAL
#-----

material properties calculated with fc

fck = fc-4
Ec = 21500*(fc/10)**(1/3) #according to CEB-fib 90
if fck<= 50:
 fct = 0.3*fck**(2/3)
else:
 fct = 2.12*log(fc, e)
Gf = (73*(fc)**0.18)/1000 #according to model code 2010
Gc = 250*Gf #according to Guideline FE RIJKSWAATERSTAAT

concrete model

Appendix D: Finite Element Models

```
addMaterial( "TSCR", "CONCR", "TSCR", [] )
setParameter( MATERIAL, "TSCR", "LINEAR/ELASTI/YOUNG", Ec )
setParameter( MATERIAL, "TSCR", "LINEAR/ELASTI/POISON", Cnu )
setParameter( MATERIAL, "TSCR", "LINEAR/MASS/DENSIT", CGamma )
setParameter( MATERIAL, "TSCR", "MODTYP/TOTCRK", "ROTATE" )
setParameter( MATERIAL, "TSCR", "TENSIL/TENCRV", "EXPONE" )
setParameter( MATERIAL, "TSCR", "TENSIL/TENCRV", "HORDYK" )
setParameter( MATERIAL, "TSCR", "TENSIL/TENSTR", fct )
setParameter( MATERIAL, "TSCR", "TENSIL/GF1", Gf )
#setParameter( MATERIAL, "TSCR", "TENSIL/POISRE/POIRED", "DAMAGE" )
setParameter( MATERIAL, "TSCR", "COMPRS/COMCRV", "PARABO" )
setParameter( MATERIAL, "TSCR", "COMPRS/COMSTR", fc )
setParameter( MATERIAL, "TSCR", "COMPRS/GC", Gc )
setParameter( MATERIAL, "TSCR", "COMPRS/REDUCT/REDCRV", "VC1993" )
setParameter( MATERIAL, "TSCR", "COMPRS/REDUCT/REDMIN", 0.6 )
#setParameter( MATERIAL, "TSCR", "COMPRS/CONFIN/CNFCRV", "VECCHI" )      # for prestressed concrete

# reinforcement model

addMaterial( "Embedded", "REINFO", "VMISES", [] )
setParameter( MATERIAL, "Embedded", "LINEAR/ELASTI/YOUNG", Es )
setParameter( MATERIAL, "Embedded", "PLASTI/YLDTYP", "KAPSIG" )
setParameter( MATERIAL, "Embedded", "PLASTI/YLDTYP", "KAPSIG" )
setParameter( MATERIAL, "Embedded", "PLASTI/HARDI2/KAPSIG", [ 0, fsy, psh, fsu ] )

# elastic load plates

addMaterial( "Steel", "MCSTEL", "ISOTRO", [] )
setParameter( MATERIAL, "Steel", "LINEAR/ELASTI/YOUNG", Es )
setParameter( MATERIAL, "Steel", "LINEAR/ELASTI/POISON", Snu )

#-----
# ASSIGN MATERIAL PROPERTIES
#-----

# BEAM

addGeometry( "Beam", "SHEET", "MEMBRA", [] )
setParameter( GEOMET, "Beam", "THICK", b )
setParameter( GEOMET, "Beam", "LOCAXS", True )
addElementData( "Beam" )
setElementClassType( SHAPE, [ "Beam" ], "MEMBRA" )
assignMaterial( "TSCR", SHAPE, [ "Beam" ] )
assignGeometry( "Beam", SHAPE, [ "Beam" ] )
assignElementData( "Beam", SHAPE, [ "Beam" ] )
setParameter( DATA, "Beam", "INTEGR", "HIGH" )

# PLATE

addGeometry( "Plate", "SHEET", "MEMBRA", [] )
setParameter( GEOMET, "Plate", "THICK", b )
addElementData( "Plate" )
setElementClassType( SHAPE, [ "Support Plate 1", "Load Plate", "Support Plate 2"], "MEMBRA" )
assignMaterial( "Steel", SHAPE, [ "Support Plate 1", "Load Plate", "Support Plate 2" ] )
assignGeometry( "Plate", SHAPE, [ "Support Plate 1", "Load Plate", "Support Plate 2" ] )
assignElementData( "Plate", SHAPE, [ "Support Plate 1", "Load Plate", "Support Plate 2" ] )
setParameter( DATA, "Plate", "INTEGR", "HIGH" )

# REINFORCEMENT

setReinforcementAspects( [ "Reinforcement" ] )
assignMaterial( "Embedded", SHAPE, [ "Reinforcement" ] ) # Material should be called embedded
addGeometry( "Reinforcement", "RELINE", "REBAR", [] )
```

```

setParameter( GEOMET, "Reinforcement", "REIEMB/CROSSE", As ) # As is the total cross section
assignGeometry( "Reinforcement", SHAPE, [ "Reinforcement" ] )
addElementData( "Reinforcement" )
assignElementData( "Reinforcement", SHAPE, [ "Reinforcement" ] )
setReinforcementDiscretization( [ "Reinforcement" ], "ELEMENT" )

#-----
# DEFINE BOUNDARY/LOADING CONDITION
#-----

createPointSupport( "Support", "Support" )
setParameter( GEOMETRY SUPPORT, "Support", "AXES", [ 1, 2 ] )
setParameter( GEOMETRY SUPPORT, "Support", "TRANSL", [ 0, 1, 0 ] )
setParameter( GEOMETRY SUPPORT, "Support", "ROTATI", [ 0, 0, 0 ] )
attach( GEOMETRY SUPPORT, "Support", "Support Plate 1", [ [ x3, -hsp, 0 ] ] )
attach( GEOMETRY SUPPORT, "Support", "Support Plate 2", [ [ x9, -hsp, 0 ] ] )

createPointSupport( "x", "Support" )
setParameter( GEOMETRY SUPPORT, "x", "AXES", [ 1, 2 ] )
setParameter( GEOMETRY SUPPORT, "x", "TRANSL", [ 1, 0, 0 ] )
setParameter( GEOMETRY SUPPORT, "x", "ROTATI", [ 0, 0, 0 ] )
attach( GEOMETRY SUPPORT, "x", "Support Plate 1", [ [ x3, -hsp, 0 ] ] )

createPointSupport( "loading point", "loading point" )
setParameter( GEOMETRY SUPPORT, "loading point", "AXES", [ 1, 2 ] )
setParameter( GEOMETRY SUPPORT, "loading point", "TRANSL", [ 0, 1, 0 ] )
setParameter( GEOMETRY SUPPORT, "loading point", "ROTATI", [ 0, 0, 0 ] )
attach( GEOMETRY SUPPORT, "loading point", "Load Plate", [ [ x6, hlp+h, 0 ] ] )

createPointLoad( "Load", "Load" )
setParameter( GEOMETRY LOAD, "Load", "LODTYP", "DEFORM" )
setParameter( GEOMETRY LOAD, "Load", "DEFORM/TR/VALUE", -0.1 )
setParameter( GEOMETRY LOAD, "Load", "DEFORM/TR/DIRECT", 2 )
attach( GEOMETRY LOAD, "Load", "Load Plate", [ [ x6, hlp+h, 0 ] ] )
a

#-----
# MESH PROPERTIES
#-----

setElementSize( [ "Beam", "Load Plate", "Support Plate 1", "Support Plate 2" ], selem, -1, True )
setMesherType( [ "Beam", "Load Plate", "Support Plate 1", "Support Plate 2" ], "HEXQUAD" )
setMidSideNodeLocation( [ "Beam", "Load Plate", "Support Plate 1", "Support Plate 2" ], "ONSHAP" )
saveProject( )
generateMesh( [ ] )

#-----
# ANALYSIS PROPERTIES
#-----

addAnalysis( "Analysis1" )
addAnalysisCommand( "Analysis1", "NONLIN", "Structural nonlinear" )
setAnalysisCommandDetail( "Analysis1", "Structural nonlinear", "TYPE/PHYSIC/CRACKI/TOLDIR, 10 ) # crack rotation with a
threshold angle of 10°
#
#incremental setting
#
addAnalysisCommandDetail( "Analysis1", "Structural nonlinear", "EXECUT(1)/LOAD/LOADNR" )
setAnalysisCommandDetail( "Analysis1", "Structural nonlinear", "EXECUT(1)/LOAD/LOADNR", 1 )
setAnalysisCommandDetail( "Analysis1", "Structural nonlinear", "EXECUT(1)/LOAD/STEPS/STEPTY", "ENERGY" )
setAnalysisCommandDetail( "Analysis1", "Structural nonlinear", "EXECUT(1)/LOAD/STEPS/ENERGY/INISIZ, 0.9 )
setAnalysisCommandDetail( "Analysis1", "Structural nonlinear", "EXECUT(1)/LOAD/STEPS/ENERGY/MINSIZ, 0.1 )
setAnalysisCommandDetail( "Analysis1", "Structural nonlinear", "EXECUT(1)/LOAD/STEPS/ENERGY/NSTEPS, 500 )

```

Appendix D: Finite Element Models

```
#
#arc-length setting
#
addAnalysisCommandDetail( "Analysis1", "Structural nonlinear", "EXECUT(1)/LOAD/STEPS/ENERGY/ARCLEN/REGULA/SET" )
setAnalysisCommandDetail( "Analysis1", "Structural nonlinear", "EXECUT(1)/LOAD/STEPS/ENERGY/ARCLEN/REG-
ULA/SET(1)/DIRECT", 2 )
addAnalysisCommandDetail( "Analysis1", "Structural nonlinear", "EXECUT(1)/LOAD/STEPS/ENERGY/ARCLEN/REG-
ULA/SET(1)/NODES" )
removeAnalysisCommandDetail( "Analysis1", "Structural nonlinear", "EXECUT(1)/LOAD/STEPS/ENERGY/ARCLEN/REG-
ULA/SET(1)/NODES(2)" )
setAnalysisCommandDetail( "Analysis1", "Structural nonlinear", "EXECUT(1)/LOAD/STEPS/ENERGY/ARCLEN/REG-
ULA/SET(1)/NODES(1)/RNGNRS", "17" )
#
#iteration setting
#
setAnalysisCommandDetail( "Analysis1", "Structural nonlinear", "EXECUT(1)/ITERAT/MAXITE", 50 ) # number of iteration per load
step
#
#convergence setting
#
addAnalysisCommandDetail( "Analysis1", "Structural nonlinear", "EXECUT(1)/ITERAT/CONVER/ENERGY" )
setAnalysisCommandDetail( "Analysis1", "Structural nonlinear", "EXECUT(1)/ITERAT/CONVER/FORCE", True )
setAnalysisCommandDetail( "Analysis1", "Structural nonlinear", "EXECUT(1)/ITERAT/CONVER/ENERGY", True )
setAnalysisCommandDetail( "Analysis1", "Structural nonlinear", "EXECUT(1)/ITERAT/CONVER/DISPLA", False )
setAnalysisCommandDetail( "Analysis1", "Structural nonlinear", "EXECUT(1)/ITERAT/CONVER/ENERGY/NOCONV", "CONTIN" )
# continue in case of not converging
setAnalysisCommandDetail( "Analysis1", "Structural nonlinear", "EXECUT(1)/ITERAT/CONVER/ENERGY/TOLCON", 0.001 )
setAnalysisCommandDetail( "Analysis1", "Structural nonlinear", "EXECUT(1)/ITERAT/CONVER/FORCE/NOCONV", "CONTIN" )
# continue in case of not converging
setAnalysisCommandDetail( "Analysis1", "Structural nonlinear", "EXECUT(1)/ITERAT/CONVER/FORCE/TOLCON", 0.01 )

#-----
# OUTPUT
#-----
#
setAnalysisCommandDetail( "Analysis1", "Structural nonlinear", "EXECUT(1)/ITERAT/LINESE", True ) # output
setAnalysisCommandDetail( "Analysis1", "Structural nonlinear", "OUTPUT(1)/SELTYP", "USER" )
addAnalysisCommandDetail( "Analysis1", "Structural nonlinear", "OUTPUT(1)/USER" )
addAnalysisCommandDetail( "Analysis1", "Structural nonlinear", "OUTPUT(1)/USER/STRAIN(1)/TOTAL" )
addAnalysisCommandDetail( "Analysis1", "Structural nonlinear", "OUTPUT(1)/USER/STRAIN(2)/TOTAL/GREEN/PRINCI" )
addAnalysisCommandDetail( "Analysis1", "Structural nonlinear", "OUTPUT(1)/USER/STRAIN(3)/CRACK/GREEN" )
addAnalysisCommandDetail( "Analysis1", "Structural nonlinear", "OUTPUT(1)/USER/STRAIN(4)/CRKWDT" )
setAnalysisCommandDetail( "Analysis1", "Structural nonlinear", "OUTPUT(1)/USER/STRAIN(4)/CRK-
WDT/GREEN/GLOBAL/LOCATI", "INTPNT" )
setAnalysisCommandDetail( "Analysis1", "Structural nonlinear", "OUTPUT(1)/USER/STRAIN(2)/TO-
TAL/GREEN/PRINCI/LOCATI", "INTPNT" )
setAnalysisCommandDetail( "Analysis1", "Structural nonlinear", "OUTPUT(1)/USER/STRAIN(1)/TO-
TAL/GREEN/GLOBAL/LOCATI", "INTPNT" )
addAnalysisCommandDetail( "Analysis1", "Structural nonlinear", "OUTPUT(1)/USER/STRESS(1)/TOTAL/CAUCHY" )
addAnalysisCommandDetail( "Analysis1", "Structural nonlinear", "OUTPUT(1)/USER/STRESS(2)/TOTAL/CAUCHY/PRINCI" )
addAnalysisCommandDetail( "Analysis1", "Structural nonlinear", "OUTPUT(1)/USER/STRESS(3)/CRACK/CAUCHY" )
setAnalysisCommandDetail( "Analysis1", "Structural nonlinear", "OUTPUT(1)/USER/STRESS(1)/TOTAL/CAU-
CHY/GLOBAL/LOCATI", "INTPNT" )
setAnalysisCommandDetail( "Analysis1", "Structural nonlinear", "OUTPUT(1)/USER/STRESS(2)/TOTAL/CAU-
CHY/PRINCI/LOCATI", "INTPNT" )
addAnalysisCommandDetail( "Analysis1", "Structural nonlinear", "OUTPUT(1)/USER/DISPLA(1)/TOTAL" )
addAnalysisCommandDetail( "Analysis1", "Structural nonlinear", "OUTPUT(1)/USER/FORCE(1)/REACTI" )

#-----
# EXECUTE MODEL
#-----
#
runSolver( "Analysis1" )
```

D-2 Results of benchmark models

Numerical results

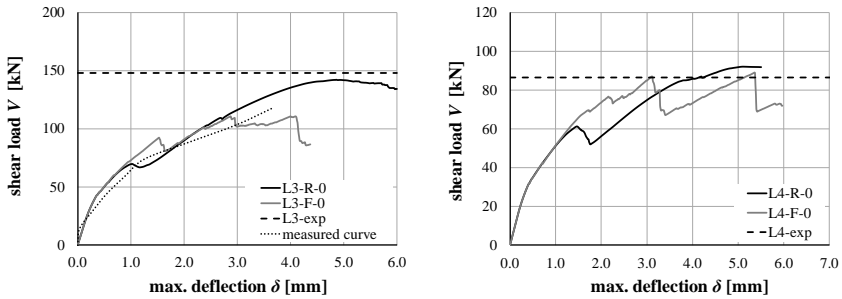


Figure D-1: Shear load –deflection curves of beams L3 and L4 for the model with the rotating crack model, the fixed crack model and the experimental measured curve (only available for L3)

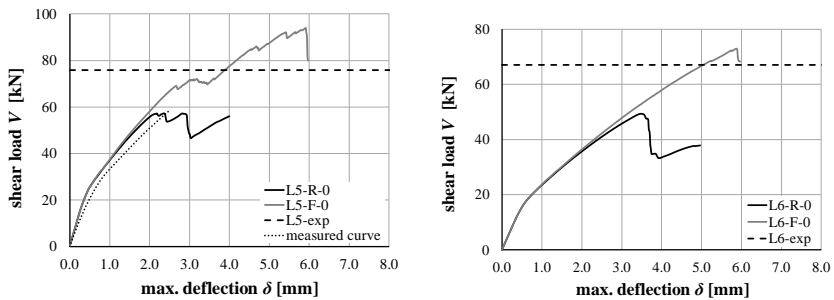


Figure D-2: Shear load –deflection curves of beams L5 and L6 for the model with the rotating crack model, the fixed crack model and the experimental measured curve (only available for L5)

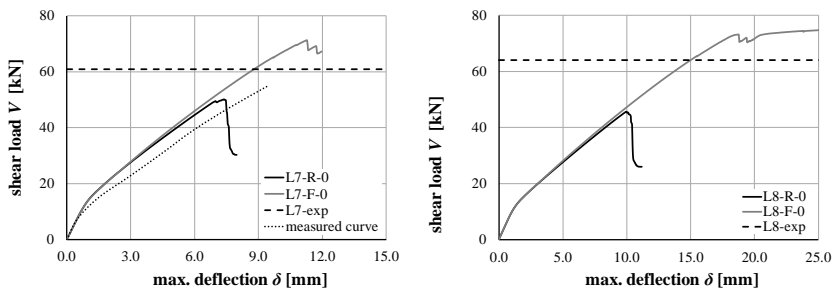


Figure D-3: Shear load –deflection curves of beams L7 and L8 for the model with the rotating crack model, the fixed crack model and the experimental measured curve (only available for L7)

Crack patterns of models with the rotating crack model (R)

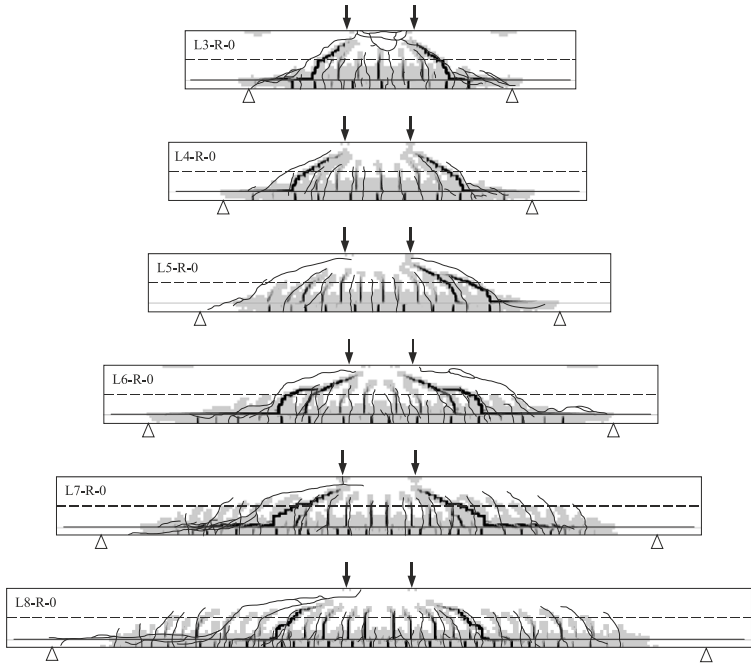


Figure D-4: Crack pattern of beams L3 to L8 modelled with the rotating crack model

Crack patterns of models with the fixed crack model (F)

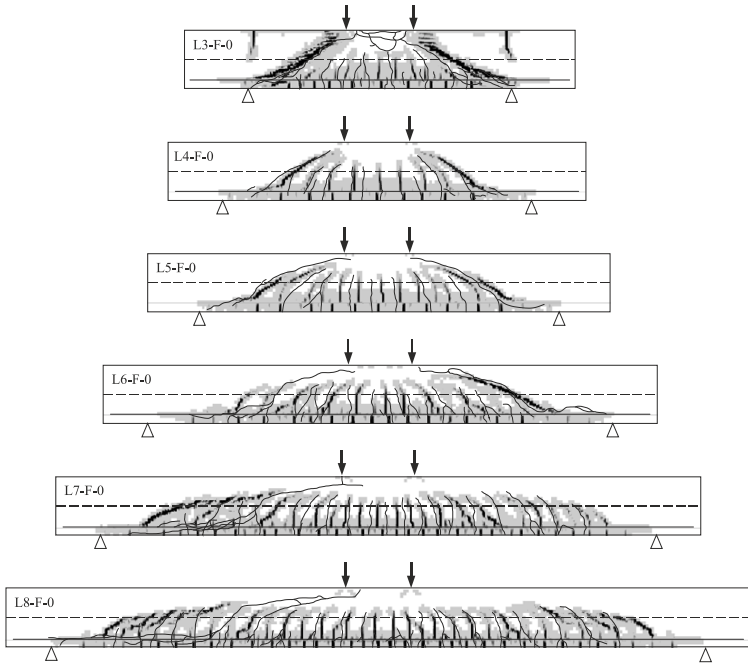


Figure D-4: Crack pattern of beams L3 to L8 modelled with the fixed crack model

Appendix D: Finite Element Models

D-3 Results of mRC beams

1	2	3	4	6					11	12	13	14	15
				Geometry									
No.	label	reference	type	b [mm]	h [mm]	d [mm]	a [mm]	ρ [%]	f_{sy} [N/mm ²]	f_s [N/mm ²]	f_c [N/mm ²]	d_g [mm]	
1	B1	[Bha-1968]	3-point	240.0	350.0	300.0	881.3	1.26	425.8	513.1	23.2	30.0	
2	B2		3-point	240.0	650.0	600.0	1762.5	1.26	425.8	513.1	29.6	30.0	
3	B3		3-point	240.0	950.0	900.0	2643.8	1.26	425.8	513.1	27.5	30.0	
4	B4		3-point	240.0	1250.0	1200.0	3525.0	1.26	425.8	513.1	25.2	30.0	
5	B5		3-point	240.0	650.0	600.0	1762.5	0.63	425.8	513.1	26.6	30.0	
6	B6		3-point	240.0	650.0	600.0	1762.5	0.63	421.8	522.4	24.7	30.0	
7	B7		3-point	240.0	950.0	900.0	2643.8	0.63	425.8	513.1	27.2	30.0	
9	B8		3-point	240.0	950.0	900.0	2643.8	0.63	421.8	522.4	27.7	30.0	
10	Bre-1		[Bre-1963]	4-point	304.8	561.3	466.1	2209.8	2.27	555.2	957.9	23.7	19.1
11	D-1	[Dia-1960]	3-point	152.4	304.8	254.0	1092.2	0.98	452.4	834.5	19.4	25.4	
12	K1-II-4A3	[Kre-1966]	3-point	203.2	457.2	390.1	850.9	2.00	364.8	512.0	30.3	16.0	
13	K2-5A3		3-point	203.2	457.2	390.1	850.9	3.00	364.8	512.0	29.9	16.0	
14	K3- 11A2		3-point	152.4	381.0	313.9	850.9	3.31	364.8	512.0	30.2	16.0	
15	K4- 12A2		3-point	152.4	304.8	237.7	850.9	4.37	364.8	512.0	30.1	16.0	
16	K5- III-18A2		3-point	152.4	381.0	316.0	850.9	2.66	370.3	512.0	19.3	16.0	
17	K6- 18B2		3-point	152.4	381.0	316.0	850.9	2.66	370.3	512.0	19.9	16.0	
18	K7- 18C2		3-point	152.4	381.0	316.0	850.9	2.66	370.3	512.0	22.6	16.0	
19	K8- 18D2		3-point	152.4	381.0	316.0	850.9	2.66	370.3	512.0	22.1	16.0	
20	K9-IV-13A2		3-point	152.4	381.0	319.0	850.9	0.80	378.6	512.0	19.9	16.0	

16	17	18	19	
$V_{Cr,FE}$ [kN]	$x_{Cr,FE}$ [mm]	$V_{d,FE}$ [mm]	numerical re- sults	Crack pattern
63.8	603	63.8		
103.8	1351	103.8		
111.4	2246	111.4		
140.5	2675	140.5		
78.7	1449	78.7		
75.5	1319	81.7		
83.6	2205	83.6		
84.3	2180	84.3		
100.3	1466	100.3		
26.0	864	26.0		
93.7	661	163.1		
99.7	615	184.8		
62.7	601	62.7		
50.8	596	50.8		
49.5	586	67.2		
49.8	586	68.7		
53.8	605	53.8		
53.2	605	53.2		
34.8	624	48.5		

Appendix D: Finite Element Models

1	2	3	4	5	6	7	8	11	12	13	14	15
No.	label	reference	type	Geometry				ρ_l [%]	steel reinforcement		concrete	
				h [mm]	h_f [mm]	d [mm]	e [mm]		f_{ky} [N/mm ²]	f_{sk} [N/mm ²]	f_c [N/mm ²]	d_c [mm]
21	K10-14A2	[Kre-1966]	3-point	152.4	304.8	242.8	850.9	1.05	378.6	512.0	20.7	16.0
22	K11-15A2		3-point	152.4	381.0	316.0	850.9	1.33	370.3	512.0	20.1	16.0
23	K12-15B2		3-point	152.4	381.0	316.0	850.9	1.33	370.3	512.0	20.7	16.0
24	K13-16A2		3-point	152.4	304.8	239.8	850.9	1.75	370.3	512.0	22.2	16.0
25	K14- 17A2		3-point	152.4	304.8	242.8	850.9	2.10	378.6	512.0	22.0	16.0
26	K15-18E2		3-point	152.4	381.0	316.0	850.9	2.66	370.3	512.0	19.8	16.0
27	K16-19A2		3-point	152.4	304.8	239.8	850.9	3.51	370.3	512.0	20.6	16.0
28	K17- 20A2		3-point	152.4	304.8	237.7	850.9	4.37	364.8	512.0	21.0	16.0
29	K18-21A2		3-point	203.2	304.8	237.7	850.9	4.92	364.8	512.0	19.9	16.0
30	K19-2AC		3-point	152.4	304.8	254.0	1155.7	1.31	393.8	512.0	23.0	16.0
31	K20- 3AC		3-point	152.4	304.8	255.5	1155.7	1.99	378.6	512.0	20.8	16.0
32	K21-4AC		3-point	152.4	304.8	254.0	1155.7	2.62	393.8	512.0	16.5	16.0
33	K22- 5AC		3-point	152.4	304.8	252.5	1155.7	3.33	370.3	512.0	18.3	16.0
34	K23- 6AC		3-point	152.4	304.8	250.4	1155.7	4.15	364.8	512.0	22.8	16.0
35	K24- 3CC		3-point	152.4	304.8	255.5	1460.5	1.99	378.6	512.0	20.5	16.0
36	K25-4CC		3-point	152.4	304.8	254.0	1460.5	2.62	393.8	512.0	20.6	16.0
37	K26-5CC		3-point	152.4	304.8	252.5	1460.5	3.33	370.3	512.0	20.3	16.0
38	K27- 6CC		3-point	152.4	304.8	250.4	1460.5	4.15	364.8	512.0	20.6	16.0
39	K28- 4EC		3-point	152.4	304.8	254.0	1765.3	2.62	393.8	512.0	21.2	16.0
40	K29-5EC		3-point	152.4	304.8	252.5	1765.3	3.33	370.3	512.0	19.5	16.0

16	17	18	19
$V_{cr,FE}$ [kN]	$x_{cr,FE}$ [mm]	$V_{u,FE}$ [mm]	numerical results Crack pattern
28.7	411	28.7	
41.8	508	44.5	
41.9	489	59.6	
33.9	564	33.9	
36.8	441	36.8	
49.8	586	68.5	
40.0	572	40.0	
42.8	611	42.8	
57.3	633	57.3	
29.6	808	29.6	
33.5	717	33.5	
33.7	762	33.7	
35.9	732	35.9	
38.7	755	38.7	
27.4	1236	27.4	
35.6	1236	35.6	
35.1	937	35.1	
35.7	1098	35.7	
31.8	1526	31.8	
30.9	1572	30.9	

Appendix D: Finite Element Models

1	2	3	4	5	6	7	8	11	12	13	14	15
No.	label	reference	type	Geometry				ρ_l [%]	steel reinforcement		concrete	
				b [mm]	h [mm]	d [mm]	a [mm]		f_{yk} [N/mm ²]	f_{tk} [N/mm ²]		f_c [N/mm ²]
41	K30- 6EC	[Kre-1966]	3-point	152.4	304.8	250.4	1765.3	4.15	364.8	512.0	19.1	16.0
42	K31- 4GC		3-point	152.4	304.8	254.0	2070.1	2.62	393.8	512.0	21.0	16.0
43	K32-5GC		3-point	152.4	304.8	252.5	2070.1	3.33	370.3	512.0	21.9	16.0
44	K33- 6GC		3-point	152.4	304.8	250.4	2070.1	4.15	364.8	512.0	21.4	16.0
45	K34-VII-6C		3-point	152.4	304.8	252.5	850.9	3.33	370.3	512.0	20.1	16.0
46	K35-VIII- 3AAC		3-point	152.4	304.8	255.5	850.9	1.99	378.6	512.0	34.6	16.0
47	K36- 4AAC		3-point	152.4	304.8	254.0	850.9	2.62	393.8	512.0	29.2	16.0
48	K37-5AAC		3-point	152.4	304.8	252.5	850.9	3.33	370.3	512.0	32.8	16.0
49	K38- 6AAC		3-point	152.4	304.8	250.4	850.9	4.15	364.8	512.0	34.4	16.0
50	K39- 3AC		3-point	152.4	304.8	255.5	1155.7	1.99	378.6	512.0	31.9	16.0
51	K40- 4AC		3-point	152.4	304.8	254.0	1155.7	2.62	393.8	512.0	30.5	16.0
52	K41- 5AC		3-point	152.4	304.8	252.5	1155.7	3.33	370.3	512.0	32.8	16.0
53	K42- 6AC		3-point	152.4	304.8	250.4	1155.7	4.15	364.8	512.0	34.1	16.0
54	K43- 4CC		3-point	152.4	304.8	254.0	1460.5	2.62	393.8	512.0	38.4	16.0
55	K44- 5CC		3-point	152.4	304.8	252.5	1460.5	3.33	370.3	512.0	37.4	16.0
56	K45- 6CC		3-point	152.4	304.8	250.4	1460.5	4.15	364.8	512.0	38.4	16.0
57	K46- 5EC		3-point	152.4	304.8	252.5	1765.3	3.33	370.3	512.0	37.4	16.0
58	K47- 6EC		3-point	152.4	304.8	250.4	1765.3	4.15	364.8	512.0	33.8	16.0
59	K48- IX-3AAC		3-point	152.4	304.8	255.5	850.9	1.99	378.6	512.0	12.6	16.0
60	K49- 4AAC		3-point	152.4	304.8	254.0	850.9	2.62	393.8	512.0	12.9	16.0

16	17	18	19
$V_{cr,FE}$ [kN]	$x_{cr,FE}$ [mm]	$V_{cr,FE}$ [mm]	numerical re- sults Crack pattern
30.9	1143	30.9	
29.4	1533	29.4	
32.2	1525	32.2	
32.3	1678	32.3	
43.9	486	43.9	
42.4	656	42.4	
45.5	457	45.5	
49.5	628	49.5	
55.2	441	55.2	
35.4	730	35.4	
39.7	701	39.7	
42.8	655	42.8	
46.1	701	46.1	
37.4	1037	37.4	
43.4	884	43.4	
44.4	915	44.4	
41.3	959	41.3	
42.3	1281	42.3	
31.7	549	31.7	
33.4	595	33.4	

Appendix D: Finite Element Models

1	2	3	4	5	6	7	8	11	12	13	14	15	
No.	label	reference	type	Geometry				steel reinforcement			concrete		
				b [mm]	h [mm]	d [mm]	a [mm]	ρ [%]	f_{sy} [N/mm ²]	f_{sw} [N/mm ²]	f_c [N/mm ²]	d_c [mm]	
61	K50- 5AAC	[Kre-1966]	3-point	152.4	304.8	252.5	850.9	3.33	370.3	512.0	15.4	16.0	
62	K51- 6AAC		3-point	152.4	304.8	250.4	850.9	4.15	364.8	512.0	13.4	16.0	
63	K52-3AC		3-point	152.4	304.8	255.5	1155.7	1.99	378.6	512.0	13.7	16.0	
64	K53- 4AC		3-point	152.4	304.8	254.0	1155.7	2.62	393.8	512.0	12.9	16.0	
65	K54-5AC		3-point	152.4	304.8	252.5	1155.7	3.33	370.3	512.0	15.4	16.0	
66	K55-6AC		3-point	152.4	304.8	250.4	1155.7	4.15	364.8	512.0	12.4	16.0	
67	K56- 3CC		3-point	152.4	304.8	255.5	1460.5	1.99	378.6	512.0	12.2	16.0	
68	K57-4CC		3-point	152.4	304.8	254.0	1460.5	2.62	393.8	512.0	17.1	16.0	
69	K58-5CC		3-point	152.4	304.8	252.5	1460.5	3.33	370.3	512.0	14.7	16.0	
70	K59- 6CC		3-point	152.4	304.8	250.4	1460.5	4.15	364.8	512.0	13.7	16.0	
71	K60- X-C		3-point	203.2	533.4	482.6	1460.5	1.55	393.8	512.0	16.8	16.0	
72	K61-XI-PCA		3-point	152.4	304.8	250.4	1765.3	4.15	364.8	512.0	36.3	16.0	
73	K62-PCB		3-point	152.4	304.8	250.4	1765.3	4.15	364.8	512.0	36.3	16.0	
74	K63-s-I-OCa		3-point	152.4	304.8	254.0	1460.5	2.62	393.8	512.0	35.7	16.0	
75	K64- OCb		3-point	152.4	304.8	254.0	1460.5	2.62	393.8	512.0	39.0	16.0	
76	K65-s-II- Oca		3-point	254.0	508.0	455.7	1765.3	2.22	370.3	512.0	38.3	16.0	
77	K66- OCb		3-point	254.0	508.0	455.7	1765.3	2.22	370.3	512.0	38.3	16.0	
78	M1- IIIa- 17		[Mat-1963]	4-point	203.2	457.2	402.8	1524.0	2.53	506.7	512.0	29.2	25.4
79	M2- VIB-22			4-point	203.2	457.2	402.8	1143.0	0.83	714.4	780.0	25.8	25.4
80	Mph1-AO-15-3c	[Mph-1984]	3-point	152.4	336.6	298.5	1041.4	3.34	413.8	512.0	94.2	9.5	

16	17	18	19
$V_{u,FE}$ [kN]	$\lambda_{c,FE}$ [mm]	$V_{u,FE}$ [mm]	numerical re- sults Crack pattern
38.6	518	38.6	
38.5	518	38.5	
27.2	855	27.2	
29.2	945	29.2	
34.9	747	34.9	
31.5	762	31.5	
24.4	1175	24.4	
32.2	930	32.2	
30.4	930	30.4	
30.3	945	30.3	
69.0	879	69.0	
41.1	1373	41.1	
41.1	1373	41.1	
43.4	976	44.8	
39.4	1190	39.4	
110.5	1179	110.5	
110.5	1182	110.5	
76.4	1014	76.4	
55.0	836	61.3	
69.3	686	69.3	

Appendix D: Finite Element Models

1	2	3	4	5	6	7	8	11	12	13	14	15
No.	label	reference	type	Geometry				steel reinforcement			concrete	
				b [mm]	h [mm]	d [mm]	a [mm]	ρ [%]	f_{sy} [N/mm ²]	f_s [N/mm ²]	f_c [N/mm ²]	d_c [mm]
81	Mph2-AO-15-2b	[Mph-1984]	3-point	152.4	336.6	298.5	720.7	3.34	413.8	512.0	71.2	9.5
82	SI-S5	[Sko-2014]	4-point	120.0	250.0	220.0	550.0	1.93	453.0	512.0	35.0	16.0
83	SI-S3		4-point	120.0	250.0	220.0	600.0	1.93	453.0	512.0	35.0	16.0

16	17	18	19
$V_{cr,FE}$ [kN]	$\lambda_{cr,FE}$ [mm]	$V_{cr,FE}$ [mm]	numerical results
78.5	585	97.3	Crack pattern
33.8	389	49.0	
32.4	359	32.4	

VERZEICHNIS DER BISHER IN DER SCHRIFTENREIHE DES IBMB ERSCHIENENEN HEFTE (ISSN 1439-3875)

In der Schriftenreihe "Institut für Baustoffe, Massivbau und Brandschutz der Technischen Universität Braunschweig - ISSN 0178-5796 (Heft 1 bis 16 als "Institut für Baustoffkunde und Stahlbetonbau der Technischen Hochschule Braunschweig", Heft 17 bis 39 als "Institut für Baustoffkunde und Stahlbetonbau der Technischen Universität Braunschweig") sind bisher die nachfolgend aufgeführten Hefte erschienen.

Sie können bezogen werden von:

Institut für Baustoffe,
Massivbau und Brandschutz
der Technischen Universität Braunschweig
Bibliothek
Beethovenstraße 52
38106 Braunschweig

Tel. (05 31) 3 91-54 54
Fax (05 31) 3 91-5900
E-Mail o.dienelt@tu-bs.de

oder über jede Buchhandlung.

Kosten:

Je nach Umfang zwischen € 7 und € 30
(zuzüglich Versandkosten)

Das aktuelle Verzeichnis unter:
www.ibmb.tu-bs.de (→ Bibliothek)

Vergriffene Hefte können als Kopien gegen Erstattung der Kopierkosten bezogen werden.

Heft 1:

Deters, R.: Über das Verdunstungsverhalten und den Nachweis öligler Holzschutzmittel. Institut für Baustoffkunde und Stahlbetonbau der Technischen Hochschule Braunschweig, 1962; Zugl.: Dissertation, Technische Hochschule Braunschweig, 1962

Heft 2:

Kordina, K.: Das Verhalten von Stahlbeton- und Spannbetonbauteilen unter Feueranriff. Institut für Baustoffkunde und Stahlbetonbau der Technischen Hochschule Braunschweig, 1963; Sonderdruck aus: Beton 13(1962), S. 11-18, 81-84

Heft 3:

Eibl, J.: Zur Stabilitätsfrage des Zweigelenkbogens mit biegeweichem Zugband und schlaffen Hängestangen. Institut für Baustoffkunde und Stahlbetonbau der Technischen Hochschule Braunschweig, 1963; Zugl.: Dissertation, Technische Hochschule Braunschweig, 1963

Heft 4:

Kordina, K.; Eibl, J.: Ein Verfahren zur Bestimmung des Vorspannverlustes infolge Schlupf in der Verankerung. Zur Frage der Temperaturbeanspruchung von kreiszylindrischen Stahlbetonsilos. Institut für Baustoffkunde und Stahlbetonbau der Technischen Hochschule Braunschweig, 1964; Sonderdruck aus: Beton- und Stahlbetonbau 58(1963), S. 265-268; 59(1964), S. 1-11

Heft 5:

Ertingshausen, H.: Über den Schalungsdruck von Frischbeton. Institut für Baustoffkunde und Stahlbetonbau der Technischen Hochschule Braunschweig, 1965; Zugl.: Dissertation, Technische Hochschule Hannover, 1965

Heft 6:

Waubke, N.V.: Transportphänomene in Betonporen. Institut für Baustoffkunde und Stahlbetonbau der Technischen Hochschule Braunschweig, 1966; Zugl.: Dissertation, Technische Hochschule Braunschweig, 1968

Heft 7:

Ehm, H.: Ein Beitrag zur rechnerischen Bemessung von brandbeanspruchten balkenartigen Stahlbetonbauteilen. Institut für Baustoffkunde und Stahlbetonbau der Technischen Hochschule Braunschweig, 1967; Zugl.: Dissertation, Technische Hochschule Braunschweig, 1967

Heft 8:

Steinert, J.: Möglichkeiten der Bestimmung der kritischen Last von Stab- und Flächentragwerken mit Hilfe ihrer Eigenfrequenz. Institut für Baustoffkunde und Stahlbetonbau der Technischen Hochschule Braunschweig, 1967; Zugl.: Dissertation, Technische Hochschule Braunschweig, 1967

Heft 9:

Lämmke, A.: Untersuchungen an dämmschichtbildenden Feuerschutzmitteln. Institut für Baustoffkunde und Stahlbetonbau der Technischen Hochschule Braunschweig, 1967; Zugl.: Dissertation, Technische Hochschule Braunschweig, 1967

Heft 10:

Rafla, K.: Beitrag zur Frage der Kippstabilität aufgehängter Träger. Institut für Baustoffkunde und Stahlbetonbau der Technischen Hochschule Braunschweig, 1968; Zugl.: Dissertation, Technische Hochschule Braunschweig, 1968

Heft 11:

Iványi, G.: Die Traglast von offenen, kreisförmigen Stahlbetonquerschnitten: Brazier-Effekt. Institut für Baustoffkunde und Stahlbetonbau der Technischen Hochschule Braunschweig, 1968; Zugl.: Dissertation, Technische Hochschule Braunschweig, 1968

Heft 12:

Meyer-Ottens, C.: Brandverhalten verschiedener Bauplatten aus Baustoffen der Klassen A und B. Institut für Baustoffkunde und Stahlbetonbau der Technischen Hochschule Braunschweig, 1969

Heft 13:

Fuchs, G.: Zum Tragverhalten von kreisförmigen Doppelsilos unter Berücksichtigung der Eigensteifigkeit des Füllgutes. Institut für Baustoffkunde und Stahlbetonbau der Technischen Hochschule Braunschweig, 1968; Zugl.: Dissertation, Technische Hochschule Braunschweig, 1968

Heft 14:

Meyer-Ottens, C.: Wände aus Holz und Holzwerkstoffen unter Feuerangriff. Institut für Baustoffkunde und Stahlbetonbau der Technischen Hochschule Braunschweig, 1970; Sonderdruck aus: Mitteilungen der Deutschen Gesellschaft für Holzforschung, H.56(1969)

Heft 15:

Lewandowski, R.: Beurteilung von Bauwerksfestigkeiten anhand von Betongüewürfeln und -bohrproben. Institut für Baustoffkunde und Stahlbetonbau der Technischen Hochschule Braunschweig, 1970; Zugl.: Dissertation, Technische Hochschule Braunschweig, 1970

Heft 16:

Neubauer, F.-J.: Untersuchungen zur Frage der Rissesicherung von leichten Trennwänden aus Gips-Wandbauplatten. Institut für Baustoffkunde und Stahlbetonbau der Technischen Hochschule Braunschweig, 1970; Zugl.: Dissertation, Technische Hochschule Braunschweig, 1969

Heft 17:

Meyer-Ottens, C.; Kordina, K.: Gutachten über das Brandverhalten von Bauteilen aus dampfgehärtetem Gasbeton: aufgestellt für den Fachverband Gasbetonindustrie. Institut für Baustoffkunde und Stahlbetonbau der Technischen Universität Braunschweig, 1970

Heft 17:

Meyer-Ottens, C.; Kordina, K.: Gutachten über das Brandverhalten von Bauteilen aus dampfgehärtetem Gasbeton. Erw. Neuaufl. Institut für Baustoffkunde und Stahlbetonbau der Technischen Universität Braunschweig, 1974

Heft 17:

Meyer-Ottens, C.; Kordina, K.: Gutachten über das Brandverhalten von Bauteilen aus dampfgehärtetem Gasbeton. Erw. Neuaufl. Institut für Baustoffkunde und Stahlbetonbau der Technischen Universität Braunschweig, 1974

Heft 18:

Bödeker, W.: Die Stahlblech-Holz-Nagelverbindung und ihre Anwendung: Grundlagen und Bemessungsvorschläge. Braunschweig. Institut für Baustoffkunde und Stahlbetonbau der Technischen Universität Braunschweig, 1971; Zugl.: Dissertation, Technische Hochschule Braunschweig, 1971, ISBN 3-89288-057-3

Heft 19:

Meyer-Ottens, C.: Bauaufsichtliche Brandschutzvorschriften: Beispiele für ihre Erfüllung bei Wänden, Brandwänden und Decken. Institut für Baustoffkunde und Stahlbetonbau der Technischen Universität Braunschweig, 1971

Heft 20:

Liermann, K.: Das Trag- und Verformungsverhalten von Stahlbetonbrückenpfeilern mit Rollenlagern. Institut für Baustoffkunde und Stahlbetonbau der Technischen Universität Braunschweig, 1972; Zugl.: Dissertation, Technische Universität Braunschweig, 1972, ISBN 3-89288-056-5

Heft 22:

Nürnberg, U.: Zur Frage des Spannungsrißkorrosionsverhaltens kohlenstoffarmer Betonstähle in Nitratlösungen unter Berücksichtigung praxisnaher Verhältnisse. Institut für Baustoffkunde und Stahlbetonbau der Technischen Universität Braunschweig, 1972; Zugl.: Dissertation, Technische Universität Braunschweig, 1972, ISBN 3-89288-054-9

Heft 23:

Meyer-Ottens, C.: Zur Frage der Abplatzungen an Betonbauteilen aus Normalbeton bei Brandbeanspruchung. Institut für Baustoffkunde und Stahlbetonbau der Technischen Universität Braunschweig, 1972; Zugl.: Dissertation, Technische Universität Braunschweig, 1972

Heft 24:

El-Arousy, T.H.: Über die Steinkohlenflugasche und ihre Wirkung auf die Eigenschaften von Leichtbeton mit geschlossenem Gefüge im frischen und festen Zustand. Institut für Baustoffkunde und Stahlbetonbau der Technischen Universität Braunschweig, 1973; Zugl.: Dissertation, Technische Universität Braunschweig, 1973, ISBN 3-89288-053-0

Heft 25:

Rieche, G.: Mechanismen der Spannungs-korrosion von Spannstählen im Hinblick auf ihr Verhalten in Spannbetonkonstruktionen. Institut für Baustoffkunde und Stahlbetonbau der Technischen Universität Braunschweig, 1973; Zugl.: Dissertation, Technische Universität Braunschweig, 1973, ISBN 3-89288-052-2

Heft 26:

Tennstedt, E.: Beitrag zur rechnerischen Ermittlung von Zwangsschnittgrößen unter Berücksichtigung des wirklichen Verformungsverhaltens des Stahlbetons. Institut für Baustoffkunde und Stahlbetonbau der Technischen Universität Braunschweig, 1974; Zugl.: Dissertation, Technische Universität Braunschweig, 1974, ISBN 3-89288-051-4

Heft 27:

Schneider, U.: Zur Kinetik festigkeitsmindernder Reaktionen in Normalbetonen bei hohen Temperaturen. Institut für Baustoffkunde und Stahlbetonbau der Technischen Universität Braunschweig, 1973; Zugl.: Dissertation, Technische Universität Braunschweig, 1973

Heft 28:

Neisecke, J.: Ein dreiparametrisches, komplexes Ultraschall-Prüfverfahren für die zerstörungsfreie Materialprüfung im Bauwesen. Institut für Baustoffkunde und Stahlbetonbau der Technischen Universität Braunschweig, 1974; Zugl.: Dissertation, Technische Universität Braunschweig, 1974, ISBN 3-89288-050-6

Heft 29:

Kordina, K.; Maack, P.; Hjorth, O.: Traglastermittlung an Stahlbeton-Druckgliedern. Schlußbericht (AIF-Nr. 956). Institut für Baustoffkunde und Stahlbetonbau der Technischen Universität Braunschweig, 1974, ISBN 3-89288-048-4

Heft 30:

Eibl, J.; Ivanyi, G.: Berücksichtigung der Torsionssteifigkeit von Randbalken bei Stahlbetondecken. Schlußbericht, Institut für Baustoffkunde und Stahlbetonbau der Technischen Universität Braunschweig, 1974

Heft 31:

Kordina, K.; Janko, B.: Stabilitätsnachweise von Rahmensystemen im Stahlbetonbau. Schlußbericht (AIF-Nr. 1388), Institut für Baustoffkunde und Stahlbetonbau der Technischen Universität Braunschweig, 1974, ISBN 3-89288-049-2

Heft 32:

Hjorth, O.: Ein Beitrag zur Frage der Festigkeiten und des Verbundverhaltens von Stahl und Beton bei hohen Beanspruchungsgeschwindigkeiten. Institut für Baustoffkunde und Stahlbetonbau der Technischen Universität Braunschweig, 1976; Zugl.: Dissertation, Technische Universität Braunschweig, 1975

Heft 33:

Klingsch, W.: Traglastberechnung instationär thermisch belasteter schlanker Stahlbetondruckglieder mittels zwei- und dreidimensionaler Diskretisierung. Institut für Baustoffkunde und Stahlbetonbau der Technischen Universität Braunschweig, 1976; Zugl.: Dissertation, Technische Universität Braunschweig, 1976

Heft 34:

Djamous, F.: Thermische Zerstörung natürlicher Zuschlagstoffe im Beton. Institut für Baustoffkunde und Stahlbetonbau der Technischen Universität Braunschweig, 1977; Zugl.: Dissertation, Technische Universität Braunschweig, 1977

Heft 35:

Haksever, A.: Zur Frage des Trag- und Verformungsverhaltens ebener Stahlbetonrahmen im Brandfall. Braunschweig. Institut für Baustoffkunde und Stahlbetonbau der Technischen Universität Braunschweig, 1977; Zugl.: Dissertation, Technische Universität Braunschweig, 1977

Heft 36:

Storkebaum, K.-H.: Ein Beitrag zur Traglastermittlung von vierseitig gelagerten Stahlbetonwänden. Institut für Baustoffkunde und Stahlbetonbau der Technischen Universität Braunschweig, 1977; Zugl.: Dissertation, Technische Universität Braunschweig, 1977, ISBN 3-89288-045-X

Heft 37:

Bechtold, R.: Zur thermischen Beanspruchung von Außenstützen im Brandfall. Institut für Baustoffkunde und Stahlbetonbau der Technischen Universität Braunschweig, 1977; Zugl.: Dissertation, Technische Universität Braunschweig, 1977, ISBN 3-89288-046-8

Heft 38:

Steinert, J.: Bestimmung der Wasserdurchlässigkeit von Kiesbeton aus dem Wassereindringverhalten. Institut für Baustoffkunde und Stahlbetonbau der Technischen Universität Braunschweig, 1977; Unveränderter Nachdruck der Erstveröffentlichung Bad Honnef, Osang, 1977 (Zivilschutzforschung, Bd. 7)

Heft 39:

Weiß, R.: Ein haufwerkstheoretisches Modell der Restfestigkeit geschädigter Betone. Institut für Baustoffkunde und Stahlbetonbau der Technischen Universität Braunschweig, 1978; Zugl.: Dissertation, Technische Universität Braunschweig, 1978, ISBN 3-89288-047-6

Heft 40:

Alda, W.: Zum Schwingkriechen von Beton. Institut für Baustoffe, Massivbau und Brandschutz der Technischen Universität Braunschweig, 1978; Zugl.: Dissertation, Technische Universität Braunschweig, 1978, ISBN 3-89288-035-2

Heft 41:

Teutsch, M.: Trag- und Verformungsverhalten von Stahlbeton- und Spannbetonbalken mit rechteckigem Querschnitt unter kombinierter Beanspruchung aus Biegung, Querkraft und Torsion. Institut für Baustoffe, Massivbau und Brandschutz der Technischen Universität Braunschweig, 1979; Zugl.: Dissertation, Technische Universität Braunschweig, 1979, ISBN 3-89288-036-0

Heft 42:

Schneider, U.: Ein Beitrag zur Frage des Kriechens und der Relaxation von Beton unter hohen Temperaturen. Institut für Baustoffe, Massivbau und Brandschutz der Technischen Universität Braunschweig, 1979; Zugl.: Dissertation, Technische Universität Braunschweig, 1979

Heft 43:

Institut für Baustoffe, Massivbau und Brandschutz: Veröffentlichungen 1967 bis 1979. Institut für Baustoffe, Massivbau und Brandschutz der Technischen Universität Braunschweig, 1979, ISBN 3-89288-037-9

Heft 44:

Kordina, K.; Fröning, H.: Druckmessungen in Silozellen mit einer neu entwickelten Sonde. Abschlußbericht, Institut für Baustoffe, Massivbau und Brandschutz der Technischen Universität Braunschweig, 1979, ISBN 3-89288-038-7

Heft 45:

Henke, V.: Ein Beitrag zur Zuverlässigkeit frei gelagerter Stahlbetonstützen unter genormter Brandeinwirkung. Institut für Baustoffe, Massivbau und Brandschutz der Technischen Universität Braunschweig, 1980; Zugl.: Dissertation, Technische Universität Braunschweig, 1980

Heft 46:

Schneider, U.; Haksever, A.: Wärmebilanzrechnungen für Brandräume mit unterschiedlichen Randbedingungen (Teil 1). Institut für Baustoffe, Massivbau und Brandschutz der Technischen Universität Braunschweig, 1980

Heft 47:

Walter, R.: Partiiell brandbeanspruchte Stahlbetondecken: Berechnung des inneren Zwanges mit einem Scheibenmodell. Institut für Baustoffe, Massivbau und Brandschutz der Technischen Universität Braunschweig, 1981; Zugl.: Dissertation, Technische Universität Braunschweig, 1981, ISBN 3-89288-039-5

Heft 48:

Svensvik, B.: Zum Verformungsverhalten gerissener Stahlbetonbalken unter Einschluß der Mitwirkung des Betons auf Zug in Abhängigkeit von Last und Zeit. Institut für Baustoffe, Massivbau und Brandschutz der Technischen Universität Braunschweig, 1981; Zugl.: Dissertation, Technische Universität Braunschweig, 1981, ISBN 3-89288-040-9

Heft 49:

Institut für Baustoffe, Massivbau und Brandschutz: Veröffentlichungen 1967 bis 1981. Institut für Baustoffe, Massivbau und Brandschutz der Technischen Universität Braunschweig, 1981, ISBN 3-89288-041-7

Heft 50:

Ojha, S.K.: Die Steifigkeit und das Verformungsverhalten von Stahlbeton- und Spannbetonbalken unter kombinierter Beanspruchung aus Torsion, Biegemoment, Querkraft und Axialkraft. Institut für Baustoffe, Massivbau und Brandschutz der Technischen Universität Braunschweig, 1982, ISBN 3-89288-042-5

Heft 51:

Henke, V.: Zusammenstellung und Anwendung Bayes'scher Verfahren bei der Stichprobenbeurteilung. Projekt D1 des SFB 148. Institut für Baustoffe, Massivbau und Brandschutz der Technischen Universität Braunschweig, 1982, ISBN 3-89288-043-3

Heft 52:

Haksever, A.: Stahlbetonstützen mit Rechteckquerschnitten bei natürlichen Bränden. Institut für Baustoffe, Massivbau und Brandschutz der Technischen Universität Braunschweig, 1982; Zugl.: Habil.-Schr., Technische Universität Istanbul, 1982, ISBN 3-89288-044-1

Heft 53:

Weber, V.: Untersuchung des Riß- und Verformungsverhaltens segmentärer Spannbetonbauteile. Braunschweig. Institut für Baustoffe, Massivbau und Brandschutz der Technischen Universität Braunschweig, 1982; Zugl.: Dissertation, Technische Universität Braunschweig, 1982, ISBN 3-89288-017-4

Heft 54:

Ranisch, E.-H.: Zur Tragfähigkeit von Verklebungen zwischen Baustahl und Beton: geklebte Bewehrung. Unveränderter Nachdruck der Ausgabe 1982. Institut für Baustoffe, Massivbau und Brandschutz der Technischen Universität Braunschweig, 1986; Zugl.: Dissertation, Technische Universität Braunschweig, 1982, ISBN 3-89288-010-7

Heft 55:

Wiedemann, G.: Zum Einfluß tiefer Temperaturen auf Festigkeit und Verformung von Beton. Institut für Baustoffe, Massivbau und Brandschutz der Technischen Universität Braunschweig, 1982; Zugl.: Dissertation, Technische Universität Braunschweig, 1982

Heft 56:

Timm, R.: Ein geometrisch und physikalisch nichtlineares Rechenmodell zur optimalen Biegebemessung ebener Stahlbetonrahmen. Institut für Baustoffe, Massivbau und Brandschutz der Technischen Universität Braunschweig, 1982; Zugl.: Dissertation, Technische Universität Braunschweig, 1982, ISBN 3-89288-018-2

Heft 57:

Diederichs, U.: Untersuchungen über den Verbund zwischen Stahl und Beton bei hohen Temperaturen. Institut für Baustoffe, Massivbau und Brandschutz der Technischen Universität Braunschweig, 1983; Zugl.: Dissertation, Technische Universität Braunschweig, 1983, ISBN 3-89288-019-0

Heft 58:

Schneider, U.: Wärmebilanzrechnungen in Verbindung mit Versuchen in Brandräumen (Teil 2). Institut für Baustoffe, Massivbau und Brandschutz der Technischen Universität Braunschweig, 1983, ISBN 3-89288-020-4

Heft 59:

Dobbernack, R.: Wärmebilanzrechnungen in Brandräumen unter Berücksichtigung der Mehrzonenmodellbildung (Teil 3). Institut für Baustoffe, Massivbau und Brandschutz der Technischen Universität Braunschweig, 1983, ISBN 3-89288-021-2

Heft 60:

Hillger, W.: Verbesserungen und Erweiterungen von Ultraschallprüfverfahren zur zerstörungsfreien Fehlstellen- und Qualitätskontrolle von Betonbauteilen. Institut für Baustoffe, Massivbau und Brandschutz der Technischen Universität Braunschweig, 1983; Zugl.: Dissertation, Technische Universität Braunschweig, 1983, ISBN 3-89288-014-X

Heft 61:

Blume, F.: Zur Wirklichkeitsnähe der Lastannahmen in Silovorschriften für Zellen aus Stahlbeton und Spannbeton. Institut für Baustoffe, Massivbau und Brandschutz der Technischen Universität Braunschweig, 1984; Zugl.: Dissertation, Technische Universität Braunschweig, 1984, ISBN 3-89288-013-1

Heft 62:

Nöling, D.: Das Durchstanzen von Platten aus Stahlbeton : Tragverhalten, Berechnung, Bemessung. Institut für Baustoffe, Massivbau und Brandschutz der Technischen Universität Braunschweig, 1984; Zugl.: Dissertation, Technische Universität Braunschweig, 1984, ISBN 3-89288-012-3

Heft 63:

Wesche, J.: Brandverhalten von Stahlbetonplatten im baupraktischen Einbauzustand. Institut für Baustoffe, Massivbau und Brandschutz der Technischen Universität Braunschweig, 1985; Zugl.: Dissertation, Technische Universität Braunschweig, 1985, ISBN 3-89288-009-3

Heft 64:

Droese, S.: Untersuchungen zur Technologie des Gleitschalungsbau. Institut für Baustoffe, Massivbau und Brandschutz der Technischen Universität Braunschweig, 1985; Zugl.: Dissertation, Technische Universität Braunschweig, 1985, ISBN 3-89288-000-X

Heft 62:

Nöltling, D.: Das Durchstanzen von Platten aus Stahlbeton : Tragverhalten, Berechnung, Bemessung. Institut für Baustoffe, Massivbau und Brandschutz der Technischen Universität Braunschweig, 1984; Zugl.: Dissertation, Technische Universität Braunschweig, 1984, ISBN 3-89288-012-3

Heft 63:

Wesche, J.: Brandverhalten von Stahlbetonplatten im baupraktischen Einbauzustand. Institut für Baustoffe, Massivbau und Brandschutz der Technischen Universität Braunschweig, 1985; Zugl.: Dissertation, Technische Universität Braunschweig, 1985, ISBN 3-89288-009-3

Heft 64:

Droese, S.: Untersuchungen zur Technologie des Gleitschalungsbaus. Institut für Baustoffe, Massivbau und Brandschutz der Technischen Universität Braunschweig, 1985; Zugl.: Dissertation, Technische Universität Braunschweig, 1985, ISBN 3-89288-000-X

Heft 65:

Institut für Baustoffe, Massivbau und Brandschutz: Forschungsarbeiten 1978 - 1983. Institut für Baustoffe, Massivbau und Brandschutz der Technischen Universität Braunschweig, 1984, ISBN 3-89288-001-8

Heft 66:

Hegger, J.: Einfluß der Verbundart auf die Grenztragfähigkeit von Spannbetonbalken. Institut für Baustoffe, Massivbau und Brandschutz der Technischen Universität Braunschweig, 1985; Zugl.: Dissertation, Technische Universität Braunschweig, 1985, ISBN 3-89288-002-6

Heft 67:

Kepp, B.: Zum Tragverhalten von Verankerungen für hochfeste Stäbe aus Glasfaserverbundwerkstoff als Bewehrung im Spannbetonbau. Institut für Baustoffe, Massivbau und Brandschutz der Technischen Universität Braunschweig, 1985; Zugl.: Dissertation, Technische Universität Braunschweig, 1985, ISBN 3-89288-003-4

Heft 68:

Sager, H.: Zum Einfluß hoher Temperaturen auf das Verbundverhalten von einbetonierten Bewehrungsstäben. Institut für Baustoffe, Massivbau und Brandschutz der Technischen Universität Braunschweig, 1985; Zugl.: Dissertation, Technische Universität Braunschweig, 1985, ISBN 3-89288-004-2

Heft 69:

Haß, R.: Zur praxisingerechten brandschutztechnischen Beurteilung von Stützen aus Stahl und Beton. Institut für Baustoffe, Massivbau und Brandschutz der Technischen Universität Braunschweig, 1986; Zugl.: Dissertation, Technische Universität Braunschweig, 1986, ISBN 3-89288-005-0

Heft 70:

Institut für Baustoffe, Massivbau und Brandschutz: 17. Forschungskolloquium des Deutschen Ausschusses für Stahlbeton, März 1986, Kurzfassungen der Beiträge. Institut für Baustoffe, Massivbau und Brandschutz der Technischen Universität Braunschweig, 1986, ISBN 3-89288-006-9

Heft 71:

Ehm, C.: Versuche zur Festigkeit und Verformung von Beton unter zweiaxialer Beanspruchung und hohen Temperaturen. Institut für Baustoffe, Massivbau und Brandschutz der Technischen Universität Braunschweig, 1986; Zugl.: Dissertation, Technische Universität Braunschweig, 1986, ISBN 3-89288-007-7

Heft 72:

Hartwich, K.: Zum Reiß- und Verformungsverhalten von Stahlfaserverstärkten Stahlbetonstäben unter Längszug. Institut für Baustoffe, Massivbau und Brandschutz der Technischen Universität Braunschweig, 1986; Zugl.: Dissertation, Technische Universität Braunschweig, 1986, ISBN 3-89288-008-5

Heft 73:

Scheuermann, J.: Zum Einfluß tiefer Temperaturen auf Verbund und Reißbildung von Stahlbetonbauteilen. Institut für Baustoffe, Massivbau und Brandschutz der Technischen Universität Braunschweig, 1987; Zugl.: Dissertation, Technische Universität Braunschweig, 1987, ISBN 3-89288-011-5

Heft 74:

Hinrichsmeyer, K.: Strukturorientierte Analyse und Modellbeschreibung der thermischen Schädigung von Beton. Institut für Baustoffe, Massivbau und Brandschutz der Technischen Universität Braunschweig, 1987; Zugl.: Dissertation, Technische Universität Braunschweig, 1987, ISBN 3-89288-015-8

Heft 75:

Institut für Baustoffe, Massivbau und Brandschutz: Fachseminar Neue Bemessungsregeln durch Änderung der Stahlbeton- und Spannbetonvorschriften DIN 1045, DIN 4227, Juni 1986, Kurzfassungen der Beiträge. Institut für Baustoffe, Massivbau und Brandschutz der Technischen Universität Braunschweig, 1986, ISBN 3-89288-022-0

Heft 76:

Budelmann, H.: Zum Einfluß erhöhter Temperaturen auf Festigkeit und Verformung von Beton mit unterschiedlichen Feuchtegehalten. Institut für Baustoffe, Massivbau und Brandschutz der Technischen Universität Braunschweig, 1987; Zugl.: Dissertation, Technische Universität Braunschweig, 1987, ISBN 3-89288-016-6

Heft 77:

Großmann, F.: Spannungen und bruchmechanische Vorgänge im Normbeton unter Zugbeanspruchung. Institut für Baustoffe, Massivbau und Brandschutz der Technischen Universität Braunschweig, 1987; Zugl.: Dissertation, Technische Universität Braunschweig, 1987, ISBN 3-89288-023-9

Heft 78:

Rohling, A.: Zum Einfluß des Verbundkriechens auf die Rißbreitenentwicklung sowie auf die Mitwirkung des Betons zwischen den Rissen. Institut für Baustoffe, Massivbau und Brandschutz der Technischen Universität Braunschweig, 1987; Zugl.: Dissertation, Technische Universität Braunschweig, 1987, ISBN 3-89288-024-7

Heft 79:

Henning, W.: Zwangrißbildung und Bewehrung von Stahlbetonwänden auf steifen Unterbauten. Institut für Baustoffe, Massivbau und Brandschutz der Technischen Universität Braunschweig, 1987; Zugl.: Dissertation, Technische Universität Braunschweig, 1987, ISBN 3-89288-025-5

Heft 80:

Richter, E.: Zur Berechnung der Biegetragfähigkeit brandbeanspruchter Spann-betonbauteile unter Berücksichtigung geeigneter Vereinfachungen für die Materialgesetze. Institut für Baustoffe, Massivbau und Brandschutz der Technischen Universität Braunschweig, 1987; Zugl.: Dissertation, Technische Universität Braunschweig, 1987, ISBN 3-89288-026-3

Heft 81:

Kiel, M.: Nichtlineare Berechnung ebener Stahlbetonflächentragwerke unter Einschuß von Brandbeanspruchung. Institut für Baustoffe, Massivbau und Brandschutz der Technischen Universität Braunschweig, 1987; Zugl.: Dissertation, Technische Universität Braunschweig, 1987, ISBN 3-89288-027-1

Heft 82:

Konietzko, A.: Polymerspezifische Auswirkungen auf das Tragverhalten modifizierter zementgebundener Betone (PCC). Institut für Baustoffe, Massivbau und Brandschutz der Technischen Universität Braunschweig, 1988; Zugl.: Dissertation, Technische Universität Braunschweig, 1988, ISBN 3-89288-028-X

Heft 83:

Grzeschkowitz, R.: Zum Trag- und Verformungsverhalten schlanker Stahlbetonstützen unter besonderer Berücksichtigung der schiefen Biegung. Institut für Baustoffe, Massivbau und Brandschutz der Technischen Universität Braunschweig, 1988; Zugl.: Dissertation, Technische Universität Braunschweig, 1988, ISBN 3-89288-030-1

Heft 84:

Wiese, J.: Zum Trag- und Verformungsverhalten von Stahlbetonplatten unter partieller Brandbeanspruchung. Institut für Baustoffe, Massivbau und Brandschutz der Technischen Universität Braunschweig, 1988; Zugl.: Dissertation, Technische Universität Braunschweig, 1988, ISBN 3-89288-031-X

Heft 85:

Rudolph, K.: Traglastberechnung zwei-achsig biegebeanspruchter Stahlbetonstützen unter Brandeinwirkung. Institut für Baustoffe, Massivbau und Brandschutz der Technischen Universität Braunschweig, 1988; Zugl.: Dissertation, Technische Universität Braunschweig, 1988, ISBN 3-89288-032-8

Heft 86:

Kordina, K.; Meyer-Ottens, C.; Noack, I.: Einfluß der Eigenbrandlast auf das Brandverhalten von Bauteilen aus brennbaren Baustoffen. Institut für Baustoffe, Massivbau und Brandschutz der Technischen Universität Braunschweig, 1989, in Vorbereitung, ISBN 3-89288-058-1

Heft 87:

Institut für Baustoffe, Massivbau und Brandschutz: Forschungsarbeiten 1984 - 1989. Institut für Baustoffe, Massivbau und Brandschutz der Technischen Universität Braunschweig, 1989, ISBN 3-89288-034-4

Heft 88:

Grossert, E.: Untersuchungen zum Tragverhalten von Massivbrücken mit zweizelligem Kastenquerschnitt. Institut für Baustoffe, Massivbau und Brandschutz der Technischen Universität Braunschweig, 1989; Zugl.: Dissertation, Technische Universität Braunschweig, 1989, ISBN 3-89288-059-X

Heft 89:

Falkner, H.; Teutsch, M. [Hrsg.]: Weiterbildungsseminar "Bauen in Europa", 15.-16. November 1990 in Braunschweig, Kurzreferate, ISBN 3-89288-063-8

Heft 90:

Falkner, H.; Teutsch, M.; Claußen, T.; Voß, K.-U.: Vorspannung im Hochbau. Institut für Baustoffe, Massivbau und Brandschutz der Technischen Universität Braunschweig, 1991, ISBN 3-89288-064-6

Heft 91:

Falkner, H.; Teutsch, M. [Hrsg.]: Fachtagung Spannbeton im Hoch- und Industriebau, Kurzreferate, 1991, ISBN 3-89288-065-4

Heft 92:

Heins, T.: Simulationsmodell zur sicherheitstechnischen Beurteilung der Rauchausbreitung in ausgedehnten Räumen. Institut für Baustoffe, Massivbau und Brandschutz der Technischen Universität Braunschweig, 1991; Zugl.: Dissertation, Technische Universität Braunschweig, ISBN 3-89288-066-2

Heft 93:

Hagen, E.: Zur Prognose des Gefährdungspotentials von Raumbränden. Institut für Baustoffe, Massivbau und Brandschutz der Technischen Universität Braunschweig, 1992; Zugl.: Dissertation, Technische Universität Braunschweig, 1991, ISBN 3-89288-072-7

Heft 94:

Falkner, H.; Teutsch, M. [Hrsg.]: Fachseminar "Instandsetzung und Ertüchtigung von Massivbauten", 14.-15. November 1991 in Braunschweig, Kurzreferate, ISBN 3-89288-068-9

Heft 95:

Qualitätssicherung im Bauwesen, VMPTagung 1992, 25.-26.06.1992, Tagungsbericht, ISBN 3-89288-071-9

Heft 96:

Weiterbildungsseminar "Brandschutz im Industriebau", 30.09.1992 in Braunschweig, Kurzreferate, ISBN 3-89288-070-0

Heft 97:

Falkner, H.; Teutsch, M. [Hrsg.]: Fachseminar "Neue Technologien im Bauwesen", 12.-13.11.1992 in Braunschweig, Kurzreferate, ISBN 3-89288-073-5

Heft 98:

Gunkler, E.: Verstärkung biegebeanspruchter Mauerwerkswände durch bewehrte Ergänzungsschichten. Institut für Baustoffe, Massivbau und Brandschutz der Technischen Universität Braunschweig, 1993; Zugl.: Dissertation, Technische Universität Braunschweig, 1992, ISBN 3-89288-074-3

Heft 99:

Dorn, T.: Zur Berechnung des Tragverhaltens brandbeanspruchter Tragwerke in Verbundbauweise unter besonderer Berücksichtigung der Träger-Stützen-Anschlüsse. Institut für Baustoffe, Massivbau und Brandschutz der Technischen Universität Braunschweig, 1993; Zugl.: Dissertation, Technische Universität Braunschweig, 1992, ISBN 3-89288-075-1

Heft 100:

Falkner, H.; Teutsch, M. [Hrsg.]: Fachseminar "Stahlfaserbeton", 04.03.1993 in Braunschweig, Kurzreferate, ISBN 3-89288-076-X

Heft 101:

Falkner, H.; Teutsch, M.: Vergleichende Untersuchungen an unbewehrten und stahlfaserbewehrten Industriefußböden. Forschungsbericht, Institut für Baustoffe, Massivbau und Brandschutz der Technischen Universität Braunschweig, 1993, ISBN 3-89288-077-8

Heft 102:

Falkner, H.; Teutsch, M.: Comparative studies of plain and steel fiber reinforced concrete industrial ground slabs. Forschungsbericht, Institut für Baustoffe, Massivbau und Brandschutz der Technischen Universität Braunschweig, 1993, ISBN 3-89288-078-6

Heft 103:

Braunschweiger Brandschutz-Tage 1993: Fachseminar Brandschutz - Forschung und Praxis. 06.-07.10.1993, Kurzreferate, ISBN 3-89288-079-4

Heft 104:

Thienel, K.-C.: Festigkeit und Verformung von Beton bei hoher Temperatur und biaxialer Beanspruchung. Institut für Baustoffe, Massivbau und Brandschutz der Technischen Universität Braunschweig, 1993
Zugl.: Dissertation, Technische Universität Braunschweig, 1993, ISBN 3-89288-080-8

Heft 105:

Falkner, H.; Teutsch, M. [Hrsg.]: Braunschweiger Bauseminar 1993 "Dauerhafte Bauwerke aus Faserbeton", 11.-12.11.1993 in Braunschweig, Kurzreferate, ISBN 3-89288-081-6

Heft 106:

Neuentwicklungen im baulichen Brandschutz. Dr. Meyer-Ottens 60 Jahre; Fachseminar 18.03.1994 in Braunschweig, ISBN 3-89288-085-9

Heft 107:

Bunte, D.: Zum karbonatisierungsbedingten Verlust der Dauerhaftigkeit von Außenbauteilen aus Stahlbeton. Institut für Baustoffe, Massivbau und Brandschutz der Technischen Universität Braunschweig, 1994
Zugl.: Dissertation, Technische Universität Braunschweig, 1993, ISBN 3-89288-086-7

Heft 108:

Holzenkämpfer, P.: Ingenieurmodell des Verbundes geklebter Bewehrung für Betonbauteile. Institut für Baustoffe, Massivbau und Brandschutz der Technischen Universität Braunschweig, 1994
Zugl.: Dissertation, Technische Universität Braunschweig, 1994, ISBN 3-89288-087-5

Heft 109:

Forschungsarbeiten 1990 - 1994. Institut für Baustoffe, Massivbau und Brandschutz der Technischen Universität Braunschweig, 1994, ISBN 3-89288-088-3

Heft 110:

Falkner, H.; Teutsch, M.; Rohde, S.: Untersuchung der Schubtragfähigkeit und der Wasserundurchlässigkeit von Arbeitsfugen unter Verwendung von Stremaform-Abschalelementen.
Falkner, H.; Teutsch, M.; Claußen, T.: Schubtragfähigkeit des Vergußbetons zwischen Köcher-, Block oder Hülsenfundamenten und Stützenfuß bei unterschiedlich profilierten Betonoberflächen.
Institut für Baustoffe, Massivbau und Brandschutz der Technischen Universität Braunschweig, 1994, ISBN 3-89288-089-1

Heft 111:

Voß, K.-U.: Zum Trag- und Verformungsverhalten bei Schwellbeanspruchung. Institut für Baustoffe, Massivbau und Brandschutz der Technischen Universität Braunschweig, 1994
Zugl.: Dissertation, Technische Universität Braunschweig, 1993, ISBN 3-89288-090-5

Heft 112:

Weiterbildungsseminar Brandschutz bei Sonderbauten: 05./06.10.1994 in Braunschweig; Kurzreferate, 1994, ISBN 3-89288-092-1

Heft 113:

Falkner, H.; Teutsch, M. [Hrsg.]: Aus der Forschung in die Praxis: 10./11.11.1994; Braunschweiger Bauseminar 1994, ISBN 3-89288-091-3

Heft 114:

Warnecke, P.: Tragverhalten und Konsolidierung von historischem Natursteinmauerwerk, 1995
Zugl.: Dissertation, Technische Universität Braunschweig, 1995, ISBN 3-89288-094-8

Heft 115:

Braunschweiger Brandschutz-Tage 1995: 6. Fachseminar Brandschutz - Forschung und Praxis: 04.-05.10.1995, Kurzreferate, ISBN 3-89288-093-X

Heft 116:

Huang, Z.: Grenzbeanspruchung gebetteter Stahlfaserbetonplatten, 1995
Zugl.: Dissertation, Technische Universität Braunschweig, 1995, ISBN 3-89288-095-6

Heft 117:

Falkner, H.; Teutsch, M.; Huang, Z.: Untersuchung des Trag- und Verformungsverhaltens von Industriefußböden aus Stahlfaserbeton. Institut für Baustoffe, Massivbau und Brandschutz der Technischen Universität Braunschweig, 1995, ISBN 3-89288-096-4

Heft 118:

Kubat, B.: Durchstanzverhalten von vorgespannten, punktförmig gestützten Platten aus Stahlfaserbeton, 1995
Zugl.: Dissertation, Technische Universität Braunschweig, 1995, ISBN 3-89288-097-2

Heft 119:

Falkner, H.; Teutsch, M. [Hrsg.]: Dichte Bauwerke: 09./10.11.1995; Braunschweiger Bauseminar 1995, ISBN 3-89288-091-3

Heft 120:

Steinert, C.: Bestimmung der Wärmeübergangsbedingungen auf Bauteile im Brandfall, Abschlußbericht, 1995, ISBN 3-89288-099-9

Heft 121:

Schütte, J.; Teutsch, M.; Falkner, H.: Fugenlose Betonbodenplatten, Forschungsbericht, 1996, ISBN 3-89288-100-6

Heft 122:

Weiterbildungsseminar Brandschutz bei Sonderbauten: 24./25.09.1996 in Braunschweig, Kurzreferate, 1996, ISBN 3-89288-101-4

Heft 123:

Droese, S.; Riese, A.: Belastungsversuche an zwei Durchlauf-Plattenstreifen aus Elementplatten mit Aufbeton aus Stahlfaserbeton, 1996, ISBN 3-89288-102-4

Heft 124:

Hankers, C.: Zum Verbundtragverhalten lachenverstärkter Betonbauteile unter nicht vorwiegend ruhender Beanspruchung, 1996
Zugl.: Dissertation, Technische Universität Braunschweig, 1996, ISBN 3-89288-103-0

Heft 125:

Schmidt-Döhl, F.: Ein Modell zur Berechnung von kombinierten chemischen Reaktions- und Transportprozessen und seine Anwendung auf die Korrosion mineralischer Baustoffe, 1996
Zugl.: Dissertation, Technische Universität Braunschweig, 1996, ISBN 3-89288-104-9

Heft 126:

Falkner, H.; Teutsch, M. [Hrsg.]: Ingenieurbauwerke mit neuen Konzepten: 14./15.11.1996, Braunschweiger Bauseminar 1996, ISBN 3-89288-105-7

Heft 127:

Forschung über Baudenkmalpflege - Arbeitsberichte: 1990 - 1993, 1996, ISBN 3-89288-106-5

Heft 128:

Festschrift zum 65. Geburtstag von Prof. Dr.-Ing. F. S. Rostásy: Baustoffe in Praxis, Lehre und Forschung, 1997, ISBN 3-89288-107-3

Heft 129:

Forschung über Baudenkmalpflege - Arbeitsberichte: 1994, 1997, ISBN 3-89288-108-1

Heft 130:

Forschung über Baudenkmalpflege - Arbeitsberichte: 1995, 1997, ISBN 3-89288-109-X

Heft 131:

Falkner, H.; Teutsch, M.; Klinkert H.: Trag- und Verformungsverhalten dynamisch beanspruchter Fahrbahnen aus Beton- und Stahl-faserbeton, Forschungsbericht, 1997, ISBN 3-89288-110-3

Heft 132:

Schütte, J.: Einfluß der Lagerungsbedingungen auf Zwang in Betonbodenplatten, 1997 Zugl.: Dissertation, Technische Universität Braunschweig, 1997, ISBN 3-89288-111-1

Heft 133:

Braunschweiger Brandschutz-Tage 1997: 7. Fachseminar Brandschutz - Forschung und Praxis: 01.-02.10.1997, Kurzreferate, ISBN 3-89288-112-X

Heft 134:

Ameler, J.: Betonverhalten bei hohen Temperaturen und triaxialer Beanspruchung - FE-Modell auf der Basis der Betonstruktur, 1997 Zugl.: Dissertation, Technische Universität Braunschweig, 1997, ISBN 3-89288-113-8

Heft 135:

Tagung Konsolidierung von historischem Natursteinmauerwerk: 06./07.11.1997 in Braunschweig, ISBN 3-89288-114-6

Heft 136:

Falkner, H.; Teutsch, M. [Hrsg.]: Innovatives Bauen: 13./14.11.1997, Braunschweiger Bauseminar 1997, ISBN 3-89288-115-4

Heft 137:

Forschung über Baudenkmalpflege - Arbeitsberichte: 1996 - 1997. 1998. ISBN 3-89288-116-2

Heft 138:

Scheibe, M.: Vorhersage des Zeitstandverhaltens unidirektionaler Aramidfaserverbundstäbe in alkalischer Umgebung. 1998. Zugl.: Braunschweig, TU, Diss., 1998. ISBN 3-89288-117-0

Heft 139:

Weiterbildungsseminar Brandschutz bei Sonderbauten : 29./30.9.1998 in Braunschweig ; Kurzreferate. 1998. ISBN 3-89288-118-9

Heft 140:

Gutsch, A.: Stoffeigenschaften jungen Betons - Versuche und Modelle. 1998. Zugl.: Braunschweig, TU, Diss. ISBN 3-89288-119-7

Heft 141:

Falkner, H. ; Teutsch, M. [Hrsg.] Beton auf neuen Wegen : 12.-13.11.1998 ; Braunschweiger Bauseminar 1998. ISBN 3-89288-120-0

Heft 142:

Betonbau - Forschung, Entwicklung und Anwendung : Festschrift zum 60. Geburtstag von Univ.-Prof. Dr.-Ing Horst Falkner am 20.4.1999. 1999. ISBN 3-89288-121-9

Heft 143:

Teutsch, M ; Klinkert, H. Leistungsklassen von Stahlfaserbeton. 1999. ISBN 3-89288-122-7

Heft 144:

Forschungsarbeiten 1995 - 1999. 1999. ISBN 3-89288-123-5

Heft 145:

Braunschweiger Brandschutztage 1999: 8. Fachseminar Brandschutz - Forschung und Praxis ; 4.-5. Oktober 1999 in Braunschweig., Kurzreferate. 1999. ISBN 3-89288-124-3

Heft 146:

Falkner, H. ; Teutsch, M. [Hrsg.] Bauen im nächsten Jahrtausend : 11.11.-12.11.1999 ; Braunschweiger Bauseminar 1999. ISBN 3-89288-125-1

Heft 147:

Weiterbildungsseminar Brandschutz bei Sonderbauten: 28./29.3.2000 in Braunschweig; Kurzreferate, 2000. ISBN 3-89288-126-X

Heft 148:

Hariri, K.: Bruchmechanisches Verhalten jungen Betons - Laser-Speckle-Interferometrie und Modellierung der Rißprozeßzone. 2000.

Zugl.: Braunschweig, TU, Diss., 2000. ISBN 3-89288-127-8

Heft 149:

Wigger, H.: Rissbildung in historischem Natursteinmauerwerk : Beobachtung, Versuche und Berechnungsmodelle. 2000.

Zugl.: Braunschweig, TU, Diss., 2000. ISBN 3-89288-128-6

Heft 150:

Neubauer, U.: Verbundtragverhalten geklebter Lamellen aus Kohlenstoffaser – Verbundwerkstoff zur Verstärkung von Betonbauteilen. 2000

Zugl.: Braunschweig, TU, Diss., 2000. ISBN 3-89288-129-4.

Heft 151:

Brandschutz in Chemikalienlagern. 2000.

ISBN 3-89288-130-8

Heft 152:

Falkner, H. ; Teutsch, M. [Hrsg.] Trends und Entwicklungen im Bauwesen : 9.-10.11.2000 ; Braunschweiger Bauseminar 2000.

ISBN 3-89288-131-6

Heft 153:

Rostásy, F.S. ; Budelmann, H. [Hrsg.] Rissbeherrschung massiger Betonbauteile : Bauwerk, Werkstoff, Simulation ; Braunschweig, 20.3.2001.

ISBN 3-89288-132-4

Heft 154:

Krauß, M. ; Hariri, K. ; Rostásy, F.S. Hydratationsgrad, Ultraschall-Technik zur Beschreibung der Erhärtung, bruchmechanisches Verhalten jungen Betons : Berichte ; Forschungsprojekt der EU (Brite Euram BE96-3843), IPACS. 2001.

ISBN 3-89288-135-9.

Heft 155:

Gutsch, A. ; Rostásy, F.S. Spannungs-Dehnungslinie, viskoelastisches Verhalten und autogenes Schwinden jungen Betons : Berichte ; Forschungsprojekt der EU (Brite Euram BE96-3843), IPACS. 2001.

ISBN 3-89288-136-7

Heft 156:

Rostásy, F.S. ; Krauß, M. ; Gutsch, A. Spannungsberechnung und Risskriterien für jungen Beton – Methoden des iMBB : Bericht ; Forschungsprojekt der EU (Brite Euram BE96-3843), IPACS. 2001.

ISBN 3-89288-137-5

Heft 157:

Rostásy, F.S. ; Krauß, M. ; Gutsch, A. Früher Zwang in massigen Sohlplatten : Bericht ; Forschungsprojekt der EU (Brite Euram BE96-3843), IPACS. 2001.

ISBN 4-89288-138-3

Heft 158:

Braunschweiger Brandschutztag 2001: 9. Fachseminar Brandschutz - Forschung und Praxis ; 1.-2. Oktober 2001 in Braunschweig., Kurzreferate. 2001.

ISBN 3-89288-139-1

Heft 159:

Falkner, H. ; Teutsch, M. [Hrsg.] Bauen im Wandel der Zeit : 8.-9.11.2001 ; Braunschweiger Bauseminar 2001. 2001.

ISBN 3-89288-140-5.

Heft 160:

Beiträge zum 40. Forschungskolloquium des Deutschen Ausschusses für Stahlbeton : 11.-12.10.2001 in Braunschweig. 2001.

ISBN 3-89288-141-3

Heft 161:

Dora, B.: Hydraulisch erhärtende Baustoffe aus Betonbrechsand – Phasenveränderungen durch Temperaturbehandlung und Einsatzmöglichkeiten.

Zugl.: Braunschweig, TU, Diss., 2001.

ISBN 3-89288-142-1.

Heft 162:

RO 70 : 50 Jahre Forschung und 25 Dissertationen ; Prof. Dr.-Ing. Dr.-Ing. E. h. Rostásy, zum 70 Geburtstag gewidmet. 2002.

ISBN 3-89288-143-X.

Heft 163:

Praxisseminar Brandschutz bei Sonderbauten : 1. und 2. Oktober 2002 in Braunschweig ; Kurzreferate.

2002.

ISBN 3-89288-144-8

Heft 164:

Stahlfaserbeton : Ein unberechenbares Material? ; 14.-15. November - Braunschweiger Bauseminar 2002.

ISBN 3-89288-145-6

Heft 165:

Niemann, P.

Gebrauchsverhalten von Bodenplatten aus Beton unter Einwirkungen infolge Last und Zwang. Zugl.: Braunschweig, TU, Diss., 2002.

ISBN 3-89288-146-4

Heft 166:

Budelmann ; H. ; Falkner, H. [Hrsg.]

Bauen im Bestand : 25. März 2003.

ISBN 3-89288-147-2

H. 167:

Blume, G.W.: Ingenieurmodell zur brandschutztechnischen Bemessung von Bauteilen auf der Basis von experimentell ermittelten Verbrennungseffektivitäten. 2003.

Zugl.: Braunschweig, TU, Diss., 2002.

ISBN 3-89288-148-0

H. 168:

Braunschweiger Brandschutztage 2003: 10. Fachseminar Brandschutz - Forschung und Praxis ; 30.9. - 1.10.2003 in Braunschweig., Kurzreferate. 2003.

ISBN 3-89288-149-9

H. 169:

Falkner, H. ; Teutsch, M. [Hrsg.]

Bauforschung und -praxis in schwierigen Zeiten : 13. und 14. November ; Braunschweiger Bauseminar 2003.

ISBN 3-89288-150-2

H 170:

Hemmy, O.: Zum Gebrauchs- und Tragverhalten von Tunnelschalen aus Stahlfaserbeton und stahlfaserverstärktem Stahlbeton.

Zugl.: Braunschweig, TU, Diss., 2003.

ISBN 3-89288-151-0

H. 171:

Dehne, M.: Probabilistisches Sicherheitskonzept für die brandschutztechnische Bemessung. 2003.

Zugl.: Braunschweig, TU, Diss., 2003.

ISBN 3-89288-153-7

H. 172:

Paliga, K.: Entstehung und Vermeidung von Betonabplatzungen bei Tunnelbränden. 2003.

Zugl.: Braunschweig, TU, Diss., 2003.

ISBN 3-89288-154-5

Heft 173:

Festschrift zum 60 Geburtstag von Univ.-Prof. Dr.-Ing. Dietmar Hosser : Brandschutz und mehr...

2003.

ISBN 3-89288-152-9

Heft 174:

Timm, M.: Verbundwirkung des Betons im Bereich von STREMAFORM - Abschalelementen : Untersuchungsbericht ; Okt. 2000. 2004.

ISBN 3-89288-156-1

Heft 175:

Zehfuß, J.: Bemessung von Tragsystemen mehrgeschossiger Gebäude in Stahlbauweise für realistische Brandbeanspruchung. Zugl.: Braunschweig, TU, Diss., 2004.

ISBN 3-89288-155-3

Heft 176:

Nause, P.: Berechnungsgrundlagen für das Brandverhalten von Druckgliedern aus hochfestem Beton. 2004.

Zugl.: Braunschweig, TU, Diss., 2004.

ISBN 3-89288-157-X

Nicht in der Schriftenreihe erschienen.

Heft 177:

Budelmann ; H. ; Falkner, H. [Hrsg.]

Bauen im Bestand : 23. März 2004.

ISBN 3-89288-158-8

H. 178:

Praxisseminar Brandschutz bei Sonderbauten : 29. – 30.9.2004 in Braunschweig ; Kurzreferate. 2004.
ISBN 3-89288-159-6

H. 179:

Krauß, M.: Probabilistischer Nachweis der Wirksamkeit von Maßnahmen gegen frühe Trennrisse in massigen Betonbauteilen. 2004.

Zugl.: Braunschweig, TU, Diss., 2004.

ISBN 3-89288-160-X.

H. 180:

Weiske, R.

Durchleitung hoher Stützlasten bei Stahlbetonflachdecken. 2004.

Zugl.: Braunschweig, TU, Diss., 2004.

ISBN 3-89288-161-8.

H. 181:

Falkner, H. ; Teutsch, M. [Hrsg.]

Qualität im Bauwesen : 11. und 12. Nov. ; Braunschweiger Bauseminar 2004.

ISBN 3-89288-162-6

H. 182:

Festschrift zum 60. Geburtstag von Univ.-Prof. Dr.-Ing. Klaus Peter Großkurth : Struktur und Anwendung der Baustoffe. 2005.

ISBN 3-89288-163-4

H. 183:

Budelmann, H. ; Laube, M. ; Hinrichs, W. [Hrsg.]

Bauen im Bestand : 23. Februar 2005.

ISBN 3-89288-164-2

H. 184:

Hinrichs, W.

Charakterisierung einer einheitlichen Messmethodik und Validierung ausgewählter Verfahren für die Bestimmung der Maschenweiten von Stahldrahtgeweben : Das Forschungsvorhaben wurde von der Stiftung Stahlanwendungsforschung im Stifterverband für die Deutsche Wissenschaft e.V. gefördert (Az: A 182/S24/10036/02. 2005).

ISBN 3-89288-166-9.

H. 185:

Braunschweiger Brandschutz-Tage '05 : 11. Fachseminar Brandschutz – Forschung und Praxis, 28. und 29. Sept. 2005 in Braunschweig, Tagungsbericht.

ISBN 3-89288-167-7.

H. 186:

Will, J.: Entwicklung eines sauerstoffkalorimetrischen Verfahrens zur Bestimmung von Brandparametern bei unterschiedlich ventilierten Bränden. 2005.

Zugl.: Braunschweig, TU, Diss., 2005.

ISBN 3-89288-168-5.

H. 187:

Rigo, E.M.: Ein probabilistisches Konzept zur Beurteilung der Korrosion zementgebundener Baustoffe durch lösenden und treibenden Angriff. 2005.

Zugl.: Braunschweig, TU, Diss., 2005.

ISBN 3-89288-169-3.

H. 188:

Budelmann, H. ; Gutsch, A.-W. [Hrsg.]

Bauen im Bestand : Beton in der Abwassertechnik ; 6. Sept. 2005.

ISBN 3-89288-170-7.

H. 189:

Gerritzen, D.P.

Zur Frage der Nutzbarkeit verbundlos vorgespannter Stahlbetondecken nach Brandeinwirkung. 2005.

Zugl.: Braunschweig, TU, Diss., 2005.

ISBN 3-89288-171-5.

H. 190:

Falkner, H. ; Teutsch, M. [Hrsg.]

Bewe(ä)rteter Betonbau : 10. und 11. November ; Braunschweiger Bauseminar 2005.

ISBN 3-89288-172-3

H. 191:

Kurzberichte aus der Forschung 2005.

2006.

ISBN 3-89288-173-1

H. 192:

Praxisseminar Brandschutz bei Sonderbauten : 26.-27. Sept. 2006 ; Kurzreferate.

ISBN-10: 3-89288-174-X

ISBN-13: 978-3-89288-174-2.

- H. 193:
 Sperling, D.
 Eine Methode zur automatisierten Überwachung von Spannbetonfahrwegträgern. 2006.
 Zugl.: Braunschweig, TU, Diss., 2006.
 ISBN-10: 3-89288-175-8
 ISBN-13: 978-3-89288-175-9.
- H. 194:
 Grunert, J.P.
 Zum Tragverhalten von Spannbetonfertigteilbalken aus Stahlfaserbeton ohne Betonstahlbewehrung. 2006.
 Zugl.: Braunschweig, TU, Diss., 2006.
 ISBN-10: 3-89288-176-6
 ISBN-13: 978-3-89288-176-6.
- H. 195:
 Budelmann, H. ; Gutsch, A.-W. [Hrsg.]
 Bau Symposium Braunschweig (BSB 2007) : Stand und Entwicklung des Trockenbaus ; 8. März. 2007.
 ISBN 978-3-89288-177-3.
- H. 196:
 Bruder, S.
 Adaptive Modellierung der Dauerhaftigkeit im Zuge der Überwachung von Betonbauwerken. 2007.
 Zugl.: Braunschweig, TU, Diss., 1996.
 ISBN 978-3-89288-178-0.
- H. 197:
 Holst, A.
 Korrosionsmonitoring und Bruchortung vorgespannter Zugglieder in Bauwerken. 2007.
 Zugl.: Braunschweig, TU, Diss.
 ISBN 978-3-89288-179-7.
- H. 198:
 Forell, B.
 A Methodology to assess Species Yields of Compartment Fires by means of an extended Global Equivalence Ratio Concept. 2007.
 Zugl.: Braunschweig, TU, Diss.
 ISBN 978-3-89288-180-3.
- H. 199:
 Braunschweiger Brandschutz-Tage '07 : 21. Fachseminar Brandschutz – Forschung und Praxis, 26. und 27. Sept. 2007 in Braunschweig, Tagungsband.
 ISBN 978-3-89288-181-0.
- H. 200:
 Nothnagel, R.
 Hydratations- und Strukturmodell für Zementstein. 2007.
 Zugl.: Braunschweig, TU, Diss.
 ISBN 978-3-89288-182-7
- H. 201:
 Riese, O.
 Ein Brandausbreitungsmodell für Kabel. 2007.
 Zugl.: Braunschweig, TU, Diss.
 ISBN 978-3-89288-183-4
- H. 202:
 Braunschweiger Brandschutz-Tage '08 : 22. Fachtagung ; Brandschutz bei Sonderbauten , 30.9. – 1.10.2008 – Tagungsband.
 ISBN 978-3-89288-185-8
- H. 203:
 Klinzmann, C.
 Methodik zur computergestützten, probabilistischen Bauwerksbewertung unter Einbeziehung von Bauwerksmonitoring. 2008.
 Zugl.: Braunschweig, TU, Diss.
 ISBN 978-3-89288-186-5.
- H. 204:
 Schnetgöke, R.
 Zuverlässigkeitsorientierte Systembewertung von Massivbauwerken als Grundlage für die Bauwerksüberwachung. 2008.
 Zugl.: Braunschweig, TU, Diss.
 ISBN 978-3-89288-187-2.
- H. 205:
 Budelmann, H. ; Gutsch, A.-W. [Hrsg.]
 Bau Symposium Braunschweig (BSB 2008): Konstruktiver Holzbau ; 4. November 2008.
 ISBN 978-3-89288-188-9.
- H. 206:
 Kampmeier, B.
 Risikogerechte Brandschutzlösungen für den mehrgeschossigen Holzbau. 2008.
 Zugl.: Braunschweig, TU, Diss., 2008.
 ISBN 978-3-89288-189-6.

- H. 207:
Husemann, U.
Erhöhung der Verbundtragfähigkeit von nachträglich aufgeklebten Lamellen durch Bügelumschließungen.
Zugl.: Braunschweig, TU, Diss., 2009.
ISBN 978-3-89288-190-2
- H. 208:
Braunschweiger Brandschutz-Tage '09 : 23. Fachtagung Brandschutz – Forschung und Praxis, 29.9.2008 – 30.9.2009 ; Tagungsband.
ISBN 978-3-89288-191-9
- H. 209:
Sperbeck, S.T.
Seismic Risk Assessment of Masonry Walls and Risk Reduction by Means of Prestressing. 2009.
Zugl.: Braunschweig, TU, Diss., 2009.
ISBN 978-3-89288-192-6
- H. 210:
Braunschweiger Brandschutz-Tage 2010 : : 24. Fachtagung ; Brandschutz bei Sonderbauten , 21. und 22.9.2010 – Tagungsband.
ISBN 978-3-89288-194-0
- H. 211:
Hohm, V.
Wärmetransportmodell für gekoppelte Prozesse in der Brandsimulation. 2010.
Zugl.: Braunschweig, TU, Diss.
ISBN 978-3-89288-195-7.
- H. 212:
Kruse, D.
Entwicklung von Hochleistungsbrandschutzbeschichtungen zum Entzündungsschutz von Holz unter Vollbrandbedingungen. 2011.
Zugl.: Braunschweig, TU, Diss., 2010.
ISBN 978-3-89288-196-4.
- H. 213:
Twelmeier, H.
Dauerhaftigkeitsprognose der Verfüugung von gipshaltigem historischem Mauerwerk. 2011.
Zugl.: Braunschweig, TU, Diss., 2010.
ISBN 978-3-89288-197-1.
- H. 214:
Braunschweiger Brandschutz-Tage 2011 : : 25. Fachtagung Brandschutz – Forschung und Praxis, 27. und 28.9.2011 – Tagungsband.
ISBN 978-3-89288-198-8
- H. 215:
Hollmann, D.W.
Grundlagen und Ingenieurmodell für den Nachweis von Holzbauteilen mit Hochleistungsbrandschutzbeschichtungen. 2011.
Zugl.: Braunschweig, TU, Diss., 2011.
ISBN 978-3-89288-199-5
- H. 216:
Rostásy, F.S.
Assessment of Mechanical Properties of Structural Materials for Cryogenic Application (June 1988). 2011.
ISBN 978-3-89288-200-8
- H. 217:
Albrecht, C.
A risk-informed and performance-based life safety concept in case of fire. 2012.
Zugl.: Braunschweig, TU, Diss., 2012.
ISBN 978-3-89288-202-2.
- H. 218:
Braunschweiger Brandschutz-Tage 2012 : : 26. Fachtagung Brandschutz bei Sonderbauten, 19. und 20.9.2012 – Tagungsband.
ISBN 978-3-89288-203-9.
- H. 219:
Wichers, M.
Bemessung von bewehrten Betonbauteilen bei Teilflächenbelastung unter Berücksichtigung der Rissbildung. 2013.
Zugl.: Braunschweig, TU, Diss. 2013.
ISBN 978-3-89288-204-6.
- H. 220:
Braunschweiger Brandschutz-Tage 2013 : : 27. Fachtagung Brandschutz – Forschung und Praxis ; 25. und 26.9.2013 – Tagungsband.
ISBN 978-3-89288-205-3

- H. 221:
 Krakowski, W..
 Rissverhalten von Flächentragwerken aus Stahlbeton mit schiefwinkliger Bewehrung. 2013.
 Zugl.: Braunschweig, TU, Diss. 2013.
 ISBN 978-3-89288-206-0
- H. 222:
 Krauss, H.-W.
 Zur Auswirkung hochfeiner inerter Zusatzstoffe auf die Hydratationskinetik und die Mikrostruktur von Zementstein. 2013.
 Zugl.: Braunschweig, TU, Diss. 2013.
 ISBN 978-3-89288-207-7
- H. 223:
 Steven, G.
 Trag- und Nachbruchverhalten von Stützen aus ultrahochfestem Beton mit hochfester Längsbewehrung. 2014.
 Zugl.: Braunschweig, TU, Diss., 2014.
 ISBN 978-3-89288-208-4
- H. 224:
 Braunschweiger Brandschutz-Tage 2014 : : 28. Fachtagung Brandschutz bei Sonderbauten ; 16. und 17.9.2014 – Tagungsband. ISBN 978-3-89288-209-1.
- H. 225:
 Heumann; G.
 Zuverlässigkeitsorientierte Bewertung bestehender Bauwerke aus Stahlbeton und Spannbeton. 2014.
 Zugl.: Braunschweig, TU, Diss., 2014.
 ISBN 978-3-89288-210-7
- H. 226:
 Leusmann, T.
 Das Verbundtragverhalten geklebter Kohlefaserkunststoffe auf Beton unter schwingen-der Beanspruchung. 2015.
 Zugl.: Braunschweig, TU, Diss., 2015.
 ISBN 978-3-89288-211-4
- H. 227:
 Braunschweiger Brandschutz-Tage 2015 : : 29. Fachtagung Brandschutz – Forschung und Praxis ; 15. und 16.9.2015 – Tagungsband. ISBN 978-3-89288-212-1
- H. 228:
 Braunschweiger Brandschutz-Tage 2016 : 30. Fachtagung Brandschutz bei Sonderbauten ; 21. und 22.9.2016 – Tagungsband. ISBN 978-3-89288-213-8
- H. 229:
 Oettel, V.V.
 Torsionstragverhalten von stahlfaserbe- wehrten Beton-, Stahlbeton- und Spannbetonbalken. 2016.
 Zugl.: Braunschweig, TU, Diss., 2016.
 ISBN 978-3-89288-214-5
- H. 230:
 Hermerschmidt, W.
 Modelle zur Beschreibung der thermome- chanischen Materialeigenschaften jungen Betons. 2016.
 Zugl.: Braunschweig, TU, Diss., 2016.
 ISBN 978-3-89288-215-2
- H. 231:
 Siemon, M.
 Ein Pyrolysemodell zur Prognose der Brand- ausbreitung. 2016.
 Zugl.: Braunschweig, TU, Diss., 2016.
 ISBN 978-3-89288-216-9.
- H. 232:
 Braunschweiger Brandschutz-Tage 2017 : 31. Fachtagung Brandschutz – Forschung und Praxis ; 13. und 14. September 2017 – Tagungsband. ISBN 978-3-89288-217-6
- H. 233:
 Lehmsberg, S.
 Herstellung und Eigenschaften von dünn- wandigen, trocken gefügten Bauteilen aus ultrahochfestem faserverstärkten Feinkorn- beton. Zugl.: Braunschweig, TU, Diss., 2017.
 ISBN 978-3-89288-218-3
- H. 234:
 Braunschweiger Brandschutz-Tage 2018 : 32. Fachtagung Brandschutz bei Sonderbau- ten ; 19. und 20. September 2018 – Tagungs- band. ISBN 978-3-89288-219-0

H. 235:

Braunschweiger Brandschutz-Tage 2019 :
33. Fachtagung Brandschutz – Forschung
und Praxis ; 25. Und 26. September 2019 –
Tagungsband.
ISBN 978-3-89288-220-6

Heft 236:

Busse, D.
Querkrafttragverhalten von Betonträgern
mit dünnwandigen, mikrobewehrten Stegen.
2019.
Zugl.: Braunschweig, TU, Diss., 2019.
ISBN 978-3-89288-221-3

Heft 237:

Reichardt, M.
Alternde Stahlbetonbauteile unter Stoßbe-
lastung im Kontext der Zwischenlagerung
hoch radioaktiver Abfälle. 2019.
Zugl.: Braunschweig, TU, Diss., 2019.
ISBN 9783-89288-222-0

Heft 238:

Javidmehr, S.
Shear Capacity of Concrete under
Monotonic and Cyclic Loading. 2019.
Zugl.: Braunschweig, TU, Diss., 2019.
ISBN 9783-89288-223-7